

LOUGHBOROUGH  
UNIVERSITY OF TECHNOLOGY  
LIBRARY

AUTHOR/FILING TITLE

EL-SAYED, A

ACCESSION/COPY NO.

088672/01

VOL. NO.

CLASS MARK

ARCHIVES  
COPY

FOR REFERENCE ONLY

CRITICAL ANALYSIS OF PORTABLE  
WEB-TENSION MEASURING EQUIPMENT

BY

AHMED ALI MOHAMMED EL-SAYED

B.Sc., M.Sc.(Eng.)

A DOCTORAL THESIS

SUBMITTED IN PARTIAL FULFILMENT OF THE REQUIREMENT FOR

THE AWARD OF THE DEGREE OF

DOCTOR OF PHILOSOPHY

OF

LOUGHBOROUGH UNIVERSITY OF TECHNOLOGY

SEPTEMBER 1976

SUPERVISOR: PROFESSOR M. GRANEEK, B.Eng., C.Eng.  
DEPARTMENT OF ENGINEERING PRODUCTION.

© BY: AHMED ALI M. EL-SAYED, 1976

## SUMMARY

For satisfactory production or conversion of continuous material in web form it is generally important to control the tension in the web. The material may be plastics, paper or metal strip; conversion processes include web-fed printing or packaging machines and strip rolling mills. As speeds of production increase, it is more likely that relatively high frequency tension perturbations may occur due to interaction between material properties and machine performance characteristics. This could result in frequent breakage of the web or unsatisfactory quality of the product. It is therefore of paramount importance to be able to measure and control tension variations accurately and with an adequate speed of response.

The objectives of this investigation are to determine, by direct experiment and analytically, the limitations in static accuracy and dynamic performance of equipment for measurement of web tension. Another objective is to investigate the effect on measurement, due to distortion of the web, caused by the use of portable devices which are narrower than the full width of the web.

Tension measuring techniques under investigation include direct mechanical displacement devices and pneumatic foil bearings using electrical pressure transducers. A prototype electro-pneumatic portable device has been developed to measure the static as well as the dynamic tension applied to the web, using the principle of externally pressurised foil bearings. Static and dynamic loadings, derived from an electro-magnetic vibrator, apply known tension variations to a fixed web of material with a load-cell connected in line. The performance of the prototype device is analysed with reference to the load-cell output signals. The effect of the width of the prototype relative to the web width is examined experimentally and an attempt is made

to include these parameters in a theoretical analysis. A continuous loop of web, running at different speeds, is used to assess the performance of the web tension measuring device under running web conditions.

The principle of externally pressurised foil bearings, when utilised for web-tension measurement, gives promising results. The prototype electro-pneumatic portable device proved to be an accurate and reliable instrument for measuring local tension in the web; both static and dynamic within the frequency range available on the test rig (i.e. up to 80 Hz).

### ACKNOWLEDGMENTS

This study was sponsored in part by the Egyptian Government; and in part by the Science Research Council.

The author owes Professor M. Graneek, his supervisor, a large debt for his esteemed guidance during this work. Such guidance provided inspiration, not only for this project, but for a life-time of research work. The numerous discussions held with him and the valuable suggestions and constructive criticism he made contributed greatly to the existence of this thesis.

Thanks are also due to Professor R.J. Sury, the director of research.

The author also acknowledges his debt to a whole host of staff at Loughborough University of Technology, Department of Engineering Production, and other departments. In particular, thanks are due to Messrs. N. Carpenter, T. Kirk, J. Manning and G. Simpson for their fruitful suggestions and their technical help in establishing the necessary arrangements for the experimental work. Mrs. D. Young, also should be singled out for the great care she has taken in typing this thesis.

Of course, any remaining errors are the author's.

My greatest debt, however, is to my wife Safa. Her editorial assistance made the thesis clearer and more readable. But, of much greater importance, her constant encouragement has helped through the most difficult parts of this study, and while the strain of completing this work has been greatest upon her, she presented me with a most precious gift; our tiny little daughter, Mai. To her my loving thanks.

Ahmed A. El-Sayed.  
September 1976.

# CONTENTS

	Page No.
List of Figures	i
List of Tables	v
List of Plates	vii
<b>1. INTRODUCTION AND LITERATURE REVIEWS:</b>	
1.1 INTRODUCTION AND THE AIM OF THE WORK	1
1.2 REVIEW OF WEB TENSION MEASUREMENT LITERATURE	11
1.3 REVIEW OF FOIL BEARINGS LITERATURE	17
<b>2. ANALYTICAL FORMULATION RELEVANT TO THE STUDY:</b>	
2.1 MINIMUM VOLUME OF PNEUMATIC CIRCUIT	24
2.2 ANALYSIS OF INERTIA-COMPENSATED TENSION CONTROL:	32
2.2.1 Introduction	32
2.2.2 Theoretical analysis	34
2.3 PRESSURE IN AIR-FILM SUPPORTING A WEB UNDER TENSION	41
2.4 FINITE ELEMENT APPROACH TO WEB-TENSION PROFILE:	43
2.4.1 Introduction	43
2.4.2 Nomenclature	44
2.4.3 Finite element analysis	45
2.4.4 Results and discussion	51
2.4.5 Conclusion	53

### 3. EXPERIMENTAL RIG:

3.1	INTRODUCTION	54
3.2	TEST RIG:	55
3.2.1	Main frame and components	55
3.2.2	Frictionless air-bearings	61
3.2.3	Web-tension measuring pad	67
3.2.4	Air supply	72
3.2.5	Web materials	74
3.2.6	Method of applying tension	75
3.3	INSTRUMENTATION	81
3.3.1	Pneumatic network	81
3.3.2	Huyck tensometer	82
3.3.3	Reference load-cell	84
3.3.4	Kistler low pressure transducer	84
3.3.5	Miniature pressure transducer	86
3.3.6	Recording oscilloscope	89

### 4. SCHEME AND PROCEDURE OF EXPERIMENTAL WORK:

4.1	INTRODUCTION	90
4.2	STATIC TESTS:	91
4.2.1	The Huyck tensometer	91
4.2.2	The sintered measuring cylinder	92
4.2.3	The measuring pad	95
4.3	DYNAMIC TESTS:	101
4.3.1	Preliminary tests on measuring cylinder	103
4.3.2	Tests on the measuring pad with the miniature pressure transducer	106

	Page No.
4.4 RUNNING WEB TESTS	108
5. CALIBRATION OF INSTRUMENTS:	
5.1 INTRODUCTION	110
5.2 MEASUREMENT OF THE RADIUS OF CURVATURE OF THE MEASURING PAD	112
5.3 TRANSDUCER CALIBRATION	115
5.4 LOAD-CELL CALIBRATION	124
5.5 DETERMINATION OF THE STIFFNESS OF THE WEB MATERIAL	132
6. RESULTS AND DISCUSSION:	
6.1 INTRODUCTION	134
6.2 TERMINOLOGY	136
6.3 STATIC TESTS	138
6.3.1 The Huyck tensometer	138
6.3.2 The sintered measuring cylinder - validity of $p = \frac{T}{R}$	139
6.3.2 The sintered measuring cylinder - Tension profile	142
6.3.4 The measuring pad - Validity of $p = \frac{T}{R}$	146
6.3.5 The measuring pad - Tension profile	148
6.3.6 The measuring pad - Optimum wrap angle	150
6.3.7 The measuring pad - Optimum position of the miniature pressure transducer	152
6.4 DYNAMIC TESTS:	155
6.4.1 Preliminary tests - Measuring cylinder	155
6.4.2 The measuring pad - Miniature pressure transducer	156



6.5	RUNNING WEB TESTS	160
7.	CONCLUSION AND RECOMMENDATIONS FOR FUTURE WORK	
7.1	conclusion	231
7.2	RECOMMENDATIONS FOR FUTURE WORK	233
8.	REFERENCES	235
9.	APPENDICES	241
	I MINIMUM VOLUME OF PNEUMATIC CIRCUIT	241
	II ADJUSTABLE SPEED DRIVE SYSTEM AND SWINGING ROLL GUIDE UNIT	247
	III PROPERTIES OF THE MELINEX WEB USED	249
	IV SPECIFICATIONS OF INSTRUMENTS USED	250
	V INTERNATIONAL SYSTEM OF UNITS (SI) CONVERSION FACTORS	254

LIST OF FIGURES

Figure No.	Legend	Page No.
1.1 to 1.3	Principles of dancing roller technique	4
1.4	Strain gauges technique	6
1.5	Pneumatic gauging and force balance systems	8
2.1	Principle of electro-pneumatic web-tension measuring technique	25
2.2	The geometry of the air pocket	27
2.3	Air pocket configuration	30
2.4 and 2.5	The principle of the "Inertia compensated dancer"	33
2.6	Analogy of the web elasticity and the dancer inertia	39
2.7	The principle of externally pressurised foil bearing	42
2.8	Diagrammatic sketch for the experimental rig	47
2.9	The idealised structure of one quarter of the loaded web in the region between two guide rollers	49
2.10	Web under uniaxial tension	52
3.1	Perspective view for the main frame	56
3.2	Components of the test rig	57
3.3	Web-end fixation	59
3.4	Frictionless air bearing	59
3.5	Alternative designs for measuring cylinder	62
3.6	Guide unit bar supporting the sliding cylinder arrangement	66

Figure No.	Legend	Page No.
3.7	The measuring pad	68
3.8	Transducer mounting	69
3.9	Wrap angle adjustment arrangement.	73
3.10	Pneumatic network layout	74
3.11	Web fixed to the reference load-cell	77
3.12	Load-carrier	78
3.13	The Huyck tensometer	83
3.14	Basic circuit for a piezo-electric measuring system	85
3.15	Low pressure quartz transducer	85
3.16	The miniature pressure transducer and the circuit associated with it	88
4.1	Huyck tensometer experimental set up	92
4.2	Experimental set up to determine the optimum position of the transducer	99
4.3	Vibrator circuit	103
4.4	Record of transducer output signal	104
4.5	Record of Transducer/Load-cell output	105
5.1 and 5.2	Principle of the measurement of a large radius of curvature	113
5.3	Miniature pressure transducer calibration data sheet.	116
5.4	Transducer calibration adapter	117
5.5	Transducer calibration curve using the adapter.	119
5.6	Transducer calibration in situ	120
5.7	Transducer calibration curve in situ	123

Figure No.	Legend	Page No.
5.8	Calibration curve supplied with the load-cell	125
5.9	Calibration certificate for the proving ring	126
5.10	Load-cell/proving ring calibration set up	127
5.11 and 5.12	Load-cell calibration curves in situ	130 131
5.13	Load-Extension curve for the Melinex film	133
6.1	Huyck tensometer dial reading vs. applied tension	164
6.2 to 6.16	Web-tension measured by the measuring cylinder	166 180
6.17	Tension profile across a 50mm wide Melinex web	182
6.18	" " 102mm "	184
6.19	" " 102mm wide steel web	186
6.20 to 6.35	Web-tension measured by the measuring pad	188 202
6.36 and 6.37	Tension profile across a 50mm wide steel web	204 206
6.38	" " " in comparison with a 50mm wide Melinex web	208
6.39 to 6.42	Optimum wrap angle	210 216
6.43	Calibration of the miniature pressure transducer against water manometer	218
6.44	Optimum stable position of the miniature pressure transducer	220
6.45	Preliminary test on the Kistler pressure transducer	222
6.46	Frequency response of the measuring cylinder with Kistler transducer	224

Figure No.	Legend	Page No.
6.47 and 6.48	Frequency response of the measuring pad	226 228
6.49 and 6.50	Tension perturbation detected by the measuring pad	229 230

LIST OF TABLES

Table No.	Legend	Page No.
3.1	Values of rate of air flow through sintered materials	63
3.2	Weight of load-carrier and dead weight	79
4.1 and 4.2	Tension profile test conditions	94 97
4.3	Wrap angle test conditions	98
4.4	Optimum position of the pressure transducer test conditions	100
5.1	Calibration of miniature pressure transducer in the adapter	118
5.2	Calibration of miniature pressure transducer in situ	122
5.3	Calibration of the load-cell in situ	129
6.1	Huyck tensometer readings vs applied tension	163
6.2 to 6.5	Web-tension measured by the measuring cylinder at different pressures	165 177
6.6	Tension profile across a 50mm wide Melinex web	181
6.7	" " 102 mm "	183
6.8	" " 102 mm wide steel web	185
6.9 to 6.12	Web-tension measured by the measuring pad at different supply pressures	187 199
6.13 and 6.14	Tension profile across a 50mm wide steel web	203 205
6.15	" " Melinex web	207
6.16 to 6.19	Optimum wrap angle	209 215
6.20	Pressure transducer calibration against water manometer	217

Table No.	Legend	Page No.
6.21	Optimum position of the pressure transducer	219
6.22 and 6.23	Frequency response of the Kistler transducer	221 223
6.24	Dynamic response of the measuring pad on a Melinex web	225
6.25	Dynamic response of the measuring pad on a steel web	227
6.26	Web speed vs. measured frequency	161

LIST OF PLATES

Plate No.	Legend	Page No.
3.1	Basic experimental set up for static tests	60
3.2	Guide unit support bar and the measuring cylinder	65
3.3	The mounting bridge with the measuring pad	71
4.1	Experimental set up for static tests	96
4.2	Experimental set up for dynamic tests	102
4.3	Experimental set up for running web tests	109



CHAPTER 1

INTRODUCTION AND LITERATURE REVIEWS

## 1.1 INTRODUCTION AND THE AIM OF THE WORK

Economic pressures and the fact that time is the most precious commodity we deal in has resulted over the years in the development and use of high speed production systems. Development of the latest techniques involving the most modern machine designs, time studies and all possible aids towards automatic production (automation) becomes a necessity. These factors alongside the development of inspection and quality control techniques are all directed to time saving and consequently cutting down the total cost in the overall production process.

There are many continuous processing systems that are linked together by the material being processed, the properties of which can sometimes have a considerable effect on the dynamic behaviour of the system. The key to the successful operation of such systems is to consider the interaction between the machine and the material. Typical examples of such machines are to be found in steel strip lines; manufacture and use of magnetic tapes; plastic, rubber and textile industries; paper making, printing presses and packaging processes.

In the foregoing systems, the material being processed is normally running under a certain value of tension. This is obtained usually by traction and braking forces acting on the material, which is in a web form, throughout its run in the system. At this stage it is worth mentioning that throughout this investigation the term "web" includes other terms that are used in other scientific or technological fields such as foil, film or thin strip of material.

Generally it is necessary to maintain the tension in the web within

the specified limits to avoid variations in the quality of the final product. In extreme cases, where the web may become slack due to very low tension or a web break may occur due to excessive peak tension, considerable disruption of the manufacturing process may follow until the fault is rectified.

It is a general rule that if you aim to control the variations in any system you must first be able to measure them. At slow speeds there is not much of a problem and there is a wide choice of adequate tension measurement and control equipment available commercially. It is at high speeds, and particularly under transient conditions, that tension fluctuations might coincide with resonant frequencies of the material/machine system resulting in unexpected web breaks.

At this stage it is advisable to give a very brief account of different methods of tension measurement. Functionally, there are two main categories of tension measuring devices; namely "Full width" or total tension sensors and "Unit tensiometers". The first category, which is also more widely used, measures the total force applied to the web. Such sensors are normally not sensitive to the distribution of tension across the web. The second category attempts to measure the web tension at specific locations or bands across the web and total or average tension can be obtained either by fitting a multiplicity of sensing heads or traversing a single tensiometer.

Technically, the earliest methods used to detect variations in web tension were mechanical. The web of material passed round a cylinder, commonly known as a dancing or floating roller, supported in bearings

mounted on a pivoted lever. The force on the lever, due to the web tension, was balanced by tension in a spring or by dead weights as shown in Fig. 1.1 and 1.2 respectively. An alternative method of regulating the desired web tension, apart from the obvious method of altering the spring tension or mass of the dead weight, is to alter the point of application of the balancing force as shown in Fig. 1.3.

An example of a recent commercial development in this respect is the "Martin Tension Control" from U.S.A. which claims to provide constant tension by the use of an "inertia compensated dancer". A general description of the technique and a theory of its operation is provided later in this thesis.

In such systems, which were described in a very simplified way, there is usually a direct linkage between the sensing roller and the web tension control device. The inertia of the sensor and the fact that the distance moved by the dancing roller, corresponding to a given change in web tension, is relatively large result in a poor speed of response of the system.

Another example of a commercially available device which operates on a mechanical basis but differs from the dancing roller technique is the "Huyck Tensometer". Its operation is based on the principle that the deflection of a flexible membrane under load is dependent upon the tensile stress in the membrane. The load is provided by an internal spring, and the web deflection is measured by a dial indicator. It is a portable, hand-held device. An analysis of its performance is given later.

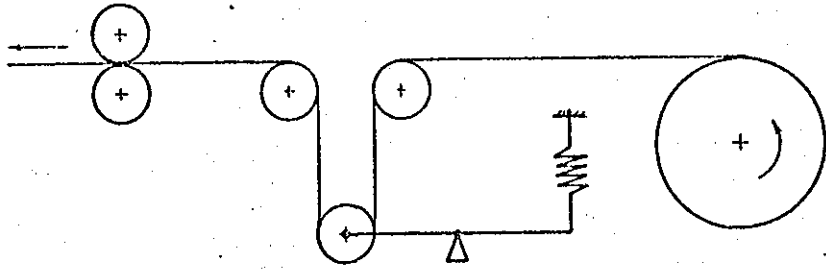


Fig. 1.1

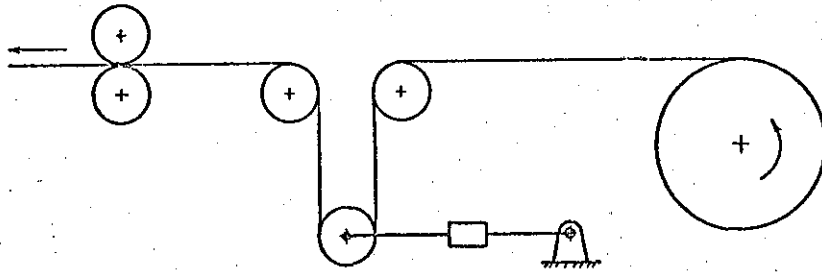


Fig. 1.2

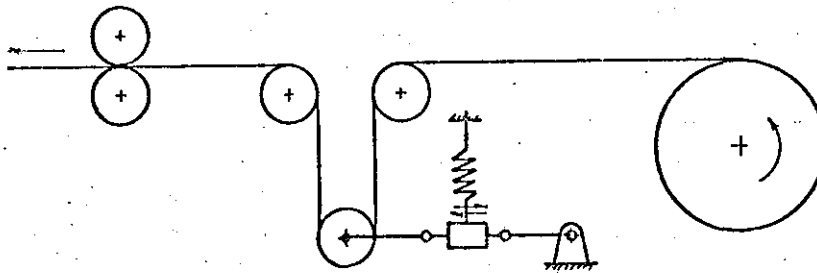
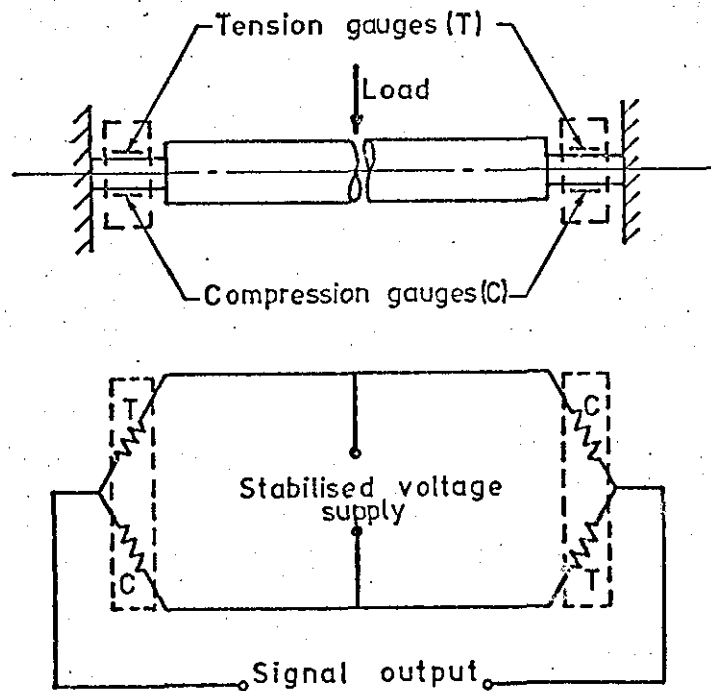
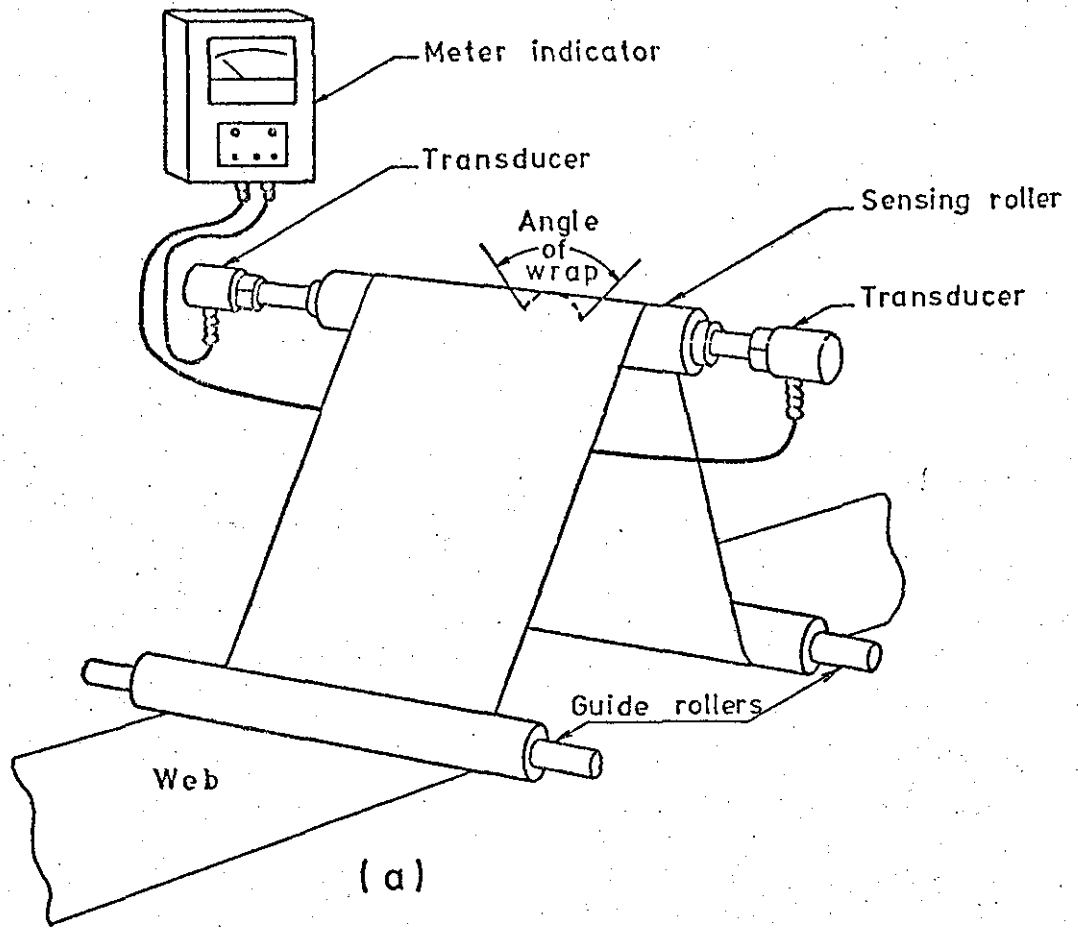


Fig. 1.3

Principles of dancing roller technique.

To provide an improved performance at higher frequencies of web tension perturbation, to overcome the previously mentioned drawbacks of the mechanical system, electric and pneumatic measuring techniques have been developed. In the former case; as the moving web passes over a stationary cylinder or a rotating roller, strain gauges can be fitted on top and underneath the non-rotating shaft at each end so that two gauges are in tension and two in compression(Fig. 1.4a.) If these are connected to form a Wheatstone bridge network as in Fig. 1.4b then a sensitive system of load measurement is provided. The output signal of such a system is largely independent of the effects of temperature change or normal electrical supply variations. The same improved performance could be achieved by using load-cells based on transducer elements to sense the change in the horizontal component of the force on the roller. If, for example, the course taken by the web is altered by passing it over a roller, in such a way that the angle formed with the horizontal on reaching the roller is not equal to that resulting after passing over it, then a horizontal force results which is proportional to the tension in the web. Vertical forces, such as the weight of the roller and the vertical component of the web tension, do not give rise to any output from the load cell. This could be achieved by the use of magneto-elastic elements, as in the case of Arencos load-cells, which are based on the fact that the permeability of certain ferromagnetic substances diminishes in the direction parallel to an applied compressive load, and increases in a direction perpendicular to that load. The load-cells are placed directly at the point of measurement and are mounted between the bearing bracket and the base plate on the machine frame.



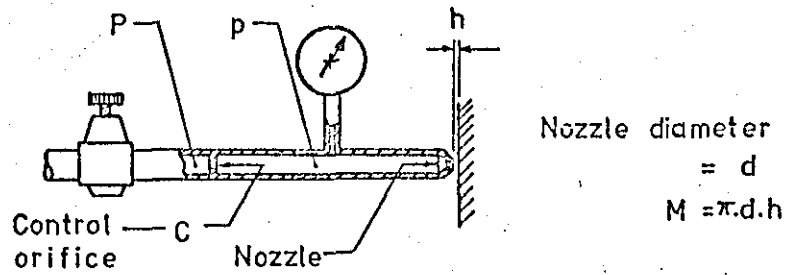
(b)  
Fig. 1.4 Strain gauges technique.

An alternative to an electric transducer is a pneumatic force-balance system which is known to have reasonable time constant. In this case the force on the end of the roller is balanced by the opposing force of a diaphragm, the pressure in which is determined by a pneumatic gauging system. The principle of such technique is shown in Fig. 1.5.

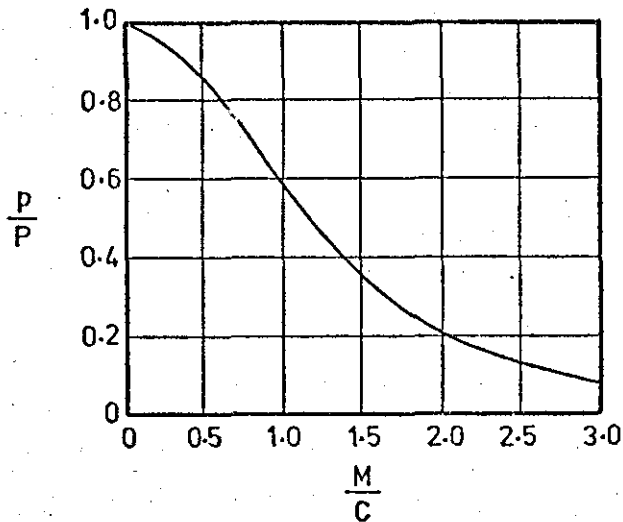
Using the electrical or the pneumatic measuring system helps a great deal in overcoming the disadvantages associated with the dancing roller technique. Both of these techniques provide a higher speed of response than the dancing roller due to the higher stiffness of the moving parts. Nevertheless, they have an inherent disadvantage when fitted into a system where the machine frame is vibrating, which is almost inevitable in practice. The weight of the roller is generally such that the vibration of the transducer mountings will give an erroneous dynamic reading. The final output will include disturbance to the signal output from the roller itself and from mechanical vibration. Filters may be used to stop these unwanted signals but only at the expense of limitations in the dynamic response of the sensing device.

As air bearings are becoming better understood, more and more uses are being found for them. Industries, such as those processing paper or plastic films, employing machines which must support, transport and guide long, wide thin webs of material may have friction and control problems. In order to reduce or eliminate these problems, air is sometimes used as a lubricant between the supports, which are normally rollers, and the web of material. Since one surface of the resultant bearing is quite flexible, the combination is called a foil bearing.

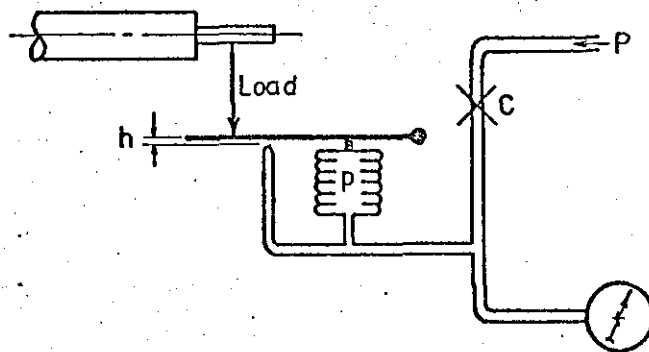




a-Pneumatic gauging system.



b-Pneumatic gauge characteristic curve.



c-Pneumatic force-balance system.

Fig. 1.5

Air is supplied by jets through small holes drilled in a stationary supporting cylinder. With this arrangement the air gap between the web and the cylinder is not constant, being greater in the vicinity of the supply orifices. Since the rate of air flow is dependent on the air gap thickness ( $Q \propto h^3$ ), the rate of air flow will increase considerably. To obviate this it was logical to aim for a much larger number of supply orifices of small diameter, arranged close together on the surface of the cylinder. This led to the development of the externally pressurized air bearings which employ a porous material as one of the bearing surfaces.

The next step is to utilize the externally pressurized air bearings to measure the tension fluctuations in a web of material. On recalling the previously described pneumatic force-balance system, it can be seen that the resistance of the sintered wall of the cylinder acts in a similar way to the fixed orifice "C" in Fig. 1.5 and the air gap between the web and the outer surface of the cylinder acts as the variable escape-ment  $h$ . Increased tension in the web will tend to reduce the air gap resulting in lessening the air flow and hence reducing the pressure drop across the sintered wall. With a fixed supply pressure this means that a higher pressure is available in the gap to balance the tension forces automatically. It will be shown later that there is a direct relation between the pressure in the gap, the outer radius of the bearing cylinder, and the tension in the web.

Vibration of the supports of the foil bearing in this case will have little effect on the apparent tension output readings due to the fact that the effective weight of the active part of the system is merely that of the

air film in the gap in addition to that of the web. Both are very small and can be practically neglected. Since the very small pores in the wall of the sintered cylinder are acting as the "Control orifices", the volume of air between them and the escapement gap is minimum. This leads to a high speed of response as long as this volume is not appreciably increased by the introduction of a pressure gauging device.

For this reason an electro-pneumatic pressure transducer is embedded in the cylinder wall. An electrical signal is provided which is proportional to the air gap pressure and therefore directly proportional to the web tension. In this way the shortcomings of either the load-cells or the pneumatic force-balance system are obviated.

It is hoped that the present study will provide a deeper insight into the problems and the limitations associated with the equipment for the measurement of web tension. The objectives of this investigation are to determine, by direct experiment and analytically, the limitations in static accuracy and dynamic performance for such equipment. Another objective is to investigate the effect on measurement, due to distortion of the web, caused by the use of portable devices which are narrower than the full width of the web.

Tension measuring techniques under investigation include direct mechanical displacement devices and pneumatic foil bearings using electrical pressure transducers. A prototype electro-pneumatic device has been developed, to measure the static as well as the dynamic tension applied to the web, using the principle of externally pressurized porous foil bearings.

1.2 REVIEW OF WEB TENSION MEASUREMENT LITERATURE

One of the early publications concerning the commercially available methods of measuring web tension appeared in the "Proceedings of the PATRA newspaper and rotary Letterpress Conference", October 1957. In his paper, Haglov<sup>1</sup>, referred to the first substantial contribution by research workers such as R.E. Gibson<sup>2</sup> and B. Steenberg<sup>3</sup> to the field of stressing the web by tension, or studying the stress in the paper material going through the machine and what this means. He went on to state the required conditions in regard to web tension regulators. The ideal web tension regulator device for a printing press, Haglov stated, is such that it maintains a very accurate web tension within few percent, independent of production speed, reel diameter, reel width, and rate of speed change of the printing press.

On the commercial side, many firms have since made their contribution to this field in their own ways by introducing devices for monitoring and controlling the web tension.

The Mount Hope Machinery Co. of USA<sup>4</sup> introduced their tension indicator for monitoring tension in moving webs. In operation, the dial indicator gives a linear response to changes in air pressure which reflect changes in web tension, the manufacturer claimed. The device has a special feature which allows either "instantaneous" response or an "averaging" response for webs subject to rapid changes or fluctuations in tension.

Another contribution was made by the John Dusenbery Co. Inc., Clifton, N.J. of the USA<sup>5</sup>. In the system they have introduced, web tension is read by a sensing idler which transmits the tension load signal to a

pair of strain gauge transducers located at each end of the idler shaft. The load cell transmits a signal, directly proportional to the tension, to an amplifier. The signal is compared to a signal from the operator's tension potentiometer, and the difference between them is used to activate the control system.

A similar technique was developed by Arenco Electronics AB of Sweden<sup>6</sup>. The system consisted of load cells based on patented magneto-elastic transducer elements. The load cells give an electric output signal which is linear and proportional to the horizontal component of the force in the web. Existing vertical forces such as the weight of the roller do not give rise to any output from the load cell.

The ATF Tensicon is the third contribution in this field made by an American firm, namely American Type Founders Company Inc., Tennessee, USA<sup>7</sup>. A frictionless air cylinder acting as a floating web-tension roller establishes the proper tension. The maker claimed that any change in "web displacement" is sensed and web speed is adjusted to compensate for it. The unit is completely mechanical and operates at all press speeds, regardless of stops, start-ups or speed changes, it is claimed.

In their paper, Endersby and Zucker<sup>8</sup> described a system for tension measurement and control for large winders and rewinders used in newsprint presses. The three major components of this system are: a strain gauge tension pick-up, the electro-pneumatic controller and disc brakes. A true average tension across the web is obtained, so it is claimed.

A quick look at these articles shows that none of them had considered any kind of analytical study of the systems described.

Turning now to the academic side of the matter, George and Kimball<sup>9</sup> gave a comprehensive treatment of the uses and differences between the two basic types of web tension measuring equipment, namely the unit tensiometers and the full width or average tensiometers. In a following publication, George and Kimball together with Oppenheimer<sup>10</sup> made an attempt to study the dynamics of a full width tensiometer system in order to be able to evaluate properly the web tension measurements. This paper has presented an analytical method for the determination of the frequency response for the mechanical tension sensing roll arrangement of a typical tensiometer system. A mass-spring system with single degree of freedom, as an equivalent to the mechanical sensing arrangement of a tensiometer system, was analysed. Experimental methods and results obtained for the evaluation of the frequency response of both the mechanical arrangement and amplifier-recorder system for a particular tensiometer system used in web tension research on rotogravure presses were then given.

Later on, Oppenheimer and Harvey<sup>11</sup> attempted to formulate a mathematical model of the gravure press system that is representative of how the real press system responds to disturbances. One of the primary objectives towards their goal was the determination of the relationship between web tension and longitudinal register. They then published another paper<sup>12</sup> in which they presented their model in a programmed form, first into an analogue and then into a digital computer. Simulation of dynamic disturbances and their effects had proven to be a valuable tool in the evaluation of actual press recordings and for prediction of press control

behaviour, the author claimed. The model is described and some typical simulations of dynamic tension and register shifts are shown.

At the INCA Convention in April 1969 a brief progress report was given on the work being carried out to develop a mathematical model of a newspaper press (published in the June 1969 issue of Newspaper Techniques). Emphasis was placed on the study of web tension behaviour between the printing nip and the pipe roller preceding that nip. Later in an interim report, D. King<sup>13</sup> illustrated the more elementary mathematics of the study of the pipe roller-web-nip combination. The mathematics were described as elementary, because only elementary differential calculus methods were used. The equations were solved both analytically and by programming an analogue computer. In his paper, King presented a typical set of results.

In a following paper<sup>14</sup>, King gave a brief review of the main categories of machine-direction tension measuring devices. He then referred to a research project at IFRA on a unit tensiometer based on pneumatic detection of an air film developed between a hollow porous bar and the paper web. The published work did not include any kind of experimental results or any analysis of the device performance. A more comprehensive report was presented by King in his paper entitled "Web tension study at Persc-ombinatic NV"<sup>15</sup>. The functions of the study were to examine further the tension behaviour in the relatively unknown region between the printing unit and folder in high-speed letterpress machines and to observe machine-direction tensions at different locations across the width of the machine using the new web tension profilemeter.

A short review of web tension control of high-speed letterpress and off-set presses was given, once more, by King<sup>16</sup> in December 1972. The paper

went on to describe a number of projects conducted by the INCA-FIEJ Research Association in the past four years. Further experimental work concerned with the influence of paper speed, tension, basis weight, etc. on web breaks, was discussed and relationships to specific strength properties of newsprint were considered.

In his paper, Grünewald<sup>17</sup> distinguished between two ways of measuring web tension on web-offset presses; viz, the partial measurement in which the force on the web at one location is measured and integral measurement, in which the mean force over the entire width of the web is determined. The relative merits of each method were summarised in a table and various methods of measuring average tension were listed. He also analysed the factors influencing web tension in five sections on an offset press.

In the same direction, studies and assessment carried out by Web Press Engineering Inc. USA, on the methods of web tension control used up to 1970 were presented by Curran<sup>18</sup>. A control unit was then produced using a Kidder tension sensor which works on the strain gauge principle. Another article followed a similar line, taking the form of a discussion between B. Blunden, head of industrial communications at PIRA, L.E. Boxall, and R.C. Jenner<sup>19</sup>. Points covered included factors affecting tension, traction, differences between tension control in web offset and in letterpress, and measurement and control of tension.

One of the latest developments in the techniques using the dancing roller as a sensing element was introduced by Martin<sup>20</sup> in 1973. In his paper, the president of the US firm of Martin Automatic analysed tension and



stretch requirements for good register in web-offset printing. He described the firm's "inertia compensated" dancer roller and associated equipment offering the printer freedom from his great dependence on "paper variation", so it was claimed.

As the battle against web breaks continues to be a focal point of the research carried out in this field, efforts of all research workers towards reducing web breaks are, as Davidson<sup>21</sup> put it, being directed in the main at the paper itself and the web tension relationships it entails.

In a paper about the technical requirements for improved newspaper production, Graneek<sup>22</sup> pointed out that high frequencies of tension variation, up to 50 Hz, may occur between reelstand and printing unit and could be an unexpected cause of web breaks. He then made reference to recently developed externally-pressurised foil bearings to act as a web tension measuring device providing a higher speed of response.

It can be seen that all the work so far seems to refer to methods of measurement, but there is almost no one who had analysed the static and dynamic capabilities of web tension measuring equipment. Even the few who did, had not considered in depth analytical or experimental results pertaining to dynamic operation of the measuring devices. In view of this fact, the author has been influenced by the necessity of making this available. Hence, it is this gap that the present investigation is aiming to fill; for the essence of measurement is not only to obtain results but to determine analytically and by direct experiment the limitation of measuring devices and to investigate possible ways of improving their accuracy and dynamic response.

### 1.3 REVIEW OF FOIL BEARINGS LITERATURE

Due to the fact that very little work was found to be published on web tension measuring techniques, this review may seem to be diverted from the main objective of the recent project. However, the author preferred to give the literature review in this form for the benefit of any other research workers who may be interested in this field. The author hopes that such a humble effort may elucidate the various parameters associated with the problem.

Air has been used as the lubricant in fluid film bearings for over 70 years, but most significant applications have occurred in the last fifteen. Recent industrial applications in instruments and machines demonstrate that gas-lubricated bearings are now accepted as precise devices with good reliability.

A bearing with at least one wall made of a thin flexible material is known as a foil bearing. In the most general sense, a foil bearing is used whenever a moving foil or thin sheet (commonly called a "web" in the paper industry) has to be supported and/or guided. The instances in which moving webs have to be supported are many, e.g. in the fabrication and handling of plastics, paper, sheet metal and flexible recording media in a variety of magnetic and light-sensitive recording and information storage-devices.

In all the examples cited, a film of air can be provided to support the moving web with the advantage of reducing dramatically the friction between the web and the supporting guide. The air film is established by either of two basic actions. The speed of the moving web relative

to the bearing surface generates a film pressure within the gap between the web and the supporting bearing and ensures separation between them as well as maintaining enough force to balance the initial tension in the web. This type of bearing is called the self-acting air bearing.

With the second basic type, air is supplied under pressure to the gap between the two mating surfaces of the bearing, i.e. the web and the supporting roller. As a result, the two are forced apart and the tension in the web is balanced by the air film pressure. Such a bearing is called an externally pressurised bearing.

The full history of gas lubrication is covered in several books<sup>23, 24</sup>, intended for the specialists. A comprehensive bibliography of publications in the field of air bearings from 1828 to 1959 has been given in the "First international symposium on gas-lubricated bearings"<sup>25</sup>. As for the foil bearings, a brief review of specific contribution made in this area could be beneficial.

Langlois<sup>26</sup> has developed a method for determining, to the first order, the deflection from a straight path of perfectly flexible tape of finite width, transported over the apex of a parabolic cylinder of infinite extent. He recognised the difficulty associated with specifying boundary conditions and the arbitrariness in the assumed extent of lubrication regions in the entrance and exit zones, in which Reynold's equation applied.

The differential equations applicable to the air film thickness beneath an infinitely wide, perfectly flexible foil bearing was furnished by

Eshel and Elrod<sup>27</sup>. The paper contained numerical solutions for the film thickness in both the entrance and exit regions. These solutions have general applicability to situations where the entrance and exit regions are separated by a third region of uniform thickness. In particular, the undulation of the foil in the exit region were discussed in detail.

Another contribution in the field of foil bearings was made by Licht<sup>28</sup>. The major part of his experimental study dealt with elastic foil bearings of finite width and the characteristic "edge effect" in particular. An elastic foil under tension was wrapped partly around a rotating cylinder and was supported on a thin film of air. Capacitance probes, coincident with the surface of the cylinder, were made to scan the air gap along the arc of wrap. Experimental results were then compared quantitatively with theoretical predictions for the perfectly flexible and for the elastic foil bearing of infinite width made by other investigators.

Eshel and Wildmann<sup>29</sup> wrote the first paper concerning dynamic behaviour in which they derived and simplified general equations for the oscillation of a foil over a lubricating fluid film. A few particular cases were discussed, and a linearised solution was obtained for the case of a massless, perfectly flexible foil moving at a speed  $U$  over an incompressible film. The solution revealed the interesting phenomenon that small disturbances in the film thickness, as well as symmetrical large disturbances, propagate at a speed  $U/2$ .

As it is difficult to analyse initial disturbances experimentally,

Barnum and Elrod<sup>30</sup> carried out a theoretical study on the dynamic behaviour of foil bearings. The differential equations and boundary conditions for the problem of a foil bearing subjected to small variations in tape tension were developed. The numerical results showed that the fluctuations of the foil tension are a function of the frequency of the disturbances and the compressibility of the lubricating fluid.

Externally pressurised foil bearings were first analysed by Barlow<sup>31</sup>, who in his report investigated an externally pressurised axisymmetrical foil bearing in order to obtain the qualitative effect of side leakage in a foil bearing. One or two circumferential pressure sources, symmetrically placed under the foil centre line, were used. In his analysis, Barlow came to the conclusion that the bending stiffness of the foil cannot be neglected. Curves which showed the effects of the various physical parameters on the gap profile were given.

Wildmann and Wright<sup>32</sup>, through their analysis, gave an overall understanding of the behaviour of foil bearings. The effects of introducing a small amount of lubricant under pressure into a self-acting foil bearing film were investigated. Foil shape and pressure distribution under the foil were obtained by combining the equilibrium equation with the Reynold's equation and solving the resulting equation. The authors showed that such a small external pressurisation has an effect of considerable importance.

Once again Barlow<sup>33</sup> put his effort to analyse an externally pressurised, axisymmetrical, foil gas bearing with the foil being treated as a thin

plate bent into a cylindrical shape. The foil had been wrapped completely around a cylindrical support, with axisymmetrical line pressure sources providing the air flow. This configuration was used by Barlow in order to eliminate the circumferential flow effects by using axial symmetry. An interesting point to notice is that when the wrap angle is large, the problem being studied could provide a good approximation except near the ends of the wrap. The solution of this problem is of value for externally pressurised foil bearings having regions where most of the flow is axial.

In the investigations on the externally pressurised, infinitely wide foil bearing it was shown that the entrance zone always behaves essentially as a self-acting bearing. In other words, the gap in the entrance region is always very small, and contact can occur in that area. To overcome this it is usually convenient to move the supply groove as close as possible to the entrance tangency points. This, of course, requires exact knowledge of the point of tangency and also results in high lubricant flow rates. One way of avoiding this hurdle is to use a porous bearing, the impedance of which will reduce the rate of air flow and because the supply is distributed over the entire bearing area, exact knowledge of the tangency point is not needed.

Because of these advantages, investigations of the porous foil bearing were undertaken by Barlow and Wildmann<sup>34</sup>. The equations for the axisymmetric, perfectly flexible foil bearing were solved for the case of an externally pressurised foil with porous inlet restriction. The results presented in graphical form for design use are useful whenever the principal flow of a porous bearing is axial. This is the case

whenever the width of the foil is small compared to its length. For comparison, results for the axisymmetric, perfectly flexible foil bearing with discrete inlet restrictors were also given.

An elegant study to analyse the porous cylindrical gas foil bearing was furnished by Baumann<sup>35</sup>. The analysis was concerned with the performance of such bearings at low pressures. It also aimed at providing an engineering design method based on the variable parameters of the bearing and the fixed parameters of the application. The theoretical analysis was divided into three parts: an analysis of flow in the porous medium, a study of the flow in the channel between the bearing cylinder and foil, and an analysis of the elastic strain in the foil.

Baumann followed his theoretical analysis, in the same paper, by an experimental study, in which a foil was supported on an air bearing at different supply pressures. The edge separation, between the foil and the bearing cylinder, was measured by microscopy techniques and compared to the prediction obtained from the computer analysis. They agreed almost perfectly, taking into consideration the experimental errors.

This review would be incomplete, and may seem to be irrelevant, without the mention of the work done by another two research workers. The first one is Deason<sup>36</sup> who studied experimentally, utilising the concept of external pressurisation of a foil bearing, an air-blown sintered metal turner bar used as an aid to web transport in printing and packaging industries. In his paper, the author described the construction, advantages, and limitations of such a turner bar.

The second research worker whose paper is indeed complementary to this

review is A.J. Munday<sup>37</sup>. Following a brief scanning to the development of gas bearing technology, the author referred to the "Shapemeter", an instrument which is based on the fact that all externally-pressurised gas bearings have a film of predictable stiffness which can be used as a calibrated spring. A bearing can therefore be the basis of a force-measuring device. The device he described consisted of a number of plain cylinders which are free to rotate separately on a fixed, externally pressurised shaft. Small pressure tappings, leading to pressure transducers, were made under the cylindrical sections of the roller. As the web passes over these plain cylinders, the transducer under each one of them measures the force on it; the result indicates the tension across the web.

Again, one has to say that almost all of the work so far did not consider in any depth, analytical or experimental results pertaining to dynamic operation of such measuring devices which is the main objective of this study.



## CHAPTER II

### ANALYTICAL FORMULATION RELEVANT TO THE STUDY

## 2.1 MINIMUM VOLUME OF PNEUMATIC CIRCUIT

When a pneumatic gauging technique is used in continuous measurement of a periodic input of variable amplitude and frequency, the dynamic response characteristics of the system have an important effect on its performance. The basic principles of pneumatic technique have been fully described by many authors<sup>38, 39, 40, 41</sup>. The main factors that affect the dynamic behaviour of the system are:

- (1) the constant operating pressure delivered to the system,
- (2) the restriction to flow imposed by the control orifice and measuring nozzle which will govern the static sensitivity of the system, and,
- (3) the volume of the pneumatic network, i.e. the connecting pipe between the orifice and the nozzle and the volume associated with the device to measure the pressure.

It has been established<sup>42</sup> that a better response could be obtained at lower operating pressure, higher rate of flow and smaller circuit volume. These conclusions could be easily explained. The lower the operating pressure the more closely does the behaviour of the air correspond to that of an incompressible fluid. Hence if friction, viscosity and inertia effects are neglected, there would be only a small attenuation of amplitude with increasing frequency. When the areas of the control orifice and measuring nozzle are small the rate of mass flow for any given pressure drop is small and appreciable time is required for a change of mass within the volume, corresponding to a change of pressure, to be established. So, when seeking high sensitivity, one must expect slow response.

As for the volume of the pneumatic network, the smaller the volume contained between the orifice and the nozzle the smaller is the mass of air which must be introduced into or expelled from this volume in order that a change of pressure may be established. Therefore a reduction in volume improves response.

Fig. 2.1 represents the principle of the electro-pneumatic system adopted to measure the variation in the tension applied to the web.

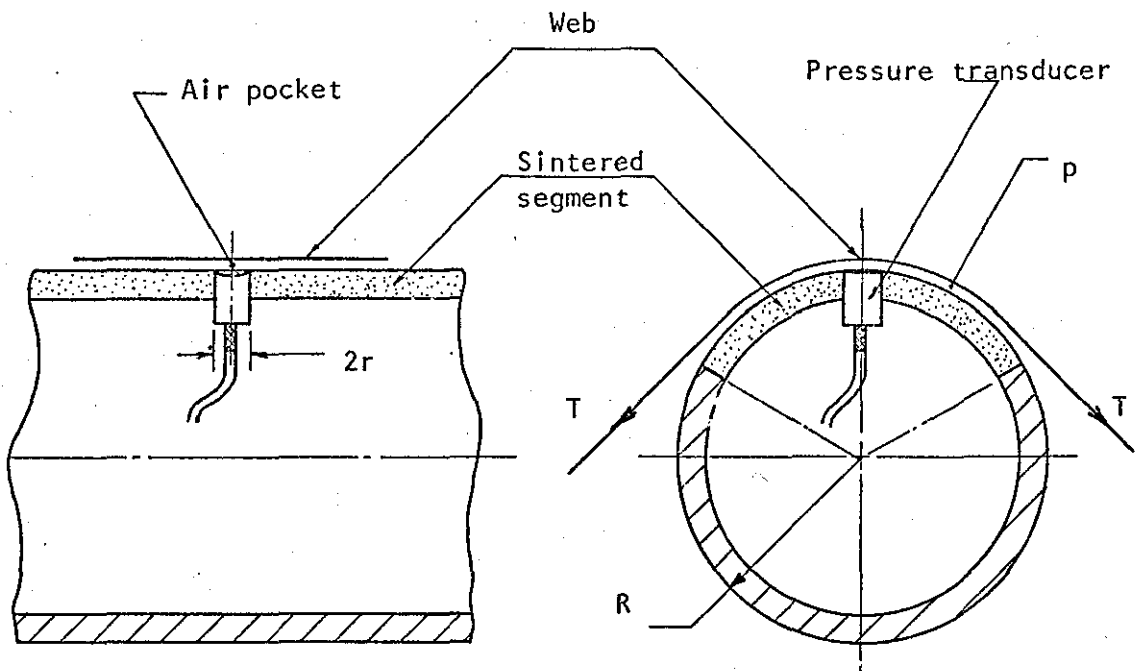


Fig. 2.1 Principle of electro-pneumatic web-tension measuring system

Air is supplied, under constant pressure  $P$ , to the cylinder. It will then flow out through the fine pores of the sintered segment of the

cylinder creating an air gap underneath the web. As the web tension varies, the pressure ( $p$ ) in the gap will vary accordingly. It has been established<sup>35, 36</sup> that there is a linear relationship between the pressure in the gap and the web tension. A pressure transducer is fitted into a hole in the sintered segment to measure the variation of pressure in the air gap.

By this arrangement the first two factors, of the three previously mentioned, affecting the frequency response of the system had been determined. In other words the constant low operating pressure delivered to the system was controlled through adequate pressure regulators while the pore size and the permeability of the sintered material controlled the rate of air flow.

This left the third factor, namely the volume of the air in the pneumatic network. The pressure transducer, being fitted directly in the cylinder wall, has virtually eliminated the volume contained between the control orifice and the measuring nozzle that existed in the conventional pneumatic system. Still there is the volume of air pocket resulting from the intersection of the sintered cylindrical segment and the pressure transducer which is also of cylindrical configuration. In this section the volume of such air pocket is determined.

Fig. 2.2 shows the geometry of the resulting minimum pocket with the following parameters:

- R outer radius of the cylindrical sintered segment
- r radius of the pressure transducer = radius of intersection circle (between sintered segment and transducer)

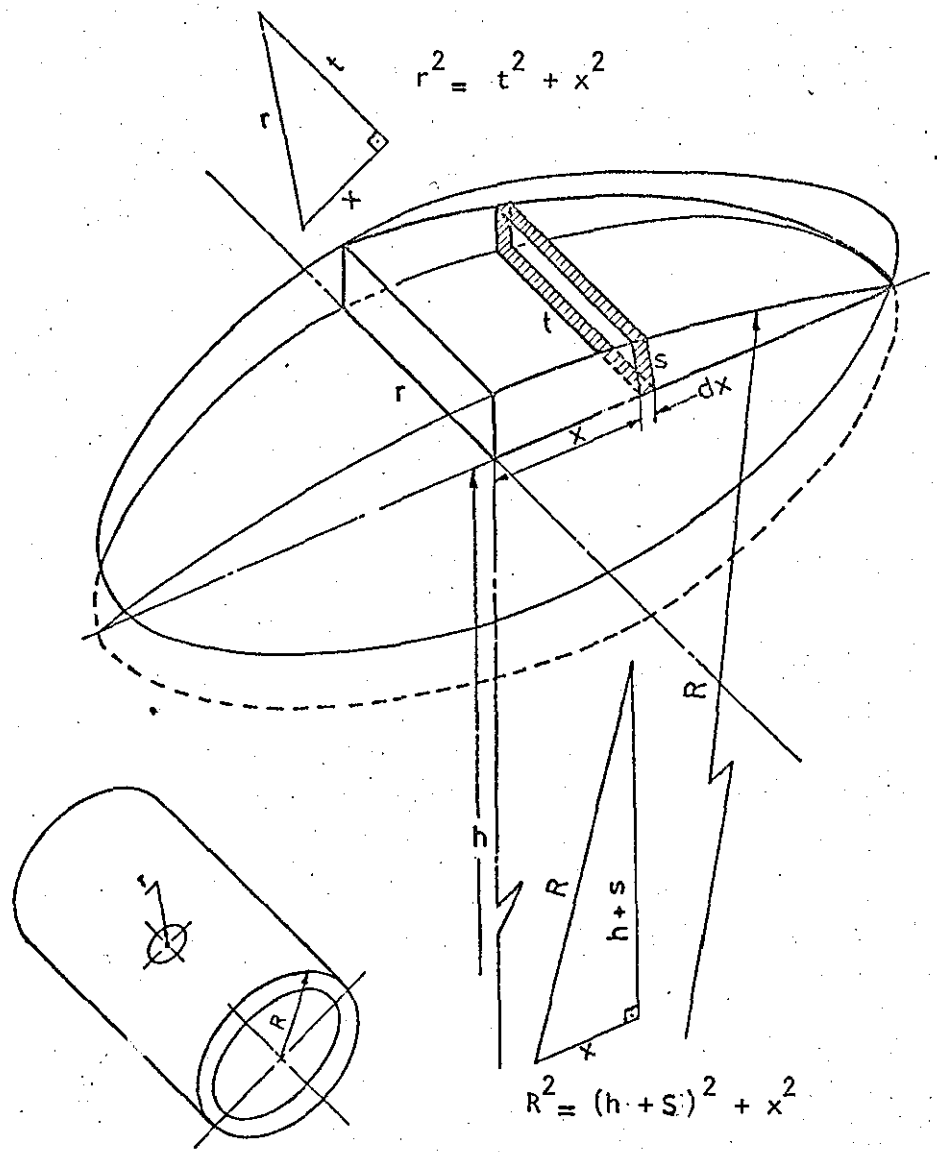


Fig. 2.2 The geometry of the "air pocket"

h distance between the centre line of the cylinder and the plane containing the intersection circle

t length of the element of volume chosen

s height of the element of volume

dx width of the element of volume

v 1/4 the resulting volume

V total resulting volume = 4v

Referring to Fig. 2.2 it can be seen that one can work on one quarter of the resulting volume. Due to symmetry the total resulting volume is four fold of the calculated one.

$$v = \int t \cdot s \cdot dx \quad (1)$$

$$\text{But we have } t = \sqrt{r^2 - x^2} \quad (2)$$

$$\text{and } h + s = \sqrt{R^2 - x^2}$$

$$\text{since } h = \sqrt{R^2 - r^2}$$

$$\text{hence } s = \sqrt{R^2 - x^2} - \sqrt{R^2 - r^2} \quad (3)$$

Substituting in (1) for t and s from (2) and (3) respectively we get

$$\begin{aligned} v &= \int_0^r \sqrt{r^2 - x^2} \cdot \left[ \sqrt{R^2 - x^2} - \sqrt{R^2 - r^2} \right] dx \\ &= \int_0^r \sqrt{r^2 - x^2} \cdot \sqrt{R^2 - x^2} \cdot dx - \sqrt{R^2 - r^2} \int_0^r \sqrt{r^2 - x^2} \cdot dx \\ &= \left[ \frac{x}{2} \sqrt{r^2 - x^2} + \frac{r^2}{2} \sin^{-1} \left( \frac{x}{r} \right) \right]_0^r \end{aligned}$$

$$\therefore v = 1 - \frac{\pi r^2}{4} \cdot \sqrt{R^2 - r^2} \quad (4)$$

$$\text{where } l = \int_0^r \sqrt{r^2 - x^2} \cdot \sqrt{R^2 - x^2} \cdot dx \quad (5)$$

Solving equation (5), hence substituting for  $l$  in (4) and multiplying the result by 4 we get:

$$V = \pi r^2 R \left\{ 1 - \frac{1}{8} \left(\frac{r}{R}\right)^2 - \frac{1}{64} \left(\frac{r}{R}\right)^4 - \frac{5}{1024} \left(\frac{r}{R}\right)^6 - \dots \right\} - \pi r^2 \sqrt{R^2 - r^2} \quad (6)$$

(See Appendix J. for detailed derivation)

$$\therefore V = \frac{3\pi}{8} \cdot \frac{r^4}{R} \left\{ 1 + \frac{7}{24} \left(\frac{r}{R}\right)^2 + \frac{59}{384} \left(\frac{r}{R}\right)^4 + \dots \right\} \quad (7)$$

It can be seen that as  $\frac{r}{R}$  gets smaller one can neglect the terms involving  $\left(\frac{r}{R}\right)^2$  and higher orders without losing significant accuracy.

For  $R = 25.4\text{mm}$  (1in) and pressure transducer of  $3.175\text{mm}$  ( $\frac{1}{8}\text{in}$ ) diameter the resulting volume is

$$V_1 = 0.29 \quad \text{mm}^3$$

Using the same transducer fitted into a sleeve of  $2.5\text{mm}$  radius which is embedded into the wall of a sintered segment of radius  $R = 258\text{mm}$ , the resulting minimum volume is

$$V_2 = 0.18 \quad \text{mm}^3$$

Turning now again to equation (7), even after neglecting the

terms involving  $(\frac{r}{R})^2$  and higher orders, one would not find it easy to give a physical meaning for

$$V = \frac{3\pi}{8} \cdot \frac{r^4}{R} \quad (8)$$

A successful attempt was made to get an expression for the volume required with an appreciable physical meaning.

Let us consider the same configuration in Fig. 2.2 but from a slightly different view as shown in Fig. 2.3.

Top of transducer (produced) in a plane just touching the highest point of the sintered segment.

Circle of intersection between transducer and sintered segment.

Pressure transducer of radius  $r$ .

Sintered segment of radius  $R$ .

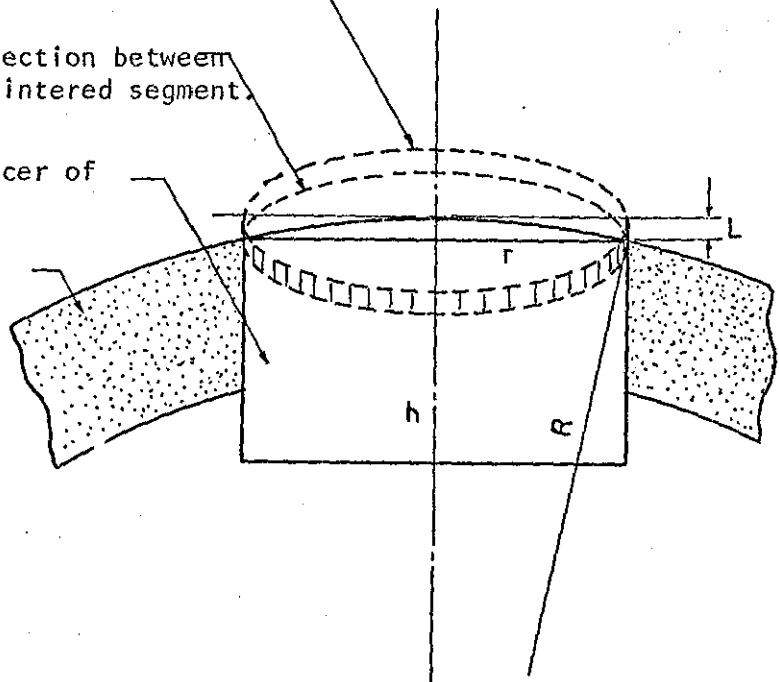


Fig. 2.3 Air pocket configuration

Rearranging equation (8) gives

$$V = \frac{3}{4} (\pi r^2) \cdot \left(\frac{r^2}{2R}\right) \quad (9)$$

But we have  $r^2 = (R-h) \cdot [2R - (R-h)] = 2R(R-h) - (R-h)^2$



For  $R-h \ll 2R$ , which will result only if  $R$  is much larger than  $r$ , we can say

$$r^2 = 2R (R-h)$$

$$\therefore \frac{r^2}{2R} = (R-h) \quad (10)$$

Now let  $A$  be the area of the top face of the transducer and  $L$  be the height of a cylindrical slice whose base is the top surface of the transducer, intersecting the sintered segment, and its top is just touching the highest point of the sintered segment.

$$\therefore A = \pi r^2 \quad \text{and} \quad L = R-h \quad (11)$$

Substituting from (10) and (11) in (9) yields:

$$V = \frac{3}{4} (AL) \quad (12)$$

It can be seen that the expression in (12) is of an appreciable physical meaning compared to that in (8). However one must emphasise the fact that this expression applies only when the diameter of the transducer is much smaller than the diameter of the sintered segment, which is the case in this study.

## 2.2 ANALYSIS OF INERTIA-COMPENSATED TENSION CONTROL

### 2.2.1 INTRODUCTION

The Martin Control System is a recent commercial development for controlling the web tension in a printing press. It is claimed by the manufacturers that "it is the only system which completely isolates the press from tension upsets occurring up to and at the infeed to the printing unit". They went on to state that "the Inertia-Compensated Dancer, included into the system, absorbs tension upsets so that tension to the press remains unchanged". It will be shown in this section that while the first claim may be right theoretically, the second one does not apply.

At this stage it was thought that a brief description, as put by the manufacturers, of their system may help to follow the theoretical analysis given later. Fig. 2.4(a) shows a typical section of a press with a dancing roller prior to the printing unit. The dancer is heavy but free turning. If the tension prior to Q increases momentarily, the dancer being heavy will resist an upward movement and because it is free turning it will convert the tension increase into a change in speed of rotation in the clockwise direction. This will result in a tension increase past the dancer C.

In Fig. 2.4(b) the dancer is replaced by another one of the same weight, but the weight is distributed further out from the centre of the dancer to give it a large flywheel effect.



If the web is subjected to the same change in tension as in the first case, the dancer will tend to rise rather than to change its speed due to the flywheel effect. Eventually, this will result in a tension decrease past the dancer.

Using a dancer of the same weight as those in the former cases but with the weight "precisely" distributed to achieve equal resistance to change in position as well as speed of rotation proved to solve the problem of tension upsets, so the manufacturers claimed.

#### 2.2.2 THEORETICAL ANALYSIS

Referring to Fig. 2.5 the diagram represents a reel (0) feeding the printing unit in a press via a typical set of rollers. Q and G are guiding rollers, C is the Inertia-Compensated dancer and D and E are driving rollers, running at a constant angular velocity, imparting a constant linear velocity U to the web in the region of the nip just prior to the printing unit. The following nomenclature is used:

- T      tension in the web entering the printing unit
- $T_1$     tension in the web prior to the dancer C
- $T_0$     tension in the web past the dancer C
- I      mass moment of inertia of the dancer C about its axis
- r      radius of the guiding rollers Q and G
- R      radius of the dancer cylinder
- m      mass of the dancer C
- $\dot{\theta}$     angular velocity of the dancer C

- $\ddot{\theta}$  angular acceleration of the dancer C
- $x$  linear displacement of the dancer C in the vertical direction
- $\ddot{x}$  linear acceleration of the dancer C in the vertical direction
- $k$  radius of gyration of the dancer C with respect to its axis
- $g$  acceleration of gravity
- $A$  viscous friction coefficient
- $B$  static friction coefficient

The equation of motion of the dancer C is given by:

$$(T_0 - T_1)R = I\ddot{\theta} + A\dot{\theta} + B$$

Neglecting the viscous and static friction effect, the equation reduces to

$$T_0 - T_1 \approx \frac{I}{R} \ddot{\theta} \quad (1)$$

Assuming the web at P to be moving with the same constant velocity  $U$ , imparted by the driving rollers, the equation of motion of the dancer can be given as:

$$\ddot{x} = -R \ddot{\theta} \quad (2)$$

Substituting in (1) for  $\ddot{\theta}$  from (2) yields:

$$T_0 - T_1 = -\frac{I}{R^2} \ddot{x} \quad (3)$$

But we have

$$T_0 + T_1 - mg = m\ddot{x} \quad (4)$$

Combining (3) and (4) gives

$$2T_0 = mg + m\ddot{x} - \frac{I}{R^2} \ddot{x}$$

Since  $I = mk^2$  by definition if the mass of non-rotating parts of the dancer C is small compared to total mass  $m$

$$\therefore T_0 = \frac{mg}{2} + \frac{mx}{2} \left( 1 - \frac{k^2}{R^2} \right) \quad (5)$$

When  $k = R$ , equation (5) becomes

$$T_0 = \frac{mg}{2} = \text{Constant}$$

This means that the tension past the dancer is constant irrespective of any tension variations prior to the dancer as long as the mass of the dancer is distributed so that the radius of the dancer cylinder is equal to the radius of gyration of its rotating mass.

Let us now consider the probable causes of cyclic tension variations in a web-fed printing machine as an example. The normal maximum diameter for a reel of paper is 1.0 m and core diameter of about 0.1 m. If the web is driven at a speed of 10 m/s, the rotational speed of the reel will vary between 3.2 and 32 revolution per second. If the reel is running excentrically at this speed this represents a frequency of tension disturbances ranging from 3.2 to 32 Hz. This sort of tension variation and

similar perturbation resulting from drift in infeed drive devices, unwind brake variation, flying pasters and irregular-shaped rollers prior to the dancer could be compensated by the Inertia-Compensated tension control system of Martin Automatic Inc. of U.S.A.

Considering the section of the machine past the dancer C, specifically between roller G and the driving rollers D and E in Fig. 2.5, D. King<sup>13</sup> showed that the mathematical model of web tension in a material passing through this section is of the form

$$\left[ D^2 + \left( \frac{U}{L} + \frac{A}{I} \right) D + \frac{Kr^2}{IL} \right] T = \frac{K}{IL} (AU + Br + T_0 r^2)$$

The involved parameters of the equation have been estimated as follows for a newspaper printing press:

Web speed (possible maximum)	$U = 10$	m/s
Free web path length (between rollers G and E)	$L = 1$	m
Paper 'stiffness'	$K = 6 \times 10^5$	N
Radius of roller G	$r = 0.05$	m
Inertia of roller G	$I = 0.07$	kg.m <sup>2</sup>
Viscous friction coefficient	$A = 0.002$	N.m.S
Static friction	$B = 0.2$	N.m
Initial tension prior to G	$T_0 = 300$	N

A practical solution to the mathematical model equation is

$$T = T_A + T_B e^{-\alpha t} \sin(\omega t + \phi)$$

where  $\alpha = \frac{1}{2} \left( \frac{U}{L} + \frac{A}{I} \right)$  ,

$$\omega = \sqrt{\frac{Kr^2}{IL} - \frac{1}{4} \left( \frac{U}{L} + \frac{A}{I} \right)^2}$$

and  $T_A = \frac{1}{r^2} (AU + Br + T_O r^2)$

Using the given values it can be seen that  $\frac{A}{I} \ll \frac{U}{L}$  and

$$\frac{1}{4} \left( \frac{U}{L} + \frac{A}{I} \right)^2 \ll \frac{Kr^2}{IL} ; \text{ hence}$$

$$\alpha = \frac{1}{2} \frac{U}{L} = 5 \text{ s}^{-1}$$

$$\omega = \sqrt{\frac{Kr^2}{IL}} = 146 \text{ rad/s}$$

$$T_A = 312 \text{ N}$$

$$T = 312 + T_B e^{-5t} \sin (146t + \phi)$$

where  $T_B$  and  $\phi$  are independent variables.

This represents a damped oscillation of tension, following disturbance, with frequency  $(\omega/2\pi)$  equal to 23Hz and exponential time constant  $(1/\alpha)$  equal to 0.2 s. Thus one should expect to find a resonant frequency, of the material/machine system, of 23 Hz between the printing unit and the previous guide roller. This would result even if the "Inertia-Compensated" device maintains a constant tension as claimed.



Furthermore, the simple analysis of the "Inertia-Compensated" tension control, given before, ignored the effect of web elasticity. To consider this, the situation can be simply described in the manner of Fig. 2.6(a) which shows the "Inertia-Compensated" dancer with the two guiding rollers and the supporting web. Fig. 2.6(b) represents an analogy of the web elasticity (stretch) and the dancer inertia.

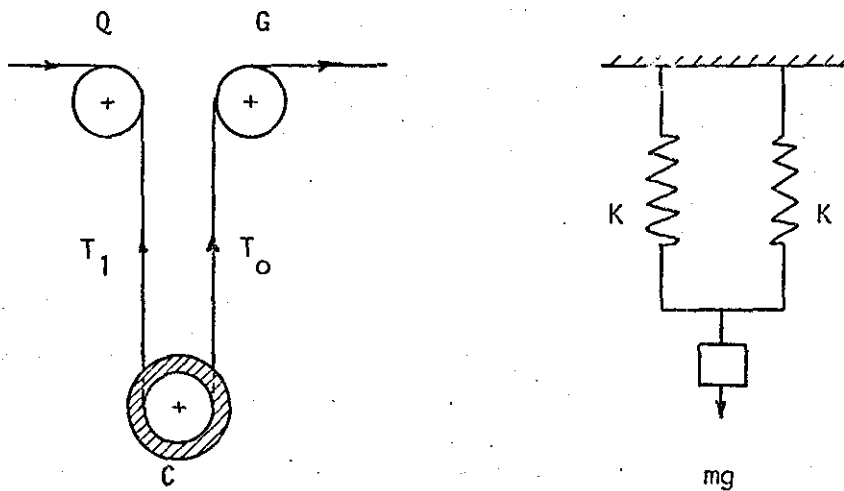


Fig. 2.6 Analogy of the web elasticity and the dancer inertia

The effective mass of the dancer, to maintain a "Constant" tension  $T_0$  of 300N, may be about 60 kg. The "stiffness" of the two supporting webs is  $2K = 12 \times 10^5$  N and the free length  $\ell$  of the paper "spring" could be about 1 m. In this case the resonant frequency of this mass-spring system is given by

$$f = \frac{1}{2\pi} \sqrt{\frac{K}{\ell m}} = 22.5 \text{ Hz}$$

which is dangerously close to the natural frequency of the material/machine system obtained from the mathematical model.

Thus, although the Martin System could compensate for the tension variation occurring prior to it in the material/machine system, the dynamic analysis showed that it can virtually do nothing for the inevitable tension perturbation occurring past it. A practical expedient is to use a tension measuring device, with appropriate frequency response, as close as possible to the printing unit to evaluate the tension variation. The tension control system can then, operating through a feed back system, compensate for this variation. The development of such measuring device is one of the aims of the recent investigation.

### 2.3 PRESSURE IN AIR-FILM SUPPORTING A WEB UNDER TENSION

The configuration considered in this analysis is illustrated in Fig. 2.7. It consists of a web, under tension, in close proximity to a cylindrical porous surface. The web, being flexible and the cylinder constitute what is known as a foil bearing. The gap between the web and the surface is maintained by a film of air provided through the porous wall of the cylinder. The tension in the web is balanced by the pressure in the air film supporting the web.

To simplify the analysis, it is assumed that the web is a perfectly flexible, inextensible membrane. A further assumption that the centre line of the web lies in a plane and that the web itself is perpendicular to this plane, rules out cases in which the web is twisted or bowed across its width. The assumption implies, also, that the gap thickness across the web is constant. Such an approach ignores completely the problem of determining the manner in which the pressure builds up underneath the web.

Consider now a web of unit width with a wrap angle  $\theta$  around the porous cylinder. The web is under tension which can be represented by a mean value  $T$  per unit width. Considering the forces acting on a polar element of the combination subtended by the two equal radii  $OA$  and  $OB$  we get

$$F = 2T \sin \frac{\delta\theta}{2} \quad (1)$$

If  $p$  is the pressure in the air gap then

$$p = \text{Force/area of the arc subtended by OA and OB}$$

$$p = F/(\text{length of arc} \times \text{width of arc})$$

Since we are considering unit width of the web

$$\therefore p = F/r \delta\theta \tag{2}$$

Substituting for  $F$  in (1) from (2) yields

$$p r \delta\theta = 2T \sin\left(\frac{\delta\theta}{2}\right)$$

Since  $\delta\theta$  is a small angle, hence  $\sin\left(\frac{\delta\theta}{2}\right) \approx \frac{\delta\theta}{2}$

$$p r \delta\theta = 2T \frac{\delta\theta}{2}$$

$$\therefore p = \frac{T}{r}$$

The supply pressure to the porous cylinder must therefore be  $\frac{4}{3} p$  to lift the web. In practice it was found that the minimum supply pressure for virtual elimination of friction between the web and the porous cylinder was  $1.5 p$ .

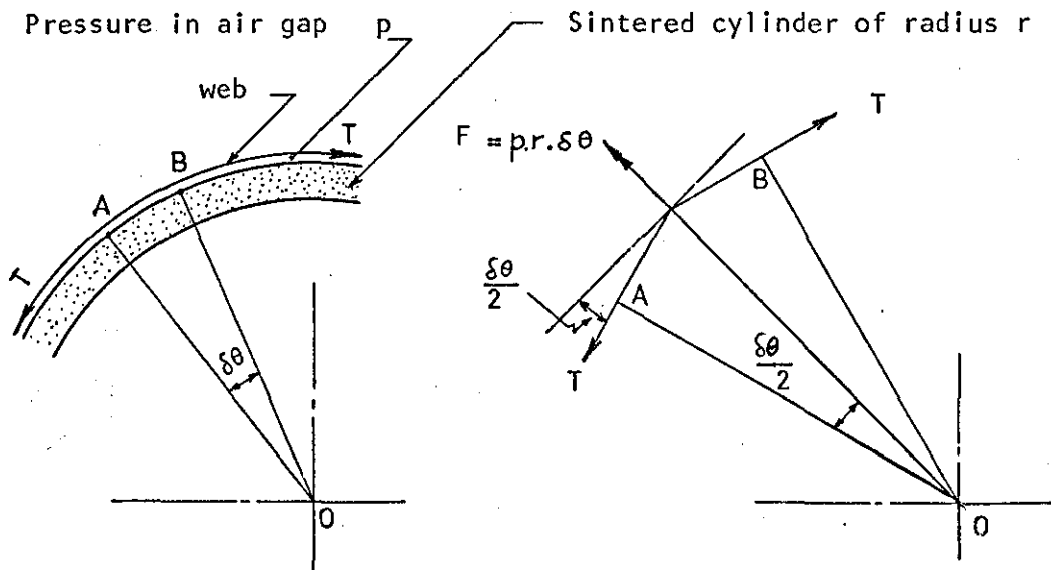


Fig. 2.7 The principle of externally pressurised foil bearings.

## 2.4 FINITE ELEMENT APPROACH TO WEB-TENSION PROFILE

### 2.4.1 INTRODUCTION

In externally pressurised foil air-bearings, the pressure in the air film deflects the flexible web. This deflection, changing the air film thickness, alters the pressure distribution along the width of the bearing.

As the tension pressure relationship was established earlier on the assumption that film thickness is constant across the web, consequently the pressure in the film was taken to be constant. This way, one is ignoring the interaction between the pressure distribution in the film and the tension in the web. To predict the tension profile across the web due to the loading conditions and the elastic characteristics of the web material only, it seemed valuable to attempt a finite element solution for the problem under consideration. Assuming that this could be achieved, one can then introduce the effect of the pressure distribution into the model to achieve a more comprehensive analysis of the problem.

The finite element method has now become recognised as a general method of wide applicability to engineering problems. It is essentially a process through which a continuum with infinite degrees of freedom can be approximated to by an assemblage of elements each with finite number of unknowns. Conventional engineering structures can be visualised as an assemblage of structural elements interconnected at a discrete number of

nodal points. If the force-displacement relationships for the individual elements are known it is possible, by using various well-known techniques of structural analysis<sup>43,44</sup>, to derive the properties and study the behaviour of the assembled structure.

#### 2.4.2 NOMENCLATURE

$\ell$	Length of web between the frictionless bearings
$t$	Web thickness
$w$	Web width
$2\theta$	Wrap angle around the pad
$E$	Young's modulus of web material
$\nu$	Poisson's ratio
$\rho$	Density of web material
$T$	Average applied tension per unit width of the web.
$X, Y, Z$	Global co-ordinates of the nodes
$x, y, z$	Local co-ordinates of the nodes
$\alpha_{11}$	Angle between $x$ and $X$
$\alpha_{12}$	" $x$ and $Y$
$\alpha_{13}$	" $x$ and $Z$
$\alpha_{21}$	" $y$ and $X$
$\alpha_{22}$	" $y$ and $Y$
$\alpha_{23}$	" $y$ and $Z$
$u$	Displacement along $x$
$v$	" $y$
$w$	" $z$

### 2.4.3 FINITE ELEMENT ANALYSIS

In the present analysis the web is treated under some assumptions and approximations, as a symmetrical cylindrical shell. The force-displacement relationships of each individual element were determined from the equations of minimisations of total potential energy. The characteristic equations of the whole structure of the elements were then derived by proper summation of the appropriate stiffness coefficients. Solution of these characteristic equations defined the nodal point displacements, hence stresses. A brief description of the procedure, assumptions, boundary conditions and loading is given below:

(i) Basic assumptions and approximations:

1. The behaviour of the web can be represented by the behaviour of a thin plate built up of small flat elements, forming the middle plane of the web.
2. The classical plate-theory assumptions are valid for the present analysis. Namely, that the plate element is thin and the deflections are small so that linear variation of stresses and strains take place on lines normal to the plane of plate elements.
3. The web material is homogeneous and isotropic, thus the elasticity constants and density remain constant throughout the web.
4. The effect of gravity on the web elements is negligible compared to other forces acting on them.
5. Linear elasticity does hold for the web material.

6. The web is symmetrical about the inplane X and Y axes, therefore one quarter of the web section under consideration represents the whole state of stress.

(ii) Selection of the type of element:

In the present problem a complete slope continuity is required on the interfaces between the various elements without violating the fundamental continuity of the displacement in the Z direction between the elements. It is, however, relatively simple to obtain shape functions which may violate the slope continuity between the elements but not at the nodes where continuity is basically imposed. If such functions satisfy the constant strain criterion then convergence may still be found<sup>45</sup>.

Rectangular elements of eight nodal points, four at the corners and the rest at the midpoints of the element sides, have been successfully used<sup>46</sup> for plate and shell analysis. With the simple geometry of the present problem, such elements appeared to be good enough to represent the web.

(iii) Finite element idealisation of the web:

Fig.2.8 shows a diagrammatic sketch for the experimental rig. The web, fixed at one end, traverses a frictionless air bearing acting as a support and guide roller. It then, in its course to the second guide roller, wraps around a pad. Both the pad and the second guide roller are frictionless air bearings. At the other end of the web, dead



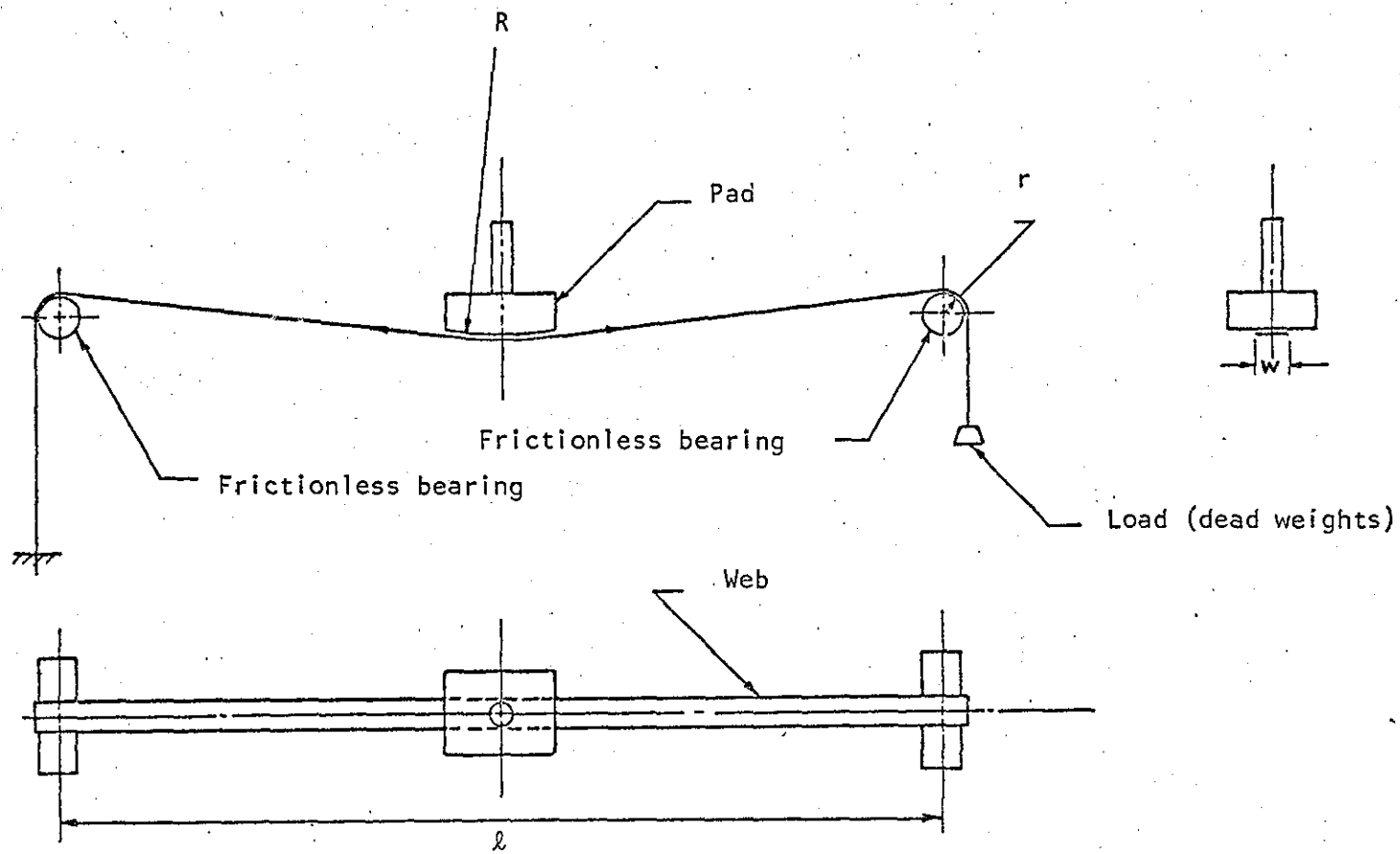


Fig. 2.8 Diagrammatic sketch for the experimental rig.

weights are used to apply tension to the web.

Fig. 2.9 shows the idealised structure of one quarter of the loaded web in the region between the two guide rollers. The two lines  $X = \frac{l}{2}$  and  $Y = 0$  are lines of symmetry and the flat elements laying within the zone  $X_0 \leq X \leq \frac{l}{2}$  are constrained in the direction normal to the element plane (the  $z$  direction). Fine mesh size was used near the lines of the steepest stress gradients.

(iv) Boundary conditions:

Due to the symmetry conditions mentioned earlier, the displacements are constrained as follows:

$$\begin{aligned} u &= 0 && \text{along the line } X = \frac{l}{2} \\ v &= 0 && \text{" } Y = 0 \\ \omega &= 0 && \text{" } X = 0 \\ \omega &= 0 && \text{within the domain } X_0 \leq X \leq \frac{l}{2} \\ &&& \text{and } 0 \leq Y \leq \frac{w}{2} \end{aligned}$$

(v) Loading conditions:

The applied loads may be described by either quantitative values of the applied force or by prescribed displacements. The procedure followed in the present analysis was to prescribe an assumed value of displacement at the edge  $X = 0$ . Thus the condition is given by

$$u = -\delta \quad \text{along the edge } X = 0$$

where  $\delta$  is an assumed small displacement in the negative direction of  $X$ .

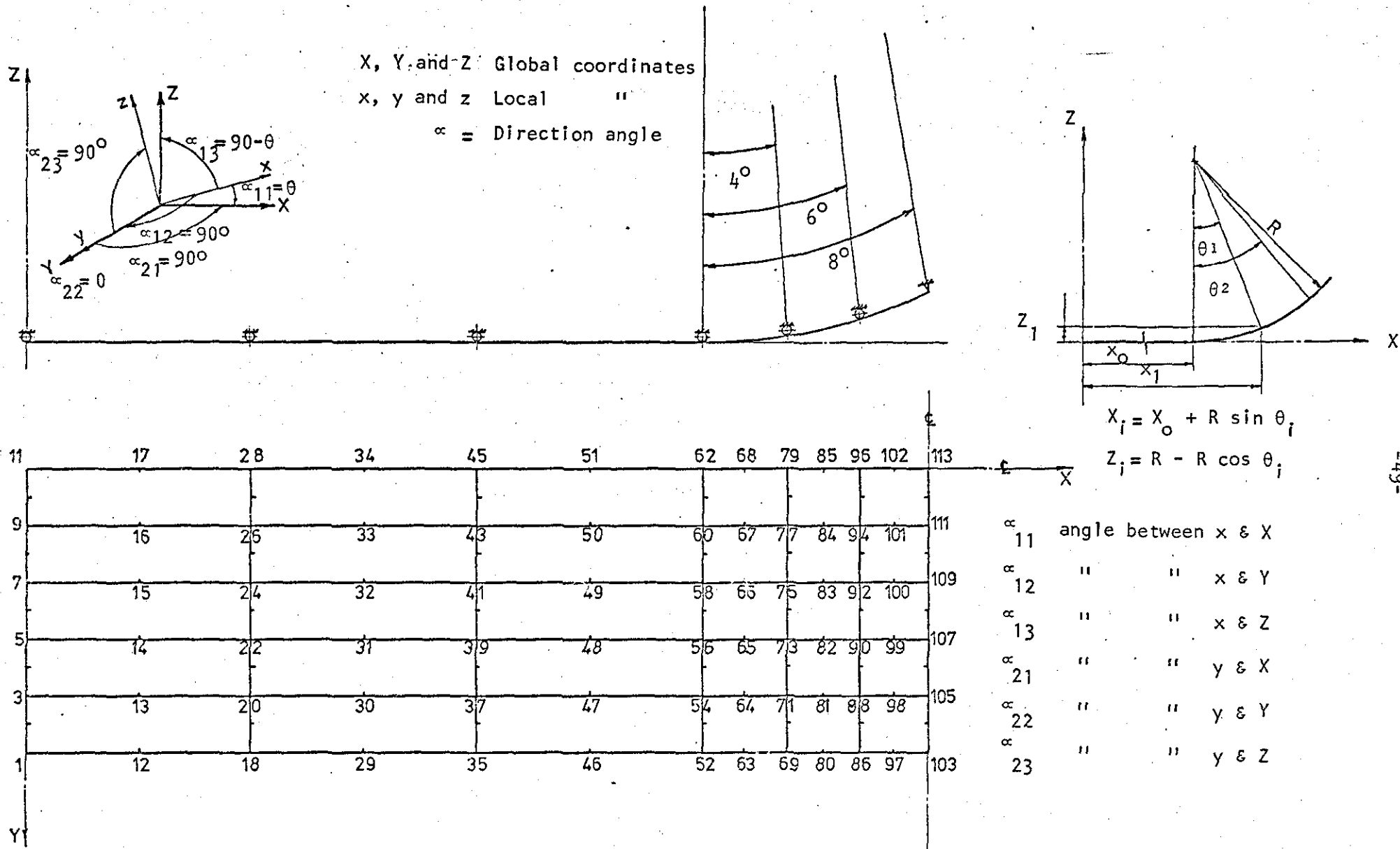


Fig. 2.9 The idealised structure of one quarter of the loaded web in the region between two guide rollers.

(vi) Method of solution:

The local stiffness matrices of the individual elements were derived, then transformed into the global co-ordinate system by using the direction cosines matrix established between the two sets (local and global) of co-ordinate systems. The structure stiffness matrix was then assembled from those of the individual elements, the boundary conditions were introduced and the prescribed displacements (resulting from the external load) were applied. The resulting  $n$  linear equations were then solved for the displacements of the discrete nodal points;  $n$  being the total number of degrees of freedom of the whole assemblage of elements. Stresses could be calculated within the elements of particular interest, e.g. near by  $X = \frac{\ell}{2}$ .

A standard computer program (PAFEC 70 +)<sup>47</sup> was used with the following data (See Fig.2.8 and 2.9) to determine the state of stresses within the region

$$-\frac{w}{2} \leq Y \leq +\frac{w}{2} \quad \text{at} \quad X = \frac{\ell}{2}$$

Total Number of nodal points	113	
Total Number of elements	30	
$\ell$	60	cm
$t$	0.010	cm
$w$	5.0	cm
$E$	$4.118 \times 10^5$	$\text{N.cm}^{-2}$
$\nu$	0.4	
$\rho$	$1.4 \times 10^{-3}$	$\text{kg.cm}^{-3}$
$R$	25.0	cm

2.4.4 RESULTS AND DISCUSSION

An inspection of the computer program results revealed the following: (see Fig. 2.9)

Stresses at nodal points 86 - 96 are identical  
 " " 97 - 102 "  
 " " 103 - 113 "

These stresses when converted to give the resultant forces acting at the centre of each element would indicate that the tension across the web is constant. Such results contradict practical observation; that is to say the side edges of any flexible web, subjected to a tensile force, appear to be slack relative to the central region of the web. This observed phenomenon could be explained as follows:

Consider the case of a web of flexible material, fixed at one end and subjected to a tensile force at the other end as shown in Fig. 2.10. Let us assume that the normal stress in the X direction is equal to that along the y direction. This would have the effect of overestimating  $\sigma_y$  at the centre of the web, since  $\sigma_y$  is only a fraction of  $\sigma_x$  ( $\sigma_y = \alpha \sigma_x$  where  $\alpha \ll 1$ ). Doing this, for simplicity, we get:

a - At the centre of the web:

$$e_x = \frac{\sigma_x}{E} - \nu \frac{\sigma_y}{E}, \quad \sigma_x = \sigma_y$$

$$e_x = \sigma_x \frac{(1-\nu)}{E}$$

$$\sigma_x = \frac{1}{(1-\nu)} E e_x \tag{1}$$



Comparing (1) and (2) yields that  $\sigma_x$  at the side edge is less than that  $\sigma_x$  at the centre which may explain the phenomenon of the slackness of the side edges relative to the centre of the web, hence the existence of a tension profile across the web.

#### 2.4.5 CONCLUSIONS

The approach presented here failed to give any conclusive results. One is inclined to believe that an improved model for the problem with more realistic features can result in a more successful outcome. Considering the difficulties involved in simulating the problem, any further attempt would have deviated this study from its original course.

CHAPTER 3

EXPERIMENTAL RIG



### 3.1 INTRODUCTION

Bearing in mind the objectives of the present work mentioned earlier, one finds that the nature of the problem has dictated the plan for experimental work. Web-tension measurement had to be carried out in situ where the web is manufactured, processed or transported. Thus it was imperative to simulate, in a test rig, conditions as near as possible to the actual working conditions to provide a deeper insight into the problem of relatively high-frequency tension perturbation. The limitations, of course, are the cost and time needed to carry out an ultimately comprehensive experimental analysis.

## 3.2 TEST RIG

### 3.2.1 MAIN FRAME AND COMPONENTS:

The main frame was designed and fabricated in such a way that it can be adapted for extended work on the study of the dynamic behaviour of moving webs. As the main requirement was rigidity, the frame was constructed of rolled hollow section steel bars (R.H.S.) The section used was 2 inch by 2 inch by 0.100 inch (50.8 x 50.8 x 2.54mm) wall thickness. The bars were cut and machined to the designed lengths, and then welded to construct the skeleton of the main frame. The essential components of the frame are illustrated in the perspective view shown in Fig. 3.1.

The frame accommodates the main drive unit, 6 guide roller units and a swinging roll displacement - guide unit as can be seen in Fig. 3.2. The web is moved (at the speed required) by a 1 horsepower, variable speed D.C. motor. The guide roller units, which were designed to be easily accommodated at any desired location on the frame, support and guide the moving closed loop of web in its designed course. The swinging roll unit is a self-contained unit that controls the lateral alignment of the moving web. Guiding is accomplished by a gentle swivel action which minimizes the distortion and wrinkling of the web as it enters and leaves the unit. The specifications of the driving motor and the swinging roll unit are given in Appendix (II).

One part of the main frame was utilised with a stationary web to carry out, experimentally, static and dynamic analyses of

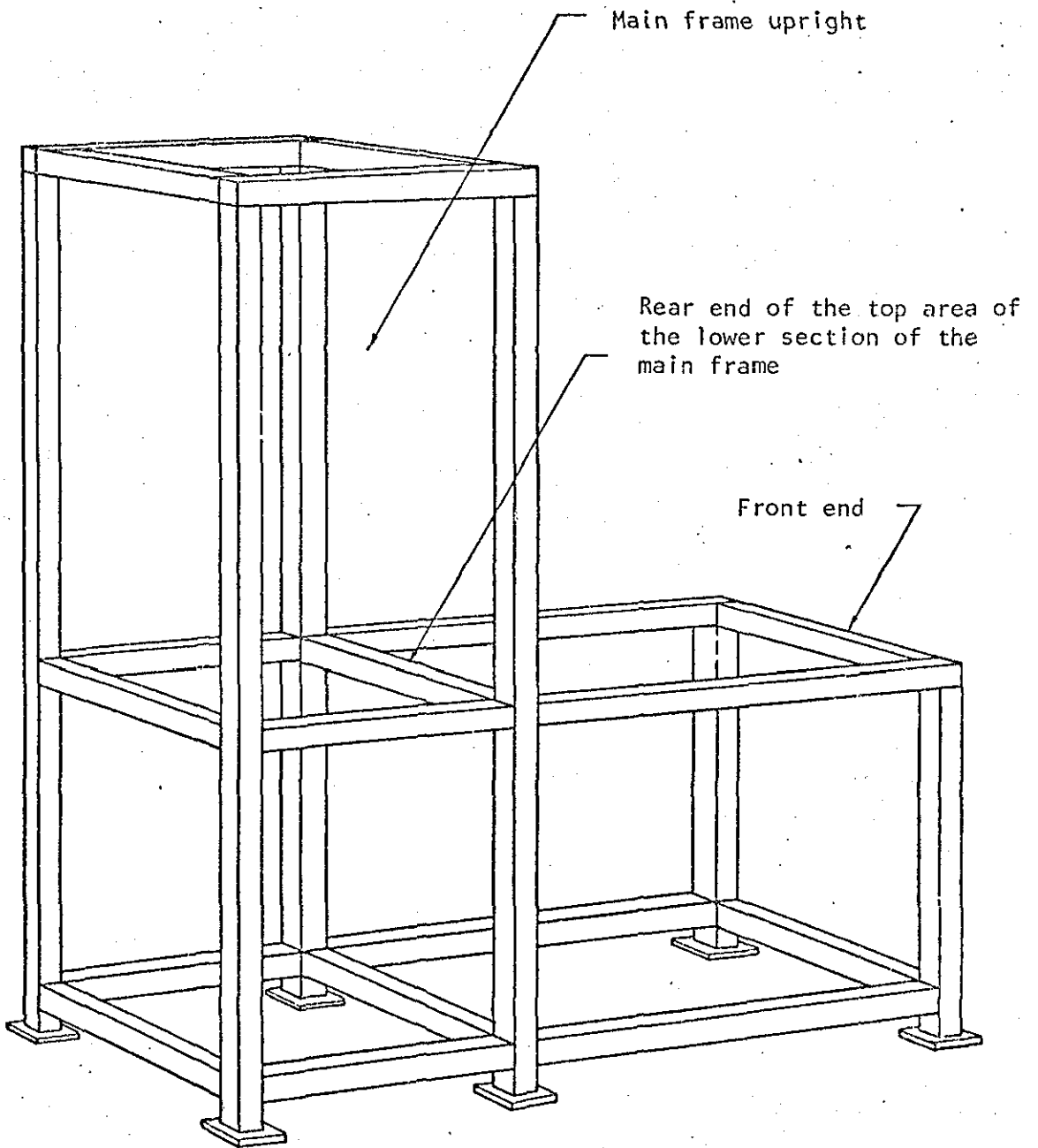


Fig. 3.1 Perspective view for the main frame.

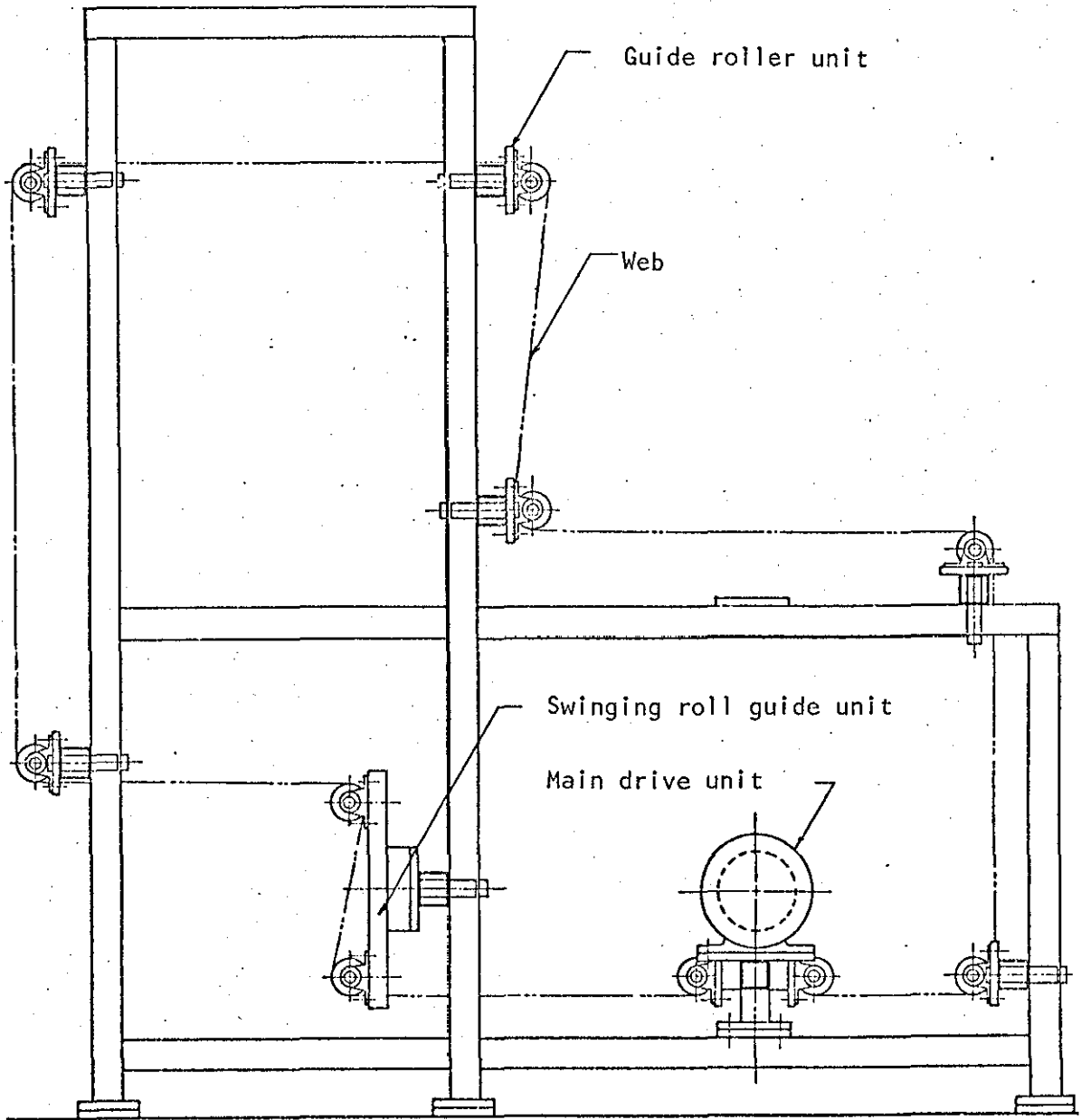


Fig. 3.2 A view showing the components of the test rig accommodated on the main frame.

web-tension measuring devices as shown in Plate 4.2. As for the analysis of measuring devices on running webs at high speeds, the investigation carried out in this study was more of a qualitative nature. The top area of the lower section of the main frame was used to build on the accessories of the experimental rig. One guide unit support bar, located at the rear end (near to the upright section of the main frame), was used to support the fixed end of the web under consideration. Another support bar, located at the front of the lower section of the main frame (about 0.6m apart from the rear one) was used to support the externally pressurised cylinder intended to measure the tension in the web traversing it.

The schematic sketch in Fig. 3.3 shows the basic arrangements for static tests. In (a) the web is fixed to a sliding cylinder at one end (near the rear end of the lower section of the main frame), traversing a frictionless air bearing at the front end of the main frame and coupled to a load carrier, through which the desired tension is to be applied at the other end of the web. In (b) the rear cylinder was replaced by another frictionless air bearing to support and guide the web, one end of which is coupled to a load cell. The load cell, acting as a reference monitoring the tension applied to the web at its other end, is mounted and fixed to a third guide unit support bar which is located across the bottom part of the lower section of the main frame. Plate 3.1 shows the second arrangement.

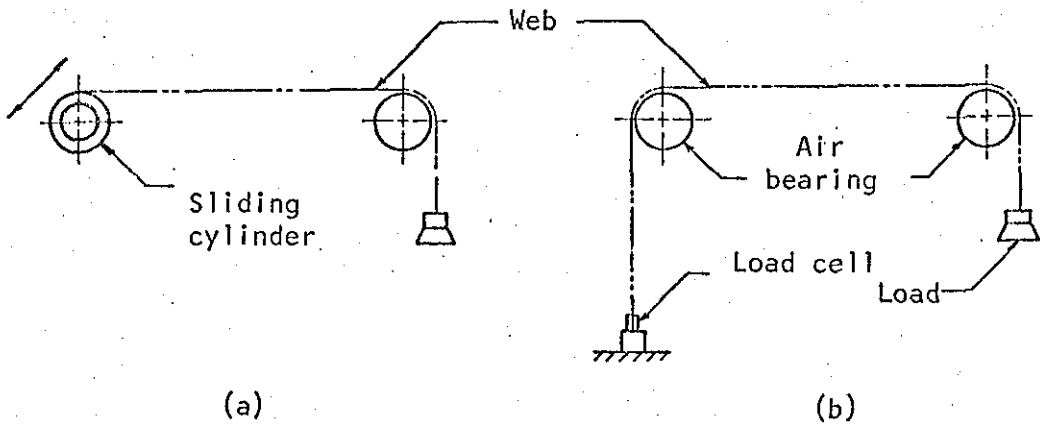


Fig. 3.3 Diagrammatic sketch showing web-end fixation

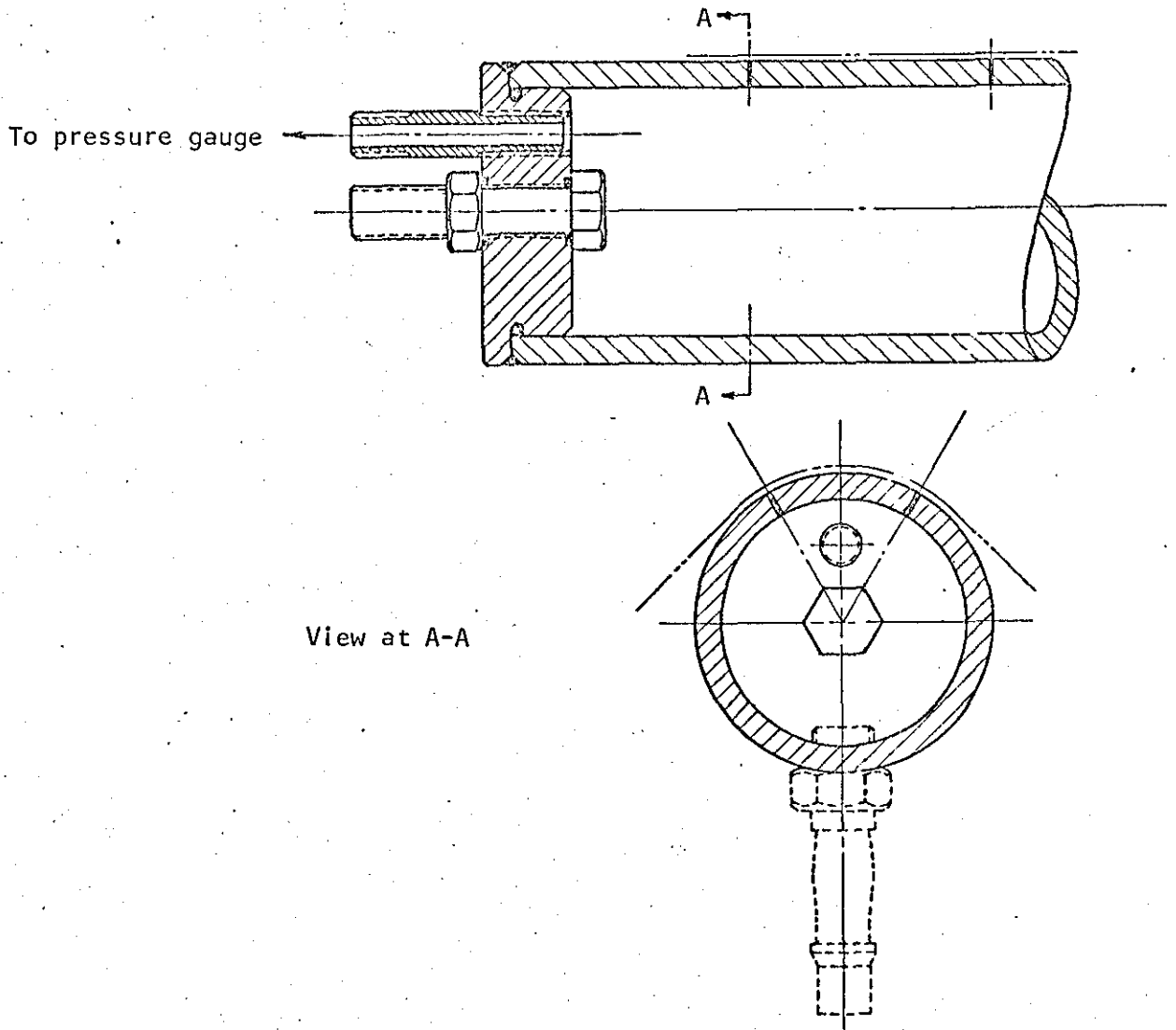


Fig. 3.4 Frictionless air bearing

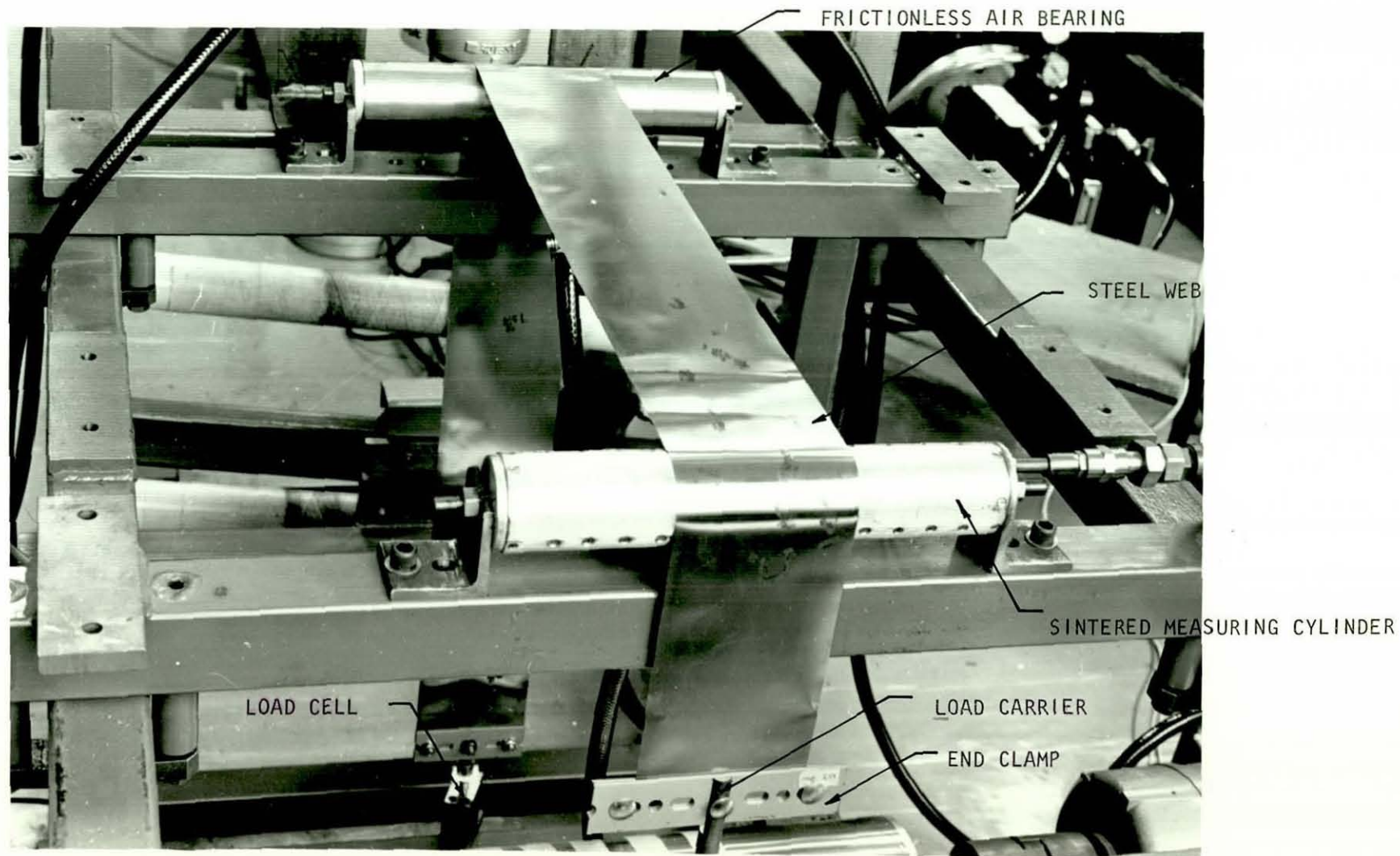


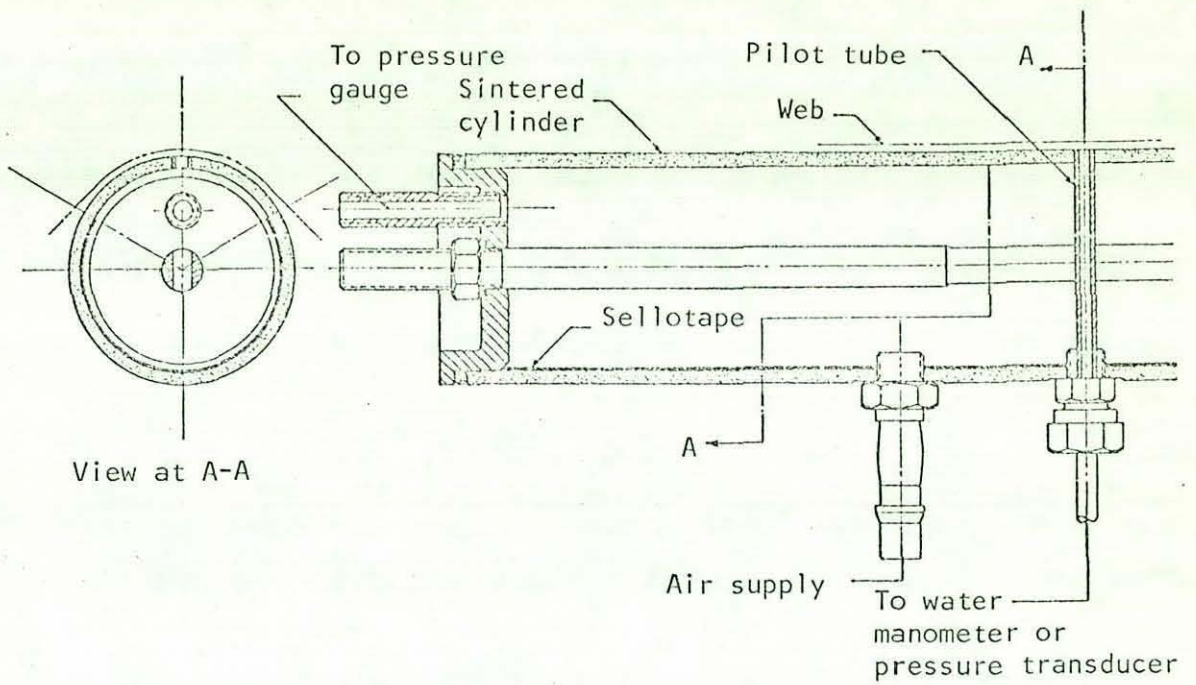
PLATE 3.1 BASIC EXPERIMENTAL SET UP FOR STATIC TESTS

### 3.2.2. FRICITIONLESS AIR-BEARINGS

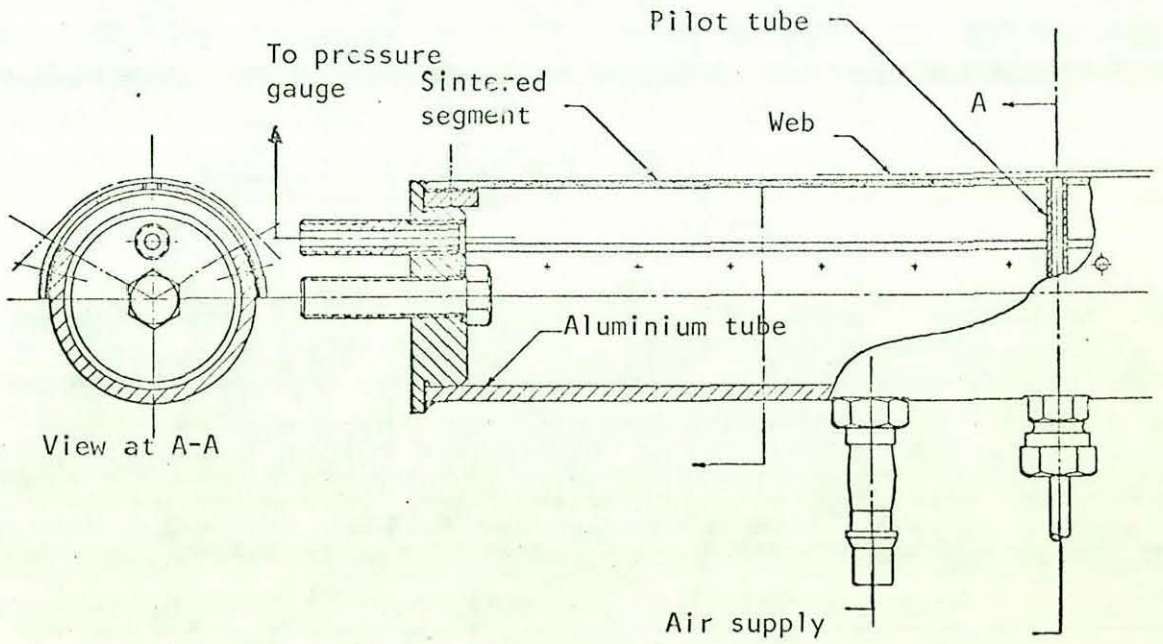
Frictionless air-bearings were used for two different purposes. First, to eliminate the friction between the rear guide roller and the web traversing it on its way to the load cell, which is a reference standard for measuring the applied tension at the other end of the web. This was achieved by using a steel tube, machined and polished to a 50mm outside diameter. Two rows of 7 small holes, (each 0.775mm diameter) were drilled, the two rows subtending an angle of  $60^{\circ}$ . The wrap angle of the web when traversing the tube was  $90^{\circ}$ . The holes were evenly spaced along the tube, 40mm apart. Fig. 3.4 shows the details of the air bearing used. As for the second purpose, the concept of porous sintered metal turner bars, described earlier, was utilised to measure the tension in the web traversing such turner bar.

Two of the possible ways in which the sintered tube could be made into an air blown turner bar are shown in Fig. 3.5. The material used for the first design was sintered bronze with a maximum pore size of  $2.5 \mu\text{m}$ , commercially available in a variety of tube sizes. The size of the tube used was 50.8mm O.D. (2 in), 44.5mm I.D. (1.75 in) and 279.4mm (11 in) length. As the intended wrap angle was  $90^{\circ}$ , a non porous sticky tape was used to blank off a sector of  $240^{\circ}$  of the inside surface of the tube leaving an active surface angle of  $120^{\circ}$ . Two drawbacks were apparent using this arrangement. Firstly, one was using a large area of sintered material and then had to blank most of it off.





(a) Sintered bronze cylinder



(b) Sintered stainless steel cylinder

Fig. 3.5 Alternative designs for measuring cylinder

Secondly, the sintered bronze material proved to have a comparatively high permeability coefficient. This meant higher rate of air flow through its porous surface (see table 3.1). To overcome these drawbacks the second design was developed. Rigid mesh, commercially available in sheets (36 x 12 x 1/16 in), which is produced by rolling and sintering of several layers of stainless steel wire mesh was used. The maximum pore size of the mesh used was 2.5  $\mu\text{m}$ . This material proved to have lower permeability coefficient, hence less air consumption as shown in table 3.1. The values listed in the table were determined experimentally under the same conditions for both materials. To economise with the use of such expensive material, the main body of the turner bar was made of aluminium tube. A sector subtending an angle of  $120^\circ$  was cut along the wall of the tube. A strip of the mesh was formed to have a 25mm radius. It was then screwed onto the outer surface of the aluminium tube, covering the slot made, to provide the active surface area of the turner bar.

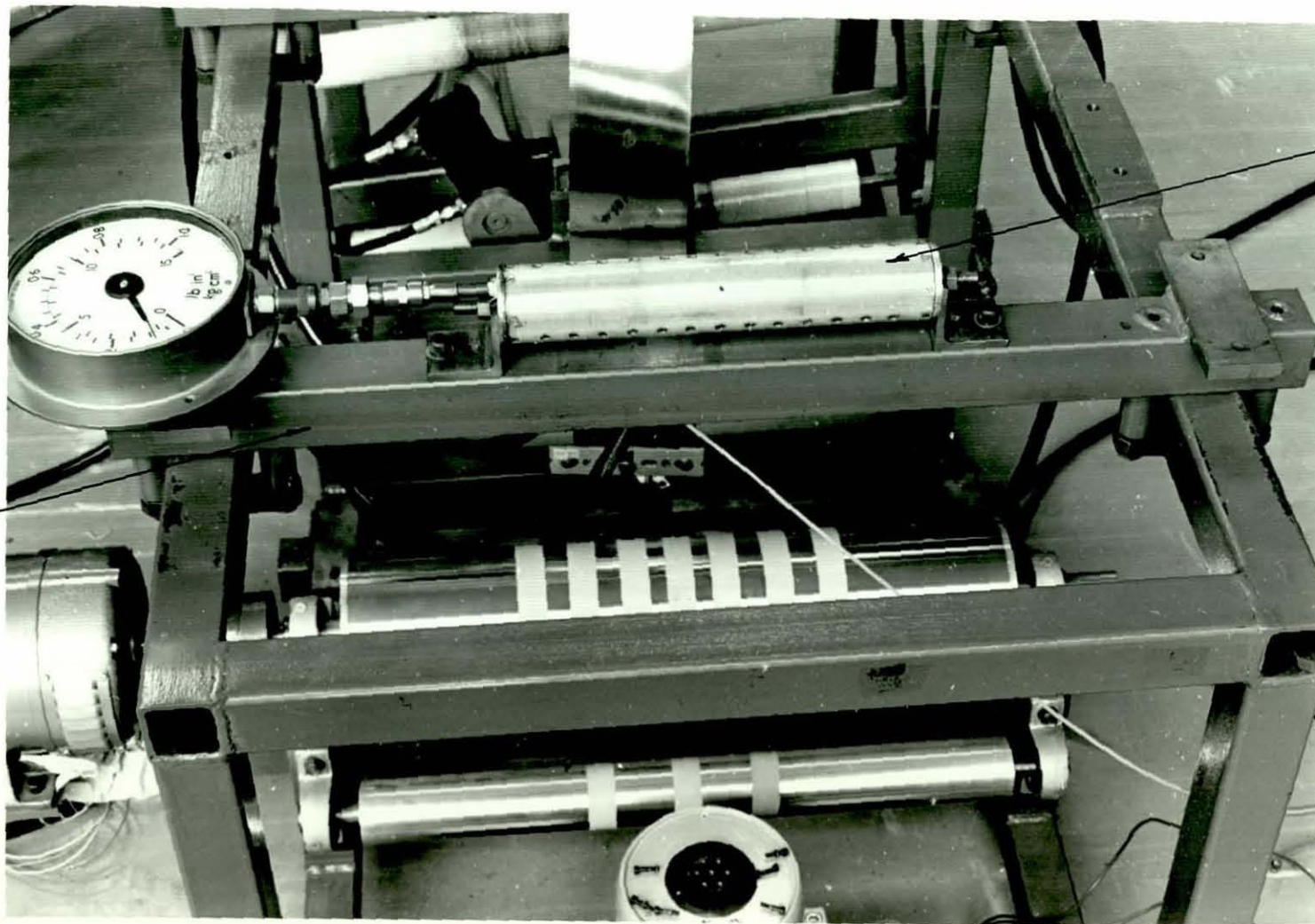
Pressure inside the cylinder (kN/m <sup>2</sup> )	Rate of air flow (m <sup>3</sup> /s.m <sup>2</sup> )	
	Bronze	Stainless Steel
20.60	0.475	-
34.34	0.60	0.198
68.67	1.283	0.41
103.01	-	0.548

Table 3.1

In both designs the materials used could be machined in the same way as similar solid materials. This made it easy to drill

a through hole of 3.2mm diameter at the middle of the active surface centre line. Every precaution was taken to ensure that the sintered surface was not in any way damaged, thereby closing the pores. A plastic pilot-tube was inserted into the hole to become flush with the outer surface of the sintered cylinder. The tube was then connected to a pressure gauge, namely a manometer at one stage of the experimental work and to a Kistler pressure transducer at another, to measure the pressure in the air gap between the active surface of the sintered cylinder and the web traversing it.

At one stage of the experimental work, the need to scan the state of tension across the web had risen. With the previous arrangement, it was found easier to move the web laterally relative to the pilot-tube fitted into the sintered cylinder. To achieve this, the rear end support frictionless bearing was replaced by a solid steel cylinder, acting as a fixed core, and an aluminium sleeve of 50mm outside diameter which slides smoothly along the core cylinder. A grub screw-v groove arrangement was made to guide and lock the sleeve along the core cylinder, hence stopping the web at the desired point relative to the measuring pilot-tube. Plate 3.2 shows one of the guide unit support bars supporting the sintered stainless steel measuring cylinder. The same arrangement was used to support either the frictionless air-bearing or the steel core cylinder with the sliding sleeve at the rear end. The latter is shown in detail in Fig. 3.6.



GUIDE UNIT  
SUPPORT BAR

SINTERED  
MEASURING  
CYLINDER

-65-

PLATE 3.2 GUIDE UNIT SUPPORT BAR & THE MEASURING CYLINDER

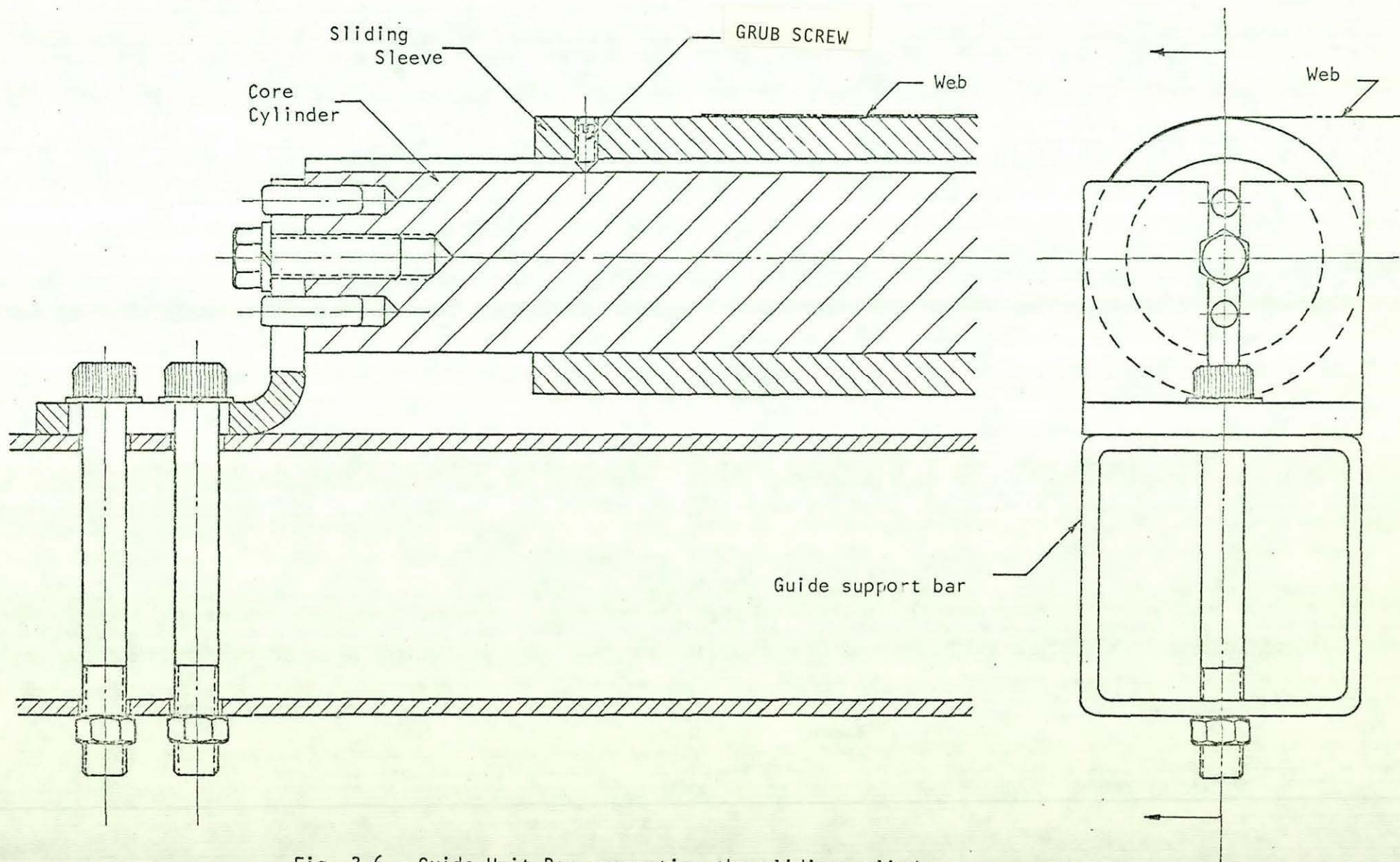


Fig. 3.6 Guide Unit Bar supporting the sliding cylinder arrangement

### 3.2.3 WEB-TENSION MEASURING PAD:

It was shown earlier that the pressure in the air gap ( $p$ ), balancing the applied web-tension ( $T$ ) is inversely proportional to the radius of curvature ( $R$ ) of the foil bearing elements ( $p = T/R$ ). The supply pressure  $P$  to the bearing must therefore be greater than  $p$  to lift the web. In practice it was found that the minimum supply pressure for virtual elimination of friction between the web and the other bearing element was 1.5 to 2.0  $p$ . Thus, for a certain value of tension, the bigger the radius of curvature of the bearing the less supply pressure would be required which means less air consumption.

Taking these considerations into account, a prototype portable device, referred to as the measuring pad, to measure web tension was designed, made and tested. Fig. 3.7 shows the detailed drawings of the pad. The porous cylindrical segment was made of a strip of the sintered stainless steel wire mesh. The strip was bent to form a shell of 250mm nominal radius. It was then screwed onto the top of a cast aluminium box, which had been machined to a radius that conformed to that of the strip, with a gasket in between to prevent leakage of compressed air supplied. A 3.2mm ( $\frac{1}{8}$  in) hole was drilled in the middle of the sintered segment to accommodate a pilot tube for measuring the static pressure in the air gap as in the case of the sintered cylinder described earlier. Later, the hole was bored to a diameter of 5.0mm (0.2 in) to fit in the pressure transducer adapter. After the assembly of the components of the pad, the radius of curvature of the sintered segment was measured and found to be

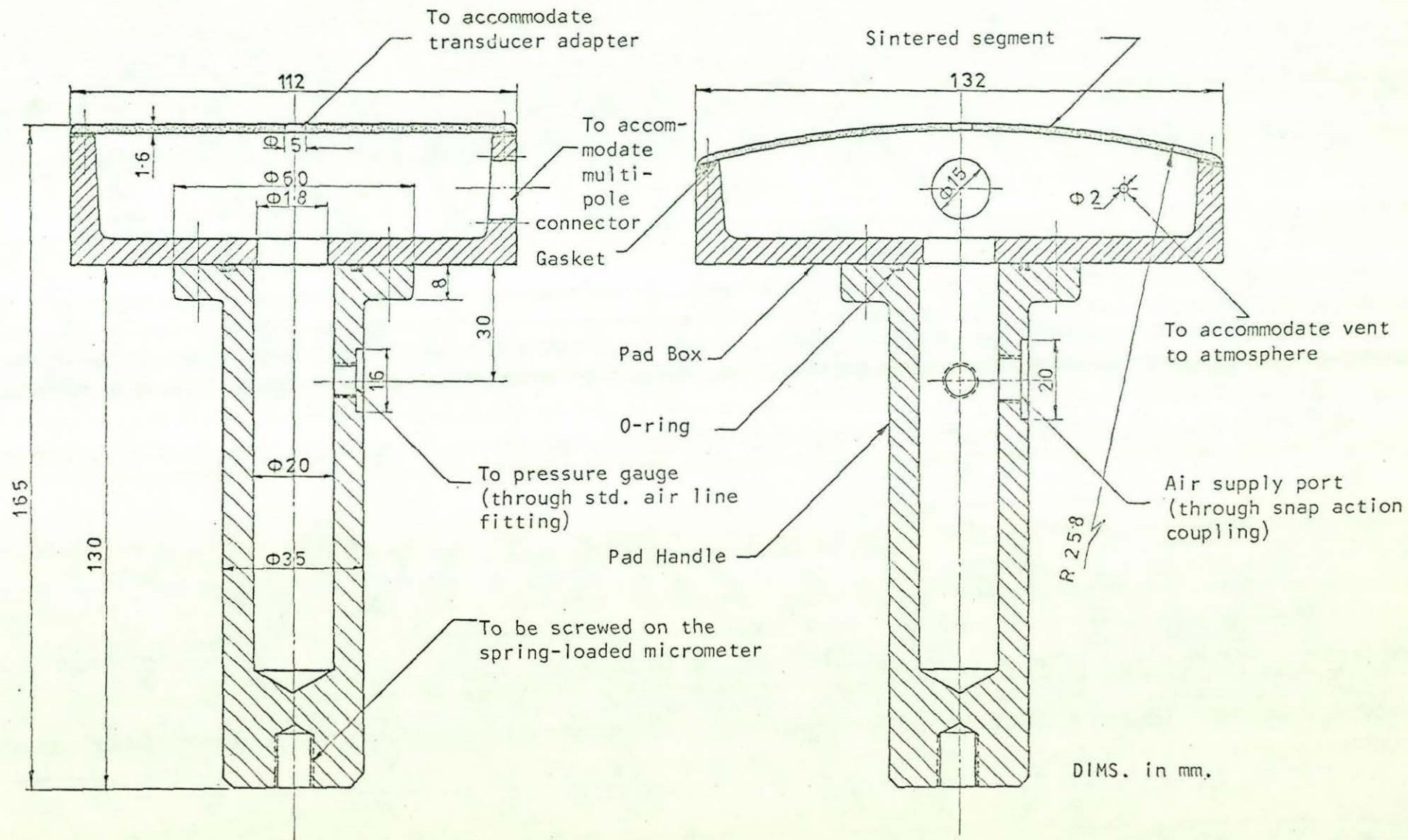


Fig. 3.7 The measuring pad

258.5mm (average value). The details of the procedure of measurement is given in (5.2).

A number of adapters were made so that the transducer, when fitted in, could be either flush with the bearing surface or pulled back from it by the prescribed distance. Such a distance was accurately measured by means of 0.0001 inch (2.54  $\mu$ m) dial indicator with a pointed stylus, which could be placed on the transducer diaphragm and bearing surface alternately. To avoid any distortion that might happen to the diaphragm of the transducer, the adapter was designed to provide some clearance around the circumference of the diaphragm while the transducer was located in position on its back body as shown in detail in Fig. 3.8

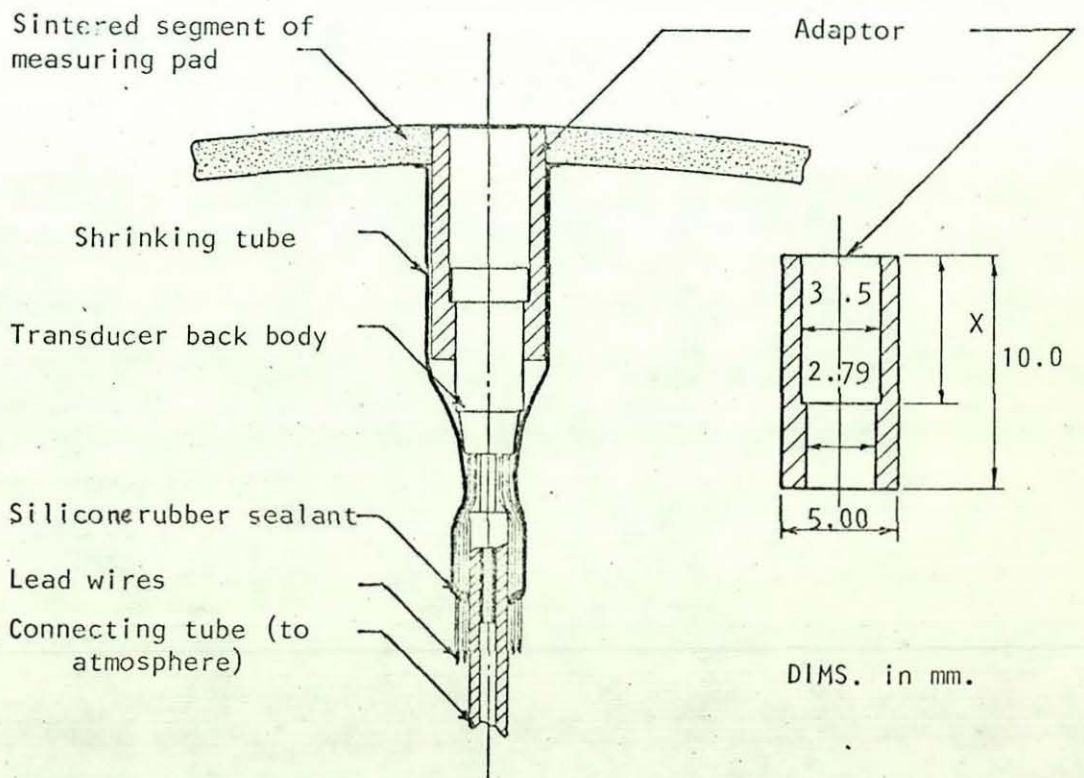


Fig. 3.8 Transducer mounting



Since the transducer used was of the differential pressure type (see 3.3.5), its reference tube was connected to atmospheric pressure (outside the pad box) via a plastic tube going through a hole drilled into the box wall. As for the electrical connections a multi-pole connector was used. It consisted of a chassis socket which was embedded into the box wall and a cable plug to connect the transducer to the power supply-pre amplifier unit. The main advantage of this multi-pole connector is that the wire and cable clamping is incorporated on the cable-mounting version to provide complete sealing to prevent leakage of the pressurised air to the outside of the pad box (Plate 3.3).

Since the supply pressure needed inside the pad box was fairly small ( $4.61 \text{ kN/m}^2$  maximum), a water manometer was used to monitor it to ensure that the required pressure was set. The manometer was connected to the pad via a plastic tube fitted to a male stud coupling screwed in the pad handle. Pressurised air was supplied to the pad through a hose fitted to a standard snap action coupling which fits in a male thread air line adapter screwed in the pad handle as shown in Fig. 3.7 and Plate 3.3.

As the measuring pad was an experimental model, facilities for achieving the optimum wrap angle of the web, around the active surface of the pad, were needed. The wrap angle is determined by the radius of curvature of the cylindrical porous segment of the pad and how far the pad is pushed against the web. Since the radius of curvature of the pad was constant, this left us with the distance the pad would move against the web.

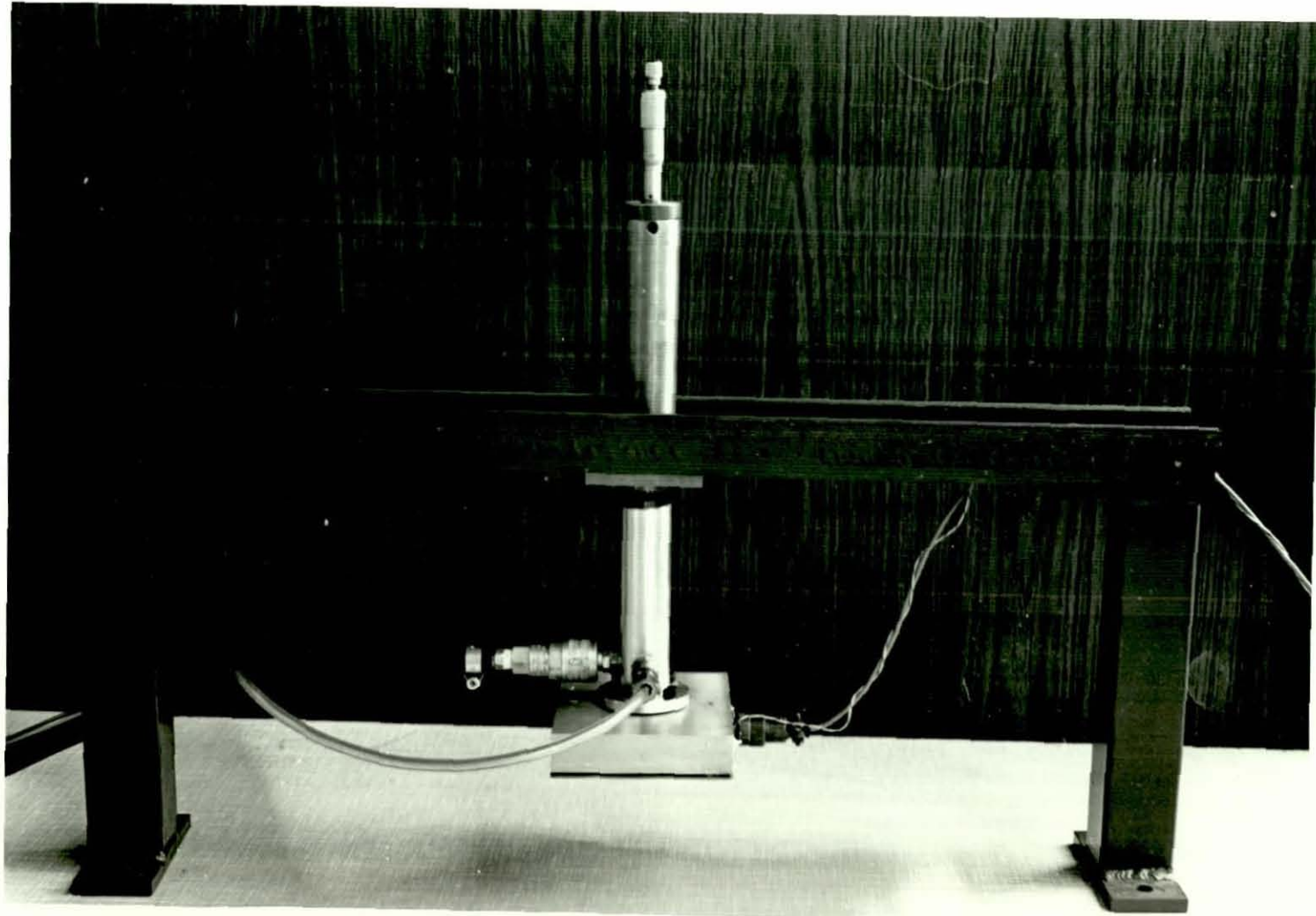


PLATE 3.3 THE MOUNTING BRIDGE WITH THE MEASURING PAD

Adjustment of this distance was made possible by the design and fabrication of a mounting bridge which could be bolted to the top area of the lower section of the main frame. A slot was made along the gantry of the mounting bridge, to which the pad is clamped, to enable the measuring pad to traverse the web passing in close proximity, underneath it. The distance moved by the pad towards the web, hence determining the wrap angle, was controlled by the use of a spring-loaded micrometer arrangement fitted to the measuring pad handle as shown in Fig. 3.9. Plate 3.3 shows the mounting bridge with the pad fitted into it.

#### 3.2.4 AIR SUPPLY

It is clearly essential for the air supply, to either the sintered cylinders or the measuring pad, to be pre-filtered by a filter of a grade similar to or finer than that of the sintered material of either of them. The air must also be dry and oil free. Although these requirements are fairly stringent, they were met by the latest commercially available filters. The filters used had a 5 micron 'Mikro-Klean II' cartridge which, according to the manufacturers, exhibits finer filtration characteristics when used on compressed air, which is the case in this work, or gas service than when used on liquid service applications. Particle removal efficiency improves and removal of particles down to 1 micron is possible, the manufacturers claim.

Two types of regulators were used in the pneumatic circuit. The first one was a general purpose type with output pressures range  $2-125 \text{ lb/in}^2$  (gauge) ( $13.79-862.19 \text{ kN/m}^2$ ) which could provide

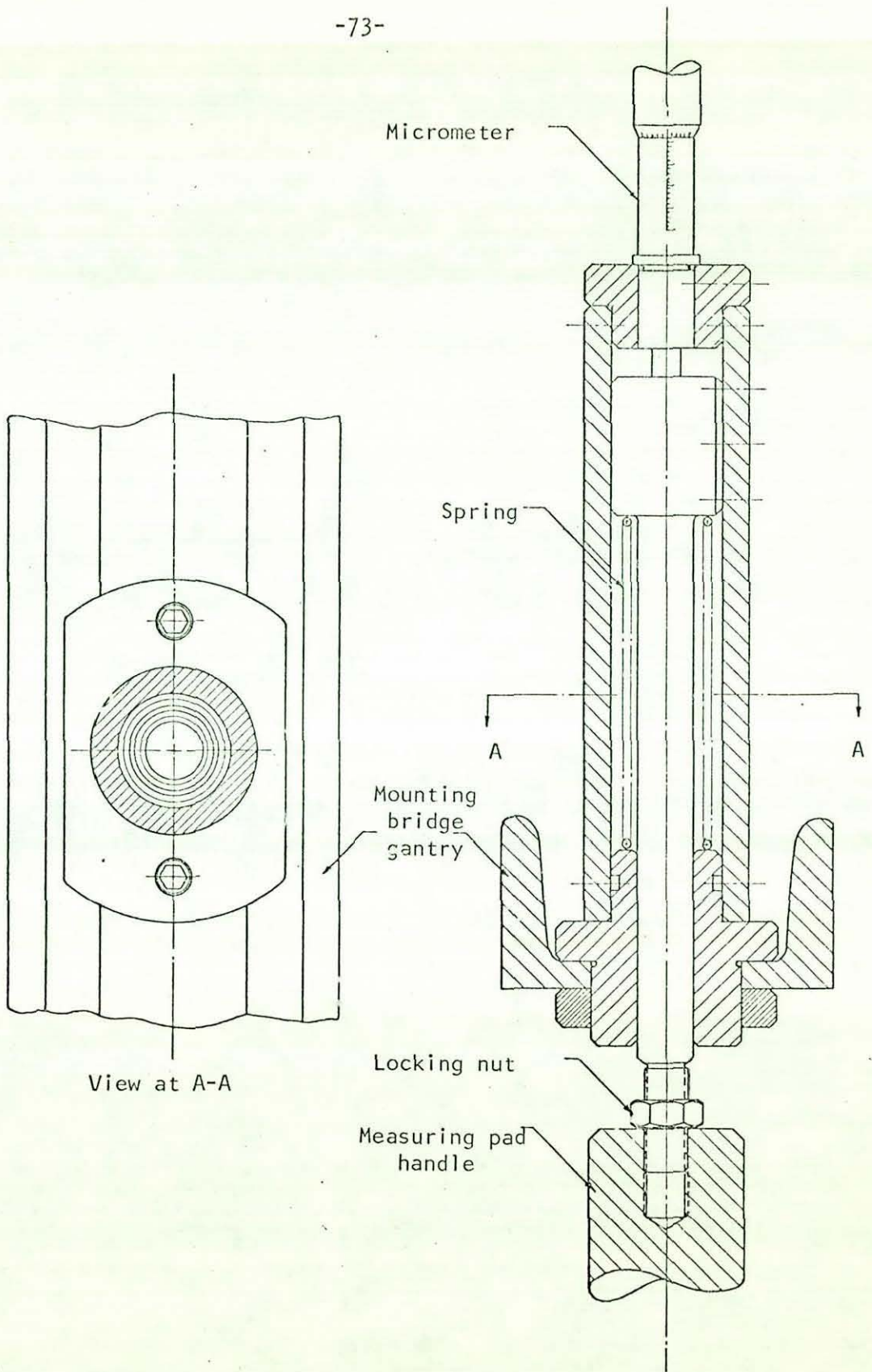


Fig. 3.9 Wrap angle adjustment arrangement

complete shut off. It was used to regulate the supply pressure to the sintered cylinder as well as the rear support air bearing. Another one, of the same type, was used as first stage regulator for the supply pressure inside the measuring pad. Since the supply pressure required inside the measuring pad was comparatively low (up to  $2 \text{ lb/in}^2 \approx 14 \text{ kN/m}^2$ ) compared to the main line pressure ( $90 \text{ lb/in}^2 \approx 620 \text{ kN/m}^2$ ) a second type of pressure regulator was used to set and control the desired value of pressure inside the pad. A diagrammatic layout of the pneumatic network used is shown in Fig. 3.10.

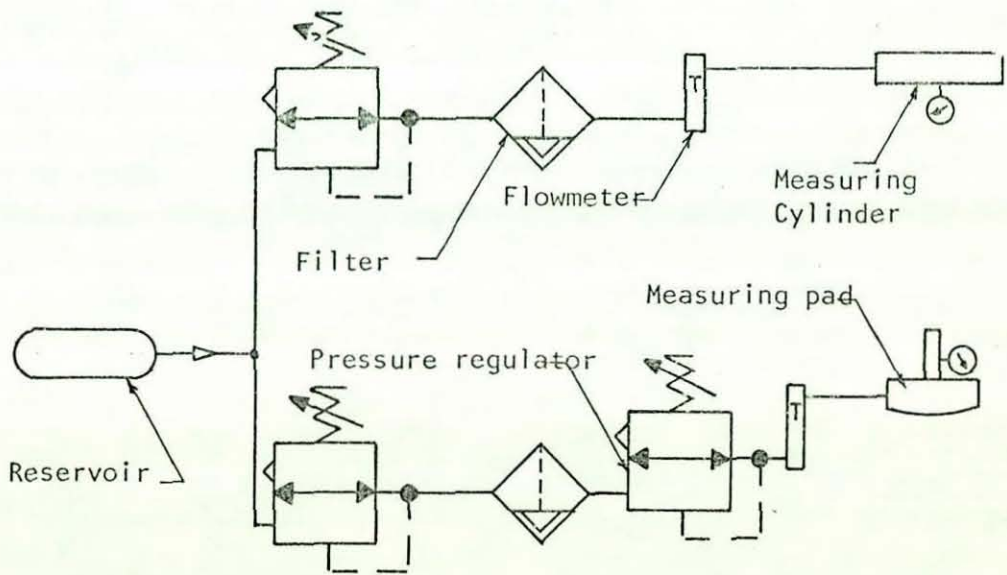


Fig. 3.10 Pneumatic network layout

### 3.2.5 WEB MATERIALS:

The webs used in the experiments were of two different materials. The choice of the materials had been influenced by the fact that

practical use of the measuring pad under consideration would be in continuous processing systems that are linked together by the material being processed. Typical examples are steel strip production lines, printing presses, manufacturing and use of magnetic tapes, plastic films and paper making industries.

"Melinex" polyester films proved to be a useful choice since they are among the most versatile and useful plastic films. They are used in printing, manufacture of magnetic tapes and photographic films and packaging industries. "Melinex" is the trade mark for a range of biaxially drawn films manufactured by ICI Plastic Division from polyethylene terephthalate polymer.

The films used were transparent, commercially available in a choice of widths and thicknesses. Throughout the experiments two "Melinex" webs of different thicknesses were used, namely  $51\ \mu\text{m}$  (0.002 in) and  $102\ \mu\text{m}$  (0.004 in). As for the width, 50, 102, 260mm wide webs were used as will be described later. (Chapter 4). The properties of the films used are given in Appendix (III). The second web material used was shim steel. A 102mm (4 in),  $51\ \mu\text{m}$  (0.002 in) thick steel strip was used.

### 3.2.6 METHODS OF APPLYING TENSION:

Tension was applied to the web by means of a load-carrier. The carrier, together with combinations of dead weights, was used to provide the prescribed static tension. An electro-magnetic vibrator capable of producing a sine vector force, coupled to the load-carrier, was used to simulate a source of tension

perturbation of different frequencies and amplitudes.

The web was fixed, at one end, either to the sliding cylinder arrangement as shown in Fig. 3.3(a) or to a load cell as in (b). The first case was described in detail earlier (3.2.1). As for the second, an adapter was made to couple the end of the web to the load cell by means of two metal strips referred to as the end clamps. To ensure that the applied load is normal to the cross-section of the web, a double sided sticky tape was used, in conjunction with a precision square and a straight edge, to position the web accurately in between the two metal strips which were then bolted together to provide the necessary grip. Fig. 3.11 shows the load cell, adapter and the end clamps. At the other end the web is coupled to the load-carrier by means of the same arrangement.

The load-carrier, shown in Fig. 3.12, consisted of 3 main components; the top part (being bolted to the web clamps through the adapter) to carry the dead weights, the middle part (which is a differential nut with right-hand thread at the top end and a left-hand thread at the bottom) to adjust the length of the carrier and the lower part to couple the carrier via its lower flange to the vibrating table of the electro-magnetic vibrator. The vibrator load mounting table is provided with 7 tapped holes for this purpose. Both the load-carrier and the vibrator are shown in Plate 4.2.

The weights used to provide the required combinations of static tension were calibrated using a "Semi-Auto" Scale of 5 kg

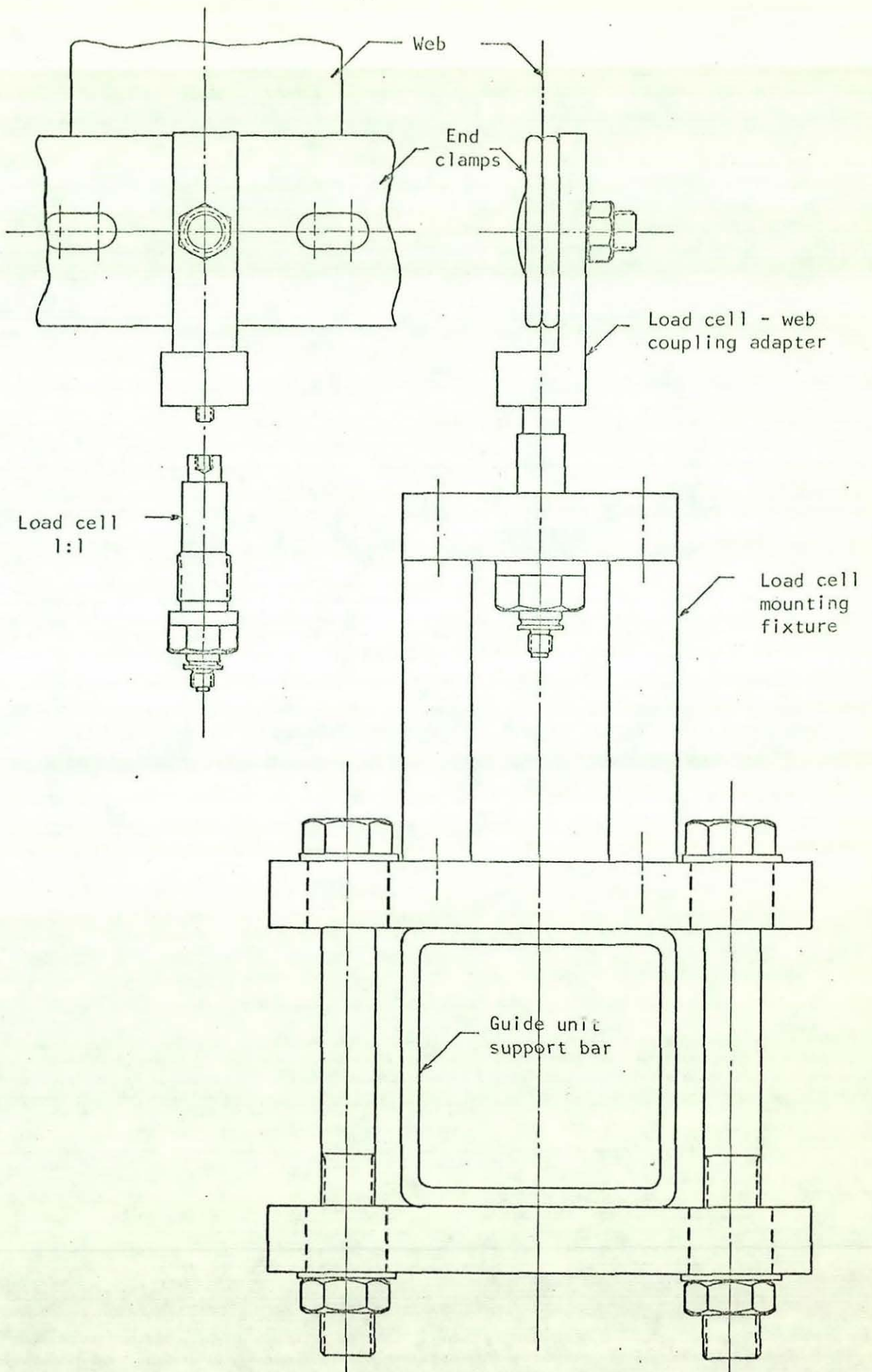


Fig. 3.11 Web fixed at one end to the reference Load-cell



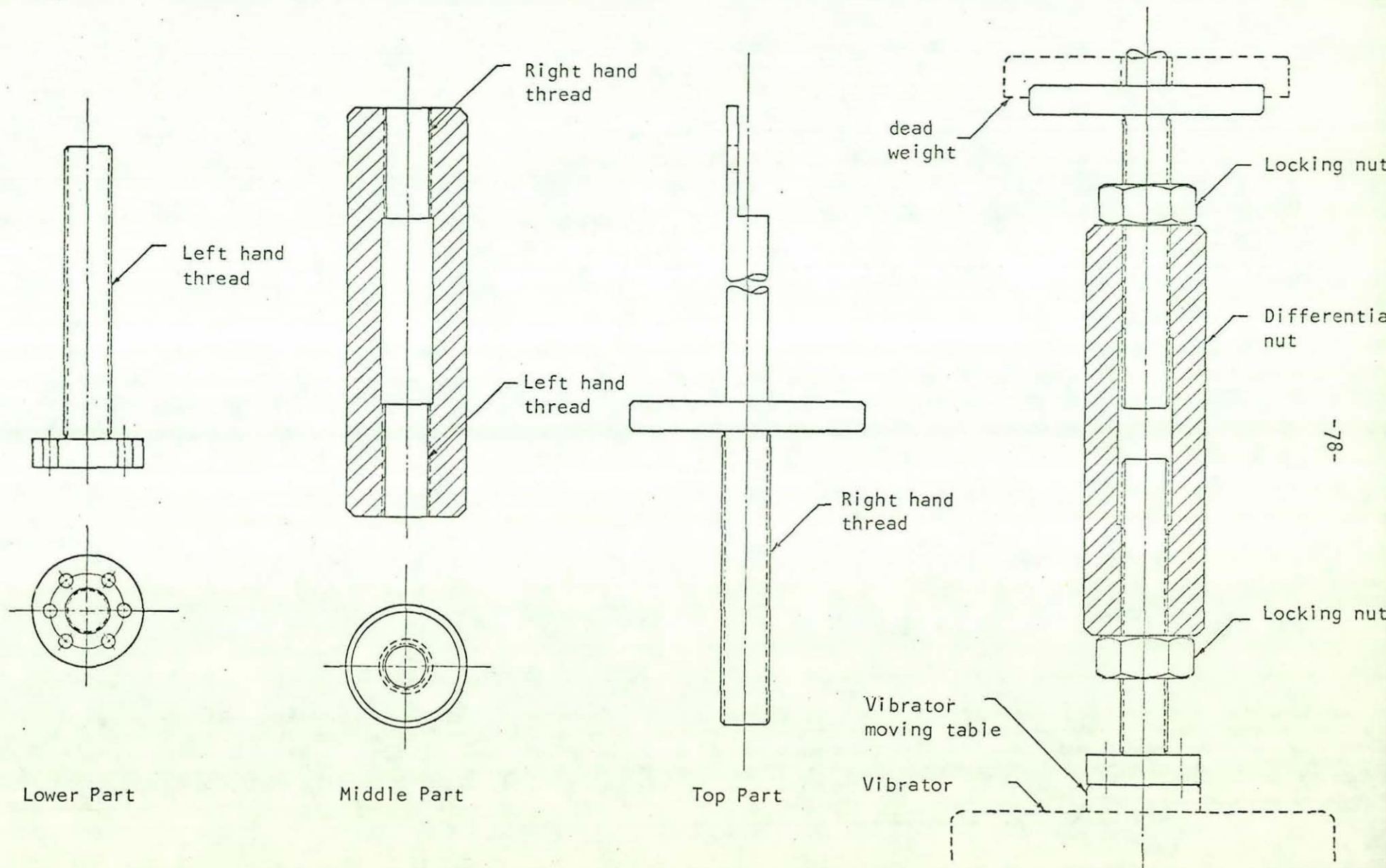


Fig. 3.12 Load-Carrier

capacity with a sensitivity of 1 g in conjunction with a calibrated set of dead weights. The accuracy of the scale readings was checked using a certified set of weights. The scale was found to be accurate within 0.5 of a gram. Table 3.2 gives the actual weight of the load carrier components as well as the set of weights used to apply the required tension.

Part and nominal weight kg	Actual weight kg
0.500 mark I	0.494
0.500 mark II	0.501
1.000	0.989
2.000 mark I	2.004
2.000 mark II	2.045
Top part of carrier	0.789
Middle and bottom parts) of the carrier )	1.217
End clamp	0.192

Table 3.2

Tension perturbation of known amplitudes and frequencies were provided by a wide frequency band electro-magnetic vibrator capable of producing a sine vector force of up to 178 N when directly coupled to the matching power amplifier unit. The specifications for both the vibrator and the power unit are given in Appendix (IV). To ensure the necessary alignment

between the load-carrier and the vibrator moving table the wave form of the current supplied to the vibrator, which is converted into mechanical force, as well as that of the load cell output signal were observed on an oscilloscope. Departure from a sine wave form is usually an indication of armature or suspension misalignment. It is also important not to exceed the maximum specified armature current. Therefore an ammeter was connected in series in the circuit to monitor the value of the current supplied to the vibrator armature.

### 3.3 INSTRUMENTATION

#### 3.3.1 PNEUMATIC NETWORK

Referring to Fig. 3.10 it can be seen that the pneumatic network consisted of: a compressor, a first stage pressure regulator with an outlet pressure gauge to monitor the regulated pressure, a fine grade filter, a second stage pressure regulator, a flowmeter, a measuring pad with the pressure transducer fitted in and a water manometer. The local compressor used had a maximum rating of  $100 \text{ lb/in}^2$  (about  $700 \text{ kN/m}^2$ ) which was far more than needed at any stage of the present work. The network was connected to the main air-line, fed by the compressor, through a connecting tube with snap action coupling at each end. Standard plastic connecting tubes were used in conjunction with standard air-line fittings to connect the different components of the pneumatic network. All of the components, except the pressure gauges and the flowmeter, were described earlier (3.2.4).

Dial indicator Bourdon-tube pressure gauges of suitable pressure ranges were used to monitor regulated pressures from the first stage pressure regulator as well as the supply pressure inside the air bearings used to support the web. Since the supply pressure required inside the measuring pad was comparatively small, a water manometer was used to monitor it. The water manometer used could be read to an accuracy of 1mm water ( $9.81 \text{ N/m}^2 \equiv 1.42 \times 10^{-3} \text{ lb/in}^2$ ). Another water manometer was used to measure the static pressure in the air film balancing the tension in the web traversing the sintered segment of the measuring pad. Mercury

column, which can be read to an accuracy of  $0.7 \text{ kN/m}^2$  ( $0.1 \text{ lb/in}^2$ ), was used to determine the pressure profile in the air gap across the web traversing the sintered cylinder (refer to 3.2.2.).

As for the rate of air flow through the sintered material, either of the sintered cylinder or the measuring pad, it was measured on an in-line "Flowbits" gap-meter placed in the air supply line prior to either the cylinder or the pad. The flow-meter outlet pressure was measured to determine the rate of air flow at standard conditions.

### 3.3.2 HUYCK TENSOMETER

The huyck tensometer is a commercially available device, made by Huyck Corporation of U.S.A., for web-tension measurements. The tensometer used is a portable, hand-held device which operates on a mechanical basis. The operation is based on the principle that the amount of deflection of a flexible membrane under load is dependent upon the tensile stress in the membrane. The load is provided by an internal spring, and the amount of web deflection is measured by a dial indicator. When using the instrument to measure the tension in a web wider than the width of the so called "picture frame" of the tensometer, which is usually the case, calibration tables must be used. The calibration differs according to the elastic properties of the material of the web under consideration, and the dial indicator readings are converted to web tension in kg. per cm of web width. The range of the tension to be measured with the instrument used is 0.88 to 4.4 kN/m (5 to 25 lb/in). Fig. 3.13 shows the Huyck Tensometer with its overall dimensions.

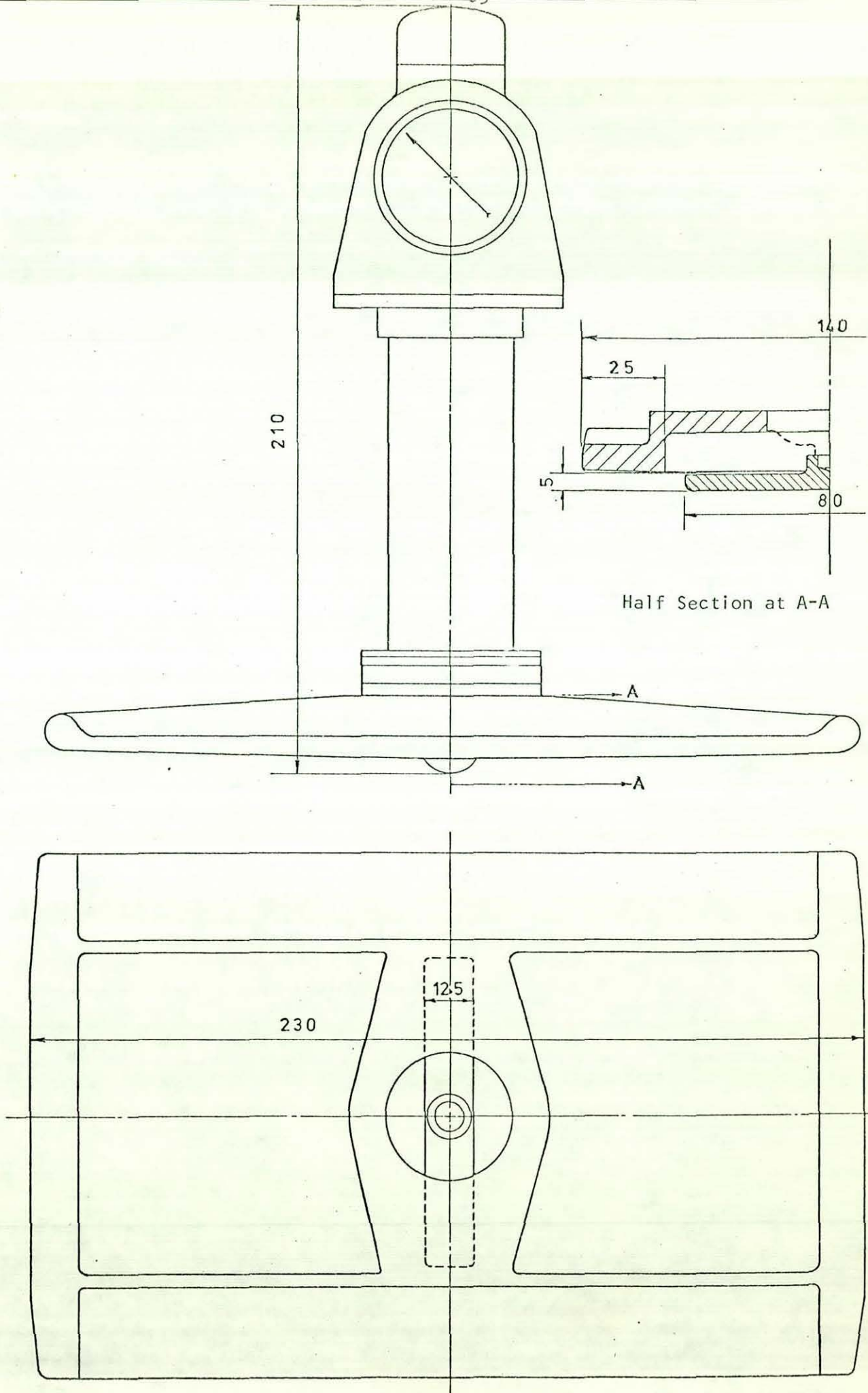


Fig. 3.13 The Huyck Tensometer

### 3.3.3 REFERENCE LOAD-CELL

As the main objective of this research is to develop a web-tension measuring technique based on an electro-pneumatic principle, the performance of the measuring device developed would have, by necessity, to be evaluated by reference to a suitable standard. Since the developed device is intended to measure dynamic tension perturbation at relatively high frequencies, a "KISTLER" load-cell of high frequency response and suitable mounting features appeared to be a favourite choice for acting as a reference standard.

The load-cell used is a quartz force transducer that, when subjected to a compressive load, develops an electrostatic negative charge which is proportional to the force applied, a tensile load results in a positive charge. The electrostatic charge given out by the load-cell (pC) is converted in a charge amplifier into a proportional voltage (mV), which could be read off the charge amplifier meter, displayed on an oscilloscope and recorded on a chart recorder. As negative charges result in positive voltages at the charge amplifier output an inverting amplifier of unity gain was used to reverse the polarity of the charge amplifier output signal.

The technical data of the load-cell used is given in appendix (IV). Fig. 3.14 shows the basic circuit used with the load-cell. The load-cell mounted in the adapter was shown earlier in Fig.3.11.

### 3.3.4 "KISTLER" LOW PRESSURE TRANSDUCER

For the purpose of conducting preliminary experiments to measure the dynamic variation of pressure in the air gap between the web and the sintered cylinder (as a result of applying a sinusoidal

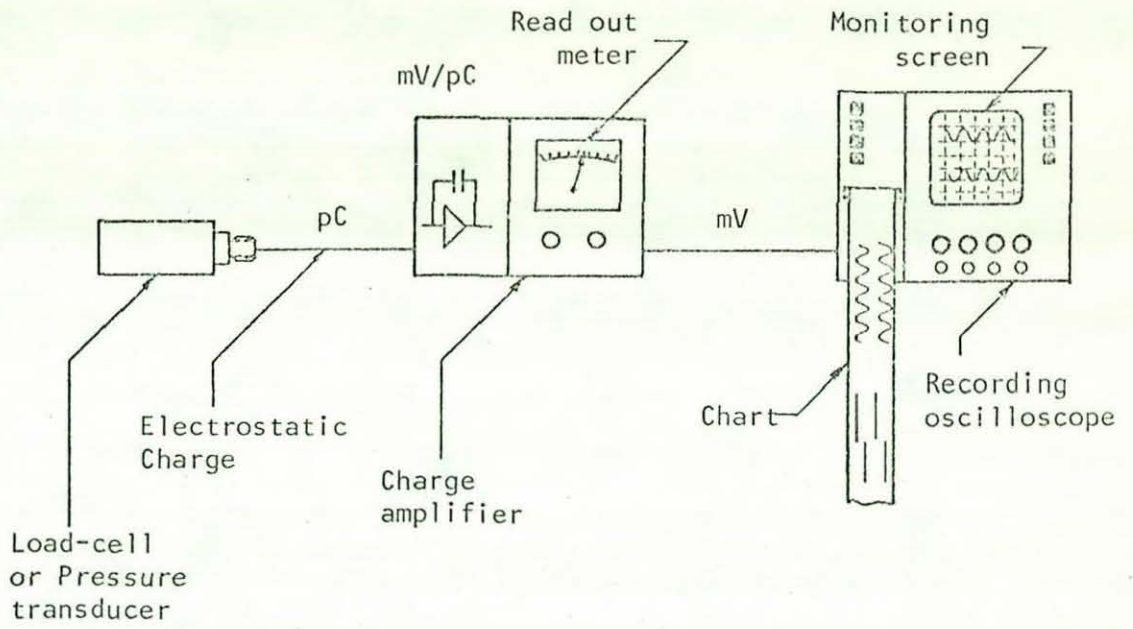


Fig. 3.14 Basic circuit for a piezo-electric measuring system

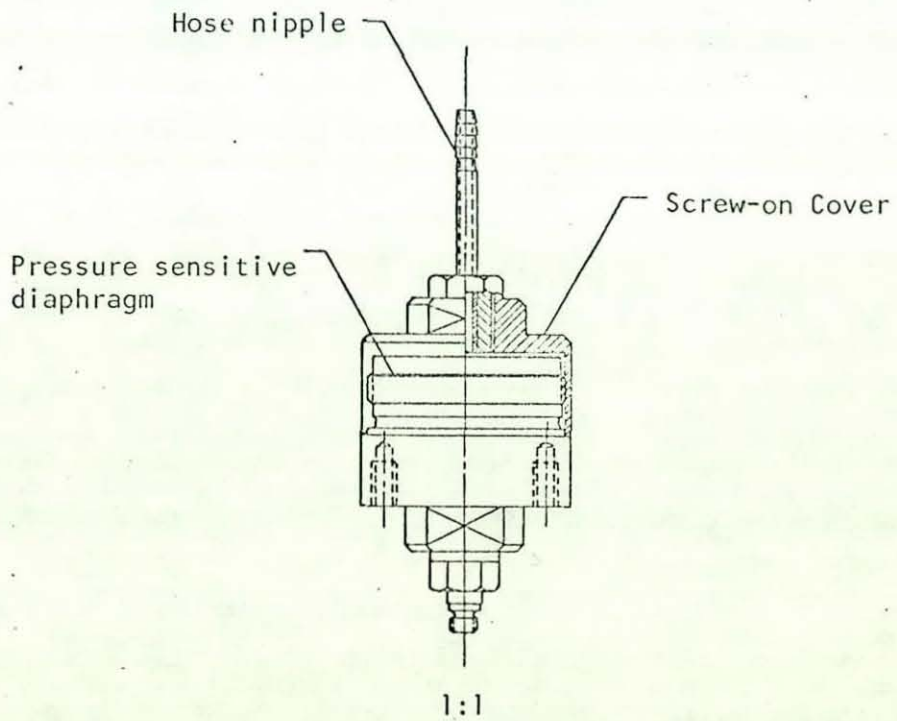


Fig. 3.15 Low pressure quartz transducer



force to the web, the pilot tube inserted into the cylinder wall (refer to 3.2.2.) was connected to a "KISTLER" pressure transducer. The transducer used was a low pressure quartz transducer for dynamic and short term static pressure from vacuum to 10 atmosphere. The measured pressure acts through a diaphragm on the quartz crystal measuring element which transforms the pressure into an electrostatic charge in the same manner as in the case of the load cell.

It can be seen from Fig. 3.15 that the transducer could be used with or without the screw-on cover and the hose nipple. Due to the large size of the transducer, it was placed outside the sintered cylinder with the cover and the hose nipple connected to the pilot tube. A similar charge amplifier to that used with the load-cell was used to transform the electrostatic charge from the transducer to voltage output.

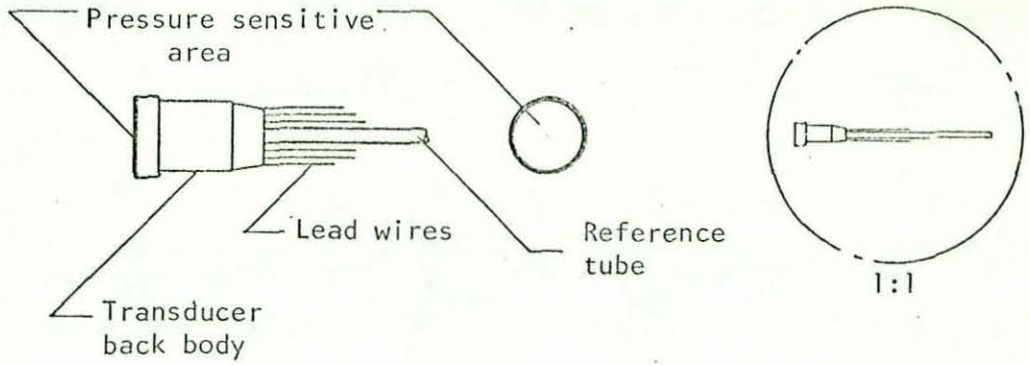
### 3.3.5 MINIATURE PRESSURE TRANSDUCER

Using the "KISTLER" pressure transducer (with the sintered cylinder) for preliminary assessment of the performance of the web-tension measuring technique, it became evident that a high frequency response, low pressure measuring range, minimum size are the primary requirements of the transducer to be used. For that, a miniature pressure transducer of 0 to  $100 \text{ kN/m}^2$  (0 to  $15 \text{ lb/in}^2$ ) range and 60 kHz resonant frequency was chosen. It is one of the piezo-resistive type transducers which combines a fully active semi-conductor Wheatstone bridge. Its semi-conductor circuitry is compensated for temperature changes in the environment and includes thermal sensitivity compensation as a standard specification. Thermal compensation is

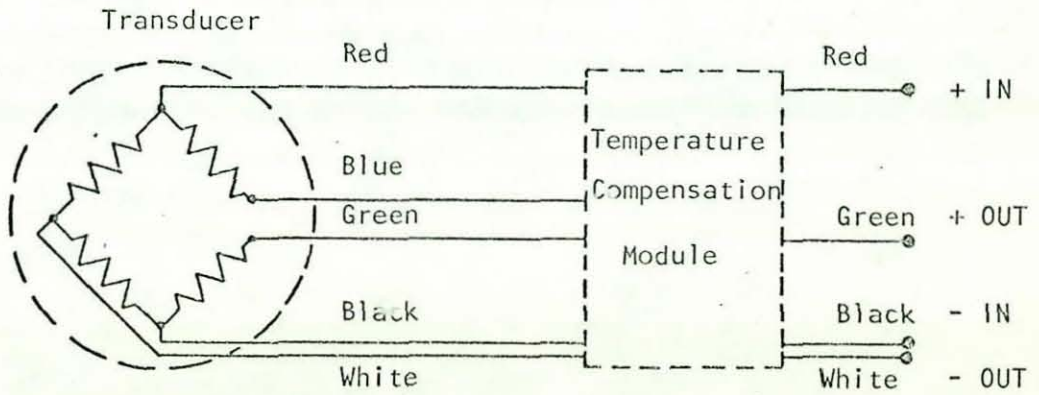
available either internal or external to the transducer. The external compensation type was used to get the minimum overall size of the transducer itself. The transducer is supplied with 0.6 m (2 feet) of teflon coated lead wire. The compensation module is located 0.450 m (18 in) from the transducer. The module is encapsulated with shrink tubing and has a diameter of 2.5mm (0.1in). Fig. 3.16(a) shows the transducer with its overall dimensions while (b) shows the basic circuit. As for the mounting details of the transducer, into the adapter made to be fitted into the measuring pad active surface wall, it was shown earlier in Fig. 3.8.

Although the transducer is a differential pressure one, it was used to measure gauge pressure by connecting its reference tube to the atmosphere via a plastic tube through a hole drilled into the wall of the measuring pad box.

A unit combining a mains stabilised DC power supply with balance facilities to cope with up to four wire bridge connections was used in the transducer circuitry. Since the output signal level of the transducer is comparatively small (1.94 mV/psi) a DC pre-amplifier was used prior to the read out system. For static pressure measurements the output signal from the pre-amplifier was read off a digital voltmeter. The technical data of the transducer used and its supporting instrumentation in the circuitry are given in Appendix (iv).



(a) The transducer



(b) The Circuit

Fig. 3.16 The miniature pressure transducer and the Wheatstone bridge associated with it.

### 3.3.6 RECORDING OSCILLOSCOPE

To monitor and record the output signals from each of the vibrator (representing the current supplied which is converted into mechanical sinusoidal force), the load cell (acting as a reference standard to measure the applied dynamic force by the vibrator) and the pressure transducer (which is the sensing element of the developed measuring pad under test), a 4 channel recording oscilloscope was used. It is a fibre-optic recording oscilloscope with a monitor tube to display the signals out of up to 4 sources even whilst a recording is being made. The monitor screen is always visible and provides an exact duplicate of the image being recorded. The recording oscilloscope used is of the type M-scope For-4, made by Medelec Ltd.

## CHAPTER FOUR

SCHEME AND PROCEDURE OF EXPERIMENTAL WORK

#### 4.1 INTRODUCTION

As the present investigation is directed primarily to give a better understanding of the limitations of the existing web-tension measuring techniques and to seek possible ways of improving their accuracy and dynamic response, the experimental scheme was laid down to serve this purpose. Experimental work was divided into three main phases.

In the first phase, three techniques were investigated for static limitations as well as the effect of various parameters associated with web-tension measurements on their accuracy. The three techniques were based on: a mechanical principle such as the Huyck Tensometer, a pneumatic system utilising the concept of an externally pressurised foil bearing such as the sintered turner bar (referred to in this thesis as the sintered measuring cylinder) and an electro-pneumatic technique, which has been developed during the course of this investigation, based on the same concept but using a pressure transducer as the sensing element of the system such as the measuring pad.

In the second phase, the last technique was investigated with a stationary web for dynamic limitations. The accuracy of the measuring device as well as the dynamic response of its sensing element were the main criteria to be investigated.

As for the last phase, concerning the analysis of the evaluation of the performance of the developed measuring pad on running webs at high speed, the main frame with the described components of the test was used to provide a closed loop of the running web under consideration. The response of the measuring pad to tension variation in the web at different running speeds was monitored and recorded.

## 4.2 STATIC TESTS

The static tests were carried out with the web fixed at one end while the other end was subjected to the desired prescribed static load. The load was always applied via the load-carrier described in 3.2.6. Three techniques; namely the mechanical, pneumatic and electro-pneumatic techniques were used to measure the applied known tension in the web. The objective of the tests was to evaluate experimentally, the static limitations and accuracy of those techniques.

### 4.2.1 THE HUYCK TENSOMETER

The web used was a Melinex film. It was fastened to a fixed roller at one end while the other end was coupled to the load-carrier via end clamps similar to those described in 3.2.7. A calibrated set of dead weights was used to provide the desired tension in the web.

The pointer of the dial indicator of the instrument was set to zero prior to every measurement. With the longer side of the instrument frame orientated in the longitudinal direction of the web, the tensometer (held by hand) was pressed slowly against the web until the pointer of the indicator stopped. The instrument was then removed and the dial reading was taken. At every applied load five readings were taken and their mean value was recorded. Fig. 4.1 shows the experimental set up diagrammatically.

The test conditions were as follows:

Web material	Melinex
Web width	260mm
Web thickness	51 $\mu$ m
Range of applied tension	0.39 - 2.06 kN/m

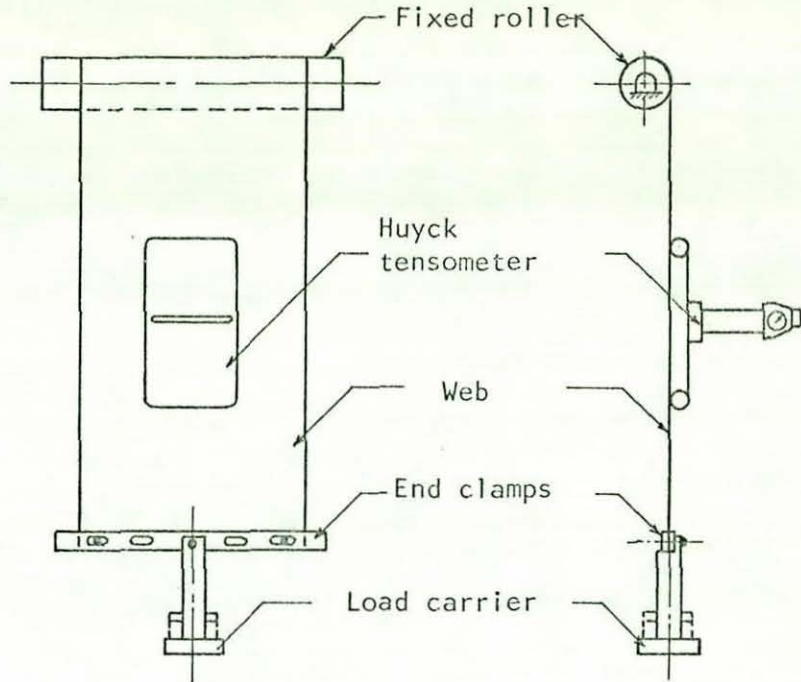


Fig. 4.1 Diagrammatic sketch of the Huyck tensometer set up

#### 4.2.2 THE SINTERED MEASURING CYLINDER:

Two possible ways in which a sintered turner bar was made into a web-tension measuring cylinder were described earlier in 3.2.2. Preliminary static tests to check experimentally the validity of the relationship  $p = \frac{T}{r}$ , where (T) is the tension in the web, (r) is the outer radius of the measuring cylinder and (p) is the pressure in the air film supporting the web (refer to 2.3), were carried out on both designs; the sintered bronze cylinder and the sintered stainless steel cylinder. These tests showed identical results under the same experimental conditions. Hence, for practical considerations mentioned earlier in 3.2.2., it was decided to carry out the experimental work in this phase on the sintered stainless steel cylinder only.



1 - Validity of  $p = \frac{T}{r}$

The theoretical relation was checked, experimentally, using two webs of the same material but with different widths and thicknesses. The experimental set up is shown in Fig. 3.3(b) and Plate 3.1. A mercury manometer, which could be read to an accuracy of  $0.7 \text{ kN/m}^2$  was used to measure the pressure ( $p$ ), in the air gap between the web and the measuring cylinder, balancing the applied tension. It has been shown earlier (2.3) that the supply pressure ( $P$ ) to the measuring cylinder must be greater or at least equal to  $1.5 (p)$ . In this set of experiments the effect of supply pressure was investigated. This was achieved by supplying the measuring cylinder with either a pressure proportional to the applied tension ( $P_v = kp$ ) or a constant pressure corresponding to the maximum applied tension throughout the experiment ( $P_c = kp_{\max}$ , where  $k$  is a constant = 1.5, 2 or 3 and  $p_{\max} = T_{\max}/r$ ).

The test conditions were as follows:

Material of web used	Melinex
(i) For web thickness	51 $\mu\text{m}$
Web width	50mm
Variable supply pressure	$P_v = 1.5, 2 \text{ and } 3 p$
Constant supply pressure	$P_c = 1.5, 2 \text{ and } 3 p_{\max}$
(ii) For web thickness	102 $\mu\text{m}$
Web width	50, 102 and 260mm
Variable supply pressure	$P_v = 1.5, 2 \text{ and } 3 p$
Constant supply pressure	$P_c = 1.5, 2 \text{ and } 3 p_{\max}$

## 2 - Tension profile

The measuring cylinder was used to measure the tension across the web. This was achieved by the use of a sliding sleeve arrangement to which one end of the web was fixed while the other end was coupled to the load-carrier. The experimental set up for these experiments was shown diagrammatically in Fig. 3.3(a) and in detail in Fig. 3.6. The same mercury manometer, previously mentioned, was used to measure the pressure in the air gap.

Two Melinex webs of the same width, but with different thicknesses, were subjected each to two values of tension whereby the tension profile across each was determined. A third Melinex web of different width was dealt with in the same manner. A similar experiment was carried out on a steel web. Table 4.1 summarises the test conditions.

Web Material	Web width mm	Web thickness $\mu\text{m}$
Melinex	50	51 102
	102	102
Steel	102	51

TABLE 4.1

#### 4.2.3 THE MEASURING PAD

The web-tension measuring pad developed during the course of the present work was described in detail in 3.2.3. In the case of the measuring cylinder, the wrap angle of the web around the cylinder was determined by the experimental set up configuration ( $90^{\circ}$ ). As for the measuring pad, the wrap angle is determined by the distance it moves against the web; the radius of curvature of the pad being constant. Hence, to determine the wrap angle a set of experiments was carried out on the measuring pad. The experimental set up is shown in Plate 4.1.

##### 1 - Validity of $p = \frac{T}{R}$

The same procedure, as in 4.2.2-1, was followed. Since the pressure in the air gap was much smaller than that when using the measuring cylinder, a water manometer, which could be read to an accuracy of 1mm water ( $9.81 \text{ N/m}^2$ ), was used to measure the pressure.

The test conditions were as follows:

- (i) For Melinex web of thickness  $51\mu\text{m}$ 
  - Web width  $50\text{mm}$
  - Variable supply pressure  $P_v = 1.5, 2 \text{ and } 3 p$
  - Constant supply pressure  $P_c = 1.5, 2 \text{ and } 3 p_{\text{max}}$
  
- (ii) For Melinex web of thickness  $102\mu\text{m}$ 
  - Web width  $50, 102 \text{ and } 260\text{mm}$
  - Variable supply pressure  $P_v = 1.5, 2 \text{ and } 3 p$
  - Constant supply pressure  $P_c = 1.5, 2 \text{ and } 3 p_{\text{max}}$

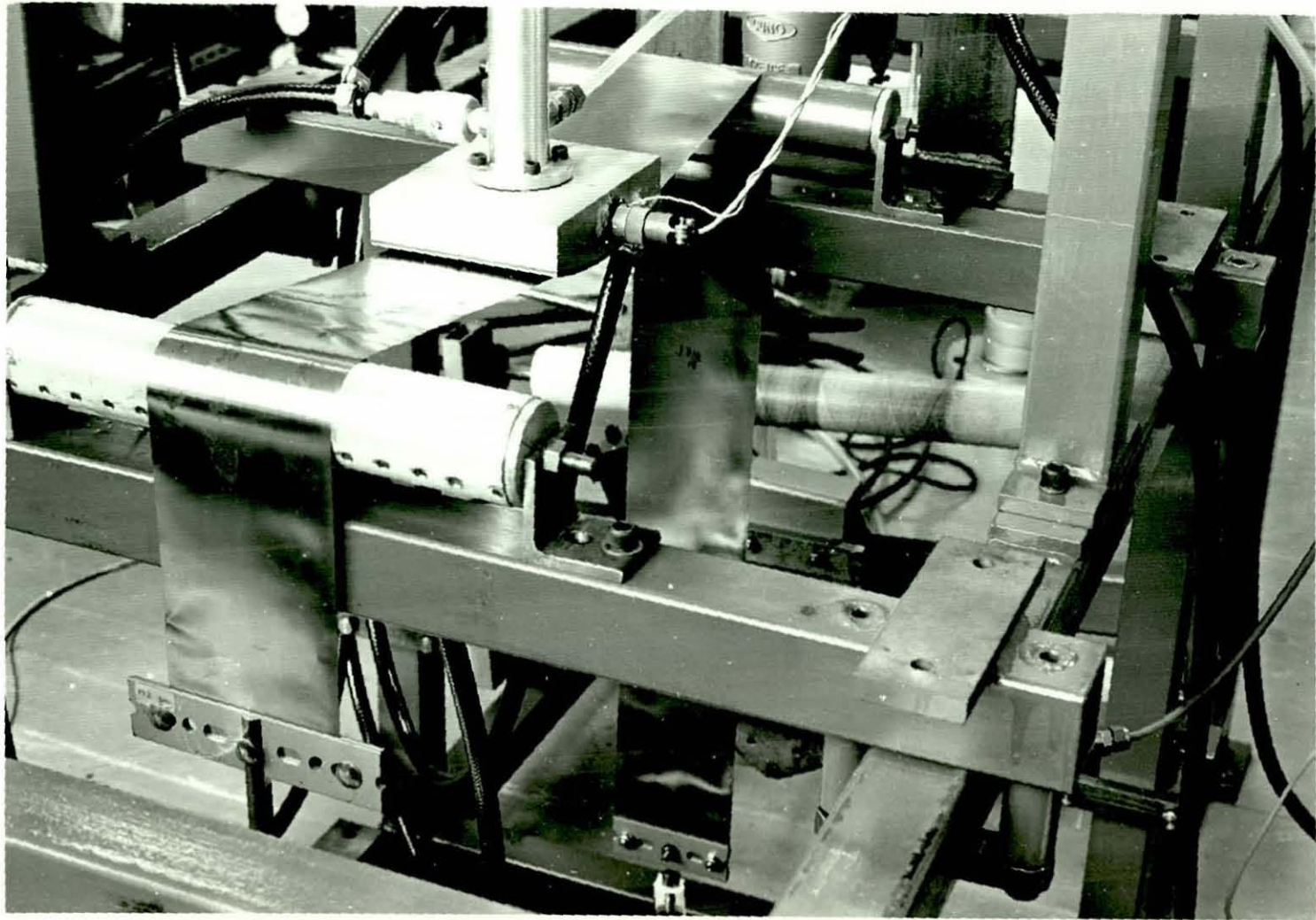


PLATE 4.1 EXPERIMENTAL SET UP FOR STATIC TESTS

2 - Tension profile

The sliding sleeve arrangement used in 4.2.2-2 was also used to determine the tension profile across two webs of different materials using the web-tension measuring pad. Table 4.2 summarises the test conditions:

Web width mm	Average tension applied kN/m	Web material	Web thickness $\mu\text{m}$
50	0.214 and 0.452	Melinex	102
		Steel	51

TABLE 4.2

3 - Optimum wrap angle

The web under consideration was subjected to a certain tensile force via the load-carrier while the measuring pad was away from the web. The measuring pad was then pushed against the web to prescribed distances controlled by the spring-loaded micrometer arrangement (refer to 3.2.3). The pressure in the air gap between the pad active surface and the web was monitored at each corresponding distance moved by the pad. A water manometer was used to measure the pressure in the air gap. The distance after which the measured pressure ceased to vary determines the optimum wrap angle. Table 4.3 gives the test conditions.

Web Material		Melinex
Web width mm	Web thickness $\mu\text{m}$	Range of applied tension kN/m
50	51 102	0.214 - 0.548
100	102	0.221 - 0.413
260		0.103 - 0.312

TABLE 4.3

4 - Optimum position of the pressure transducer

At one stage of the experimental work a miniature pressure transducer was embedded into the wall of the sintered segment of the measuring pad. When the transducer pressure sensitive diaphragm was flush with the active surface of the measuring pad, the output showed an intolerable instability and inaccuracy. Therefore a series of tests were designed to determine, experimentally, the optimum position of the transducer relative to the active surface of the measuring pad which would give both accurate and stable output.

This was achieved in two stages. In the first, the plastic pilot-tube, fitted into the wall of the sintered segment of the measuring pad, was connected via a T-junction outside the pad box to both the transducer and a water manometer through equal lengths of plastic tube. In this way the known applied tension in the



Table 4.4 gives the test conditions with an illustrative sketch of the experimental set up for each stage.

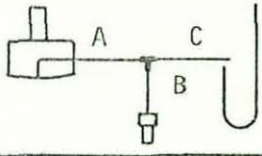
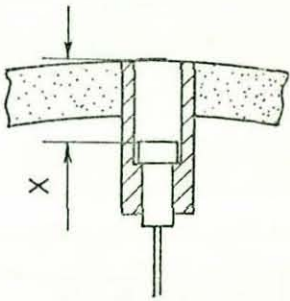
Stage	Tension range kN/m	Expt. No.	Length of tubes mm			Sketch
			A	B	C	
I	0 - 0.598	1	1000	2300	2300	
		2	10	50	2300	
II	0 - 0.598	Expt. No.	Transd. depth X (mm)			
		1	2.31			
		2	3.25			
		3	3.81			
		4	5.08			
		5	5.72			
		6	6.17			

TABLE 4.4



#### 4.3 DYNAMIC TESTS

In this phase the electro-pneumatic technique used for the web-tension measurements was investigated for accuracy and dynamic response on a stationary web. The web was coupled at one end to a load-cell which acted as a reference standard to measure the dynamic tension applied at the other end of the web by means of the electro-magnetic vibrator, described in 3.2.6, via the load-carrier. Plate 4.2 shows the experimental set up for this phase. It can be seen that the web in its course from the load-cell to the load-carrier (bolted to the vibrator) was supported and guided by frictionless air bearings to ensure that the applied tension at one end is transmitted through the web, without friction losses, to both the measuring device under test and the reference load-cell at the other end. The same set up was used, when the sintered measuring cylinder was under test, with the pad being moved away from the set up.

Some preliminary experiments were carried out on the sintered measuring cylinder. The pilot tube inserted into the cylinder wall (for static tests) was connected to the Kistler low pressure transducer which was placed outside the cylinder. As for the measuring pad, a miniature pressure transducer replaced the pilot tube. The device performance was then tested for accuracy and dynamic response with the transducer mounted flush with the pad active surface and when it was set at its optimum position from the surface as indicated in 4.2.3-4.

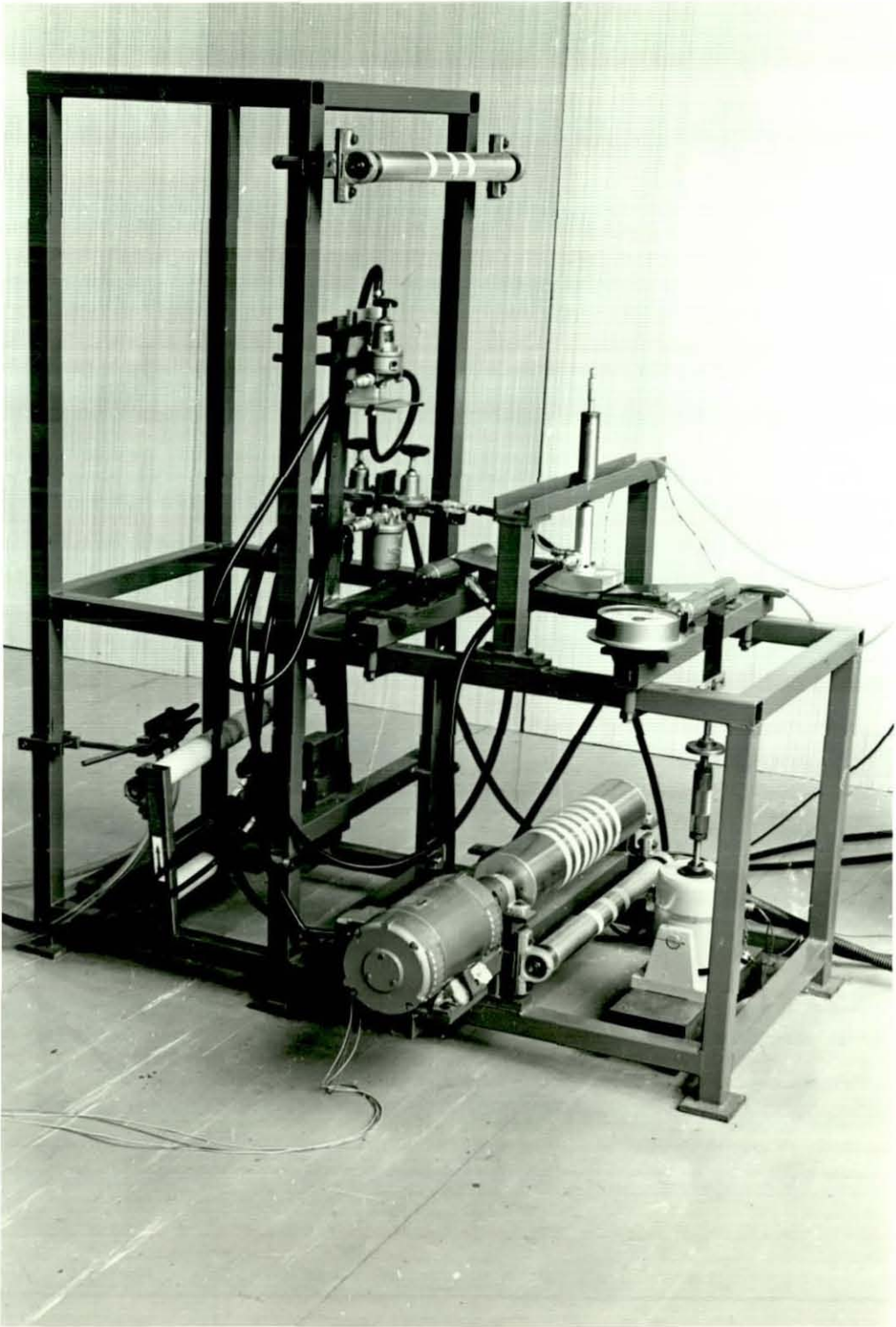


PLATE 4.2 EXPERIMENTAL SET UP FOR DYNAMIC TESTS

#### 4.3.1 PRELIMINARY TESTS ON MEASURING CYLINDER

The objective of the preliminary tests was to test the accuracy and response of the Kistler transducer to pressure variations, resulting from dynamic variations in tension, with reference to the load-cell. Tension perturbations of different known frequencies were provided by the electro-magnetic vibrator which is bolted to the load-carrier. The vibrator when connected to its matching power amplifier unit is capable of producing a sine vector force proportional to the current supplied to its moving coil. The produced force was monitored on the recording oscilloscope to ensure that it is not distorted from its true sinusoidal wave form. The load-cell, being the reference, was used to measure the applied dynamic force and to ensure that it was transmitted to the web with no distortion in its form and to monitor phase shift if it was there. The objective of the preliminary tests was achieved in two ways.

- (i) The vibrator was connected to its matching a.c. power supply unit and alternatively to a 6 V d.c. power supply as shown in Fig. 4.3.

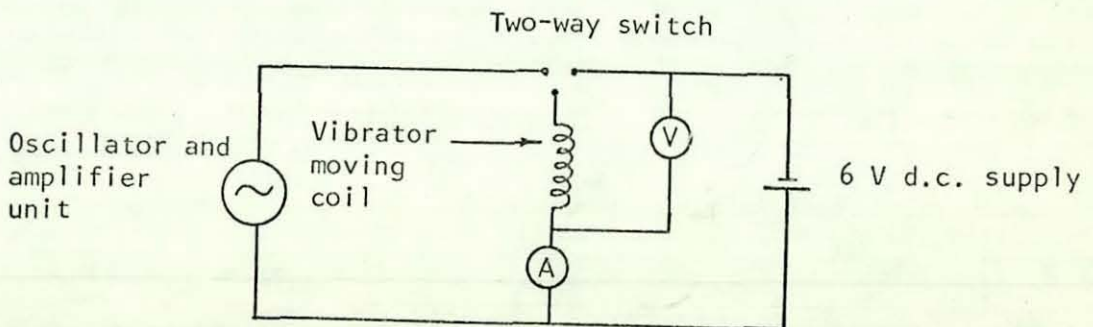


Fig. 4.3 Vibrator Circuit

When the moving coil is supplied with a direct current (i) a static force is produced which is proportional to (i). This force is measured by the transducer and the reference load cell. The output from the transducer is of the form of a step  $A_{\omega=0}$ , where  $\omega=0$  indicates that the force was applied at zero frequency and A is the amplitude of that force. Then the vibrator coil was supplied with the same value of (i) from the a.c. power supply unit at different frequencies. The resulting sinusoidal force was measured by the web-tension measuring pad and the load-cell. The output signal of both was recorded on the recorder chart. Fig. 4.4 shows a typical example of a record for this test.

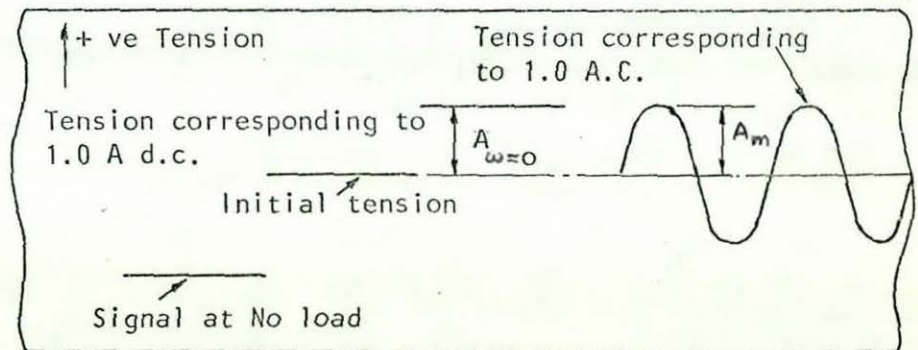


Fig. 4.4 Record of transducer output signal

The ratio  $A_m/A_{\omega=0}$  throughout the range of frequencies of the applied sinusoidal force was taken to determine the dynamic response of the web-tension measuring cylinder over the frequency range,  $A_m$  being the amplitude of the sinusoidal force as measured by the transducer.

The test conditions were as follows:

Web material	Melindex and Steel
Web width	102mm
Web thickness	51 $\mu$ m
Initial static tension	0.52 kN/m
Current supplied to the vibrator moving coil	(i) 1 A d.c. 1 A a.c.
Range of frequency	( $\omega$ ) 1.5-50 Hz

(ii) In this method the reference load-cell was used to ensure that a constant dynamic force was provided by the vibrator, irrespective of the current supplied to its moving coil, and transmitted to the web (via the load-carrier) throughout the frequency range. This dynamic force was measured by the load-cell and the transducer of the web-tension measuring cylinder at the same time, monitored and recorded on the recording oscilloscope. Fig. 4.5 shows an example of such a record.

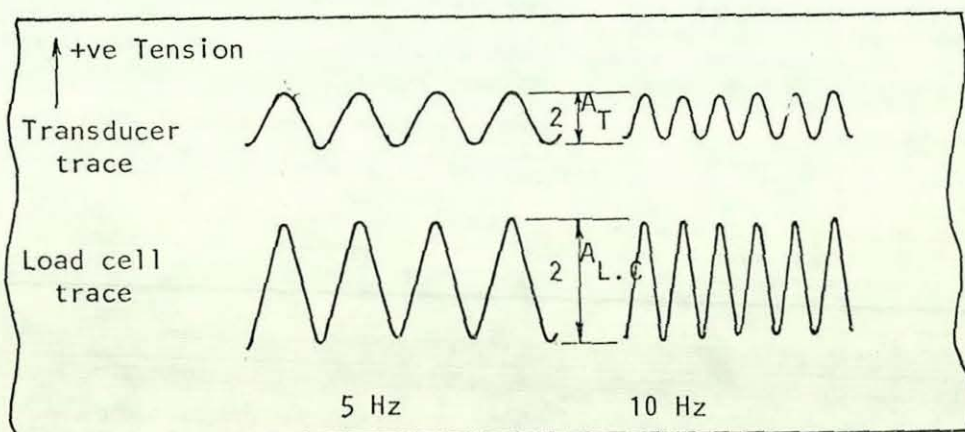


Fig. 4.5 Record of Transducer/Load-cell output

The ratio of the amplitude of the force measured by the transducer to that measured by the reference load-cell, which was kept constant, over the frequency range was taken to determine the dynamic response of the web-tension measuring cylinder.

The test conditions were as follows:

Web material	Steel
Web width	102 mm
Web thickness	51 $\mu$ m
Initial tension	0.52 kN/m
Frequency range	1.5 - 60 Hz

#### 4.3.2. TESTS ON THE MEASURING PAD WITH THE MINIATURE PRESSURE TRANSDUCER

The web-tension measuring pad was tested for dynamic response with the miniature pressure transducer, described earlier in 3.3.5, fitted flush with the outer surface of the sintered segment of the pad. The dynamic response of the device was again tested when the transducer was mounted within the appropriate adapter at its optimum stability position. The experimental set up is shown in Plate 4.2.

Test conditions were as follows:

i - Transducer flush with the surface

Web material	Melinex
Web width	102 mm
Web thickness	102 $\mu$ m
Initial tension	0.211 kN/m
Frequency range	1.5 - 80 Hz

ii - Transducer at optimum stability position

a - Melinex web

Web width	102 mm
Web thickness	102 $\mu\text{m}$
Initial tension	0.211, 0.307, 0.402 and 0.594 kN/m
Frequency range	1.5 - 80 Hz

b - Steel web

Web width	102 mm
Web thickness	51 $\mu\text{m}$
Initial tension	0.211 and 0.594 kN/m
Frequency range	1.5 - 80 Hz

#### 4.4 RUNNING WEB TESTS

Plate 4.3 shows the experimental set up for this phase of the work. Two Melinex films of different widths were used, one at a time, to form a continuous loop of running web. In both cases the two ends of the web were bonded together using a "Permabond" contact adhesive, resulting in an overlap joint. The adhesive used proved to stand a tensile force well beyond the initial tension applied to the web.

With the web-tension measuring pad located in position, the guide roller (marked A) in Plate 4.3 was pulled away from the pad until the required value of initial tension to be applied to the web was reached. This was determined by the output of the pad transducer monitored on the digital voltmeter. The guide roller unit was then secured in position. The closed loop of the web was moved at the required speed by means of the variable speed motor coupled to the main drive roller.

The tension perturbations, resulting from the interaction between the stiffness of the web and the inertia of the guide rollers, were measured by the web-tension measuring pad under test. The output signal was monitored and recorded on the recording oscilloscope.

Test conditions were as follows:

Web material	Melinex
Web thickness	102 $\mu$ m
Web width	102 and 260mm
Initial tension	0.354 kN/m
Running speed	1.22, 2.44, 3.66, 6.10 and 7.11 m/s



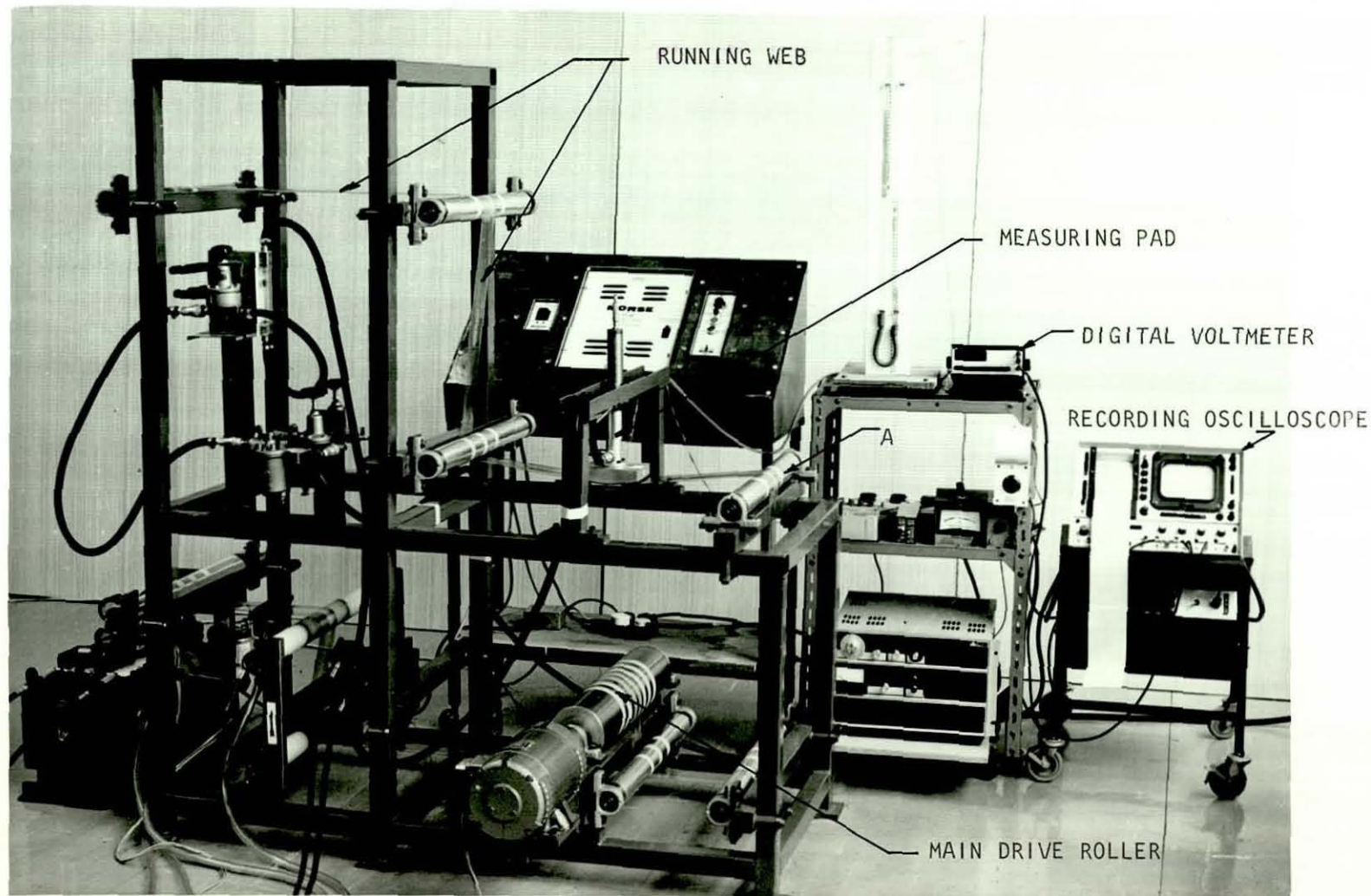


PLATE 4.3 EXPERIMENTAL SET UP FOR RUNNING WEB TESTS

CHAPTER FIVE

CALIBRATION OF INSTRUMENTS

## 5.1 INTRODUCTION

A summary of analytical formulation pertinent to the present study has been given in Chapter 2. A correlation of theoretical and of experimental results requires a knowledge of some, if not all, of the following quantities:

- t      Web thickness
- w      Web width
- K      "Stiffness" of web material (defined here as the product of the Modulus of Elasticity of the material and the cross-sectional area of the web under test, i.e.  
$$K = E.w.t.$$
- T      Tension in the web
- R      Radius of the measuring pad
- p      Pressure in the air film supporting the web

It has not been possible, of course, to determine each and everyone of the foregoing quantities to the same order of accuracy. However, each one of them was determined with the appropriate accuracy by the available means.

Throughout this investigation the main devices used for measurement and the corresponding parameters (shown between brackets) were: the web-tension measuring device (R), the miniature pressure transducer fitted into it as the sensing element of the device (p) and the reference load-cell (T). Another important element in each experimental set up, all the way through this study, was the web. Although not an instrument, the web properties can sometimes have a considerable effect on the dynamic behaviour of the system. Among those properties is the web stiffness.

Thus it can be seen that the source of measuring errors should, wherever possible, be determined and due allowances made for them in the measured quantity. For a start, the measuring instrument itself might give rise to different sources of errors due to the inaccuracies of manufacturing its elements. Since measurements are no more reliable than the devices used in making them, it is of vital importance, in the field of research, to commence with the calibration of the instruments used.

## 5.2 MEASUREMENT OF THE RADIUS OF CURVATURE OF THE MEASURING PAD

The radius of curvature of the measuring pad was measured, after its components were finally assembled, on the SIP universal measuring machine using a method based on that described by K.J. Hume and G.H. Sharp<sup>48</sup>. In their method, a surface plate, a straight edge, a set of slip gauges and a pair of standard rollers are used to determine the radius of curvature of a plate gauge of large radius. The same principle was used on the SIP machine. Fig. 5.1 shows the principle of the method described by Hume and Sharp whilst Fig. 5.2 shows the equivalent used in this calibration.

A locating indicator, with its arm set at a known radius about the vertical spindle of its holder, acted as the pair of standard rollers. The travel of the longitudinal carriage, from one point on the cylindrical segment of the pad ( $x_1$ ) to another point ( $x_2$ ) at the same y coordinate ( $y_1 = y_2$ ), determined the span along which the radius of curvature was measured ( $2e = x_2 - x_1$ ); the measuring pad being fixed to the carriage working table. As for the gap C, it was determined by the distance travelled by the locating indicator from the position  $y_1 = y_2$  to where it touched the apex of the cylindrical segment ( $y_0$ ) at the middle of the prescribed span.

The radius of curvature was measured along 6 parallel spans in the longitudinal direction of the measuring pad. The SIP machine scales could be read to an accuracy of  $1.25\mu\text{m}$ . The average value of the 6 measurements was taken as the radius of curvature of the measuring pad. A typical set of measurements is given below as an example:

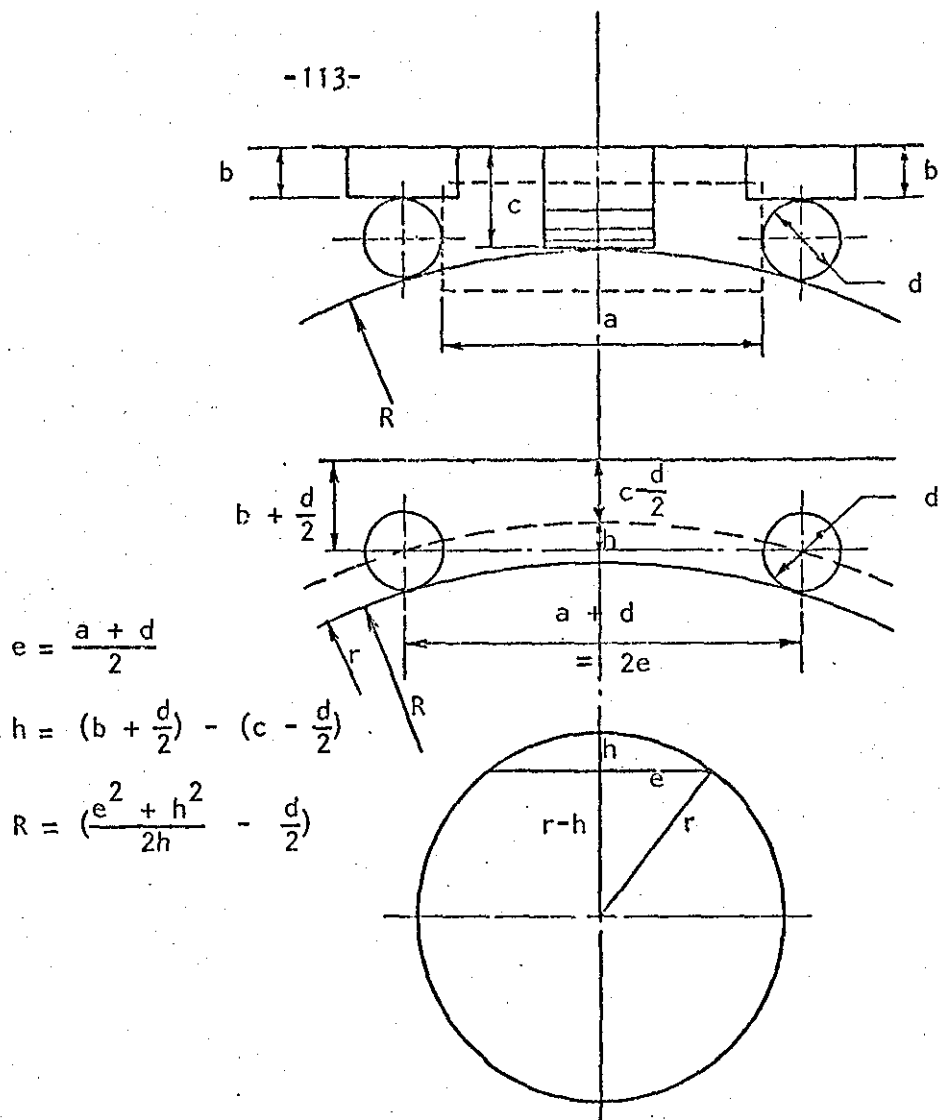


Fig. 5.1 Principle of the measurement method on a surface plate.

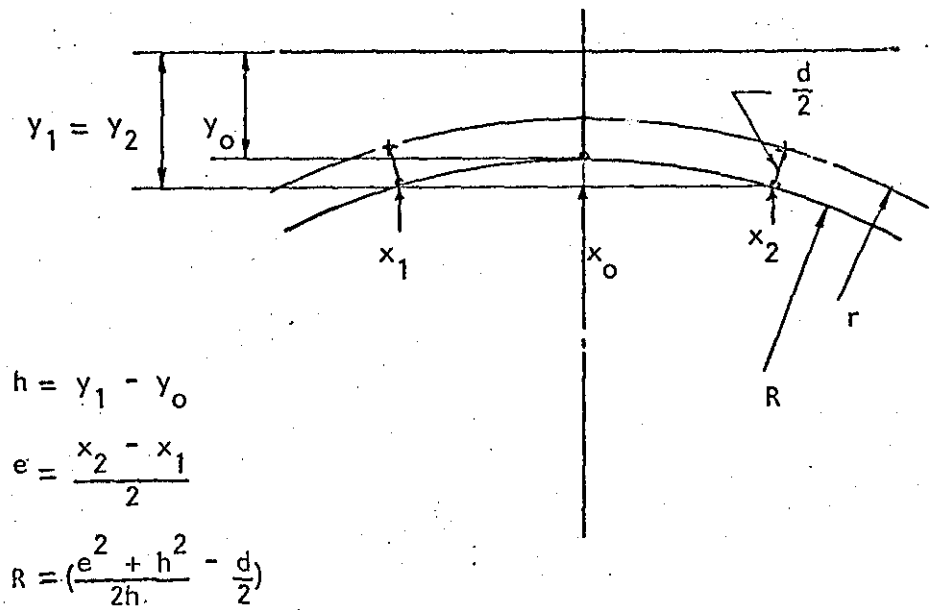


Fig. 5.2 Principle of the measurement method on the SIP machine

Mounting indicator set at a radius of 15.300mm

$$\left. \begin{aligned} x_2 &= 10.44908 \text{ in} = 265.407 \text{ mm} \\ x_1 &= 5.50000 \text{ in} = 139.700 \text{ mm} \end{aligned} \right\} \text{ at } y_1 = y_2 = 1.22154 \text{ in} \\ = 31.027 \text{ mm}$$

$$\begin{aligned} 2e &= x_2 - x_1 \\ &= 125.707 \text{ mm} \end{aligned}$$

$$e = 62.854 \text{ mm} (2.47454 \text{ in})$$

$$\begin{aligned} x_0 &= 202.554 \text{ mm} (7.97454 \text{ in}) \text{ at which } y_0 = 0.93452 \text{ in} \\ &= 23.737 \text{ mm} \end{aligned}$$

Referring to Figs. 5.1 and 5.2 we have

$$h = \left(b + \frac{d}{2}\right) - \left(c - \frac{d}{2}\right) = y_1 - y_0$$

$$r = \frac{e^2 + h^2}{2h}$$

$$R = r - \left(\frac{d}{2}\right), \text{ where } \frac{d}{2} \text{ is the radius at which the mounting indicator was set.}$$

Substituting in the foregoing equations with the corresponding measured quantities yields

$$R = \left[ \frac{(62.854)^2 + (7.290)^2}{2 \times 7.290} \right] - 15.300 = 259.307 \text{ mm}$$

The average value of six measurements was found to be:

$$\underline{\underline{R = 258.501 \text{ mm}}}$$

### 5.3 TRANSDUCER CALIBRATION

The miniature pressure transducer used was supplied with a calibration data sheet, a photocopy of which is included (Fig. 5.3). Since the transducer was the corner stone of the developed device, its calibration was of paramount importance. Therefore it was calibrated in two different ways; first on its own in a specially made adapter and second being fitted in position in the developed measuring pad.

(i) Calibration in the adapter:

Figure 5.4 shows the adapter made to accommodate the transducer to calibrate it. The applied pressure was measured by a water manometer which could be read to an accuracy of 1mm water ( $9.8 \text{ N/m}^2 = 1.42 \times 10^{-3} \text{ psi}$ ). Enough clearance was maintained around the periphery of the transducer cap to avoid any distortion that might happen to the diaphragm when mounted into the adapter. The transducer reference tube was open to the atmosphere. Silicon rubber sealant was used to seal the calibration adapter. The transducer was connected to a digital voltmeter via the pre-amplifier which was set to its maximum magnification range, namely 1000 times. With the digital voltmeter set at 2 mV range the transducer output could be read to an accuracy of 0.001 mV.

The result of the calibration proved the figure quoted by the manufacturers to be accurate as the measured sensitivity was found to be  $0.28 \text{ mV/kN.m}^{-2}$  (1.935 mV/psi). The plotted values in Fig.5.5 were the means of four sets of readings taken with both increasing and decreasing the applied pressure. It was found that, for any set of readings, either increasing or decreasing the supply



# Entran Devices, Inc.

## Pressure Calibration

PLEASE READ TRANSDUCER OPERATING INSTRUCTIONS BEFORE POWERING UNIT

Model No.: EPA-125E-15G Serial No.: 17L5A6-D3-1  
 Type: Miniature Pressure Transducer  
 Range: 15 psi g Overrange: 50 psi g  
 Recommended Excitation: 6.00 V DC or AC Max. Voltage: 8.00 V  
 Pressure Reference:  psia  psis  psig  psid  
 Operating Temperature Range: -40 °F to 250 °F  
 Compensated Temperature Range: 80 °F to 180 °F

CAUTION: DO NOT PRESS ON PRESSURE SENSITIVE AREA WITH SHARP OBJECT

### CALIBRATION DATA

Excitation: 6.000 V DC  
 Sensitivity: 1.94 mV/psi g at 77 °F  
 Zero Offset:          mV  
 Thermal Sensitivity Shift:          mV/100°F  $< \pm 2$  %/100°F  
 Thermal Zero Shift:          mV/100°F  $< \pm 3$  % FS/100°F  
 Combined Non-Linearity and Hysteresis:           $< \pm 1\%$  F.S.  
 Non-Linearity:          Hysteresis:           
 Repeatability:          Descriptive:           
 Descriptive:         

### WIRING

+ Input:  Red  Orange  Pin          + Output:  Green  Blue  Pin           
 - Input:  Black  Brown  Pin          - Output:  White  Yellow  Pin           
 Shield:  Pin          : : : :  
 Transducer Connector:          Mating Connector:         

Input Impedance 384 ohms

Output Impedance 230 ohms

Signature: *D.S.*

Date: 1/7/76

Form No. C002-1173

Fig. 5.3 A copy of the miniature pressure transducer calibration data sheet (supplied with it).

pressure, the repetition of the digital voltmeter readings was of the order of 0.003 mV. The plotted values in Fig. 5.5 are listed in Table 5.1.

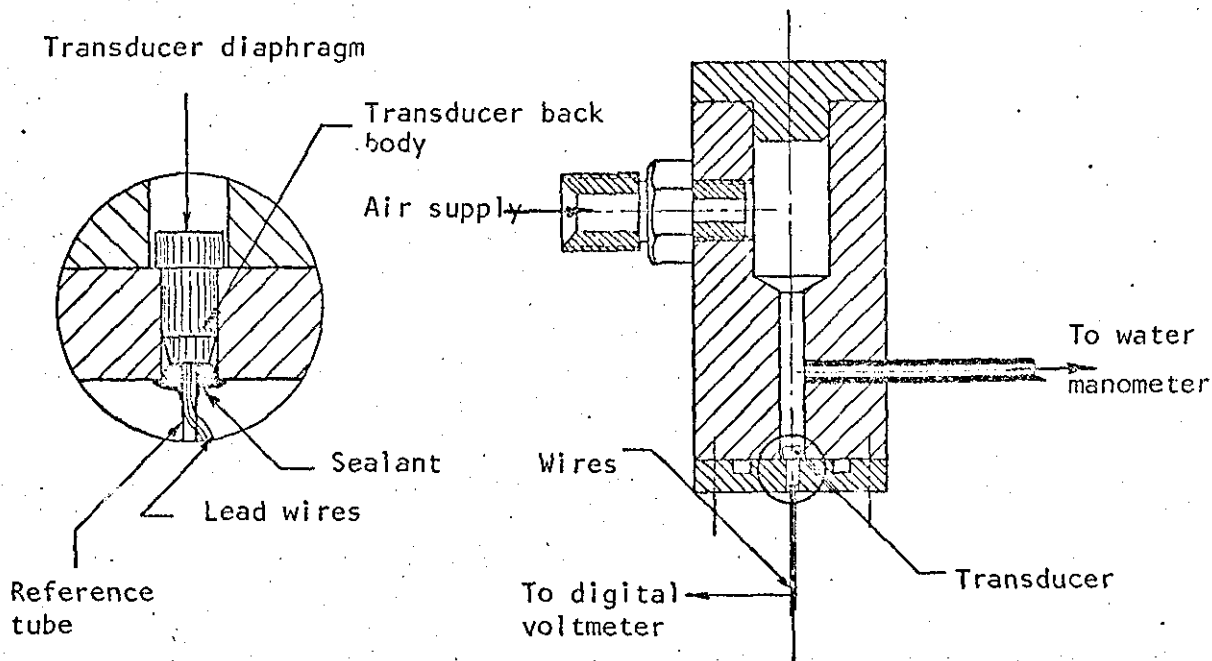


Figure 5.4 Calibration Adapter

(ii) Calibration in situ:

The second calibration was carried out with the transducer fitted in situ in the measuring pad at its optimum stable position. A Cap was made to fit the measuring pad box as shown in Fig. 5.6. The intention here was to provide closed chamber on top of the active surface area of the measuring pad. Once more, the silicon rubber sealant proved to be an adequate means to prevent leakage of air from the produced closed chamber. The cap had two ports, one for supplying the pressurised air and the other was connected to the water manometer to measure the applied pressure to which the transducer was subjected.

CALIBRATION OF THE MINIATURE PRESSURE TRANSDUCER  
IN THE ADAPTER

Applied pressure kN/m <sup>2</sup>	Transducer output mV
0.00	0.00
1.08	0.30
2.60	0.55
2.95	0.81
3.43	0.95
3.97	1.10
4.93	1.37
5.88	1.64
6.87	1.94
13.7	3.91
20.6	5.90
27.5	7.89

TABLE 5.1

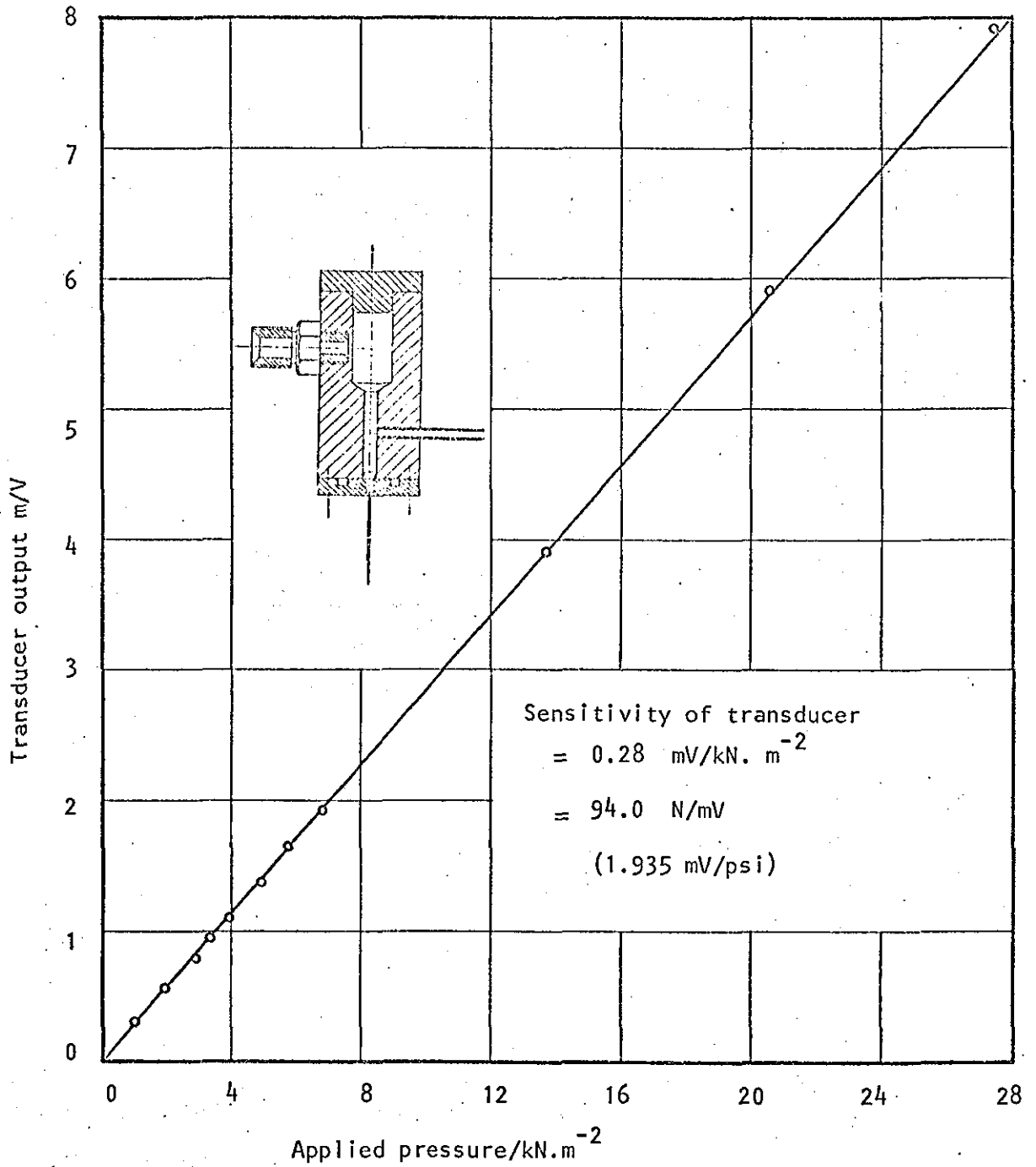


Fig. 5.5 Miniature transducer calibration curve using calibration adapter.

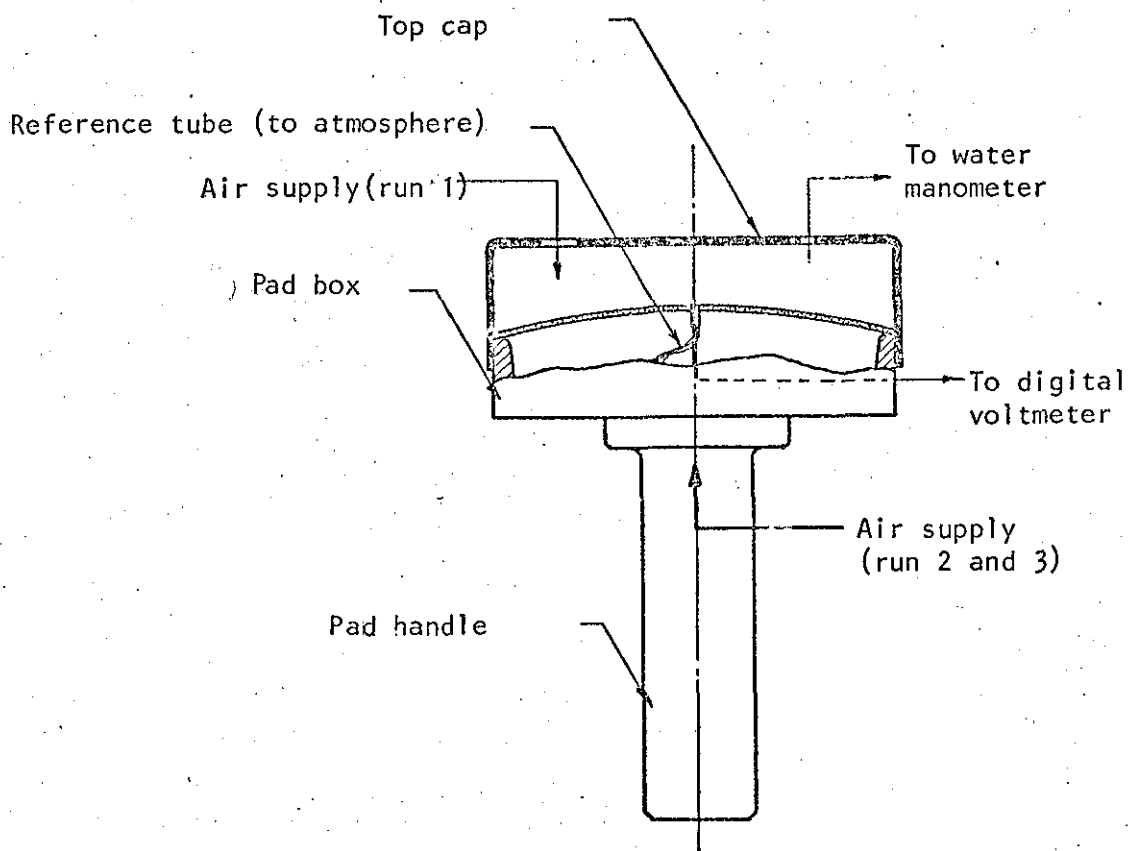


Fig. 5.6 Calibration arrangement for miniature transducer in situ

Three calibration runs have been made with the same procedure described in (i), except that the applied pressure range was limited to  $6.87 \text{ kN/m}^2$  ( $\approx 1 \text{ lb/in}^2$ ). However, this pressure range was more than the actual working range of the transducer throughout the experimental work.

In the first run the air was supplied to the closed chamber through the air supply port at the top of the cap shown in Fig. 5.6, whilst in the second and third runs pressurised air was supplied to the pad box through the port made in its handle as in the actual operating conditions (refer to Fig. 3.7). In the second run the air supply port at the top of the cap was closed

(no air flow through the system) whilst in the third run the port was opened resulting in an air flow to the atmosphere.

It can be seen, from the experimental values for Fig. 5.7 listed in Table 5.2, that there is no significant differences between the outcome of the three calibration runs. At the same time, Fig. 5.7 reveals, almost, a complete agreement with the result obtained when the transducer was calibrated in the adapter made for this purpose.

CALIBRATION OF MINIATURE TRANSDUCER

IN SITU

Applied pressure kN/m <sup>2</sup>	Transducer output*		
	Run 1	Run 2	Run 3
0.00	0.00	0.00	0.00
0.49	-	0.13	0.13
0.98	0.25	0.26	0.26
1.47	-	0.40	0.40
1.96	0.52	0.53	0.54
2.45	-	0.67	0.68
2.94	0.79	0.81	0.81
3.43	-	0.95	0.95
3.92	1.08	1.08	1.08
4.42	-	1.21	1.23
4.91	1.33	1.35	1.36
5.40	-	1.49	1.50
5.89	1.61	1.63	1.64
6.38	-	1.77	1.78
6.87	1.90	1.91	1.91

TABLE 5.2

- \* Run 1     Air supplied from the port at the top of the cap  
              (no air flow through the system)
  
- Run 2     Air supplied through the pad handle and the port  
              at the top of the cap closed (no air flow)
  
- Run 3     Air supplied as in Run 2 but the port in the cap  
              was open

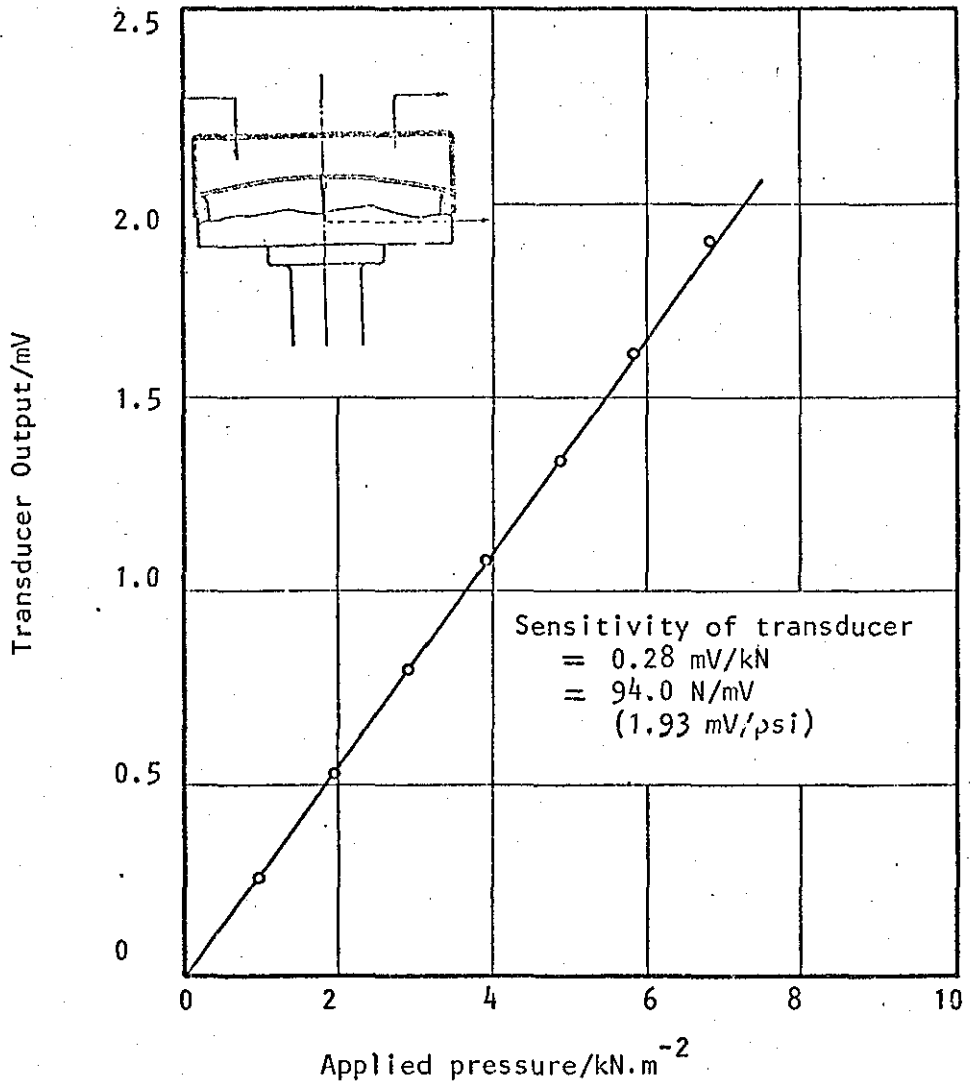


Fig. 5.7 Miniature transducer calibration in situ



#### 5.4. LOAD-CELL CALIBRATION

The load cell used was calibrated by the manufacturers and the calibration curve shown in Fig. 5.8 was supplied with it. The specified sensitivity in pC/kp together with known sensitivity of charge amplifier in mV/pC yields a known output sensitivity in mV/kp (1 kp = 1 kg force ; 1N = 0.102 kp).

However, since the load-cell was acting, in the experimental set up, as a standard reference for the measurement of the applied tension to the web, the need for recalibrating it against a proving ring was imperative. On top of that, the load-cell was calibrated once more under the working conditions, in the experimental set up, using a calibrated set of dead weights as a means of applying the tension to the web.

##### (i) Calibration against Proving ring:

The proving ring used was calibrated against a NPL certified proving ring. A photocopy of the certificate is included (Fig. 5.9). Fig. 5.10 shows the calibration set up. The proving ring bottom end was clamped to the table of a vertical milling machine with its axis in line with the centre line of the machine spindle. An adapter, made to accommodate the load-cell, was then screwed into the top end of the proving ring. The load was applied by the machine spindle via a spherical contact to ensure alignment of the applied load with both the load-cell and the proving ring axes.

The applied load was measured on the proving ring dial gauge and plotted against the measured load by the load-cell. The load-

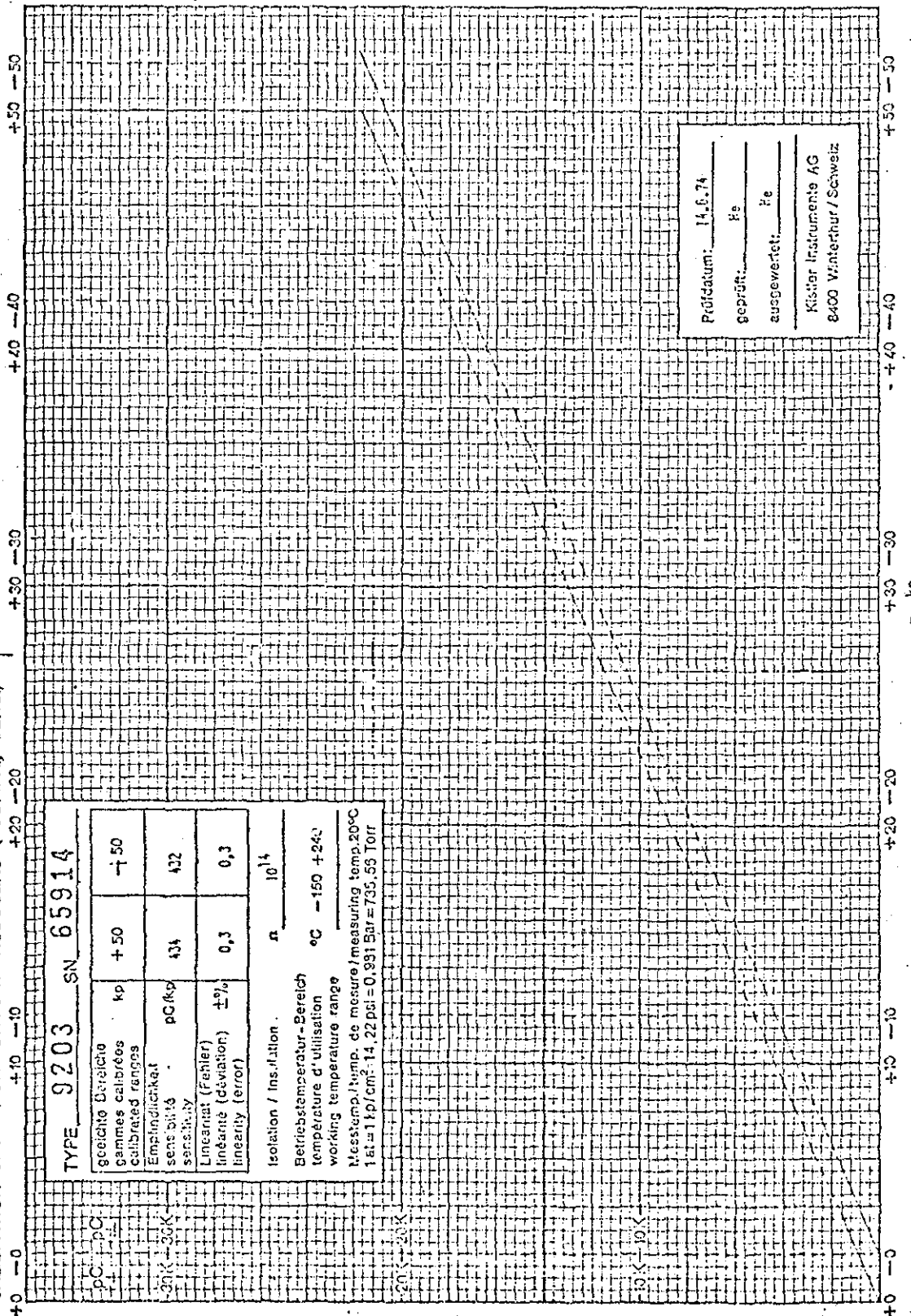
Type 9203

SN 65914

KISTLER

9201/9203-23  
Dr. 177

EICHELBLATT FÜR KRAFTAUFNEHMER (+DRUCK, -ZUG)  
FEUILLE DE CALIBRATION POUR CAPTEURS DE FORCE (+COMPR., -TRAC.)  
CALIBRATION SHEET FOR FORCE TRANSDUCERS (+COMPR., -TENS.)



TYPE 9203 SN 65914	
Speichle Bereiche gammes calibrées calibrated ranges	kp +50
Empfindlichkeit sensibilité	pC(kp) 434
Linearität (Fehler) linéarité (déviation) linearity (error)	±0,3
Isolation / Insulation	n 10 <sup>14</sup>
Betriebstemperatur-Bereich température d'utilisation working temperature range	°C -150 +240
Mess-temp./temp. de mesure / measuring temp. 20°C 1 st. = 1 kp/cm <sup>2</sup> = 14,22 psi = 0,991 Bar = 735,56 Torr	

Prüfdatum: 14.6.74  
geprüft: He  
ausgewertet: He  
Kistler Instrumente AG  
8400 Winterthur / Schweiz

Fig. 5.8 Calibration curve supplied with the reference Load-cell

# CERTIFICATE of CALIBRATION

200 lb Proving Ring No. 1527  
fitted with Dial Gauge No. 74462

LOAD ( lb )	DIAL GAUGE READING			
	TEST 1	TEST 2	TEST 3	AVERAGE
20	147	147	147	147
40	294	294	294	294
60	444	444	444	444
80	593	593	593	593
100	740	740	740	740
120	893	893	893	893
140	1041	1041	1041	1041
160	1193	1193	1193	1193
180	1343	1343	1343	1343
200	1502	1502	1502	1502

MEAN SENSITIVITY .1332 lb PER DIVISION

This proving ring has been calibrated in Compression at 62 °F against an NPL certified proving ring. It has been prestressed once to a 10% overload and three times to its maximum rated load.

Regular checking and recalibration ensure continued accuracy. We operate a 48-hour service at fixed prices.

Date of calibration  
1st October, 1962.

*J. T. ...*  
CHIEF ENGINEER



**Clockhouse Engineering Limited**

BROOKHILL ROAD · NEW BARNET · HERTFORDSHIRE · ENGLAND

Fig. 5.9 A copy of Calibration Certificate for the proving ring

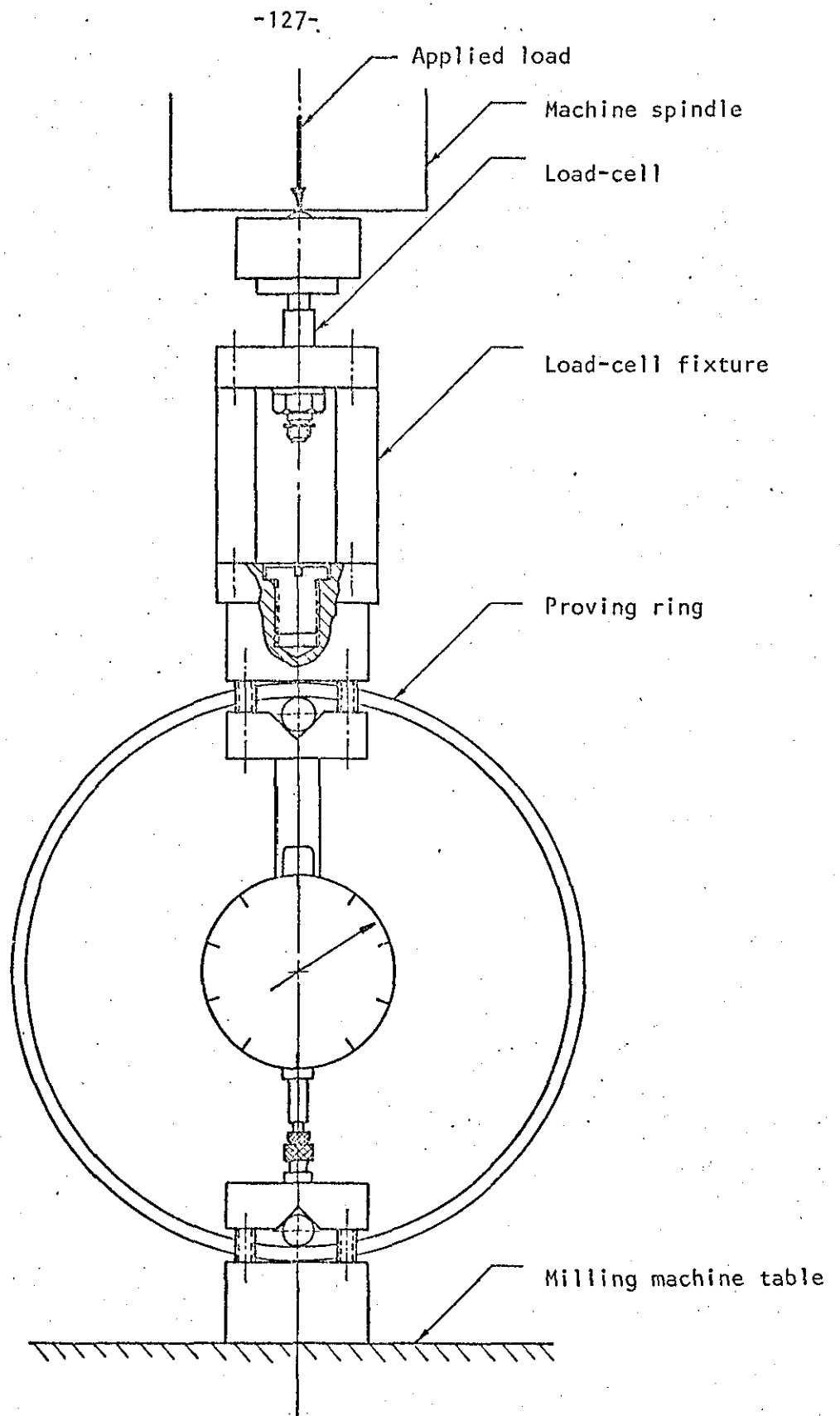


Fig. 5.10 Load-cell - Proving ring calibration set up

cell was connected to a charge amplifier which was set to the range and the resolution required to calibrate the load-cell over its maximum range (50 kp). The output from the load-cell was read off the charge amplifier meter. The sensitivity of the load-cell over this range was found to be 43.38 pC/N (425.5 pC/kp), a value which differs from that stated by the manufacturers by 1.7%.

(ii) Calibration in situ:

The second calibration was carried out under typical experimental conditions, i.e. with the load-cell in situ within the experimental set up as shown in Plate 3.1 and illustrated diagrammatically in Fig. 3.3-(b). Load was applied to the web at one end via the load-carrier using a calibrated set of dead weights while the other end of the web was fixed to the load-cell by means of the end clamps. Frictionless air bearings ensured virtual elimination of friction in the system so that the applied load at one end of the web is transmitted to the load-cell without friction losses.

The load-cell output in pC was read off the charge amplifier meter and plotted against the load applied as shown in Fig. 5.11. A record of the output signal of the amplifier was obtained using the recording oscilloscope and corresponding output in volts was plotted against the applied load as shown in Fig. 5.12. The sensitivity of the load-cell in situ was found to be 43.11 pC/N on the charge amplifier meter or 11.733N/V on the recorder chart. The 2mV/pC range on the charge amplifier was used throughout the experimental work. Table 5.3 gives the calibration results.

CALIBRATION OF THE LOAD-CELL IN SITU

Applied load	Load-cell output	
	On the meter	On the chart
N	pC	V
0.00	0.0	0.00
1.88	75.0	0.20
9.62	400.0	0.80
21.56	912.5	1.80
26.41	1137.5	2.23
31.32	1325.0	2.63
36.11	1550.0	3.05
41.03	1762.0	3.50
46.07	1975.0	3.90
50.98	2187.5	4.35
55.77	2400.0	4.75
60.68	2625.0	5.15

TABLE 5.3

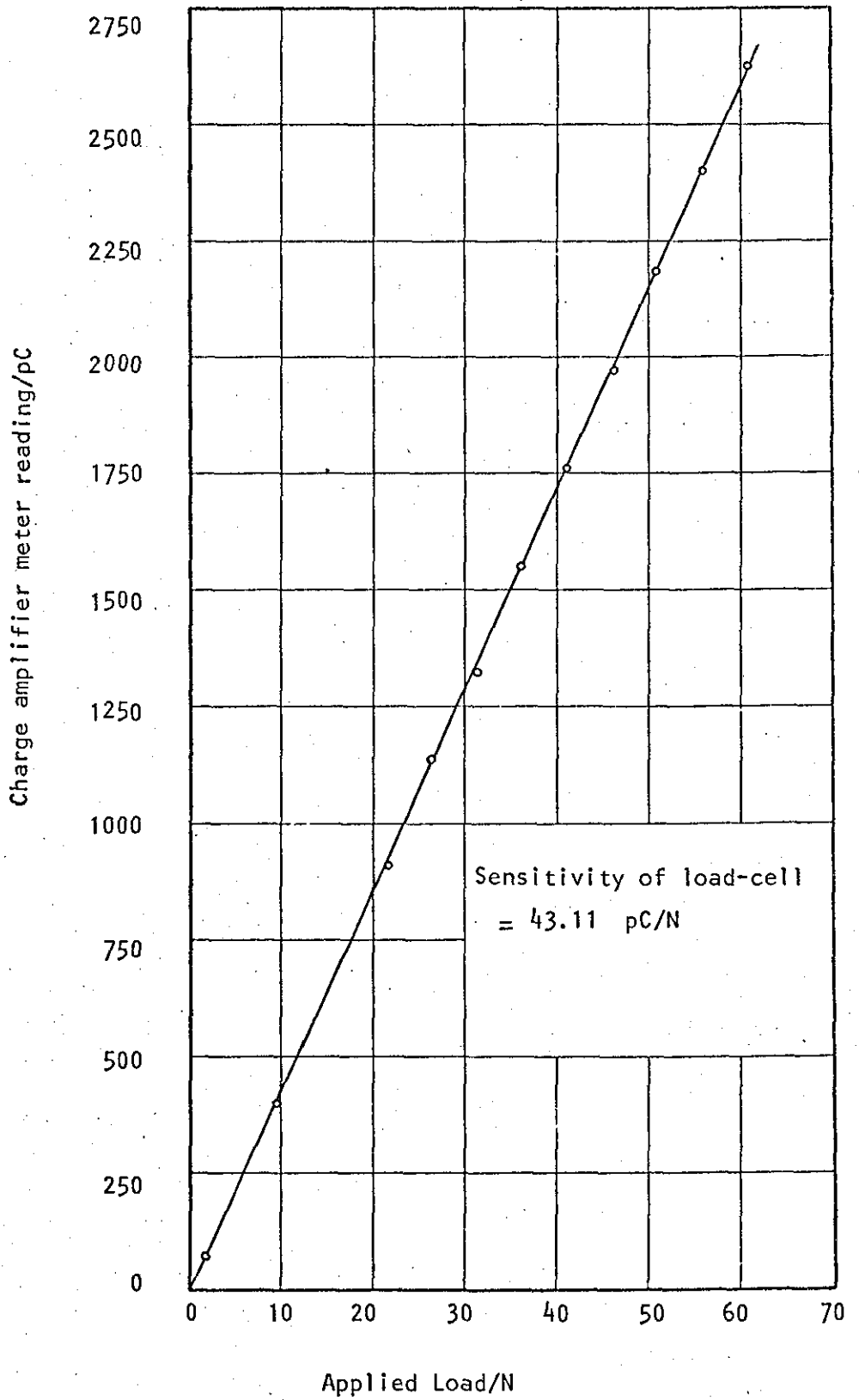


Fig. 5.11 Load-cell calibration curve in situ using charge amplifier meter as the readout system

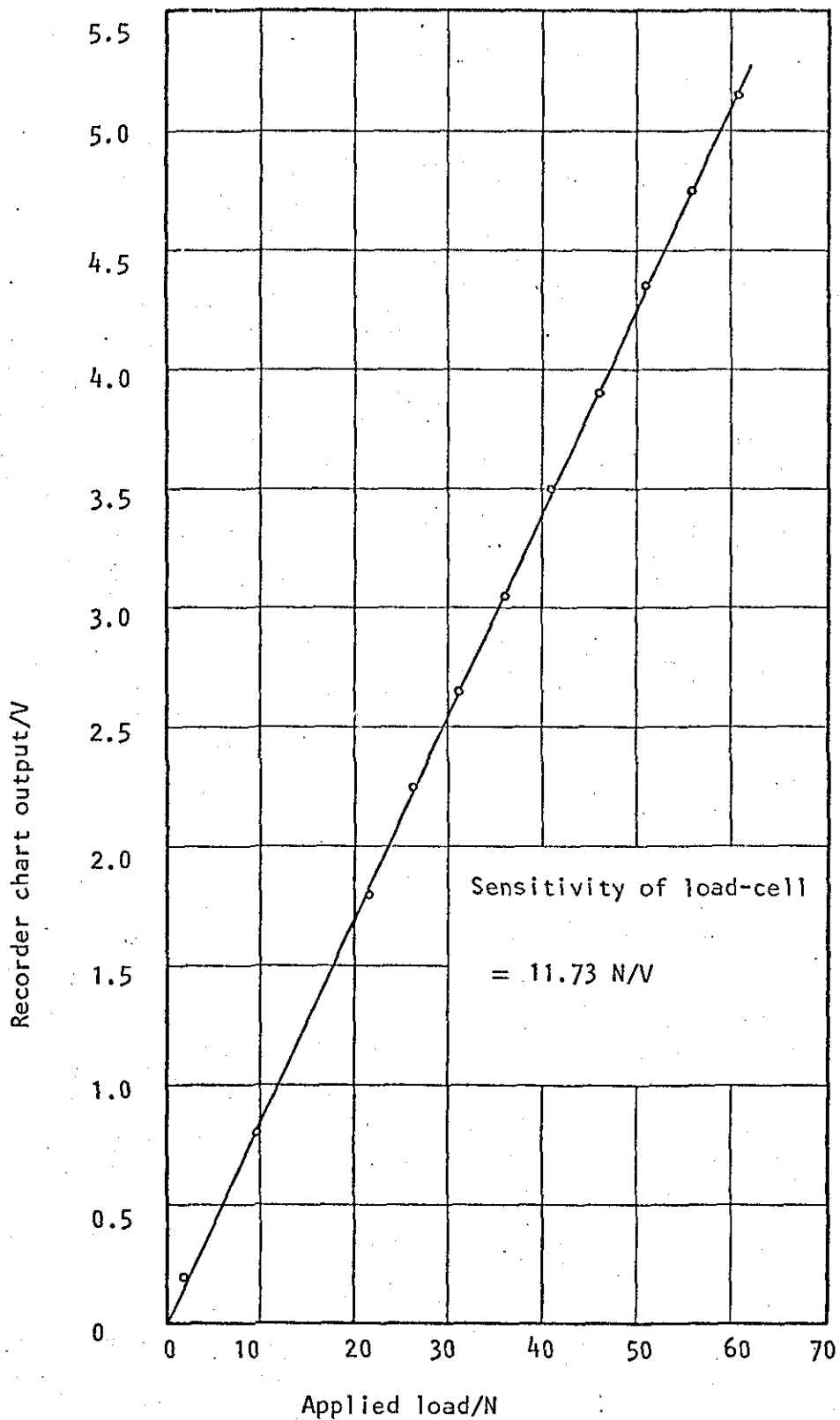


Fig. 5.12 Load-cell calibration curve in situ using the chart of the recording oscilloscope as the readout system



### 5.5 DETERMINATION OF THE STIFFNESS OF THE WEB MATERIAL

A J.J. tensile testing machine of the type T5002, made by J.J. Lloyd Instruments Ltd., was used to determine, experimentally, the stiffness (S) of the melinex web used in this study. The machine enabled the specimen to be fitted between a fixed base and a movable crosshead via a pair of general purpose grips of the eccentric roller type. The force applied to the specimen under test was measured by means of an electric load-cell of 500 N capacity. The distance travelled and the speed of movement of the crosshead were controlled and monitored whilst the loading developed on the specimen was measured and recorded. For this purpose an X-Y plotter, provided as an integral part of the system, was used. With the Y-axis connected to the load-cell output, whilst the X-axis was directly coupled to the crosshead displacement, the applied force was plotted automatically against the extension resulting in the specimen.

The test conditions were as follows:

Specimen material	Melinex
Specimen thickness	102 $\mu$ m
Specimen width	25.4mm
Distance between the gripped sections of the specimen	75mm
Capacity of the load-cell used	500 N
Load full scale on chart paper	200 N
Crosshead speed	50mm/min
Chart paper/crosshead ratio	10:1

Referring to Fig. 5.13, which shows the load-extension curve obtained, it has been found that the stiffness (S) of the Melinex specimen is

44.4 N/mm.

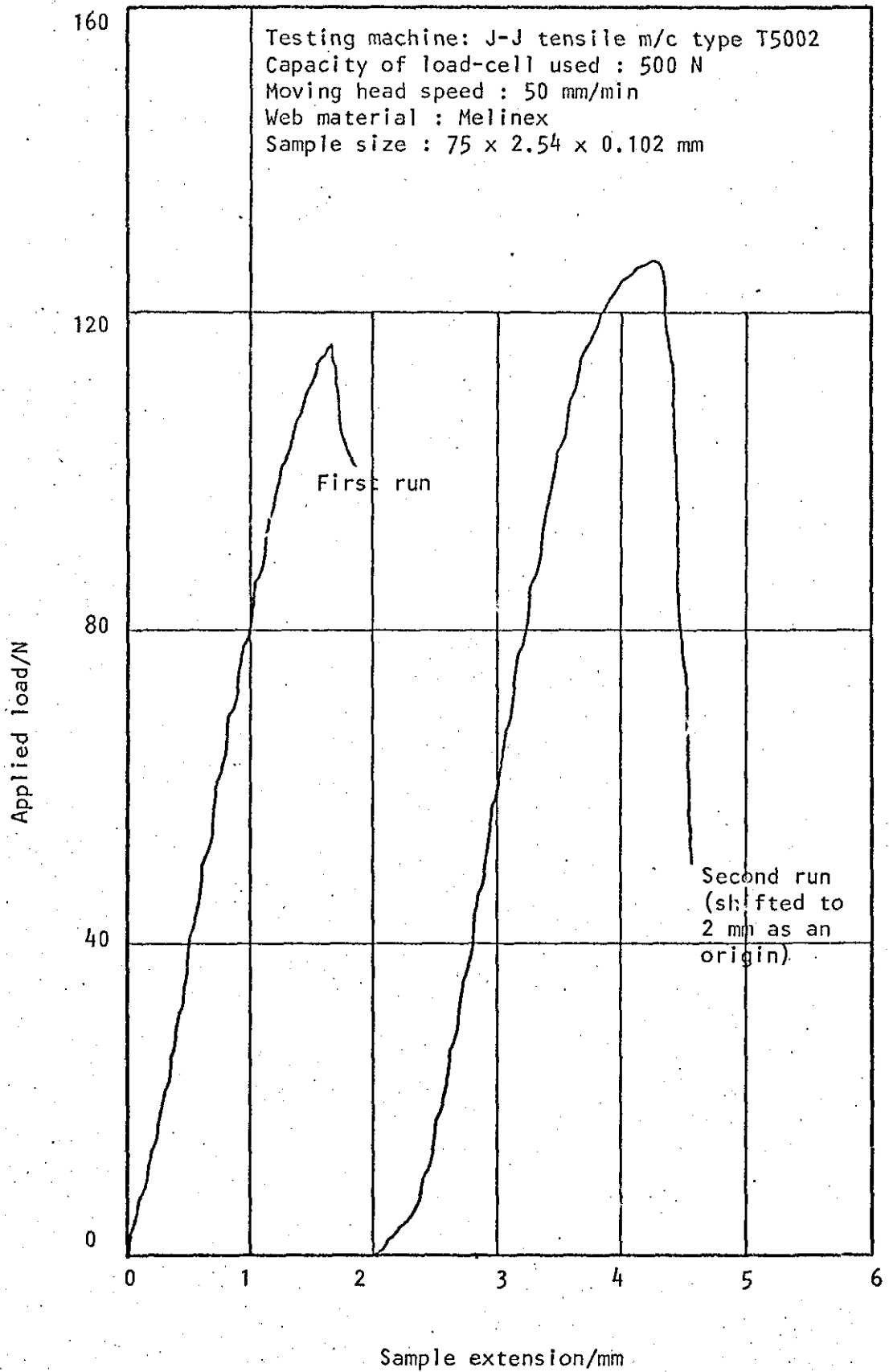


Fig. 5.13 Load-extension curve

CHAPTER SIX

RESULTS AND DISCUSSION

## 6.1 INTRODUCTION

The key to the successful operation of any continuous processing system that is linked together by the material being processed is positive control of the various parameters involved in the system. Among those parameters is the tension applied to the web of the material being processed. The automatic control of the web-tension comprises three basic elements : the measuring device, which senses the variations ; the controller, which interprets the measuring device signal and amplifies it, if need be, to indicate control action ; and the transmission link, which operates from the controller to compensate for the undesired variations. It is the first element of the three which has been the sole concern of this study.

A brief account of different methods of web-tension measurement was given at the very beginning of this thesis (refer to 1.1). Various techniques, which are in use nowadays, have been described. Due to practical limitations, namely the cost and time needed, it was not possible to investigate all the existing techniques experimentally. However, a theoretical analysis was made for one of them, viz the "Inertia Compensated dancer" (refer to 2.2). Another commercial instrument, the "Huyck Tensometer", was tested experimentally. Then a prototype of a device based on the electro-pneumatic principle was developed and tested for static and dynamic accuracy, limitations and most important of all dynamic response.

The results achieved are given and discussed in this Chapter in the same order that their corresponding experiments were laid down and

described in more detail in Chapter 4. An attempt has been made to present the graphs in the most self-explanatory way. Every graph is preceded by a table listing the corresponding experimental values. A terminology including all the symbols used throughout the discussion, or those appearing on the graphs, is given in the next section of this Chapter. The SI units were used and a table for conversion is given in Appendix (V ).

6.2 TERMINOLOGY

w web width

t web thickness

L web length

r radius of measuring cylinder

R radius of curvature of measuring pad

2b width of the pad

y distance moved by the pad against the web (see Fig. 6-iii)

2ℓ span between guiding rollers

θ wrap angle of the web

$p_t$  theoretical value of the pressure in the air gap

$p_{max}$  maximum theoretical pressure corresponding to maximum applied tension ( $p_{max} = \frac{T_{max}}{r}$  or  $= \frac{T_{max}}{R}$ )

k constant = 1.5, 2 or 3

$P_v = k.p_t =$  variable supply pressure (function of theoretical pressure)

$P_c = k.p_{max} =$  constant supply pressure

All pressures are gauge pressures, i.e. measured above atmospheric pressure.

$T_t$  theoretical tension per unit width of the web =  $p_t \times r$  or  $p_t \times R$

$T_a$  applied mean tension per unit width of the web  
=  $\frac{\text{gravitational force of applied dead weights}}{\text{width of the web}}$

$T_m$  measured tension per unit width of the web

$T_{\ell}$  local tension per unit width measured across the web

$\omega$  frequency of applied tension perturbations

$A_{\omega=0}$  amplitude of the measured tension at zero frequency

$A_m$  amplitude of the measured tension perturbations

$A_T$  " " " " by transducer

$A_{L.C}$  " " " " by load-cell

## 6.3 STATIC TESTS

### 6.3.1 THE HUYCK TENSOMETER

The objective of carrying out experimental tests on the Huyck tensometer was to evaluate its performance under static conditions by measuring different applied tensions of known values. The tension was measured in the longitudinal direction of the web along its centreline. The deflection of the web under tension, which is dependent upon the tensile stress in the web, was plotted against the applied tension as shown in Fig. 6.1 (the corresponding data are tabulated in Table 6.1).

In web-fed printing presses web-tension may be of the order of 0.1 to 0.5 kN/m (values vary according to printing processes)<sup>49</sup>. but in practice experience has shown that the level of tension, to reduce the possibility of a web break, is normally somewhere between 0.06 and 0.3 kN/m<sup>14</sup>. In steel strip rolling lines, the range of tensions encountered varies from 5 kN/m in first stage foil rolling to some 500 kN/m on stainless steel rolling mills<sup>50</sup>. These figures are reported for comparison with the range of web-tension measurable by the Huyck tensometer which is 0.9 to 4.4 kN/m, intended primarily for measurement of "felt" tension in paper mills. It can be seen that such a range is too high for a web-fed printing press and too low for a steel strip line. Although this fact should not be considered as a criticism of the device, the experimental results obtained show obvious non-linearity in the output of the tensometer even within its specified measuring range.



In Fig. 6.1, data obtained from the "tension versus deflection conversion tables", given in the manufacturer's instruction manual, are plotted resulting in curves (2) and (3) for comparison with the experimental results obtained on a Melinex web (refer to 4.2.1). The data corresponding to curve (2) and (3) are for web-tension measurements encountered in paper mills, namely Formex\* fabrics (design 22) and super plate press felt respectively. Both curves confirm the non-linearity in the instrument output shown by curve (1). It can also be seen that the instrument reading depends on the material of the web under consideration due to the fact that the web is wider than the instrument.

#### 6.3.2 THE SINTERED MEASURING CYLINDER - Validity of $p = \frac{T}{r}$

The main objective of the series of experiments carried out on the sintered measuring cylinder was to check the validity of the theoretical relationship  $p = \frac{T}{r}$  reported earlier in 2.3, where  $p$  is the pressure in the air film supporting the tension  $T$  in the web passing in close proximity to the porous surface of the sintered cylinder of radius  $r$ . The relation suggests a linear correlation between the pressure in the air gap and the tension in the web.

It has been pointed out in Section 2.3 of this thesis, that the minimum supply pressure to the sintered cylinder to provide an air film capable of supporting the web under tension should be 1.5 times the pressure required in that film. A higher

---

\*Trade mark of Huyck Corporation. Registered in USA and other countries.

figure than this merely increases slightly the gap between the web and the cylinder surface<sup>36</sup>. The experiments dealt with here were carried out at different variable and constant supply pressures (refer to 4.2.2-1) to achieve another objective, namely the study of the effect of supply pressure on the validity of the theoretical relationship.

The measured value of the pressure in the air film was substituted in the equation  $p = \frac{T}{r}$  to get the corresponding measured tension, which was then plotted against the applied tension as shown in Figs. 6.2 to 6.16. The corresponding experimental values are listed in tables 6.2 to 6.5.

Figs. 6.2, 6.6, 6.9 and 6.13 show the web-tension measured at different variable supply pressures, proportional to the applied tension ( $P_v = k p$ ). The results obtained reveal an excellent confirmation of the linearity suggested by the theoretical relation  $p = \frac{T}{r}$ .

A comparison of theoretical and experimental curves in these figures indicate that the measured values exceed the theoretical ones linearly. It can be seen that the increase in the experimental values depends on the supply pressure inside the cylinder; the higher the supply pressure the higher the increase in the tension measured values relative to the theoretical ones.

Fig. 6.2, as an example, shows that the measured values are higher than the theoretical by 7.4, 12 and 16% corresponding to supply pressures  $P_v = 1.5, 2$  and  $3 p$  respectively for a

Melinex web of 51  $\mu\text{m}$  thickness and 50mm width. The deviation from theoretical values for other webs of different thicknesses and widths, as shown in Figs. 6.2, 6.6, 6.9 and 6.13, at  $P_v = 1.5 p_t$  is 7.4, 6.4, 8.0 and 2.0% respectively. The difference between the first three values of deviation appear to be rather insignificant considering the experimental errors. This may suggest that relatively small differences in web thickness  $t$  or width  $w$  bear no significant effect on the amount of deviation (7.4% for  $t = 50 \mu\text{m}$  and  $w = 50 \text{ mm}$ , 6.4% for  $t = 102 \mu\text{m}$  and  $w = 102 \text{ mm}$ ). No further attempt was made at this point to confirm this suggestion. As for the 260 mm wide web (Fig. 6.13) the deviation appear to be significantly lower than the previous ones (2% compared to an average value for the previous three cases of about 7%). This and the entire phenomenon of the deviation from theoretical values is attributed to the variation across the web of pressure distribution in the air film, the effect of which is demonstrated and discussed in 6.3.3.

In Figs. 6.3 to 6.16, with the exception of Figs. 6.6, 6.9 and 6.13, the calculated tension values, based on the measured pressure in the air film at constant supply pressures corresponding to the maximum applied tension throughout each experiment ( $P_c = k p_{\text{max}}$  where  $k$  is a constant = 1.5, 2 or 3 and  $p_{\text{max}} = T_{\text{max}}/r$ ), are plotted against the corresponding values of applied tension. The results of the series of experiments described herewith show that the tension calculated at  $P_c = k p_{\text{max}}$  is higher than that calculated at  $P_v = k p_t$  at the bottom end

of the applied tension range as a result of the measured pressure in the air gap being higher in the former case than the latter. It can also be seen that as  $P_c$  approaches  $P_v$ , i.e. at the top end of the applied range, the difference diminishes. This suggests that the increase in the supply pressure would result in a distortion in the web and higher value of pressure in the air gap at the central region of the web. Bearing in mind that the porous wall of the cylinder has a constant "impedance", this explanation seems plausible in view of the fact that at relatively low tensions the rate of air flow, monitored on the flowmeter, showed a clear increase.

### 6.3.3 THE SINTERED MEASURING CYLINDER - Tension Profile

A comparison between the applied and experimentally determined values of tension in the previous section, namely in Figs. 6.2, 6.6, 6.9 and 6.13, showed the measured values to be higher than the theoretical ones in a linear manner. The objective of the series of experiments dealt with here was to seek an explanation for such a phenomenon.

One of the assumptions made, when deriving the relation  $p = \frac{T}{r}$ , was that the air gap thickness across the web is constant (refer to 2.3). In a more elaborate analysis concerning a porous gas foil bearing, Baumann<sup>35</sup> arrived at the formula

$$p = Et \frac{h - h_0}{r_0^2} \text{ where}$$

$p$  = pressure in the air gap

$E$  = Young's modulus for the web material

$t$  = web thickness

$r_o$  = outer radius of the bearing element (cylinder)

$h$  = separation between the web and the bearing (cylinder)

$h_o$  = " " " at  
the edge of the web

For more details the reader is referred to reference 35, in which the author included graphs of predicted separation and pressure profiles across the web. No experimental determination of such profiles have been reported in the open literature with the exception of the experiments done by Licht<sup>28</sup> to scan the separation across a foil bearing of finite width, but not the pressure.

Bearing in mind that the tension determined in the previous experiments was measured along the centreline of the web, a series of experiments was carried out to determine the tension profile across the web. The pressure in the air gap was measured at equal intervals underneath the web and the calculated tension was plotted against the corresponding position across webs of different materials, thicknesses and widths as shown in Figs. 6.17 to 6.19. Since it was not possible to measure the pressure in the air gap right underneath the edges of the web, the corresponding values of tension were extrapolated, taken as half the tension values of the nearest points to them on the web (2.5mm from the edges). The corresponding data of the figures are listed in tables 6.6 to 6.8 respectively. The areas under the resulting curves were then integrated by Simpson's rule and the average values of the measured tension per unit width of the web

were calculated and shown on the figures compared to the average values of the applied tension.

A comparison between the applied values of tension and the average values obtained experimentally reveals a good correlation considering the experimental errors. A qualitative comparison could also be made with the predicted profiles by Baumann. The reader is referred again at this point to reference 35 page 462, wherein it is shown that local tension across the web varies in the same manner as in Figs. 6.17 to 6.19.

Although these experiments were confined to 50mm and 102mm wide webs only, it is reasonable to expect the tension profile for a 260mm wide web, in view of the behaviour determined experimentally for the narrower webs, to take the shape marked (3) on the illustrative diagram (6-i) compared to those of the 50 and 102mm wide webs marked (1) and (2) respectively on the same graph.

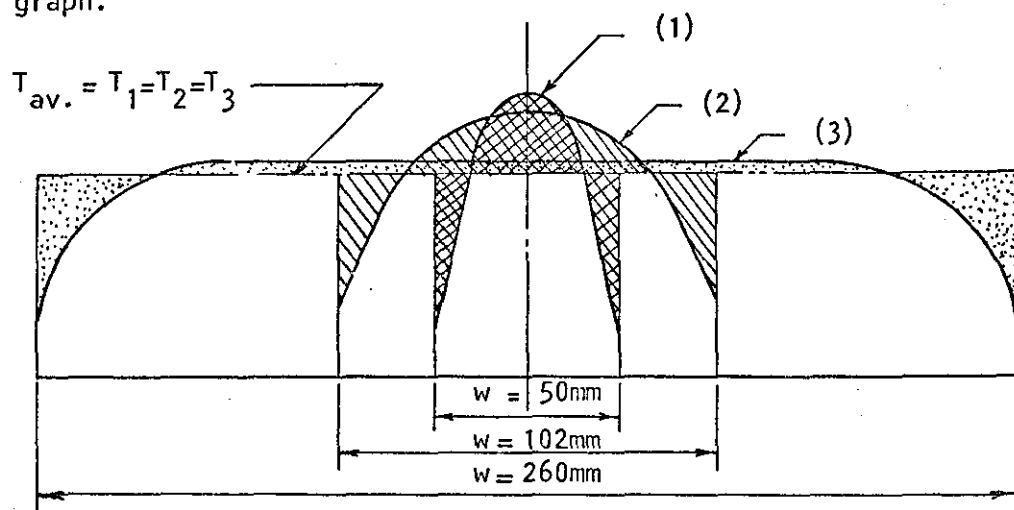


Diagram (6-i)

Proceeding outwards from the centre line of the diagram, which represents the centreline of the web under consideration, the pressure in the air gap decreases at first gradually and then with a faster rate in the vicinity of the edges for the 50 and the 102mm wide webs. As for the 260mm wide web, one would expect the pressure, the peak value of which is lower than those of (1) and (2), to remain fairly constant along a wider span on both sides of the centreline and then decreases rapidly towards both edges of the web. In all these cases the average value of the calculated tensions, based on the measured pressure in cases (1) and (2) and postulated in (3), is the same within the experimental error.

Recalling the value of 2% reported in 6.3.2, representing the amount by which the measured value of tension at the centreline of the 260mm wide web exceeded the average value of applied tension in Fig. 6.13 compared to an average increase of 7% for the 50 and the 102mm wide webs (Figs. 6.2, 6.6 and 6.9), the explanation given with the aid of the illustrative diagram (6-i) seems reasonable.

The significance of the verification of the behaviour of a flexible web of finite width, as predicted by Baumann, does not lie only in being the first to be done (to the best of the author's knowledge), but in establishing the fact that the measuring cylinder, as a web-tension measuring device, does measure the actual local tension in the web with a reliable accuracy at the point of measurement. It also provides the reason behind the

higher values of tension, measured by the device along the centre-line of the web, relative to the average applied values in the experiments dealt with in the previous section.

#### 6.3.4 THE MEASURING PAD - Validity of $p = \frac{T}{R}$

As the series of experiments carried out on the measuring cylinder, which is a web-tension measuring device based on an electro-pneumatic principle, gave promising results, a similar series was carried out to validate the relation  $p = \frac{T}{R}$  on the measuring pad. It can be seen from Figs. 6.20, 6.24, 6.28 and 6.32 that  $p = \frac{T}{R}$  still holds good over the whole range of the web widths used in this series. A similar trend to that observed in the case of the measuring cylinder, that is the measured values of tension being higher than those applied, are apparent in the mentioned figures. This phenomenon could be accounted for in the same way as in the case of the measuring cylinder (refer to 6.3.3).

A comparison between the results shown in Figs. 6.2 and 6.20, whereby the web thickness and width, the applied tension and the supply pressures ( $P_v = 1.5, 2$  and  $3 p_t$ ) were the same whilst the radii of the measuring device and the wrap angles of the web were different, reveals that the amount by which the measured values of tension exceed the applied ones is higher for the pad than for the cylinder (16, 19 and 22% for the pad and 7.4, 12 and 16% for the cylinder). These higher values, with the pad, proved to be genuine when the tension profile across the web was determined experimentally as will be seen in 6.3.5. However, it remains to be seen if these higher values, compared to those in Fig. 6.2,



are due to the change in either the radius of curvature of the device or the wrap angle of the web around it or both since no further experimental information was obtained to clarify this point.

Results in Fig. 6.32 whereby the web under test was 260mm wide (about twice the width of the measuring pad) indicate that the measured tension exceeds the applied values by as much as 50% at a supply pressure of  $P_v = 1.5 p_t$  and even higher percentage at higher values of supply pressures (94 and 126% at  $P_v = 2$  and  $3 p_t$  respectively). In viewing these values it should be remembered that the value of the applied tension is equal to the gravitational force of the dead weight divided by the width of the web to give the applied tension per unit width of the web. In the experiment described herewith, slackness in the lateral direction of the web was observed over the region:

$$0 < x < \left(\frac{w}{2} - b\right) \quad \text{and} \quad \left(\frac{w}{2} + b\right) < x < w$$

as shown in the diagrammatic sketch (6-ii).

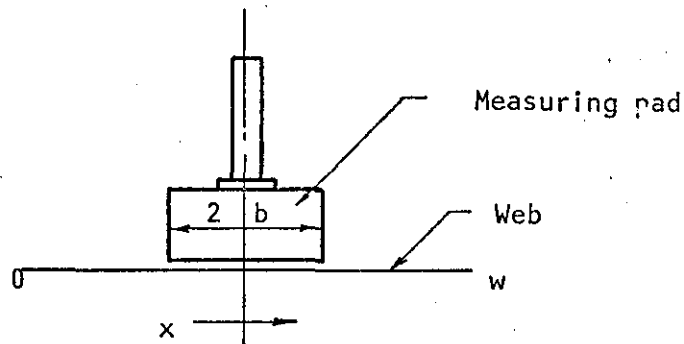


Diagram (6-ii)

This implies that the applied tensile force is concentrated in that region resulting in a higher value of tension per unit width than that calculated on the full width of the web. A theoretical attempt was made to predict the tension profile across the web in the region underneath the web using the Finite Element Method. The formulated model for the problem was oversimplified, hence it failed to give any conclusive results (refer to 2.4).

Figs. 6.21 to 6.35, with the exception of Figs. 6.24, 6.28 and 6.32, show similar results to those obtained on the measuring cylinder, i.e. the tension measured at  $P_c = kp_{max}$  is higher than that measured at  $P_v = kp_t$  at the lower end of the applied tension range and the difference diminishes as  $P_c$  approaches  $P_v$ . The explanation offered for the measuring cylinder still holds for the measuring pad (see 6.3.2).

Experimental values for Figs. 6.20 to 6.35 are listed in tables 6.9 to 6.12; each figure is preceded by the corresponding table.

#### 6.3.5 THE MEASURING PAD - Tension profile

The tension profile across a 50mm wide steel web (51 $\mu$ m thick) was determined for two average values of applied tension, namely 0.21 and 0.45 kN/m. The results obtained, as shown in Fig. 6.36, reveal that the measuring pad measures the local tension in the web at the points of measurement since the average values of measured tension agree, within experimental errors, with the applied values. The corresponding experimental data are listed in table 6.13.

A most interesting result can be seen in Fig. 6.37, whereby the tension profile across another section on the same steel web used in the previous experiment, was determined. The average applied tension was the same for both sections. In the figure described herewith the profile presented in Fig. 6.36, corresponding to an average applied tension of 0.21 kN/m, is plotted (marked A) together with the profile across the other section (marked B) for comparison. It can be seen that profile B is skewed to the left with a higher peak value than that of profile A. The interesting remark is that the values of average measured tension, determined by integrating the area under both curves and dividing each by the web width, were found to agree with the average applied value (+ 0.5% for profile A and -1% for profile B).

A close inspection of the section of the web, corresponding to profile B, has shown distortion and kinks across the section; believed to be due to cutting the web used from a wider steel strip and mishandling of the web when set in position for the experiment. Hence the higher peak value is thought to be due to stress concentration at a kinked point on the section.

The overall agreement between the measured average values of tension at both sections and the applied value confirms, yet again, the argument put forward earlier stating that the measuring pad does, in fact, measure the local tension in the web with a reliable accuracy.

Tension profiles were determined across a 50mm wide Melinex web (102 $\mu$ m thick) for the same two values of average applied tension

on the steel web dealt with earlier. Fig. 6.38 shows the results obtained, which comply with the trend indicated by the steel web on the measuring pad and the Melinex web on the measuring cylinder. It should be noted that the two profiles have a very wide plateau, covering about 60% of the web width around its centreline, in sharp contrast with those of the steel web (of the same width) in Fig. 6.36; one of them is replotted in Fig. 6.38 for comparison. This would suggest that with a stiff web greater resistance to bending manifests itself as we proceed outwards from the centreline resulting in a higher value of local tension at the centreline. The important fact, however, is that the average measured tension, determined from the graph for both the steel and Melinex web agrees with the value of the applied tension.

#### 6.3.6 THE MEASURING PAD - Optimum wrap angle

When using the sintered cylinder to measure web-tension, the wrap angle of the web around the measuring cylinder is determined by the set-up configuration. The wrap angle resulting from the configuration used was  $90^{\circ}$ . As for the measuring pad, it was imperative to find out the optimum wrap angle, if it exists, defined here as the angle beyond which the output signal from the web-tension measuring device remains unchanged. To achieve this objective a series of experiments, described with the associated condition in 4.2.3-3, were carried out on webs of different materials and widths. The diagrammatic sketch shown in Fig. (6-iii) illustrates how an expression for the wrap angle ( $2\theta$ ) was derived;

$\theta \approx \tan^{-1} \frac{y}{l}$  where  $y$  is the distance moved by the pad against the web and  $l$  is half the span between the guide rollers.

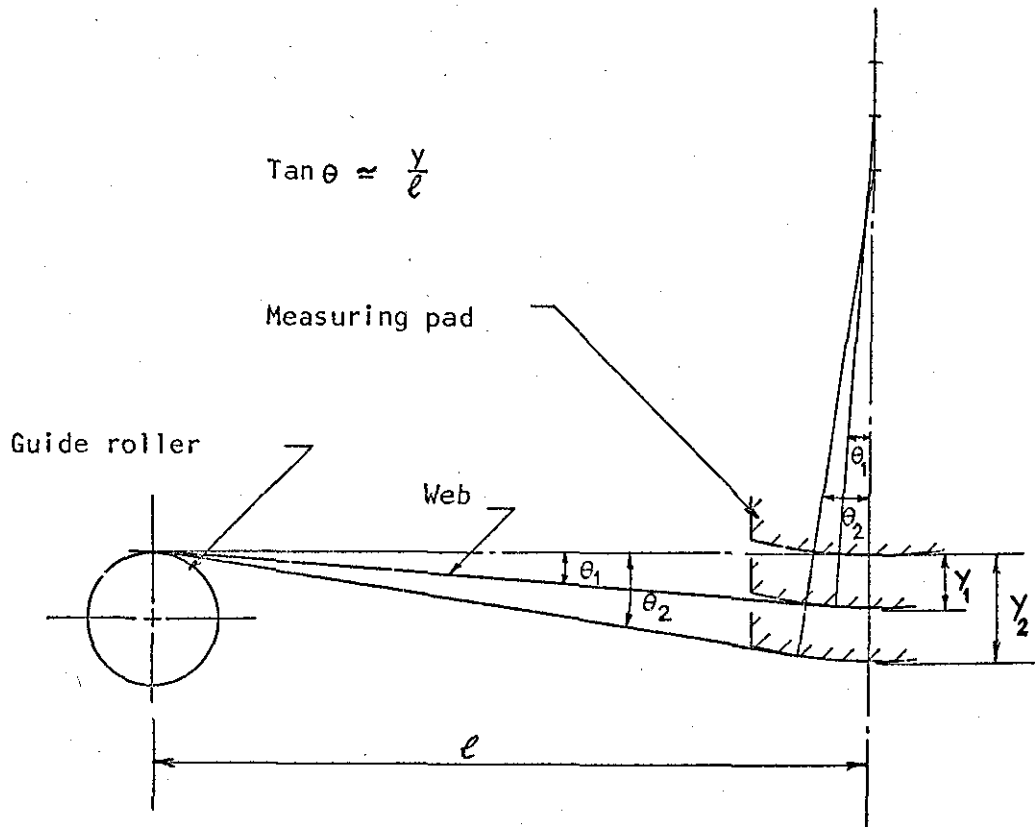


Diagram (6-iii)

The results obtained are shown in Figs. 6.39 - 6.42 and their corresponding experimental data are given in tables 6.16 to 6.19 respectively. It can be seen that neither the thickness (see Figs. 6.39 and 6.40) nor the width (see Figs. 6.40, 6.41 and 6.42) of the web has any significant effect on the value of the optimum wrap angle, which was found to be about  $13.5^\circ$  in all cases. It was also found that the material of the web has no effect on the wrap angle as can be seen in Fig. 6.39.

6.3.7 THE MEASURING PAD - Optimum position of the miniature pressure transducer

In the foregoing experiments the pressure in the air gap between the web under tension and the active surface of the measuring pad was measured by a water manometer via a pilot tube inserted into a hole made in the centre of the sintered segment of the pad. For dynamic measurements, the miniature pressure transducer replaced the pilot tube - water manometer arrangement (refer to 3.2.3). Therefore, before proceeding to the next phase of this investigation, which deals with the determination of the dynamic performance of the measuring pad, it was thought to be instructive to test the sensing element of the device, namely the transducer, under static conditions.

When the transducer was fitted, with its pressure sensitive diaphragm flush with the active surface of the measuring pad, the output signal was found to be erratic, intolerably unstable and inaccurate. The transducer was giving negative readings at lower values of applied tension implying that the pressure in the air gap corresponding to these values is subambient. One tends to believe that this could be due to a turbulent flow in the vicinity of the area where the transducer is fitted. Considering the difficulties involved in working out the flow pattern in such an area theoretically, no attempt is made here to confirm this explanation.

However, to overcome these shortcomings, and to elucidate such a phenomenon, experimental tests were carried out in two stages

(refer to 2.2.3-4). The results of the first stage, whereby the pressure in the air gap between the web and the pad, and consequently the tension in the web, was measured by both the transducer and the water manometer at the same time, are shown in Fig. 6.43. With the transducer being placed outside the pad box, the results indicated a complete agreement between the output of the transducer and the water manometer. The resulting straight line, correlating the measured and applied tension, in this stage was then considered as the reference for the transducer in the second stage. The transducer was then fitted into the wall of the sintered segment of the pad within different adapters, one at a time, resulting in the pressure sensitive diaphragm of the transducer being placed at different depths from the outer surface of the sintered segment of the pad. With the transducer set at depths less than 2.31mm (the smallest listed in table 6.21), an erratic output from the transducer was still observed. It was required, therefore, to set the transducer further back from the disturbed area. The tension measured by the transducer at each depth is plotted against the applied tension and the results of these experiments are plotted together with the reference straight line, from the first stage, for comparison as shown in Fig. 6.44. Table 6.21 includes the measured values of tension in the first stage in addition to those obtained in the second.

Referring to Fig. 6.44, it can be seen that at a depth of 2.31mm the transducer was still giving negative output at the lower end of

the range of applied tension. At larger depths the negative output ceased to prevail but up to a depth of 5.08mm nonlinearity of the lower part of the resulting curves was evident. The values of measured tension with the transducer set at the last two positions in this series of experiments, namely at a depth of 5.72 and 6.17mm, were plotted; although not joined on the graph both show obvious linearity. It would be noted that the points corresponding to the depth of 6.17mm could be represented, confidently, by the reference straight line obtained in the first stage and shown on the same graph. Hence, it was concluded that this is the optimum stable position for the transducer. Therefore it was decided to set the miniature pressure transducer at this position for the rest of the experimental work in this investigation.

In view of the experimental fact revealed by the previous set of experiments, the derivation of the minimum volume of the pneumatic circuit, introduced earlier in 2.1, may seem irrelevant. However, the erratic behaviour of the transducer used in the present investigation, when fitted within a depth less than 5.72mm from the active surface of the web-tension measuring device, should not imply that this is an inherent characteristic of miniature pressure transducers under different conditions.

The mathematical formulation for the minimum volume of the pneumatic circuit was derived before the turbulent behaviour of this arrangement became apparent and is included in the earlier part of the text (2.1) for completeness.



## 6.4 DYNAMIC TESTS

### 6.4.1 PRELIMINARY TESTS - Measuring cylinder

The main objective of these preliminary tests was to evaluate the dynamic performance of the electro-pneumatic technique, tested earlier under static conditions, when used to measure web-tension perturbations of relatively high frequencies.

Fig. 6.45 shows the result of the first experiment. The ratio of a dynamic tension ( $A_m$ ) to a static tensile force ( $A_{\omega=0}$ ) is plotted against the frequency of the applied dynamic force. In this case  $A_m$  corresponds to 1.0 A a.c. supplied to the vibrator at different frequencies and  $A_{\omega=0}$  corresponds to 1.0 A d.c. Both static and dynamic forces were measured by the Kistler pressure transducer while the dynamic force was monitored at the same time by the reference load-cell via the recording oscilloscope (refer to 4.3 and 4.3.1). In the figure described herewith it can be seen that for the Melinex web the ratio starts to exceed unity at 5 Hz, rises rapidly to a maximum and then decreases at a resonant frequency of about 13 Hz indicating that the natural frequency of the load-web system lies around that value. The load-cell, monitoring the dynamic force at the same time, showed the same rapid increase in the ratio followed by a decrease at the same value of frequency, i.e. 13 Hz. A steel web of the same dimensions was used under the same conditions to extend the natural frequency of the load-web system; the steel web being about 80 times as stiff as the Melinex one. The result of the test presented by the curve shifted to the right of the Melinex

curve, extended the natural frequency of the system to a value around 20 Hz, which is far below what was expected.

One way of overcoming this hurdle was to keep the magnitude of the applied dynamic tension constant by adjustment of the value of the current supplied to the moving coil of the vibrator. The ratio of amplitude of the measured tension by the transducer ( $A_T$ ) to the amplitude of the constant applied tension by the reference load-cell ( $A_{L.C}$ ) was then plotted against the frequency of the applied force as shown in Fig. 6.46. Thus the frequency response of the web-tension measuring system, namely the measuring cylinder associated with the Kistler pressure transducer, was determined.

It can be seen that the frequency response of the system under consideration proved to be satisfactory up to a frequency of 25 Hz, after which attenuation of the transducer output signal starts to take place. This is attributed to the relatively large volume of air contained within the screw-on cover and the hose nipple of the transducer (refer to 3.3.4) in addition to that contained in the connecting pilot-tube.

Experimental data of Figs. 6.45 and 6.46 are given in tables 6.22 and 6.23 respectively.

#### 6.4.2 THE MEASURING PAD - Miniature pressure transducer

Prior to proper analysis of any recordings of measured changes in web-tension the frequency response as well as the dynamic accuracy of the measuring system should be known. The frequency response of the measuring pad associated with the miniature

pressure transducer was tested against the reference load-cell following the procedure described in 4.3.1-ii. The reader is also referred to Fig. 4.5 whereby a typical example of a record of transducer/load-cell output signals is given. Inspection of such a trace would reveal any distortion in the "wave" form of the measured tension variation compared to the applied dynamic tension as well as any phase shift, if it exists, between the two.

Fig. 6.47 shows the results of a series of experiments carried out on a Melinex web for different values of initial (static) tension with the transducer fitted in the appropriate adapter at its optimum stable position (refer to 6.3.7). The result of a similar experiment, but with the transducer flush with the active surface of the pad, is present in the same figure for comparison. In addition, two more experiments were carried out on a steel web at the lowest and highest values of the range of tension applied in the first series. The results of these two experiments are shown in Fig. 6.48. Tables 6.24 and 6.25 give the experimental data of Figs. 6.47 and 6.48 respectively.

Referring to both figures, it can be seen that the measuring pad associated with the miniature pressure transducer has a very good dynamic response up to a frequency of 80 Hz. It was not possible to extend the frequency range of the applied tension perturbations due to the limitation on the maximum working current of the vibrator. However, it is quite evident that up to 80 Hz there was no trace of any tendency of attenuation in the transducer

output signal. A comparison between the result obtained with the transducer flush and those obtained with the transducer mounted at 6.2mm (stable position) reveals that the dynamic response of the measuring pad was not affected by setting the transducer back by that distance over the frequency range used throughout the experiments. With the transducer flush, the negative drift reported in 6.3.7 had no effect on the dynamic measurements due to the fact that the transducer output during this phase of the experimental work was coupled to an a.c. built in amplifier, within the recording oscilloscope, thus blocking any d.c. component.

An inspection of table 6.24 shows that the calculated ratio is higher than unity. The average value of the ratio as calculated for the transducer at optimum position, was found to be 1.19 with a standard deviation of 0.04. This confirms, yet again, that while the load-cell measures the average value of the applied tension the transducer measures the local variations in web-tension (at the centre of the web), which has proved to be higher than the average applied (refer to 6.3.4). The agreement between the excess of the average over the local tension, determined under static and dynamic conditions, is remarkable (19% in both cases). The reader is referred to 6.3.4 wherein it was shown that local measured tension, along the centreline of the web, is 19% higher than the average applied at a supply pressure  $P = 2p_t$  which was the case when these dynamic tests were carried out. Thus it could be concluded that the measuring pad associated

with the miniature pressure transducer is capable of measuring tension perturbation with a reliable accuracy.

The recording oscilloscope traces of the transducer output signal showed no significant distortion in the sinusoidal form of the measured tension compared with that monitored and recorded by the reference load cell at the same time, on the same chart. In some cases where the loading conditions were not accurately aligned resulting in a distorted output signal from the transducer, identical distortion was monitored by the reference load-cell. This implies that the transducer, and consequently the measuring pad as a web-tension measuring device, is detecting what is actually happening to the web under consideration.

As for phase shift between the two output signals, from the transducer and the reference load-cell, no measurable time lag could be detected.

## 6.5 RUNNING WEB TESTS

The last phase of the experimental work in the present study was to investigate the performance of the measuring pad, as a web-tension measuring technique, under running web conditions. A closed loop of a Melinex web, run at the required speeds, was used to achieve this objective, the experiment being repeated with two different web widths. The procedure of setting up the experiments is described in detail in 4.4. The output signal was monitored on the oscilloscope screen and recorded on the recording oscilloscope chart.

In the first experiment, a 102mm wide web was run at three different speeds, namely 1.22, 2.44 and 3.66m/s. Fig. 6.49 shows the trace of the tension variations, measured by the pad, at a web speed of 1.22m/s over three consecutive running cycles of the closed loop of the web. The traces of the three cycles are put one below the other for the sake of comparison. It can be seen that the three cycles are almost repetitive. The figure described herewith, although concerning the first running speed only, is a typical example of the output at the other two speeds. In other words, at every speed of the three, the measuring pad was reproducing its output at the speed under consideration.

In Fig. 6.50 tension variations, recorded at the three speeds mentioned in the previous paragraph, are shown over a complete cycle of the running web. A qualitative comparison between the three traces reveals that although they correspond to different speeds they show the same pattern of cyclic variation in tension. This and the remark made earlier about the results shown in Fig. 6.49, were also noted on the traces of tension variations measured by the pad on a 260mm wide web running at

six different speeds in the second experiment. Table 6.26 summarises the running speeds and the corresponding frequencies of tension variations as determined from the traces obtained in the two experiments.

Web speed (U) m/s	Measured frequency of tension variations (f) , Hz		U/f	
	102mm wide web	260mm wide web	102mm	260mm
1.22	6-7	6-7	0.188	0.188
2.44	13	13	0.188	0.188
3.66	19-20	19-20	0.188	0.188
6.10	-	32-33	-	0.188
7.32	-	38-39	-	0.190
8.53	-	47	-	0.182

Average value of ratio U/f = 0.187

Table 6.26 Web speed vs. measured frequency

The numerical data listed in table 6.26 reveal that the frequency of tension variations measured by the pad increases linearly with the running speed of the web. This would suggest that the pad is detecting tension variation resulting from a possible out of balance in the guide rollers.

The well known expression for the rotational frequency of a roller is:

$$f = \frac{1}{2\pi} \cdot \frac{U}{r_o} \quad (1)$$

in which U is the peripheral speed of the roller and  $r_o$  is its outside radius.

$$r_o = \frac{1}{2\pi} \cdot \left(\frac{U}{f}\right) \quad (2)$$

Substituting in equation (2) for  $\left(\frac{U}{f}\right)$  with the average value of those listed in table 6.26 yields

$$r_o = 0.0298 \text{ m}$$

A comparison between the calculated value of  $r_o$  (0.0298 m), which is based on the measured frequencies and the running speeds of the web, and the radius of the guide rollers actually used on the test rig (0.0302 m) indicate that the tension variations measured by the measuring pad under test are those resulting from out of balance in the guide rollers.

For the measuring pad to detect tension perturbations resulting from the interaction between the stiffness of the web material and the inertia of the guide rollers, the interference of any out of balance in the rollers or any other sources of tension variations must be kept to a minimum. If not, frequencies of such variations may overshadow the sought frequency, which is believed to be the case in the experiments carried out in this phase of the work.

The analysis presented here gives an overall understanding of the performance of the measuring pad under test on a running web. It should nevertheless be remembered that the significance of the results should not be extended too far before carrying out more comprehensive studies, considering all the associated factors, such as web width and material stiffness.



STATIC TESTS - Huyck tensometer

- Web Material : Melinex

w = 260mm

t = 51 $\mu$ m

Applied Tension	Dial indicator readings*
kN/m	division
0.425	13.5
0.618	31.0
0.811	40.0
1.004	50.0
1.197	54.5
1.373	62.0
1.548	66.0
1.723	72.0
1.899	74.0
2.047	79.5

\* Average value of 5 readings

Table 6.1 Huyck tensometer readings vs applied tension

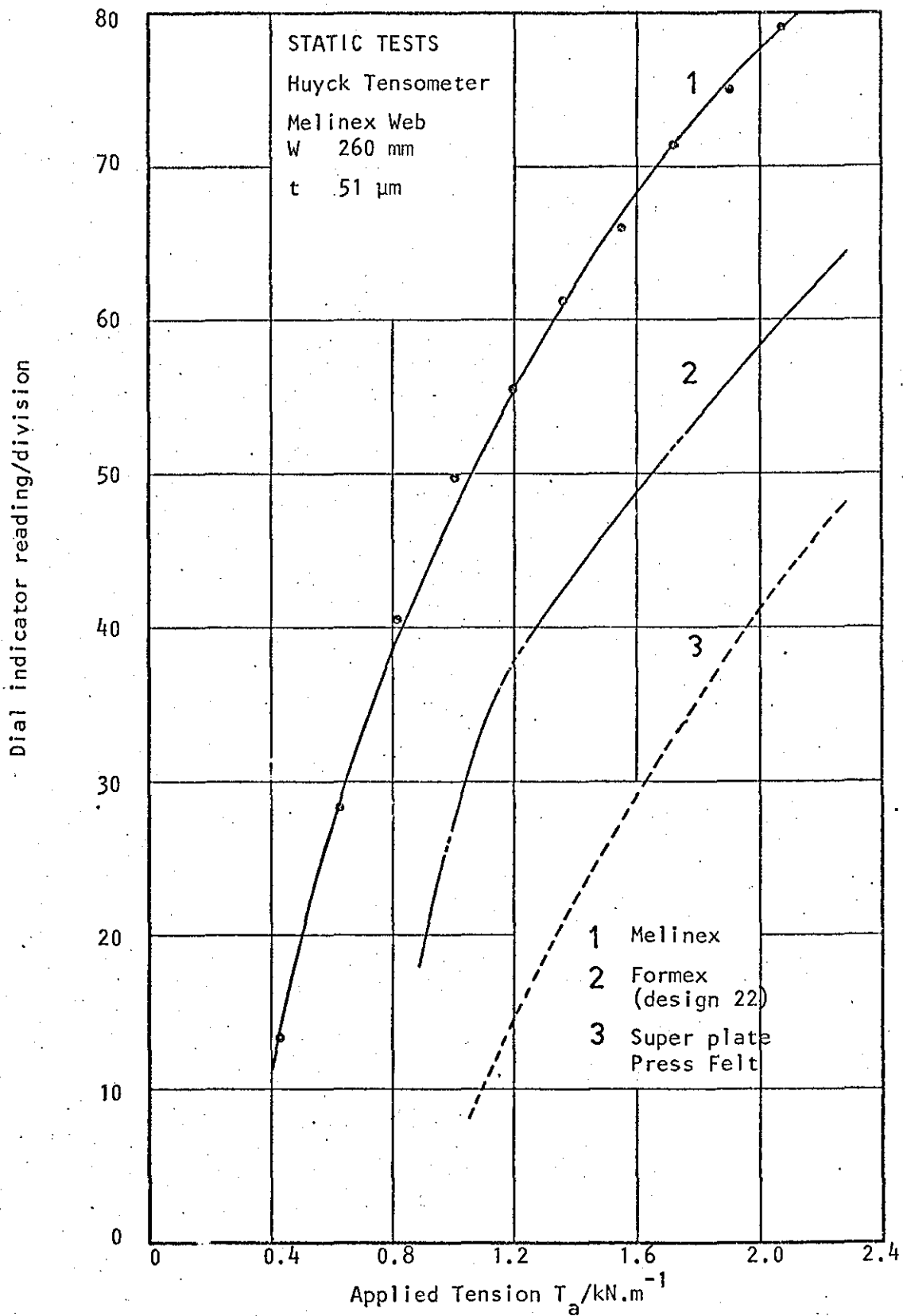


Fig. 6.1 Huyck tensometer dial reading vs. applied tension

STATIC TESTS - Validity of  $p = T/r$

- Measuring cylinder ;  $r = 25.65 \text{ mm}$
- Web Material : Melinex ; Thickness  $t = 51\mu\text{m}$   
 $w = 50\text{mm}$
- $P_v = 1.5, 2 \text{ and } 3 p_t$  ;  $P_c = 1.5, 2, 3 p_{\text{max}}$

$T_a$ kN/m	$p_t$ kN/m <sup>2</sup>	$T_m$ kN/m at $P_v$	$T_m$ kN/m at $P_c$
0.214	8.339	0.239	0.257
		0.244	0.264
		0.252	0.269
0.311	12.164	0.340	0.360
		0.350	0.370
		0.362	0.377
0.452	17.658	0.486	0.496
		0.501	0.513
		0.521	0.531
0.548	21.386	0.584	0.584
		0.604	0.604
		0.627	0.627

Table 6.2. Web-tension measured by the measuring cylinder at different supply pressures.

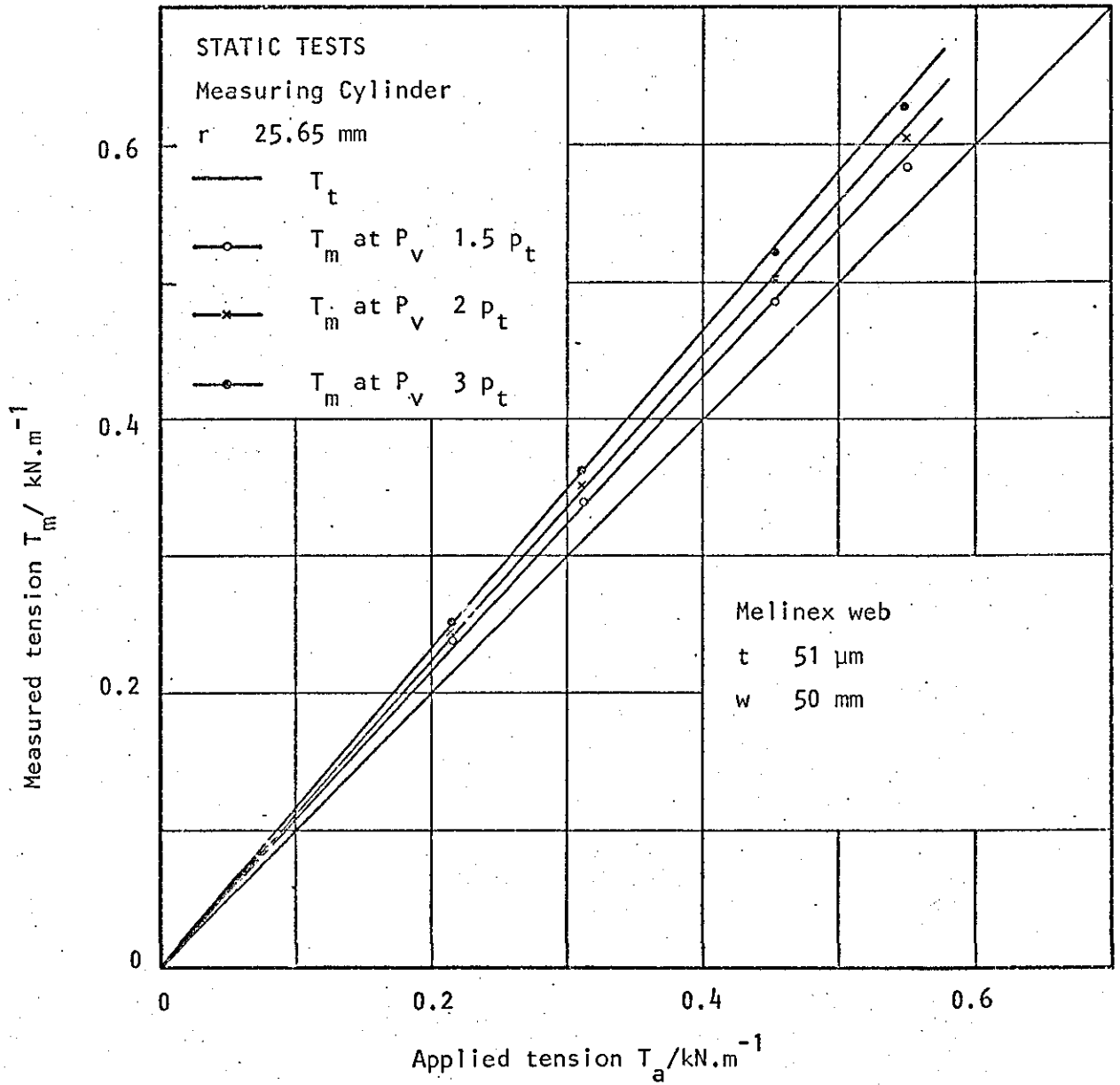


Fig. 6.2 Web-tension measured by the measuring cylinder at different variable supply pressures.

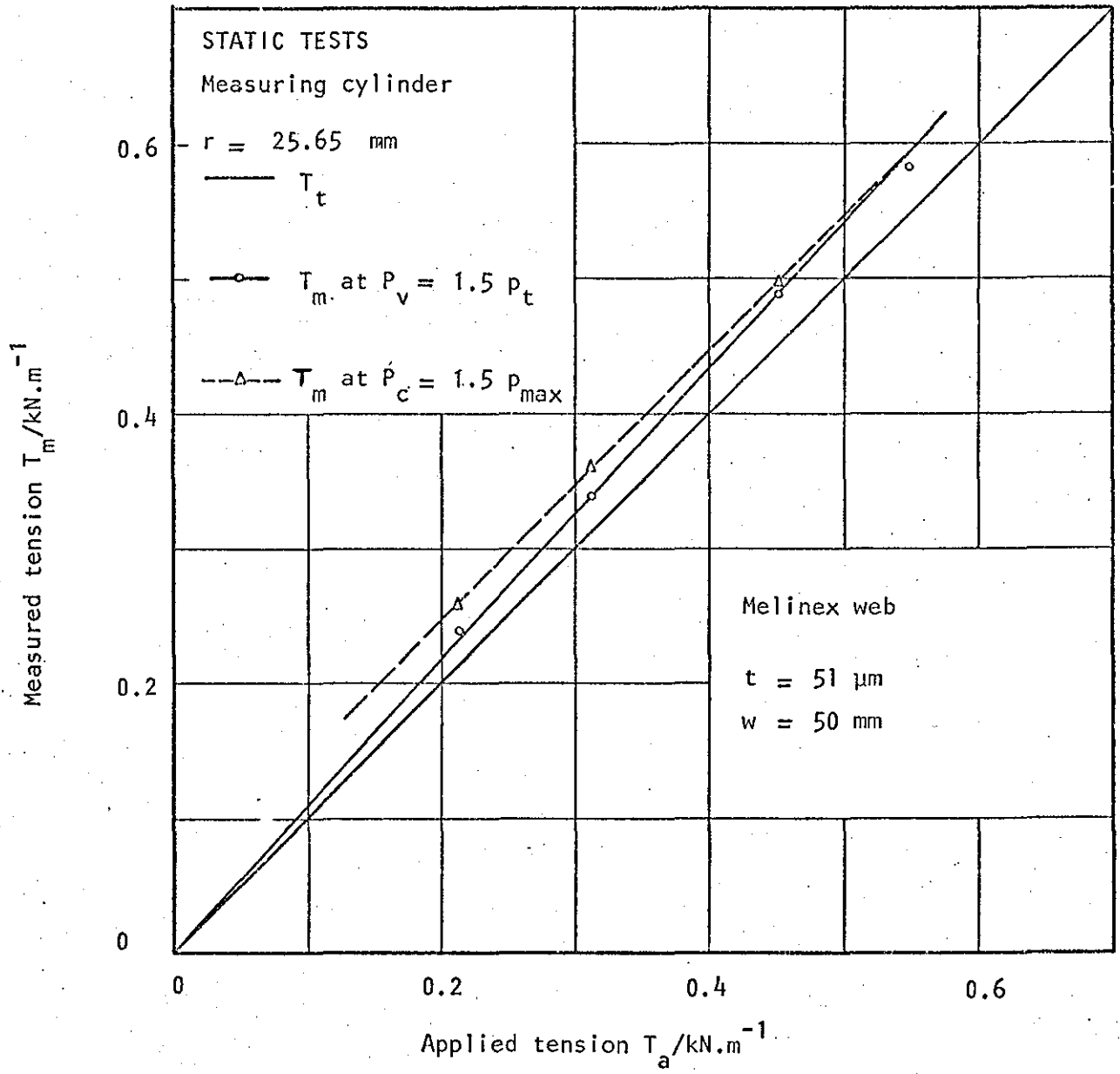


Fig. 6.3 Web-tension measured by the measuring cylinder at variable and constant supply pressure.

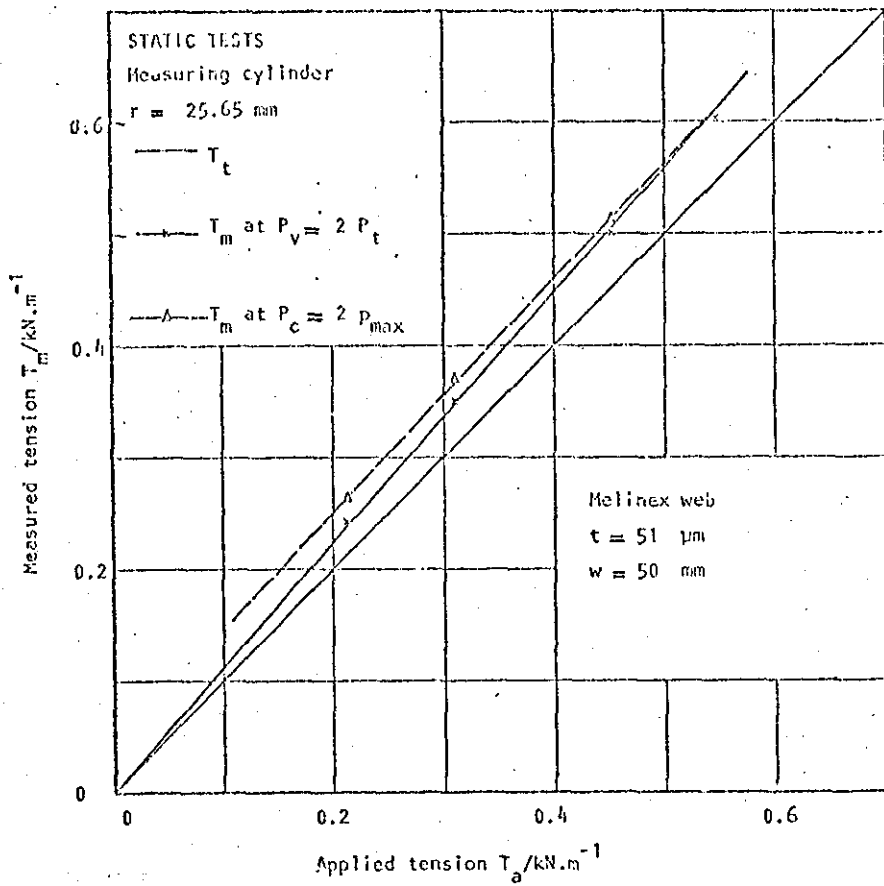


Fig. 6.4 Web-tension measured by the measuring cylinder at variable and constant supply pressure.

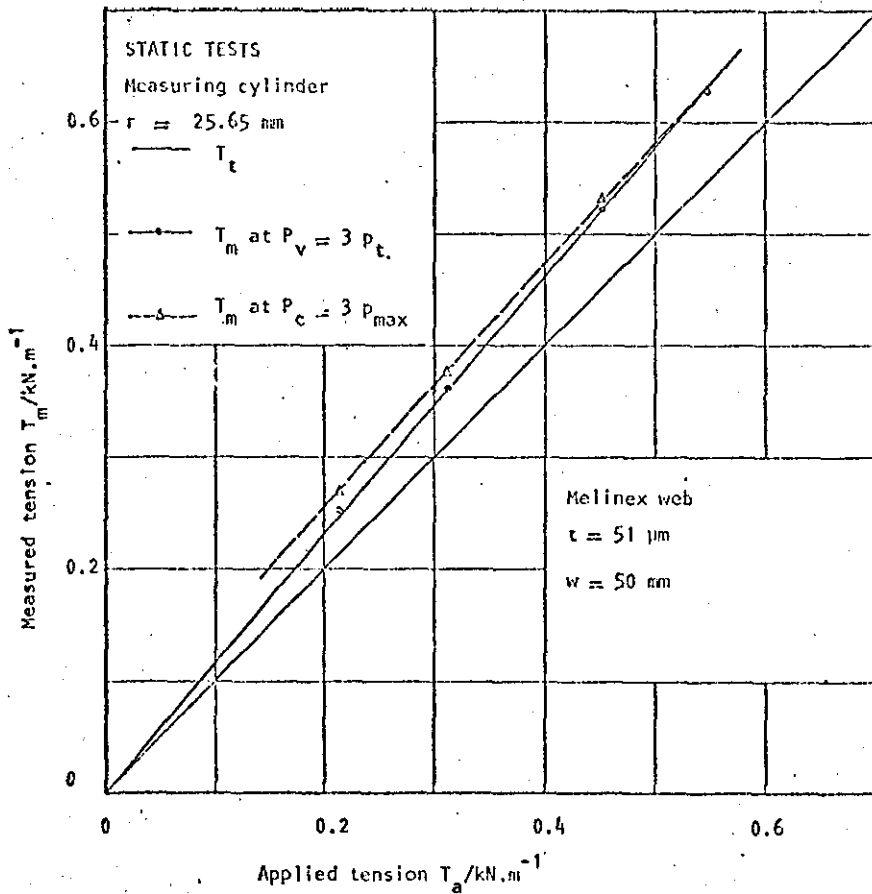


Fig. 6.5 Web-tension measured by the measuring cylinder at variable and constant supply pressure

STATIC TESTS - Validity of  $p = T/r$

- Measuring Cylinder ;  $r = 25.65$  mm
- Web Material : Melinex ; Thickness  $t = 102$   $\mu$ m  
 $w = 50$  mm
- $P_v = 1.5, 2$  and  $3 p_t$  ;  $P_c = 1.5, 2$  and  $3 p_{max}$

$T_a$ kN/m	$P_t$ kN/m <sup>2</sup>	$T_m$ kN/m	
		at $P_v$	at $P_c$
0.214	8.339	0.234	0.252
		0.242	0.259
		0.247	-
0.311	12.164	0.335	0.350
		0.342	0.357
		0.352	-
0.452	17.658	0.478	0.486
		0.491	0.498
		0.511	-
0.548	21.386	0.574	0.574
		0.594	0.594
		0.625	-

Table 6.3 Web-tension measured by the measuring cylinder at different supply pressures.

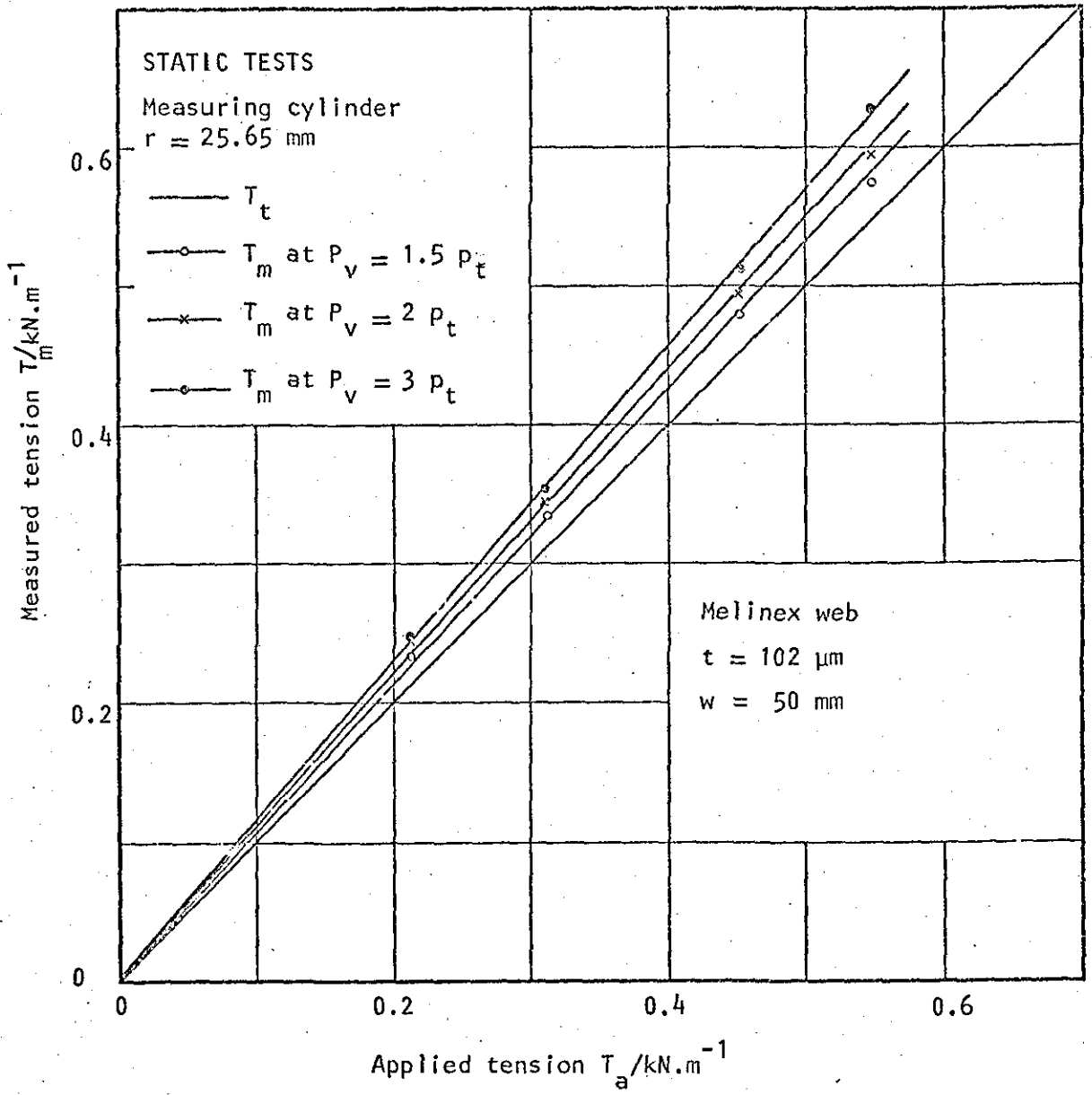


Fig. 6.6 Web-tension measured by the measuring cylinder at different variable supply pressures.



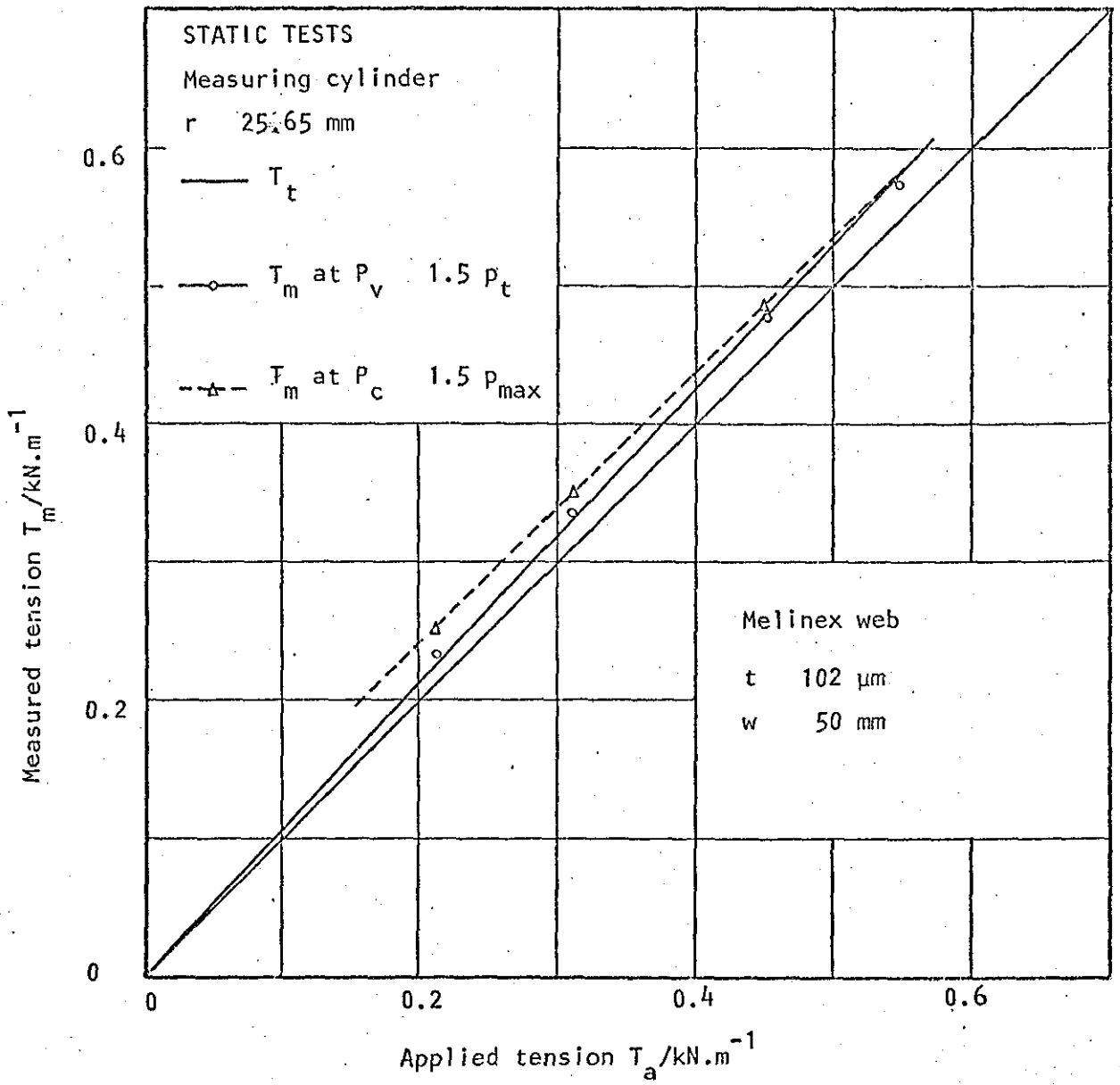


Fig. 6.7 Web-tension measured by the measuring cylinder at variable and constant supply pressure

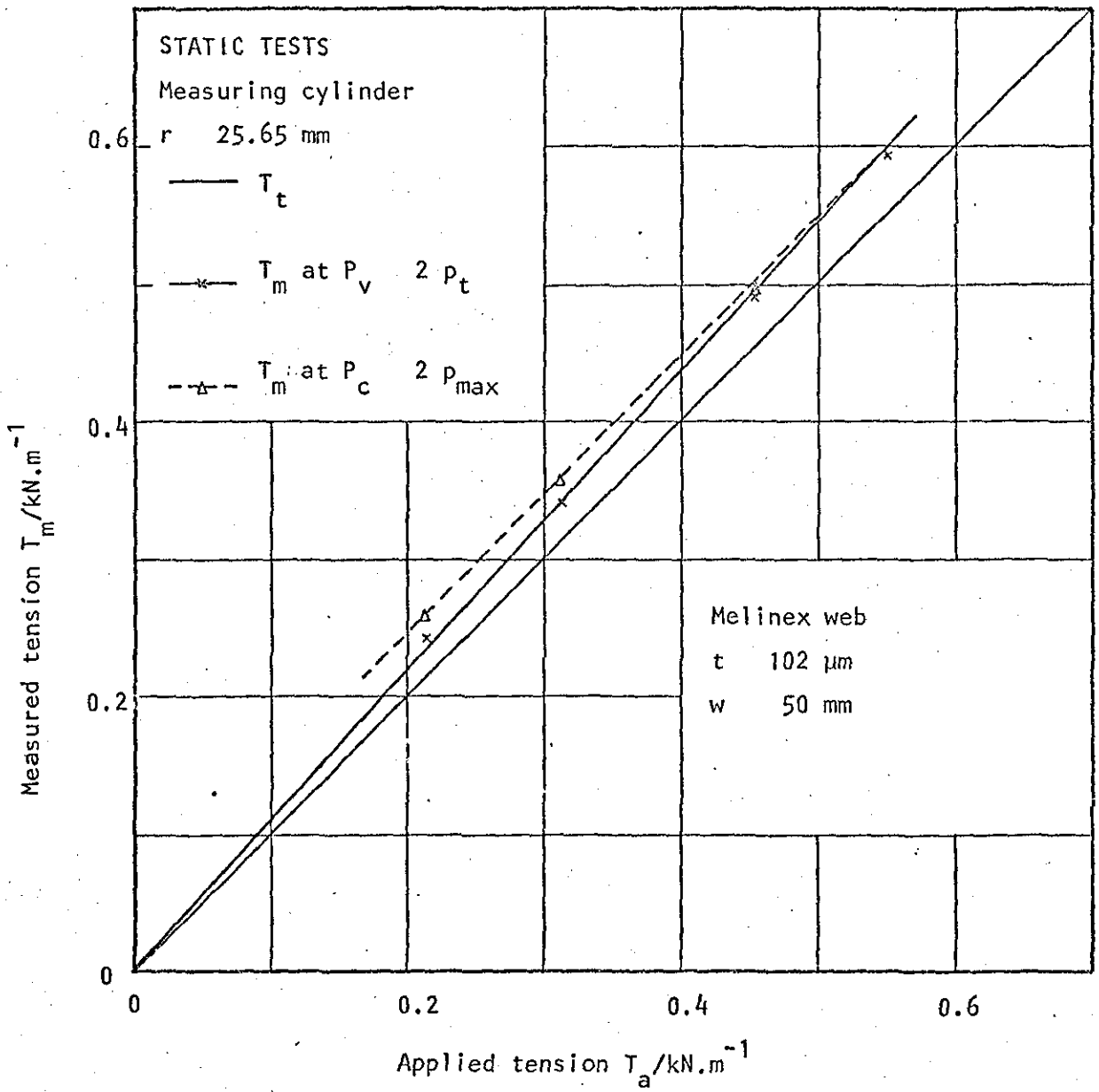


Fig. 6.8 Web-tension measured by the measuring cylinder at variable and constant supply pressure

STATIC TESTS - Validity of  $p = T/r$

- Measuring Cylinder ;  $r = 25.65 \text{ mm}$
- Web Material : Melinex ; Thickness  $t = 102 \mu\text{m}$   
 $w = 102\text{mm}$
- $P_v = 1.5, 2 \text{ and } 3 p_t$  ;  $P_c = 1.5, 2 \text{ and } 3 p_{\text{max}}$

$T_a$ kN/m	$P_t$ kN/m <sup>2</sup>	$T_m$ kN/m	
		at $P_v$	at $P_c$
		0.247	0.262
0.222	8.633	0.252	0.269
		0.259	0.274
		0.292	0.307
0.269	10.497	0.305	0.320
		0.315	0.327
		0.345	0.355
0.318	12.361	0.357	0.367
		0.372	0.377
		0.398	0.403
0.364	14.225	0.410	0.415
		0.425	0.428
		0.448	0.445
0.413	16.088	0.461	0.461
		0.478	0.481

Table 6.4 Web-tension measured by the measuring cylinder at different supply pressures.

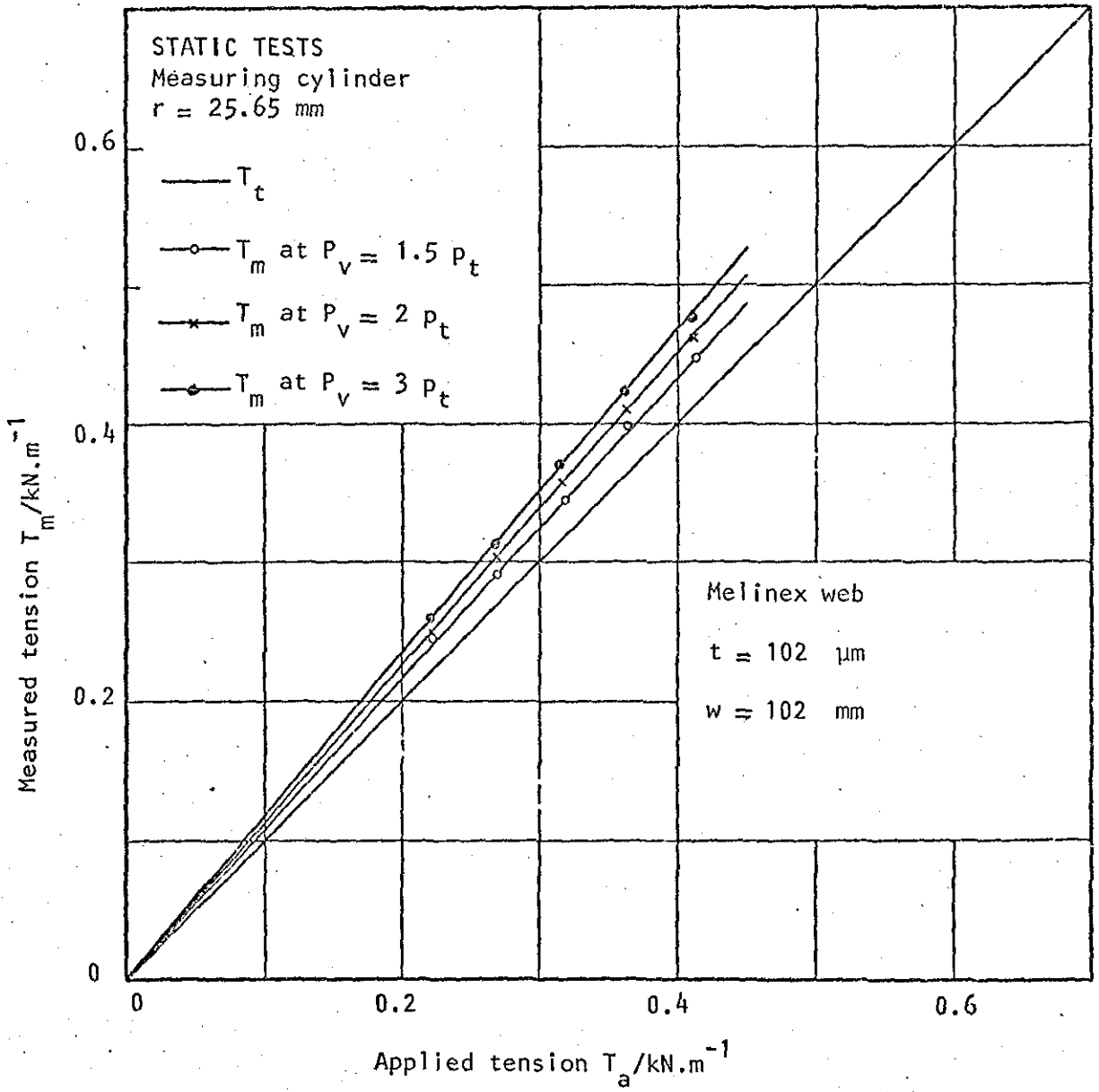


Fig. 6.9 Web-tension measured by the measuring cylinder at different variable supply pressures.

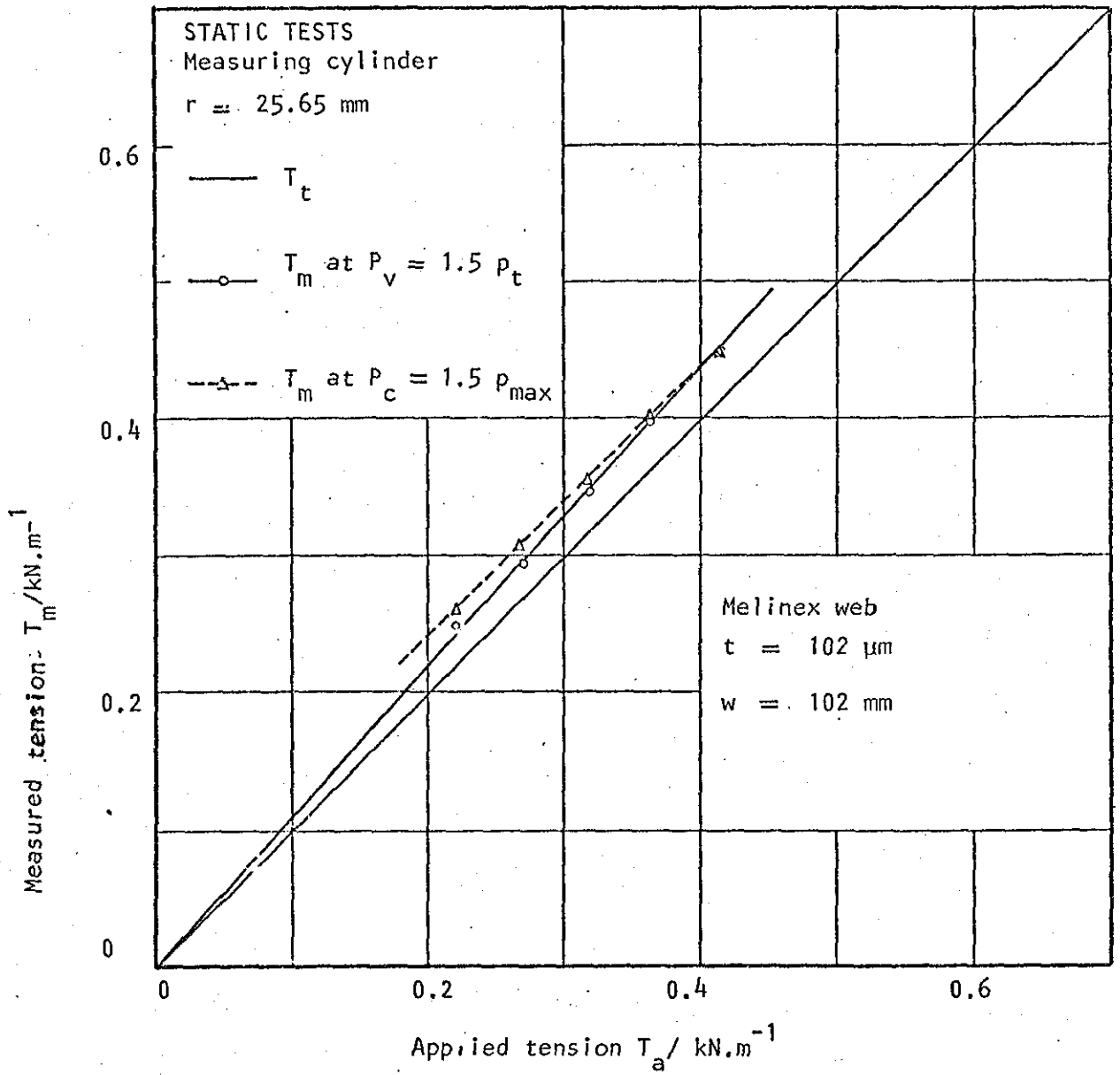


Fig. 6.10 Web-tension measured by the measuring cylinder at variable and constant pressure.

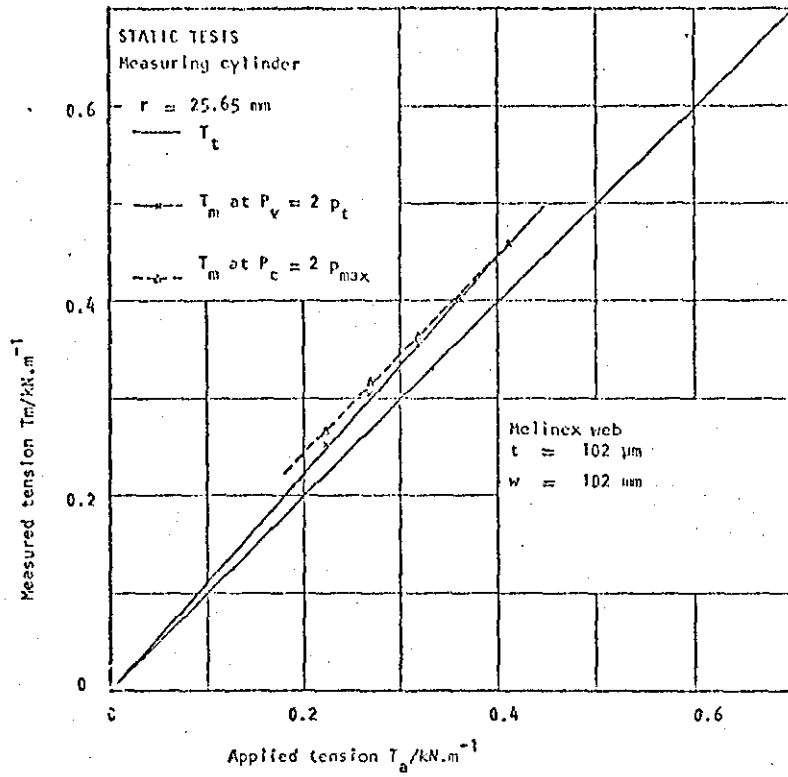


Fig. 6.11 Web-tension measured by the measuring cylinder at variable and constant supply pressure

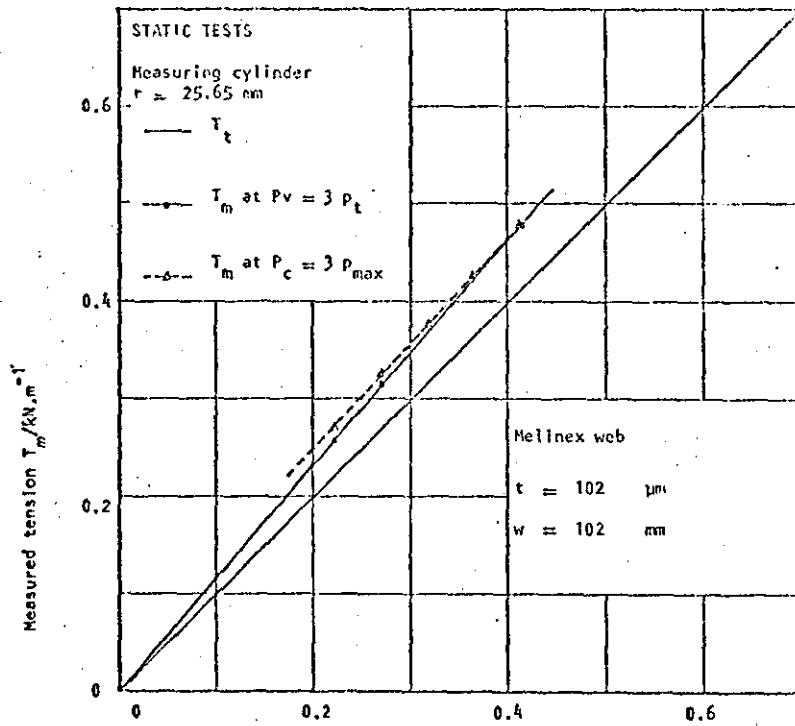


Fig. 6.12 Web-tension measured by the measuring cylinder at variable and constant supply pressure.

STATIC TESTS - Validity of  $p = T/r$

- Measuring Cylinder ;  $r = 25.65 \text{ mm}$
- Web Material : Melinex ; Thickness  $t = 102 \mu\text{m}$   
 $w = 260 \text{ mm}$
- $P_v = 1.5, 2 \text{ and } 3 p_t$  ;  $P_c = 1.5, 2 \text{ and } 3 p_{\text{max}}$

$T_a$ kN/m	$P_{t2}$ kN/m <sup>2</sup>	$T_m$ kN/m	
		at $P_v$	at $P_c$
0.103	4.022	0.106	0.121
		0.111	0.123
		0.118	0.128
0.122	4.709	0.123	0.138
		0.128	0.143
		0.133	0.148
0.159	6.180	0.164	0.176
		0.169	0.181
		0.176	0.191
0.236	9.221	0.244	0.252
		0.252	0.259
		0.262	0.269
0.312	12.164	0.322	0.322
		0.330	0.330
		0.345	0.342

Table 6.5 Web-tension measured by the measuring cylinder at different supply pressures.

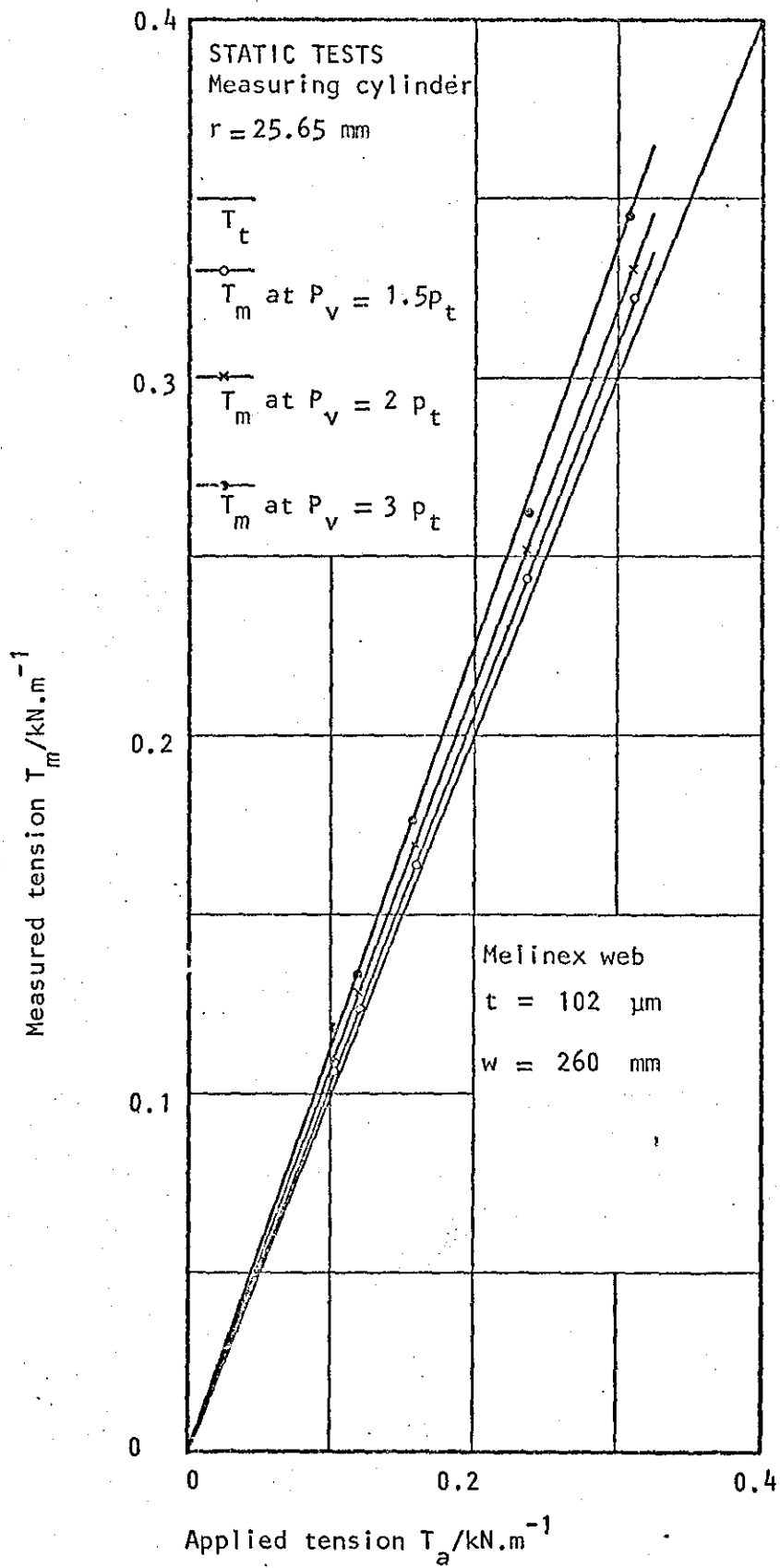


Fig. 6.13 Web-tension measured by the measuring cylinder at different variable supply pressures.



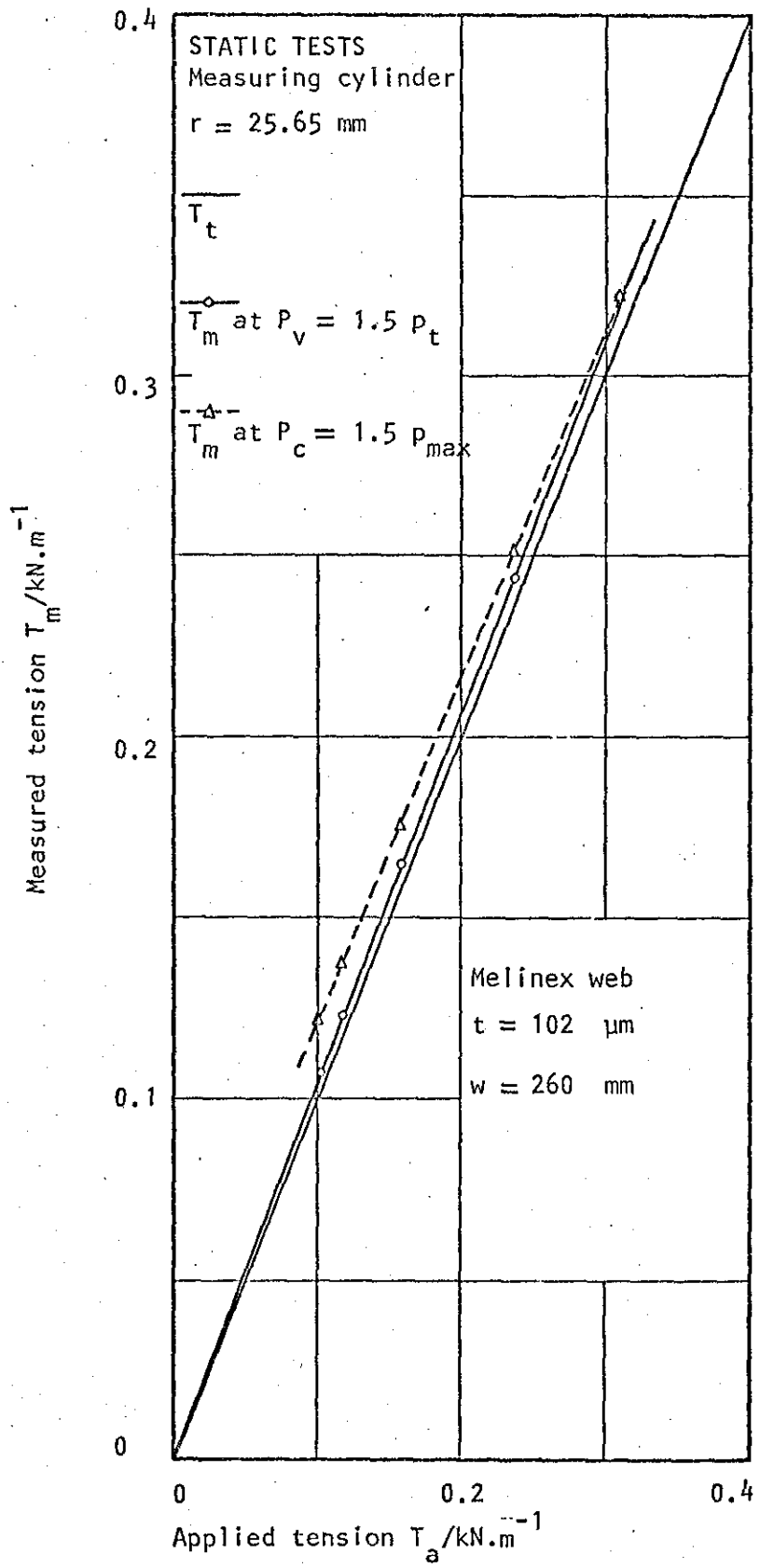


Fig. 6.14 Web-tension measured by the measuring cylinder at variable and constant supply pressure.

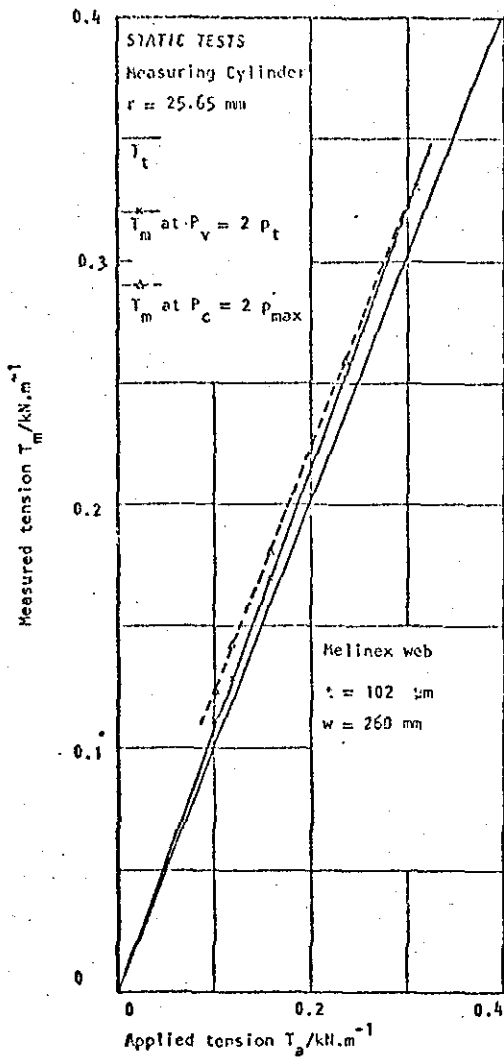


Fig. 6.15 Web-tension measured by the measuring cylinder at variable and constant supply pressure.

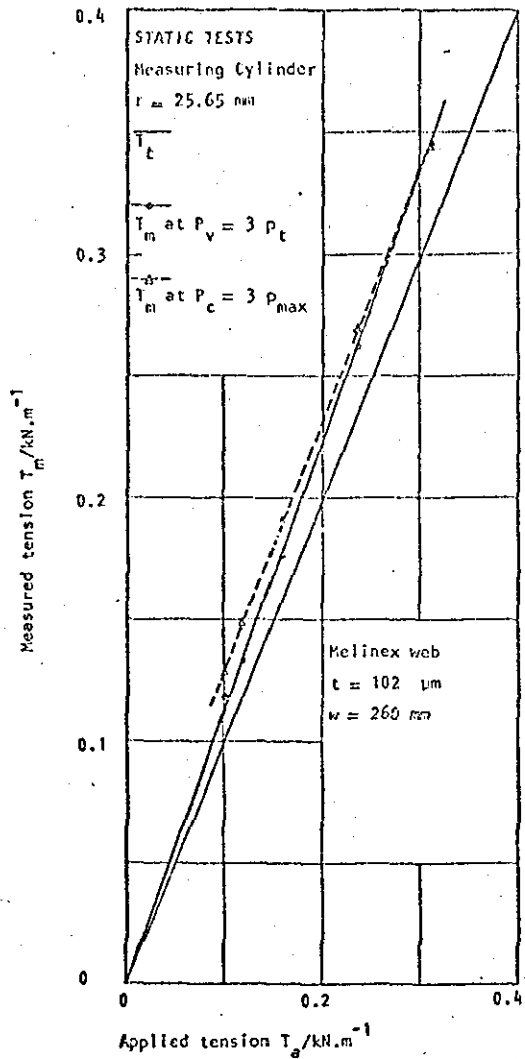


Fig. 6.16 Web-tension measured by the measuring cylinder at variable and constant supply pressure.

STATIC TESTS - Tension profile

- Measuring Cylinder ;  $r = 25.65 \text{ mm}$
- Web Material : Melinex ;  $t = 51 \mu\text{m}$   
 $w = 50 \text{ mm}$
- Average applied tension  $T_a = 0.438 \text{ \& } 0.933 \text{ kN/m}$

$$T_l = P_l \cdot r$$

Position across the web mm	Local tension $T_l$ kN/m	
	(1) at $T_a = 0.438$	(2) at $T_a = 0.933$
0	(0.149)*	(0.39)*
2.5	0.298	0.779 Experimental average
5.0	0.376	0.901 tension (1) = 0.441 kN/m
10.0	0.455	0.988 (+ 0.7%)
15.0	0.492	1.035
20.0	0.515	1.058
25.0	0.525	1.067
30.0	0.525	1.062 Experimental average
35.0	0.507	1.035 tension (2) = 0.941 kN/m
40.0	0.463	0.983 (+ 0.7%)
45.0	0.363	0.865
47.5	0.227	0.706
50.0	(0.114)*	(0.353)*

\* Values between brackets are extrapolated.

Table 6.6 Tension profile across a 50mm wide Melinex web.

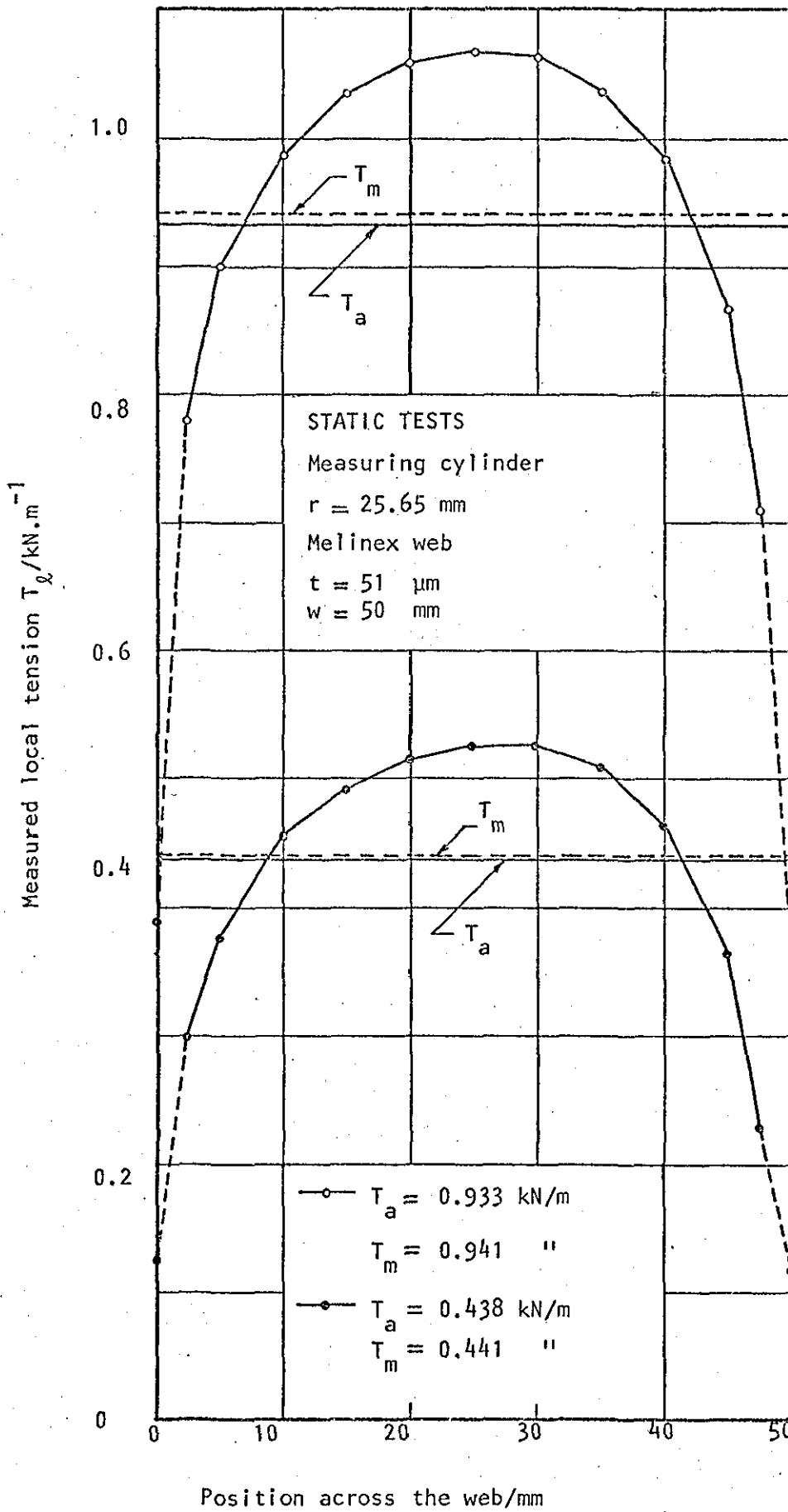


Fig. 6.17 Tension profile across a 50 mm wide Melinex web

STATIC TESTS - Tension profile

- Measuring Cylinder ;  $r = 25.65 \text{ mm}$
- Web Material : Melinex ;  $t = 102 \text{ }\mu\text{m}$   
 $w = 102 \text{ mm}$
- Average applied tension  $T_a = 0.214 \text{ kN/m}$

$$T_\ell = P_\ell \cdot r$$

Position across the web mm	Local tension $T_\ell$ kN/m	
0	(0.061)	
3.5	0.121	
6	0.141	
11	0.182	
15	0.206	
21	0.222	
26	0.229	
31	0.239	Experimental average tension = 0.210 kN/m (- 1.9%)
36	0.244	
41	0.246	
46	0.249	
51	0.249	
56	0.249	
61	0.246	
66	0.246	
71	0.244	
76	0.239	
81	0.232	
86	0.222	
91	0.209	
96	0.182	
98.5	0.156	
102	(0.078)	

Table 6.7 Tension profile across a 102 mm wide Melinex web.

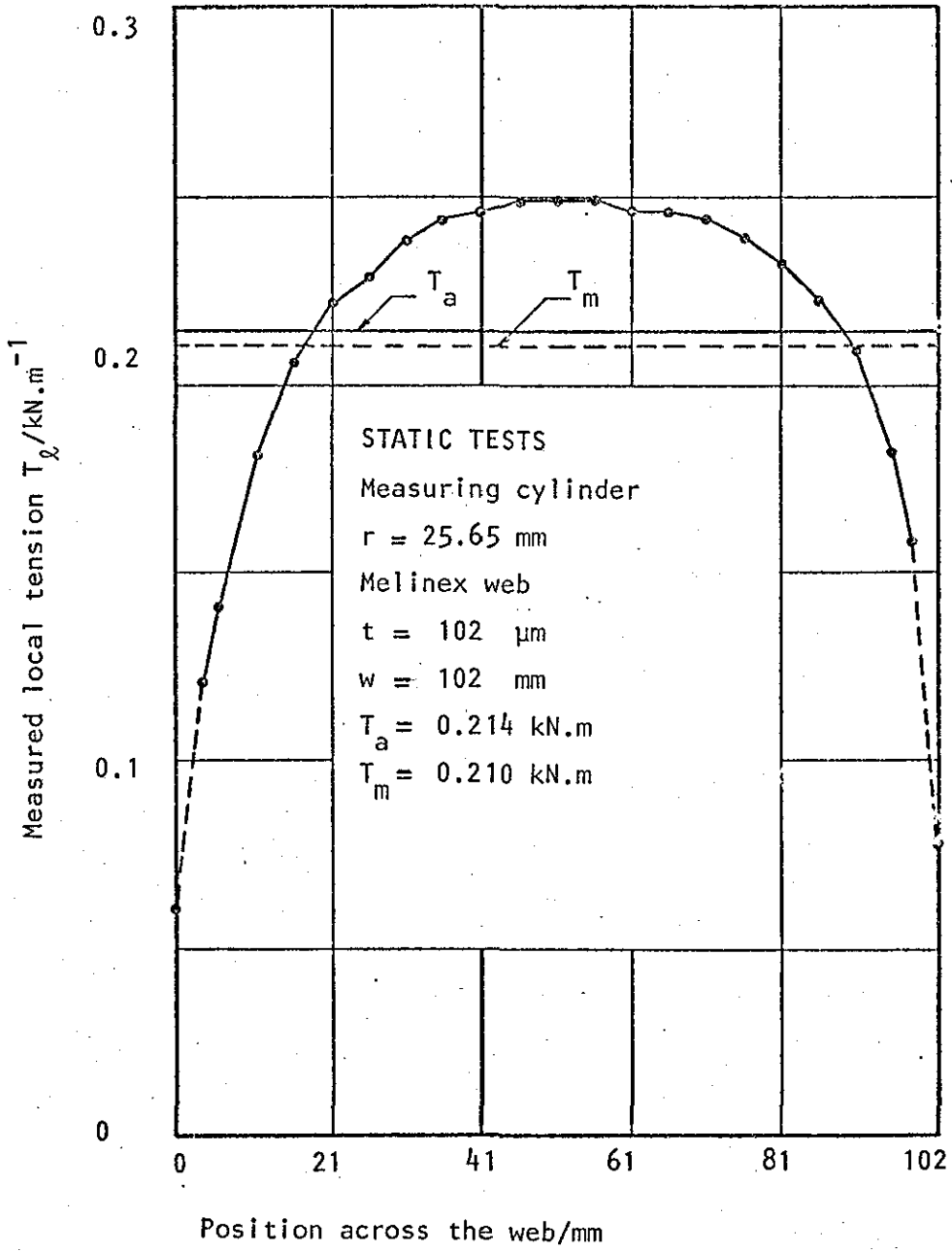


Fig. 6.18 Tension profile across a 102mm wide Melinex web.

STATIC TESTS - Tension profile

- Measuring Cylinder ;  $r = 25.65 \text{ mm}$
- Web Material : Steel ;  $t = 51 \mu\text{m}$   
 $w = 102 \text{ mm}$
- Average applied tension  $T_a = 0.221 \text{ kN/m}$

$$T_l = p_l \cdot r$$

Position across the web mm	Local tension $T_l$ kN/m	
0	(0.025)	
3.5	0.053	
6	0.098	
11	0.151	
16	0.186	
21	0.215	
26	0.229	
31	0.244	Experimental average tension = 0.218 kN/m (- 1%)
36	0.254	
41	0.259	
46	0.264	
51	0.269	
56	0.269	
61	0.269	
66	0.267	
71	0.263	
76	0.257	
81	0.246	
86	0.229	
91	0.206	
96	0.151	
98.5	0.119	
102	(0.060)	

Table 6.8 Tension profile across a 102 mm wide steel web.

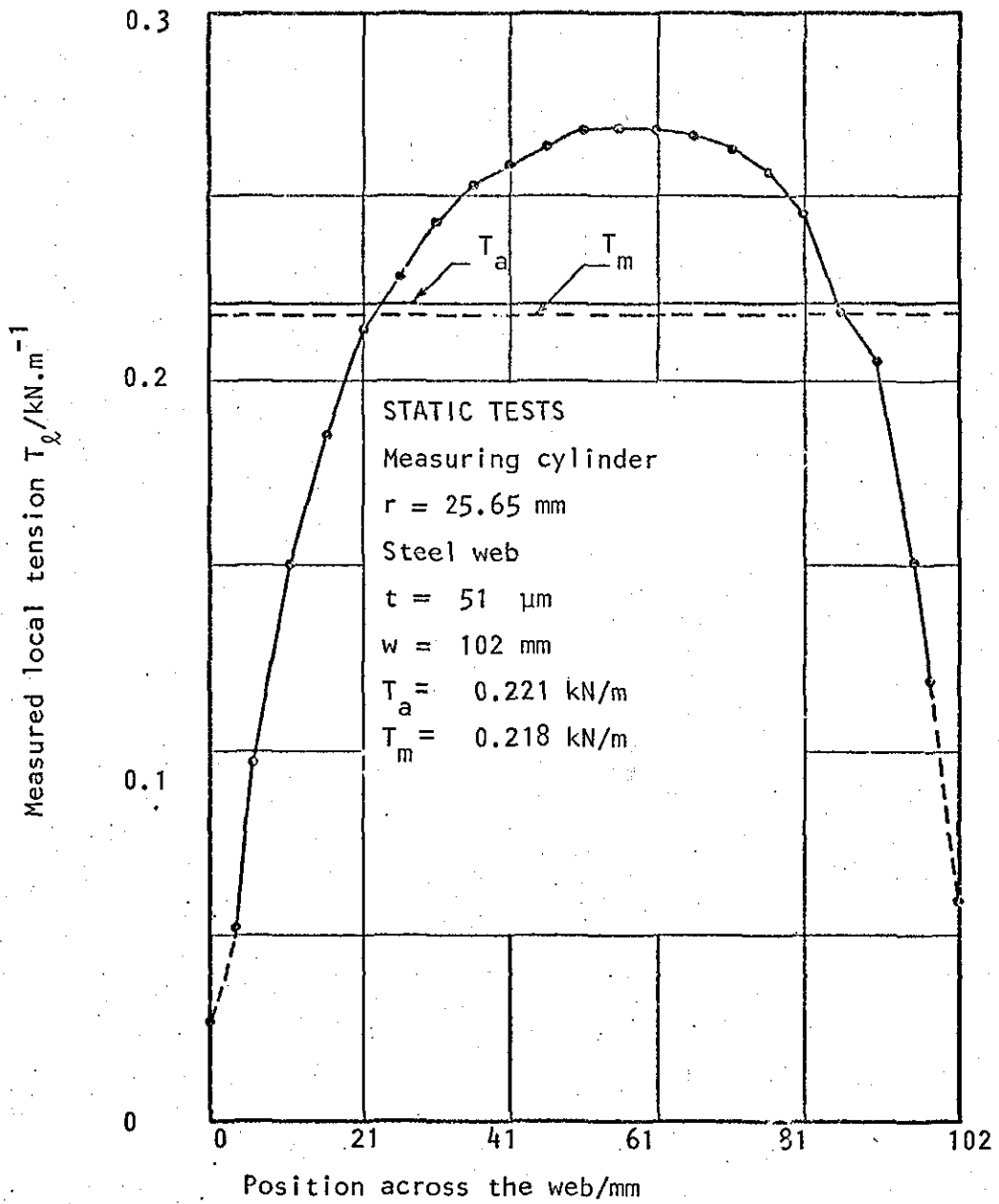


Fig. 6.19 Tension profile across a 102mm wide Steel web.



STATIC TESTS - Validity of  $p = T/R$

- Measuring Pad ;  $R = 258.5 \text{ mm}$
- Web Material : Melinex ; thickness  $t = 51 \mu\text{m}$   
 $w = 50 \text{ mm}$
- $P_v = 1.5, 2 \text{ and } 3 p_t$  ;  $P_c = 1.5, 2 \text{ and } 3 p_{\text{max}}$

$T_a$ kN/m	$P_t$ kN/m <sup>2</sup>	$T_m$ kN/m	
		at $P_v$	at $P_c$
0.214	0.824	0.254	0.271
		0.259	0.274
		0.264	0.279
0.311	1.207	0.360	0.375
		0.370	0.380
		0.378	0.393
0.452	1.746	0.525	0.533
		0.535	0.540
		0.548	0.555
0.548	2.119	0.629	0.629
		0.649	0.649
		0.664	0.664

Table 6.9 Web-tension measured by the measuring pad at different supply pressures.

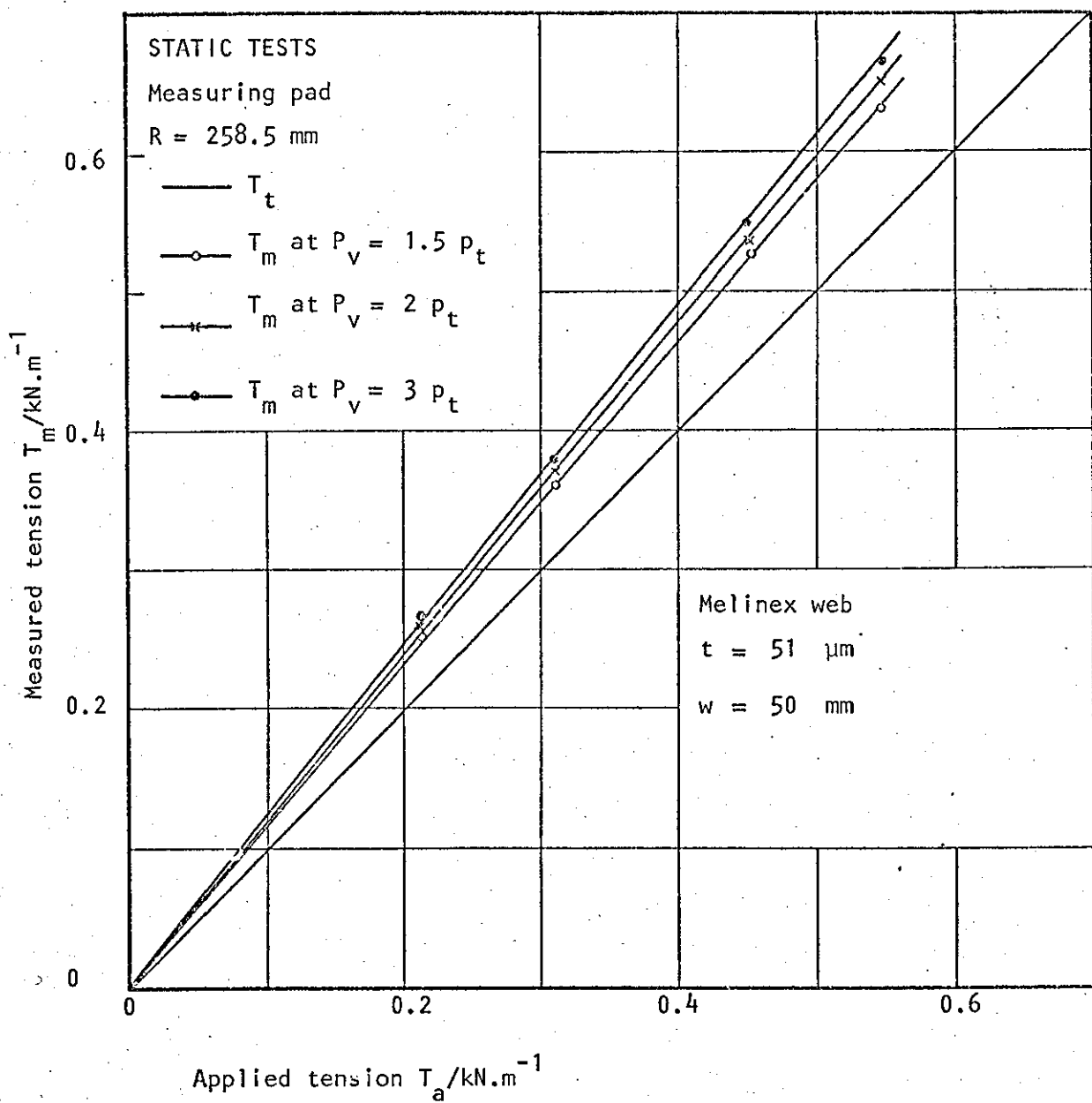


Fig. 6.20 Web-tension measured by the measuring pad at different variable supply pressures.

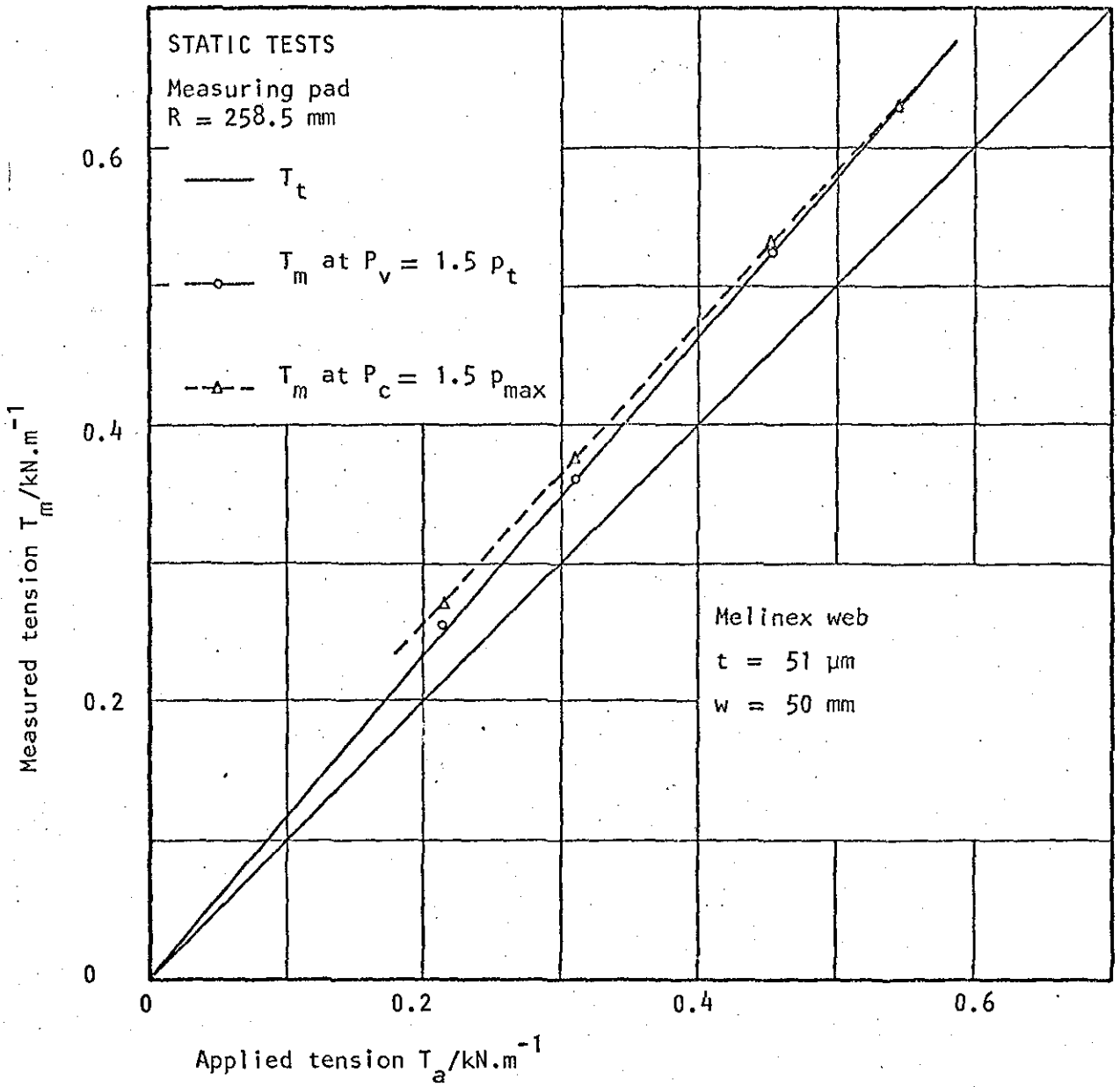


Fig. 6.21 Web-tension measured by the measuring pad at variable and constant supply pressure.

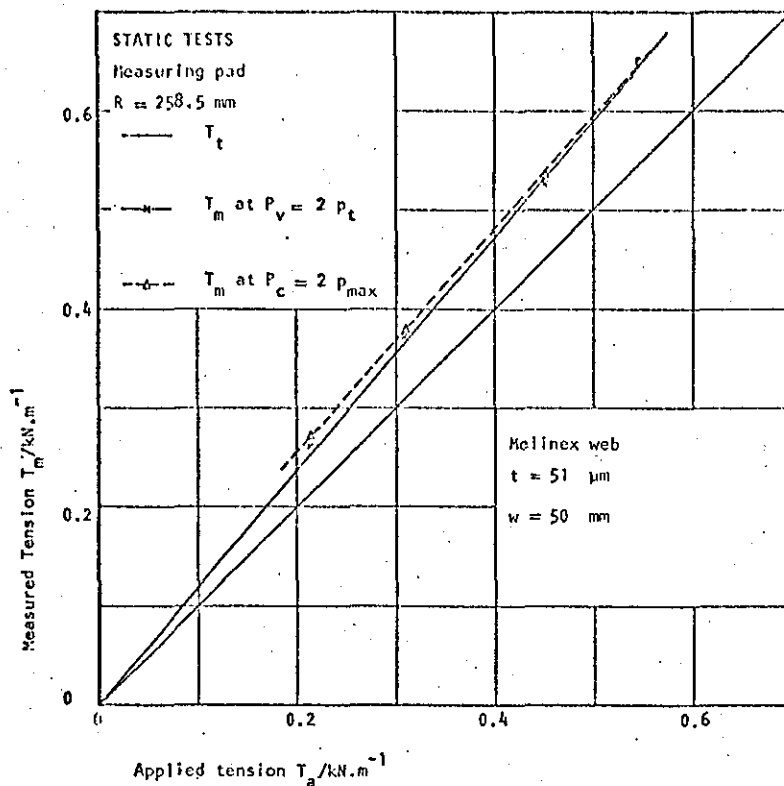


Fig. 6.22 Web-tension measured by the measuring pad at variable and constant supply pressure.

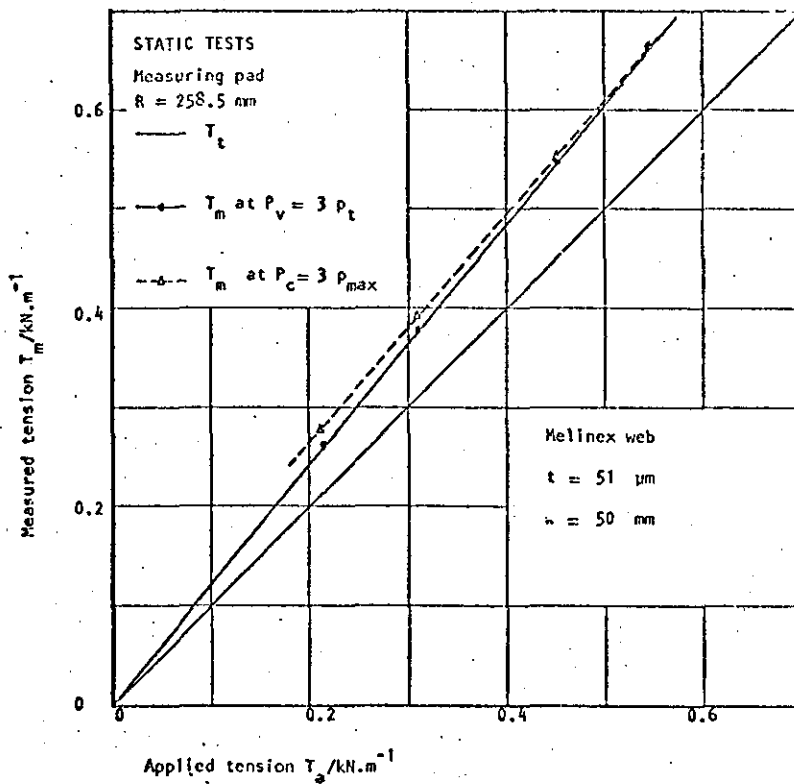


Fig. 6.23 Web-tension measured by the measuring pad at variable and constant supply pressure.

STATIC TESTS - Validity of  $p = T/R$

- Measuring Pad ;  $R = 258.5 \text{ mm}$
- Web Material : Melinex ; thickness  $t = 102 \text{ }\mu\text{m}$   
 $w = 50 \text{ mm}$
- $P_v = 1.5, 2 \text{ and } 3 p_t$  ;  $P_c = 1.5, 2 \text{ and } 3 p_{\text{max}}$

$T_a$ kN/m	$P_t$ kN/m <sup>2</sup>	$T_m$ kN/m	
		at $P_v$	at $P_c$
0.214	0.824	0.251	0.274
		0.263	0.278
		0.272	0.284
0.311	1.207	0.360	0.381
		0.376	0.390
		0.388	0.399
0.452	1.746	0.521	0.530
		0.542	0.549
		0.550	0.564
0.548	2.119	0.625	0.627
		0.654	0.653
		0.675	0.675

Table 6.10 Web-tension measured by the measuring pad at different supply pressures.

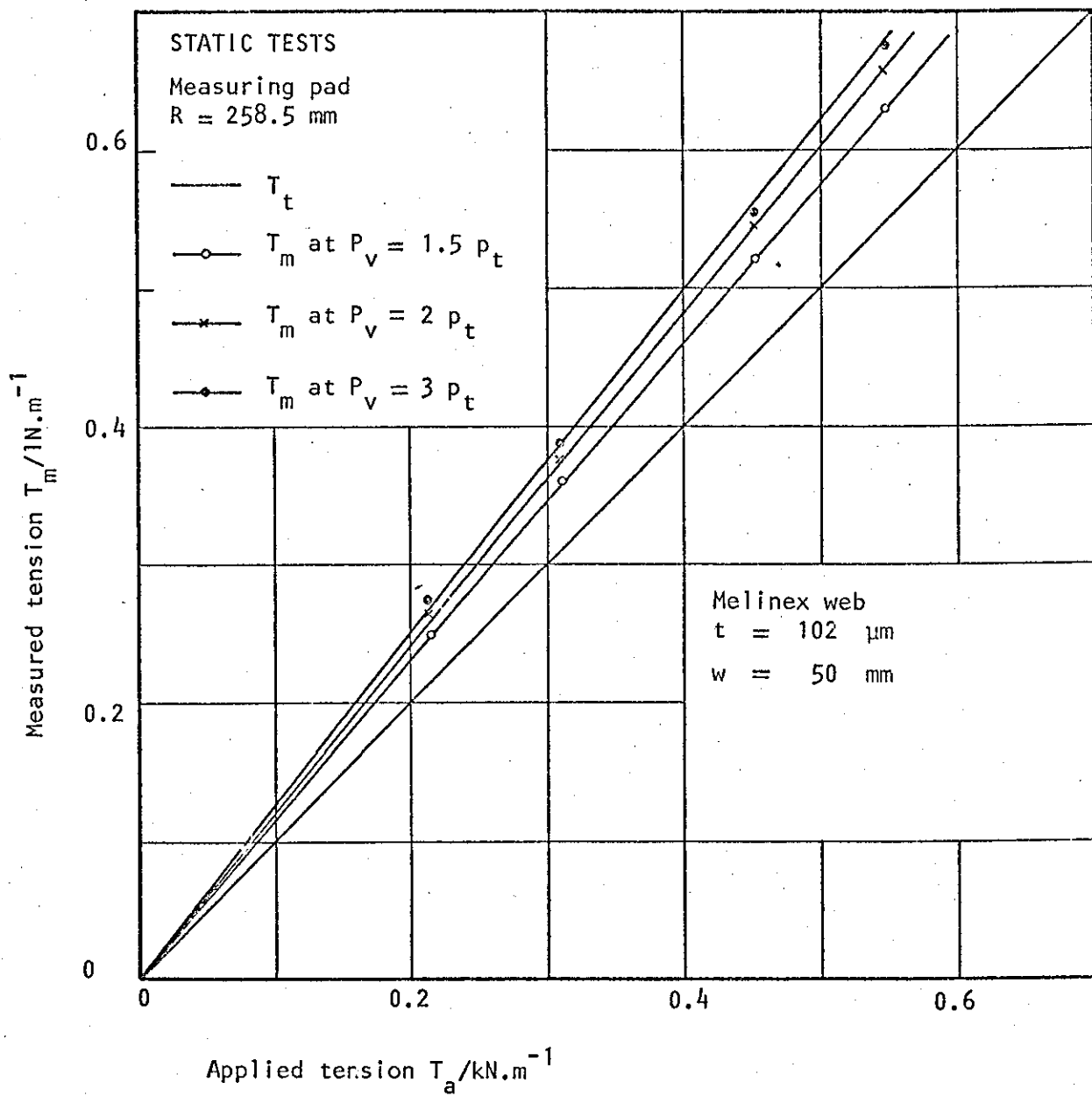


Fig. 6.24 Web-tension measured by the measuring pad at different variable supply pressures.

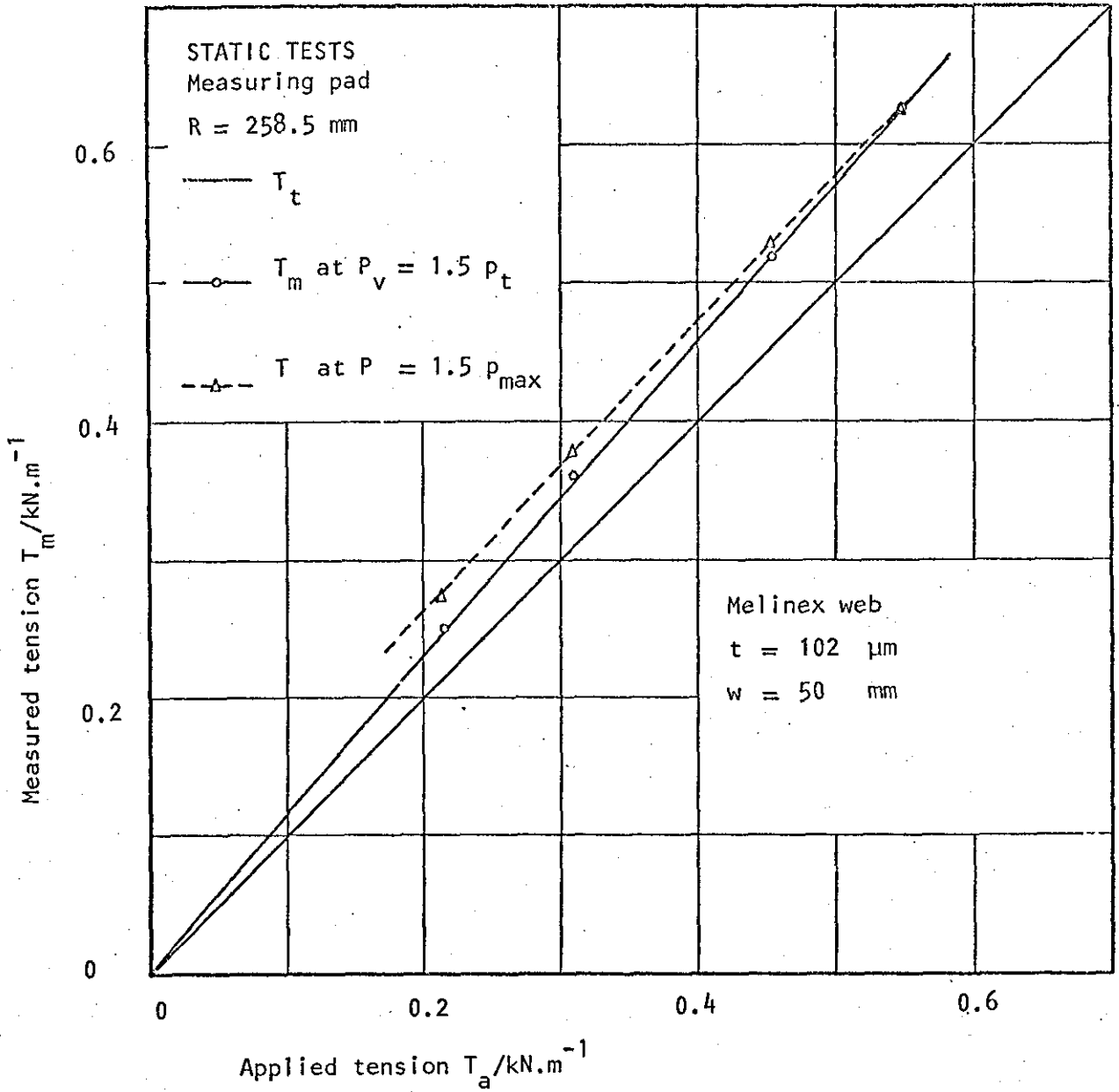


Fig. 6.25 Web-tension measured by the measuring pad at variable and constant supply pressure.

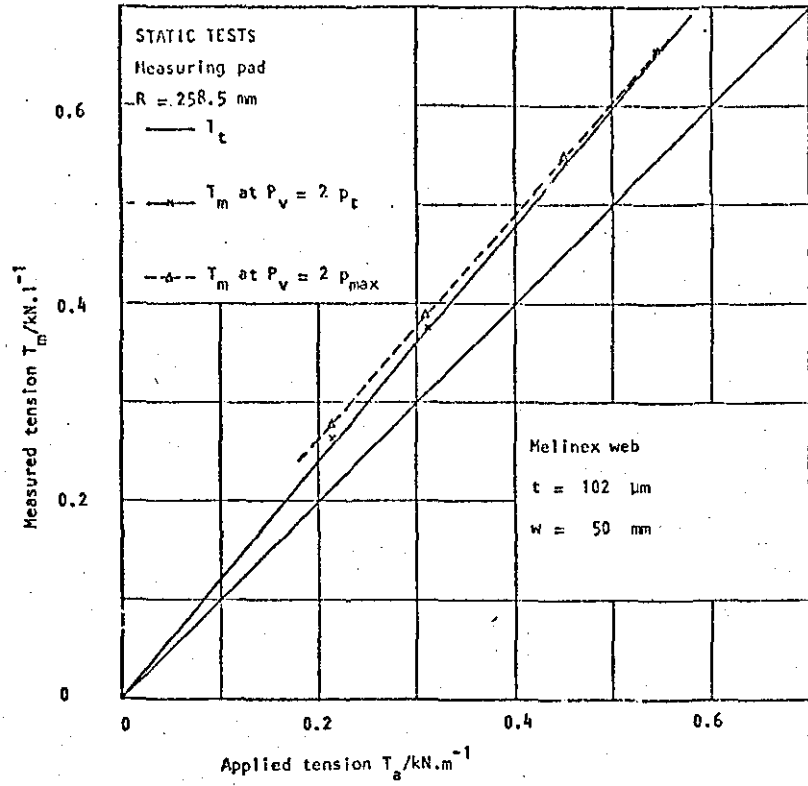


Fig. 6.26 Web-tension measured by the measuring pad at variable and constant supply pressure.

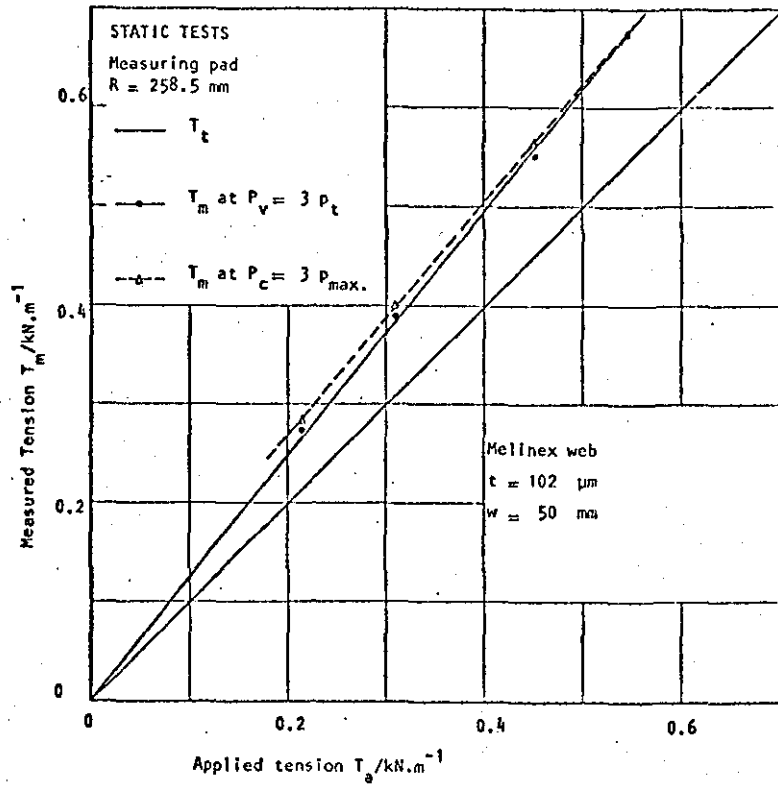


Fig. 6.27 Web-tension measured by the measuring pad at variable and constant supply pressure.



STATIC TESTS ; Validity of  $p = T/R$

- Measuring Pad ;  $R = 258.5 \text{ mm}$
- Web Material : Melinex ; thickness  $t = 102 \text{ }\mu\text{m}$   
 $w = 102 \text{ mm}$
- $P_v = 1.5, 2 \text{ and } 3 p_t$  ;  $P_c = 1.5, 2 \text{ and } 3 p_{\text{max}}$

$T_a$ kN/m	$P_t$ kN/m <sup>2</sup>	$T_m$ kN/m	
		at $P_v$	at $P_c$
0.222	0.853	0.250	0.267
		0.256	0.273
		0.267	0.284
0.269	1.040	0.301	0.318
		0.311	0.324
		0.323	0.341
0.319	1.226	0.354	0.367
		0.369	0.378
		0.381	0.387
0.364	1.413	0.412	0.418
		0.427	0.429
		0.437	0.443
0.413	1.599	0.463	0.464
		0.481	0.480
		0.491	0.491

Table 6.11 Web-tension measured by the measuring pad at different supply pressures.

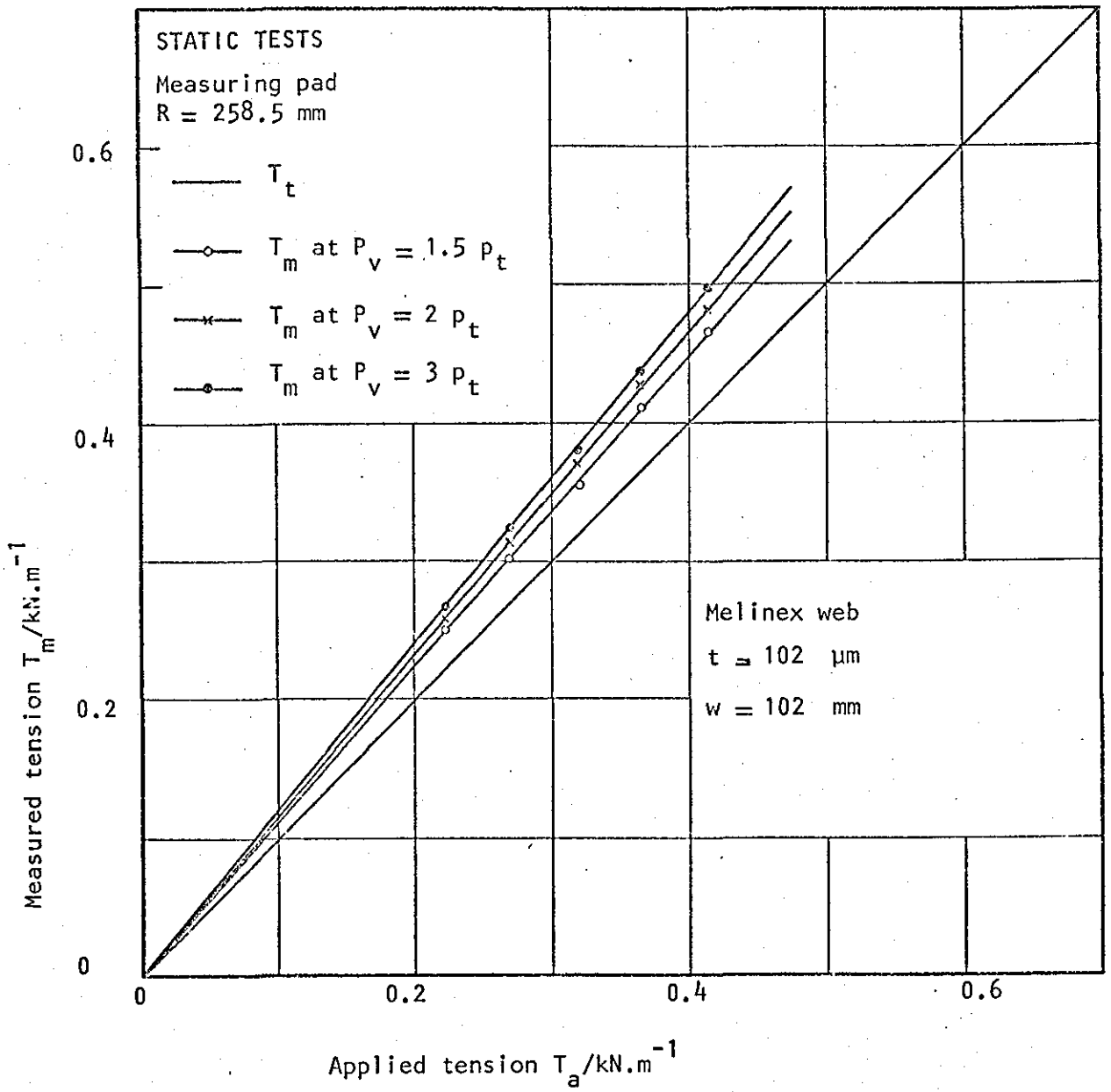


Fig. 6.28 Web-tension measured by the measuring pad at different variable supply pressures.

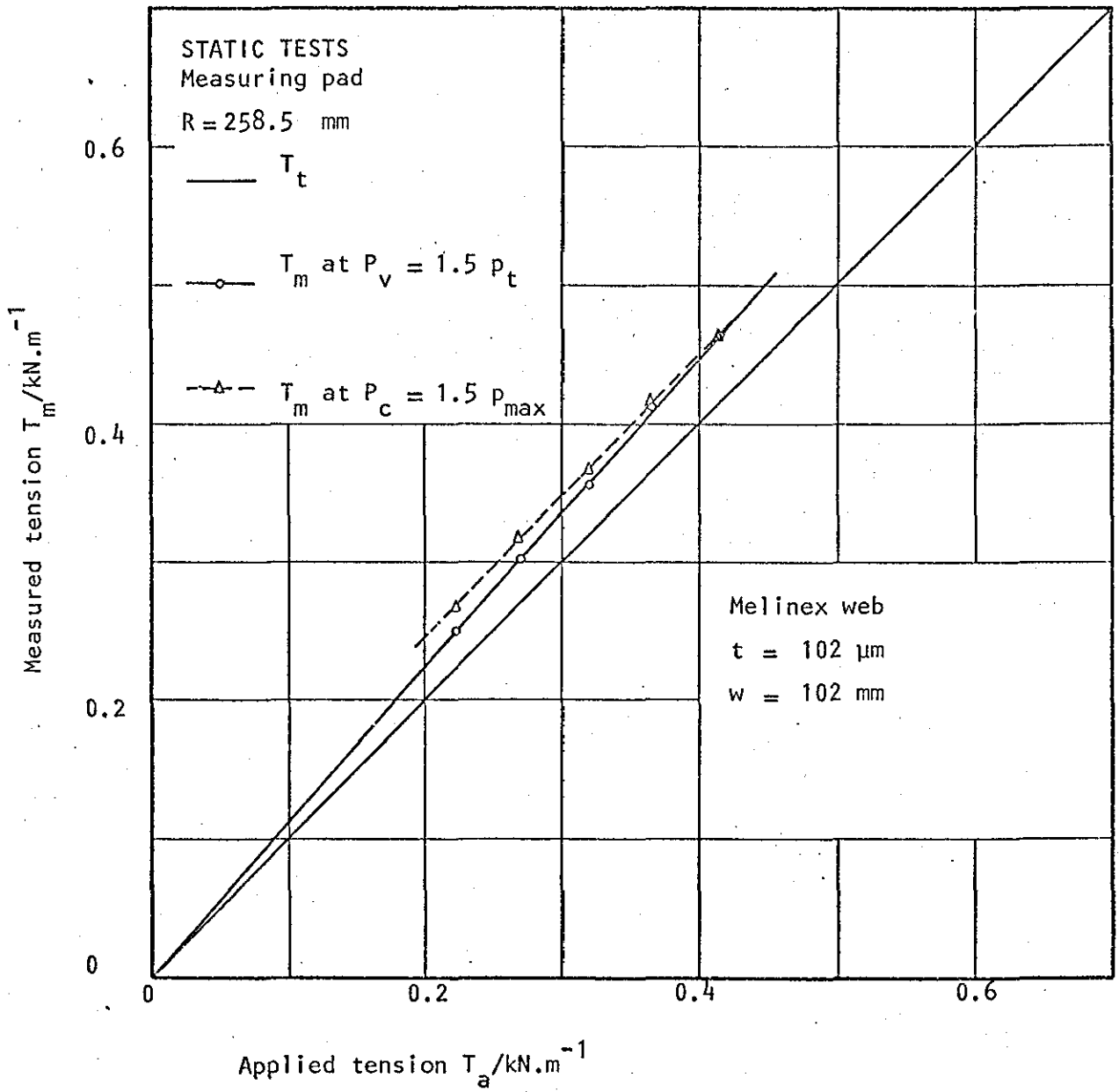


Fig. 6.29 Web tension measured by the measuring pad at variable and constant supply pressure.

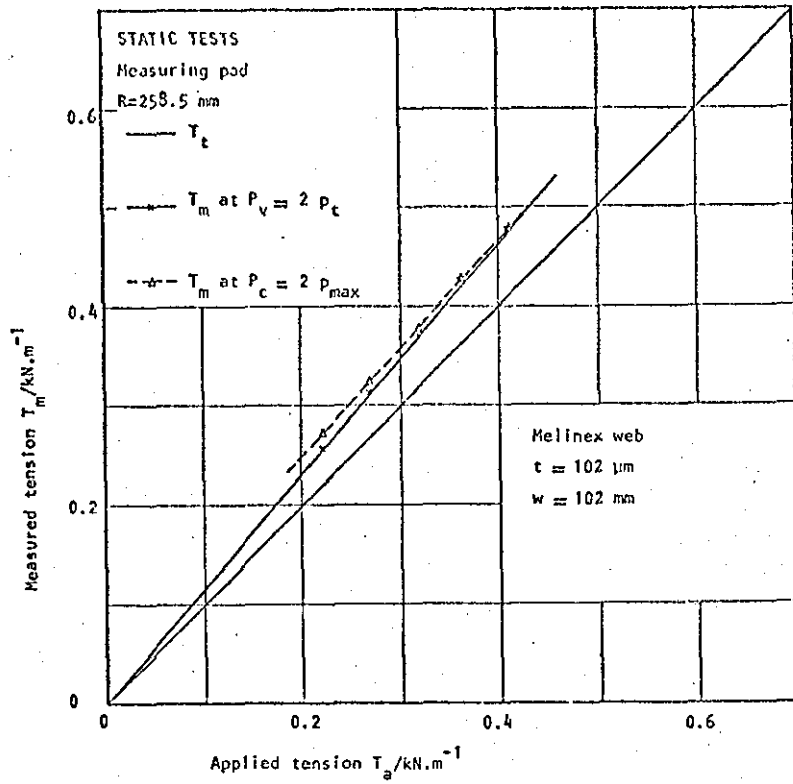


Fig. 6.30 Web-tension measured by the measuring pad at variable and constant supply pressure.

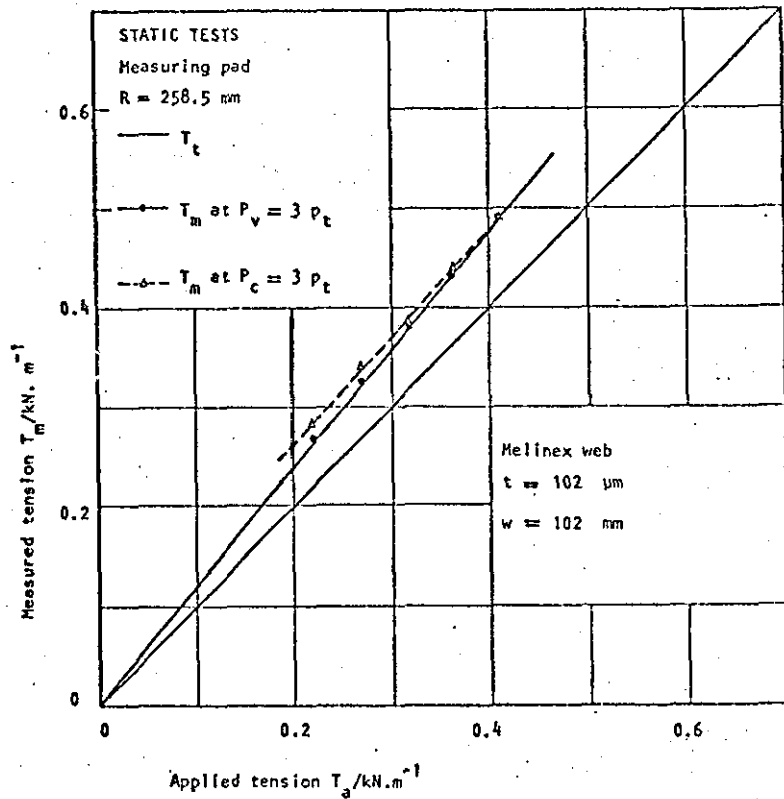


Fig. 6.31 Web-tension measured by the measuring pad at variable and constant supply pressure.

STATIC TESTS - Validity of  $p = T/R$

- Measuring Pad ;  $R = 258.5 \text{ mm}$
- Web Material : Melinex ; thickness  $t = 102 \text{ }\mu\text{m}$   
 $w = 260 \text{ mm}$
- $P_v = 1.5, 2 \text{ and } 3 p_t$  ;  $P_c = 1.5, 2 \text{ and } 3 p_{\text{max}}$

$T_a$ kN/m	$P_t$ kN/m <sup>2</sup>	$T_m$ kN/m	
		at $P_v$	at $P_c$
0.103	0.392	0.155	0.261
		0.202	0.268
		0.246	0.276
0.122	0.491	0.190	0.298
		0.251	0.304
		0.287	0.315
0.159	0.589	0.229	0.325
		0.304	0.376
		0.364	0.390
0.236	0.785	0.350	0.391
		0.450	0.484
		0.535	0.539
0.312	1.177	0.455	0.456
		0.601	0.603
		0.675	0.676

Table 6.12 Web-tension measured by the measuring pad at different supply pressures

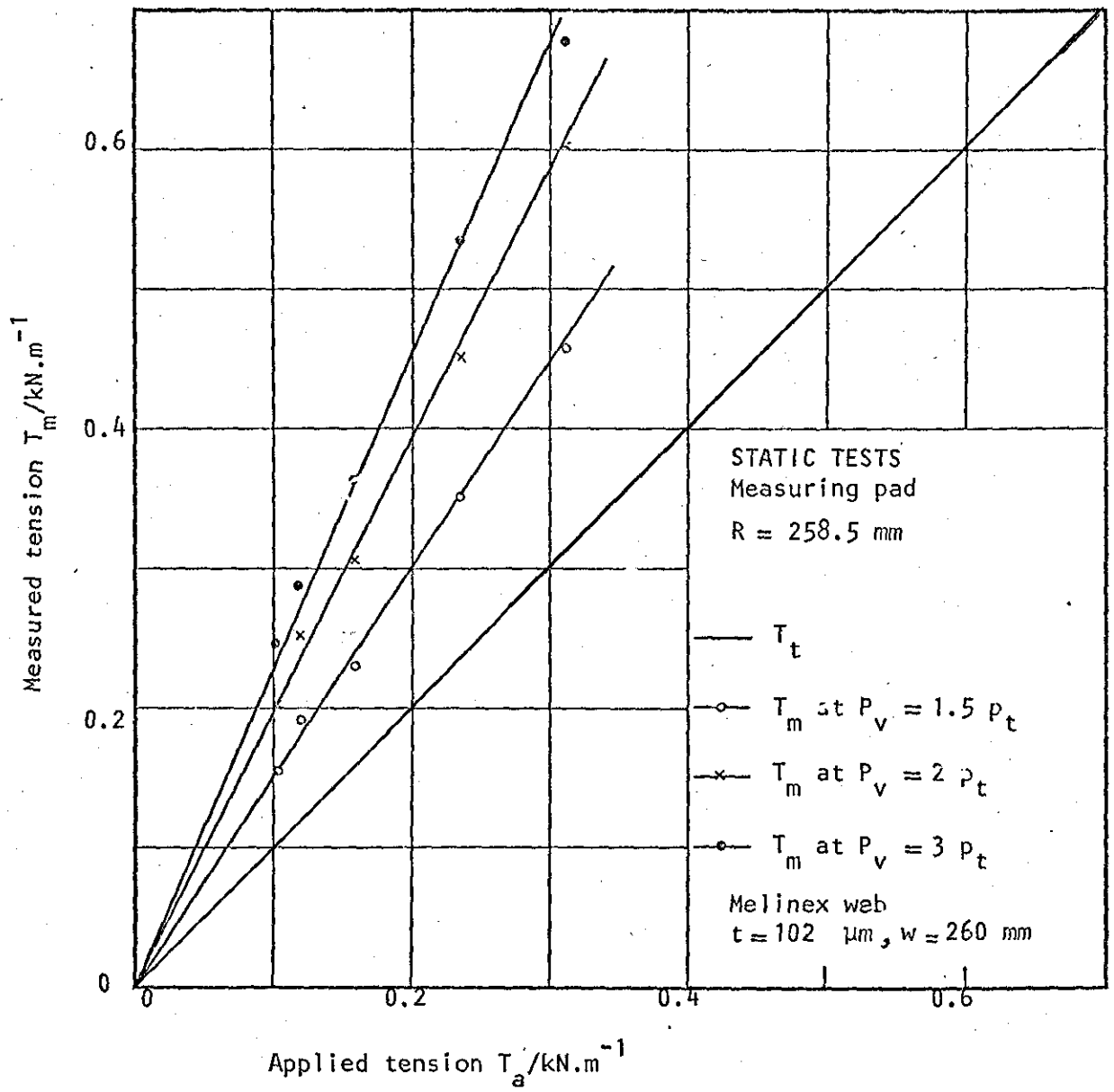


Fig. 6.32 Web-tension measured by the measuring pad at different variable supply pressures.

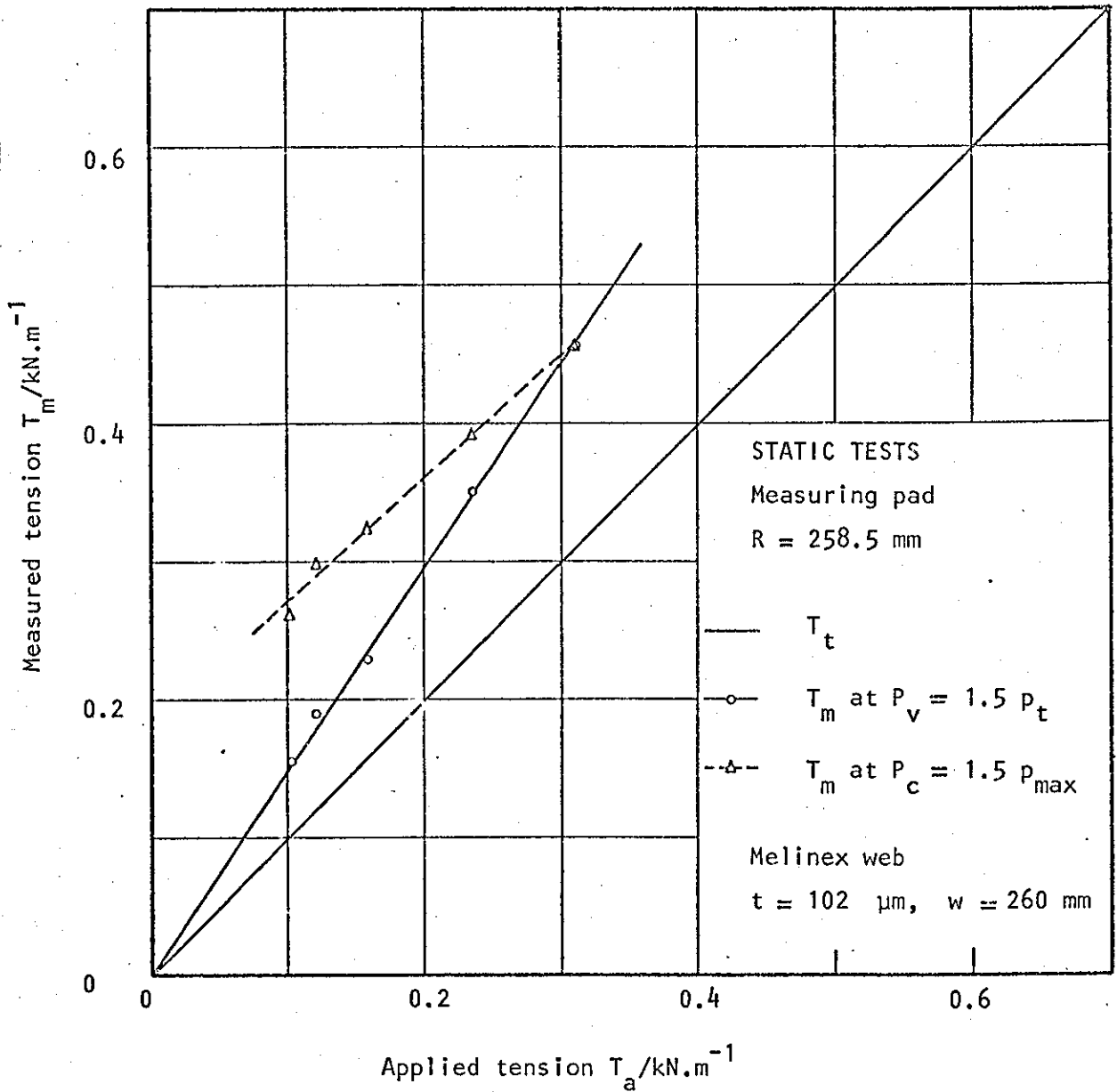


Fig. 6.33 Web-tension measured by measuring pad at variable and constant supply pressure.

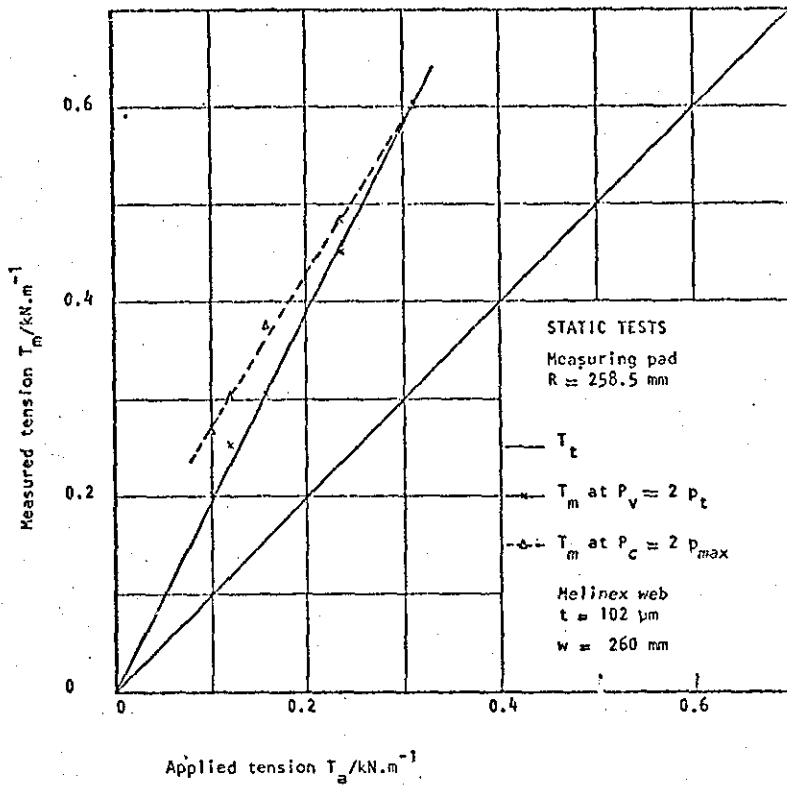


Fig. 6.34 Web-tension measured by the measuring pad at variable and constant supply pressure

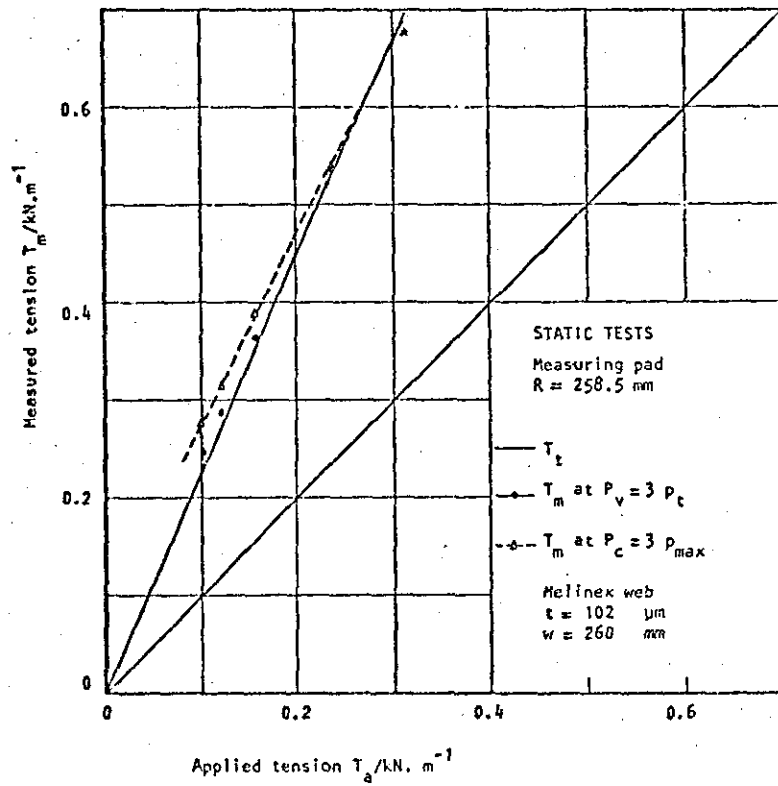


Fig. 6.35 Web-tension measured by the measuring pad at variable and constant pressure.



STATIC TESTS - Tension Profile

- Measuring Pad ; R = 258.8 mm
- Web Material : Steel ; t = .51 μm  
w = 50 mm
- Average applied tension  $T_a = 0.214 \text{ \& } 0.452 \text{ kN/m}$

$$T_\ell = p_\ell \cdot R$$

Position across the web mm	Local tension $T_\ell$ kN/m	
	at $T_a = 0.214$	at $T_a = 0.452$
0	(0.029)	(0.017)
2.5	0.058	0.033
5.0	0.107	0.114
10.0	0.218	0.505
15.0	0.296	0.560
20.0	0.327	0.611
25.0	0.333	0.643
30.0	0.322	0.619
35.0	0.291	0.553
40.0	0.199	0.512
45.0	0.061	0.259
47.5	0.022	0.173
50.0	(0.011)	(0.086)
Experimental average tension	= 0.215 (+ 0.5%)	0.443 (- 1.9%)

Table 6.13 Tension profile across a 50 mm wide steel web.

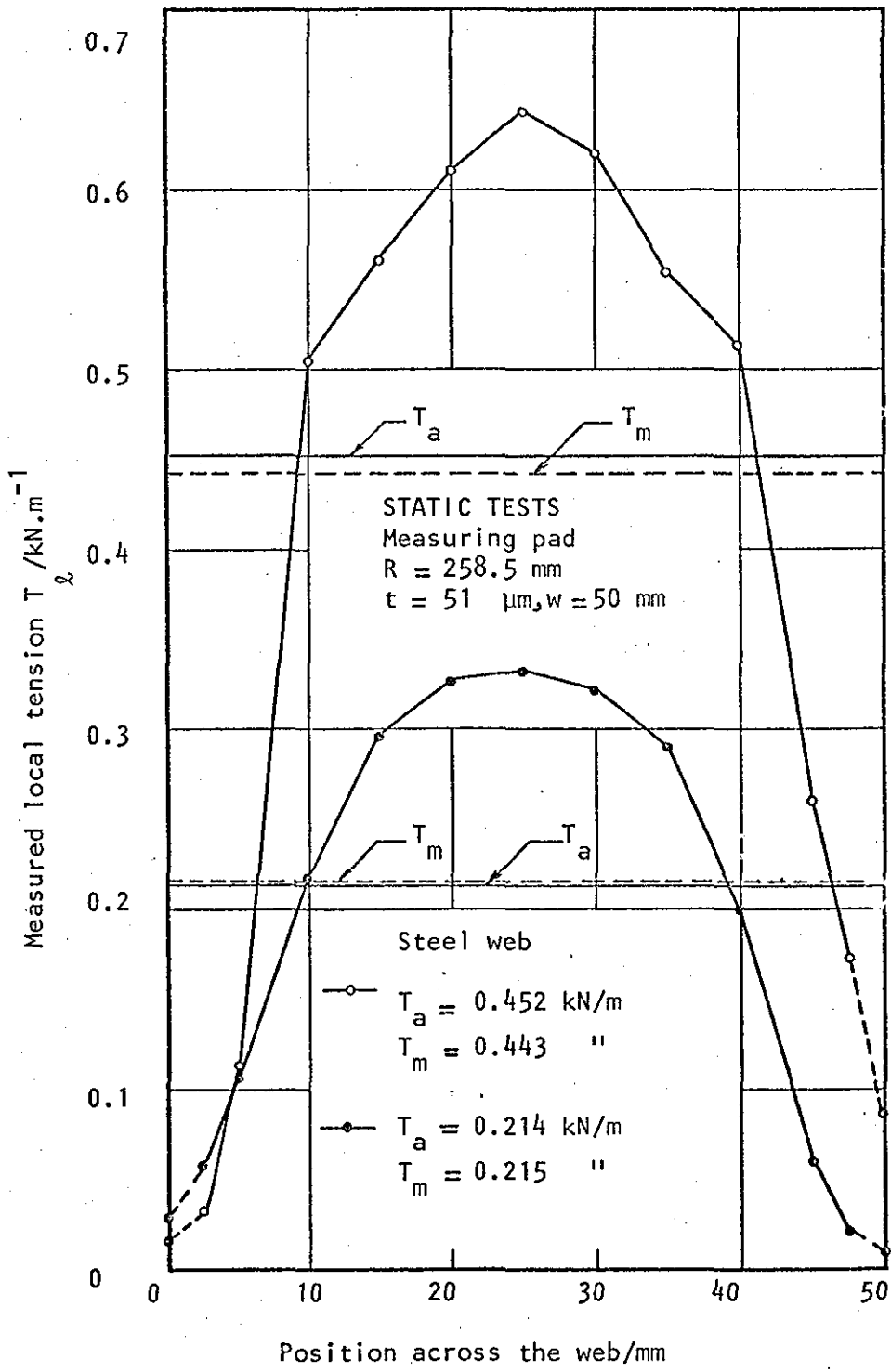


Fig. 6.36 Tension profile across a 50mm wide Steel web.

STATIC TESTS - Tension Profile

- Measuring Pad ; R = 258.5 mm
- Web Material : Steel ; t = .51 μm  
w = 50 mm
- Average applied tension  $T_a = 0.214$  kN/m

$$T_\ell = p_\ell \cdot R$$

Position across the web mm	Local tension $T_\ell$ kN/m	
	across distorted Section (B)	across a true Section (A)
0	(0.050)	(0.029)
2.5	0.101	0.058
5.0	0.205	0.107
10.0	0.346	0.218
12.5	0.360	-
15.0	0.351	0.296
20.0	0.309	0.327
25.0	0.274	0.333
30.0	0.237	0.322
35.0	0.168	0.291
40.0	0.121	0.199
45.0	0.039	0.061
47.5	0.021	0.022
50.0	(0.010)	(0.011)
Experimental average tension	= 0.212 (- 1.0%)	0.215 (+ 0.5%)

Table 6.14 Tension profile across a 50mm wide steel web at different sections.

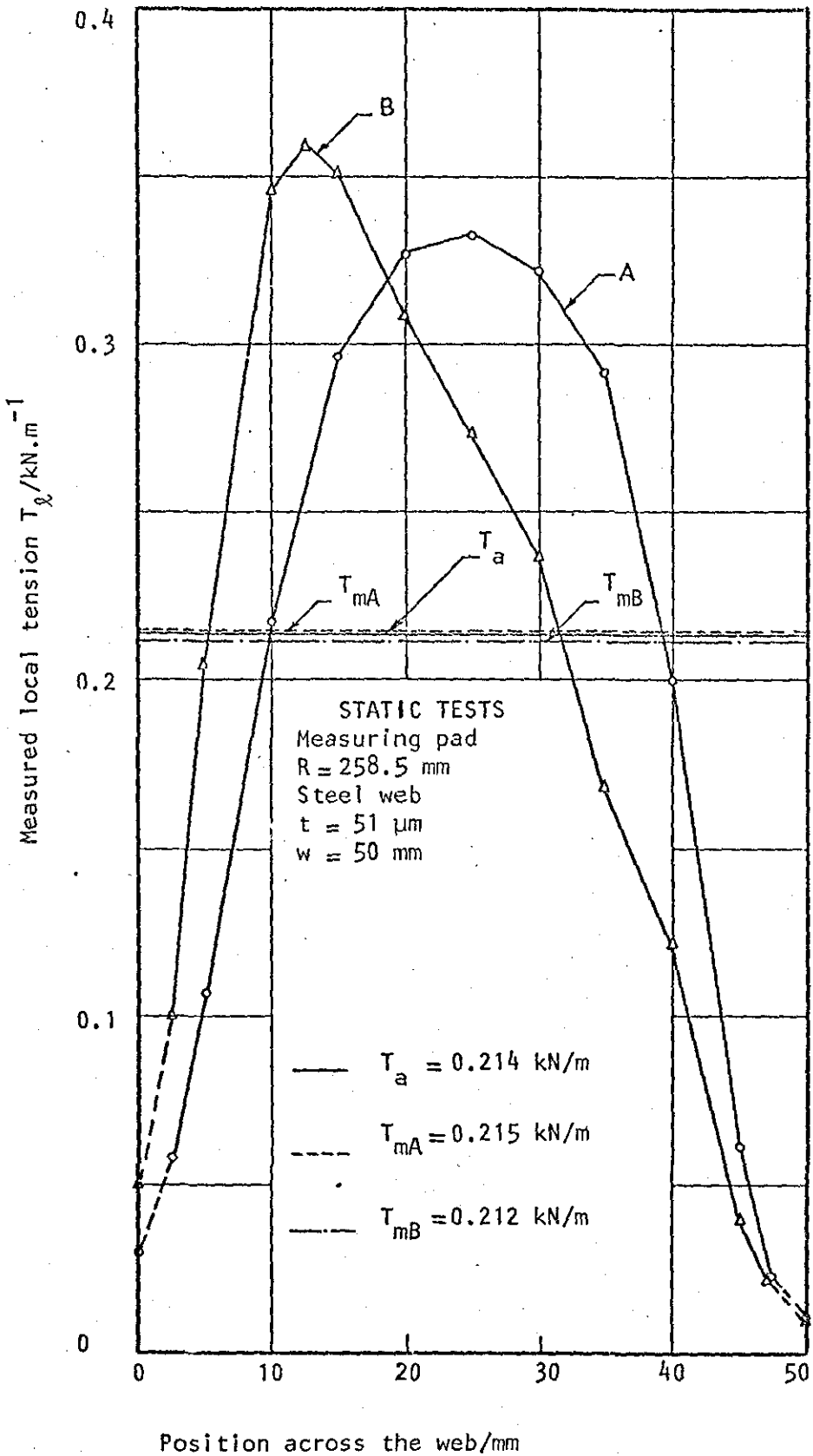


Fig. 6.37 Tension profile across a 50mm wide steel web at two different sections.

STATIC TESTS - Tension Profile

- Measuring Pad ; R = 258.5 mm
- Web Material : Melinex ; t = 102 μm  
w = 50 mm
- Average applied tension  $T_a = 0.214$  &  $0.452$  kN/m

$$T_l = P_l \cdot R$$

Position across the web mm	Local Tension $T_l$ kN/m	
	at $T_a = 0.214$	at $T_a = 0.452$
0	(0.044)	(0.113)
2.5	0.088	0.226
5.0	0.218	0.494
10.0	0.248	0.522
15.0	0.252	0.533
20.0	0.253	0.535
25.0	0.255	0.535
30.0	0.256	0.535
35.0	0.253	0.535
40.0	0.253	0.533
45.0	0.218	0.507
47.5	0.066	0.248
50.0	(0.032)	(0.124)
Experimental average tension	= 0.218 (+ 1.9%)	0.460 (+ 1.8%)

Table 6.15 Tension profile across a 50 mm wide Melinex web.

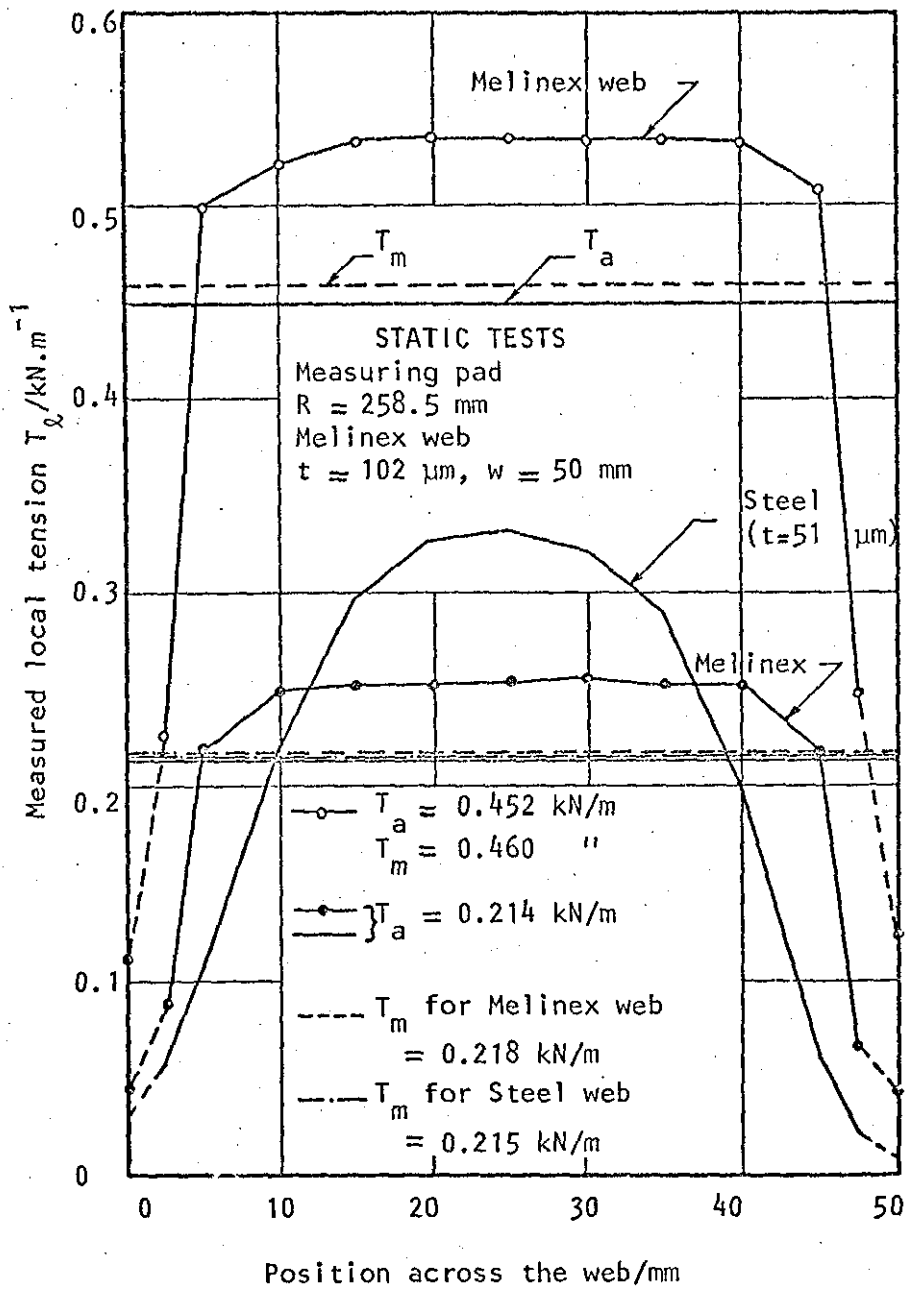


Fig. 6.38 Tension profile across a 50mm wide Melinex web in comparison with a 50mm wide Steel web.

STATIC TESTS - Optimum Wrap Angle

- Measuring Pad ;  $R = 258.5 \text{ mm}$  ;  $P = 2 p_t$
- Web Material : Melinex \* ;  $t = 51 \mu\text{m}$   
 $w = 50 \text{ mm}$

Distance moved by the pad against the web		Wrap Angle degrees	Measured tension in the web at different applied tensions ( $T_m = p_m \cdot R$ ) kN/m				
mm	in.		$T_{a1}$	$T_{a2}$	$T_{a3}$	$T_{a4}$	$T_{a5}^*$
0.00	0.0	0.0	0.000	0.000	0.000	0.000	0.000
2.54	0.1	0.98	0.005	0.013	0.020	0.025	0.018
5.08	0.2	1.88	0.018	0.030	0.038	0.048	0.030
7.62	0.3	2.92	0.038	0.058	0.089	0.104	0.051
10.16	0.4	3.88	0.076	0.114	0.172	0.213	0.086
12.70	0.5	4.84	0.127	0.193	0.284	0.355	0.134
15.24	0.6	5.82	0.178	0.261	0.385	0.472	0.183
17.78	0.7	6.78	0.213	0.304	0.449	0.548	0.228
20.32	0.8	7.76	0.228	0.335	0.487	0.593	0.264
22.86	0.9	8.72	0.243	0.350	0.507	0.616	0.287
25.40	1.0	9.68	0.251	0.360	0.514	0.634	0.294
27.94	1.1	10.64	0.254	0.368	0.525	0.642	0.309
30.48	1.2	11.60	0.256	0.370	0.533	0.647	0.317
33.02	1.3	12.56	0.259	0.373	0.535	0.649	0.322
35.56	1.4	13.52	0.259	0.373	0.535	0.649	0.322
38.10	1.5	14.48	0.259	0.373	0.535	0.649	0.322
40.64	1.6	15.44	0.259	0.373	0.535	0.649	0.322
43.18	1.7	16.38	0.259	0.373	0.535	0.649	0.322

$T_{a1} = 0.214, T_{a2} = 0.311, T_{a3} = 0.452, T_{a4} = 0.548, T_{a5}^* = 0.214 \text{ kN/m}$

\* The same experiment was carried out on a steel web, for comparison, at  $T_{a5} = T_{a1}$ . The steel web had the same dimensions as the Melinex one.

Table 6.16 Optimum wrap angle for a 50 mm wide web, 51  $\mu\text{m}$  thick

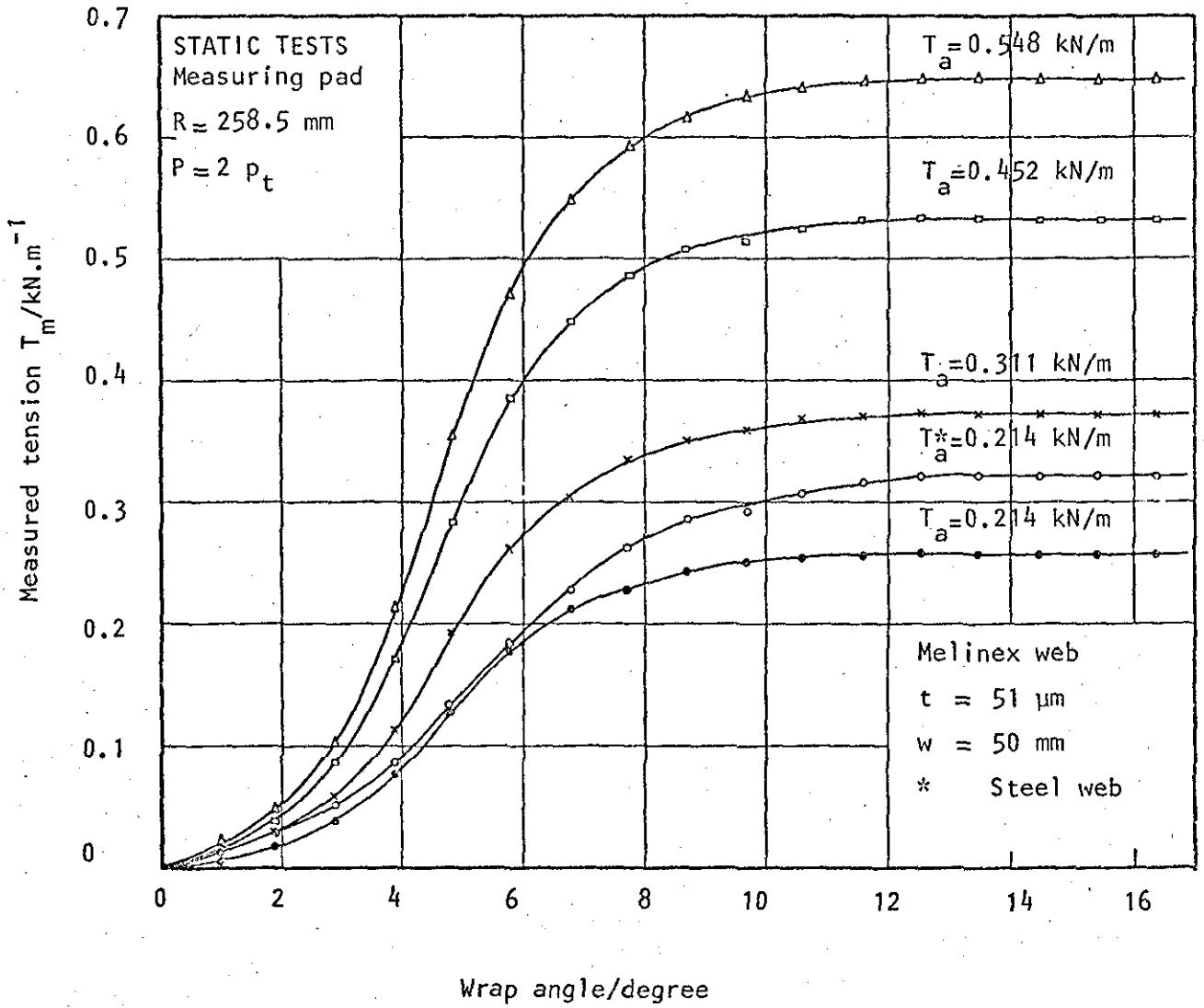


Fig. 6.39 Optimum wrap angle for a 50mm wide Melinex web ( $t = 51 \mu\text{m}$ )



STATIC TESTS - Optimum Wrap Angle

- Measuring Pad ;  $R = 258.5 \text{ mm}$  ;  $P = 2 p_t$
- Web Material : Melinex ;  $t = 102 \mu\text{m}$
- $w = 50 \text{ mm}$

Distance moved by the pad against the web		Wrap Angle degrees	Measured tension in the web at different applied tensions ( $T_m = p_m \cdot R$ ) kN/m			
mm	in		$T_{a1}$	$T_{a2}$	$T_{a3}$	$T_{a4}$
0.00	0.0	0.0	0.000	0.000	0.000	0.000
2.54	0.1	0.98	0.014	0.019	0.025	0.032
5.08	0.2	1.88	0.027	0.037	0.052	0.066
7.62	0.3	2.92	0.048	0.071	0.112	0.136
10.16	0.4	3.88	0.082	0.128	0.202	0.251
12.70	0.5	4.84	0.126	0.190	0.302	0.382
15.24	0.6	5.82	0.161	0.251	0.383	0.475
17.78	0.7	6.78	0.188	0.288	0.434	0.535
20.32	0.8	7.76	0.207	0.314	0.465	0.571
22.86	0.9	8.72	0.221	0.330	0.489	0.600
25.40	1.0	9.68	0.236	0.344	0.507	0.617
27.94	1.1	10.64	0.240	0.352	0.520	0.633
30.48	1.2	11.60	0.247	0.361	0.527	0.640
33.02	1.3	12.56	0.251	0.368	0.535	0.649
35.56	1.4	13.52	0.256	0.369	0.539	0.653
38.10	1.5	14.48	0.258	0.373	0.540	0.653
40.64	1.6	15.44	0.261	0.373	0.540	0.653
43.18	1.7	16.38	0.261	0.373	0.540	0.653

$$T_{a1} = 0.214, T_{a2} = 0.311, T_{a3} = 0.452, T_{a4} = 0.548$$

Table 6.17 Optimum wrap angle for a 50 mm wide web,  
102  $\mu\text{m}$  thick.

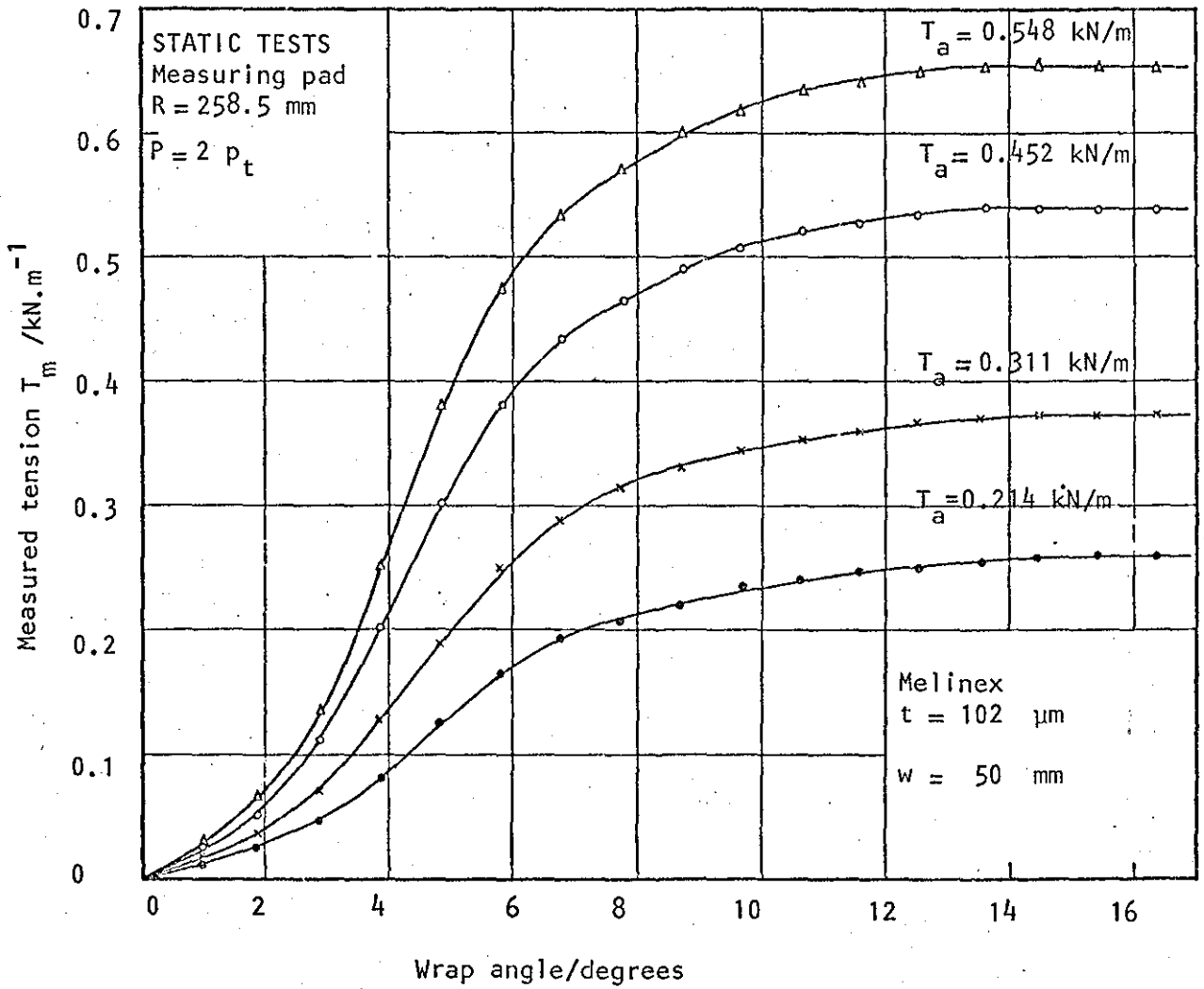


Fig. 6.40 Optimum wrap angle for a 50 mm wide Melinex web  
( $t = 102 \text{ }\mu\text{m}$ )

STATIC TESTS - Optimum Wrap Angle

- Measuring Pad ; R = 258.5 mm ; P = 2 p<sub>t</sub>
- Web Material : Melinex ; t = 102 μm
- w = 102 mm

Distance moved by the pad against the web		Wrap angle degrees	Measured tension in the web at different applied tensions (T <sub>m</sub> = p <sub>m</sub> · R) kN/m				
mm	in		T <sub>a1</sub>	T <sub>a2</sub>	T <sub>a3</sub>	T <sub>a4</sub>	T <sub>a5</sub>
0.00	0.0	0.0	0.000	0.000	0.000	0.000	0.000
2.54	0.1	0.98	0.009	0.013	0.015	0.019	0.022
5.08	0.2	1.88	0.023	0.028	0.037	0.042	0.049
7.62	0.3	2.92	0.049	0.063	0.076	0.090	0.099
10.16	0.4	3.88	0.091	0.117	0.143	0.169	0.189
12.70	0.5	4.84	0.141	0.181	0.219	0.257	0.295
15.24	0.6	5.82	0.183	0.228	0.275	0.321	0.368
17.78	0.7	6.78	0.205	0.260	0.308	0.358	0.410
20.32	0.8	7.76	0.219	0.276	0.330	0.380	0.435
22.86	0.9	8.72	0.231	0.288	0.344	0.397	0.455
25.40	1.0	9.68	0.240	0.297	0.354	0.408	0.464
27.94	1.1	10.64	0.249	0.304	0.360	0.417	0.472
30.48	1.2	11.60	0.252	0.308	0.364	0.420	0.475
33.02	1.3	12.56	0.256	0.311	0.368	0.423	0.479
35.56	1.4	13.52	0.257	0.313	0.370	0.426	0.481
38.10	1.5	14.48	0.257	0.313	0.370	0.426	0.482
40.64	1.6	15.44	0.257	0.313	0.370	0.426	0.482
43.18	1.7	16.38	0.257	0.313	0.370	0.426	0.482

T<sub>a1</sub> = 0.222, T<sub>a2</sub> = 0.268, T<sub>a3</sub> = 0.319, T<sub>a4</sub> = 0.364, T<sub>a5</sub> = 0.413 kN/m

Table 6.18 Optimum Wrap Angle for a 102 mm wide web.

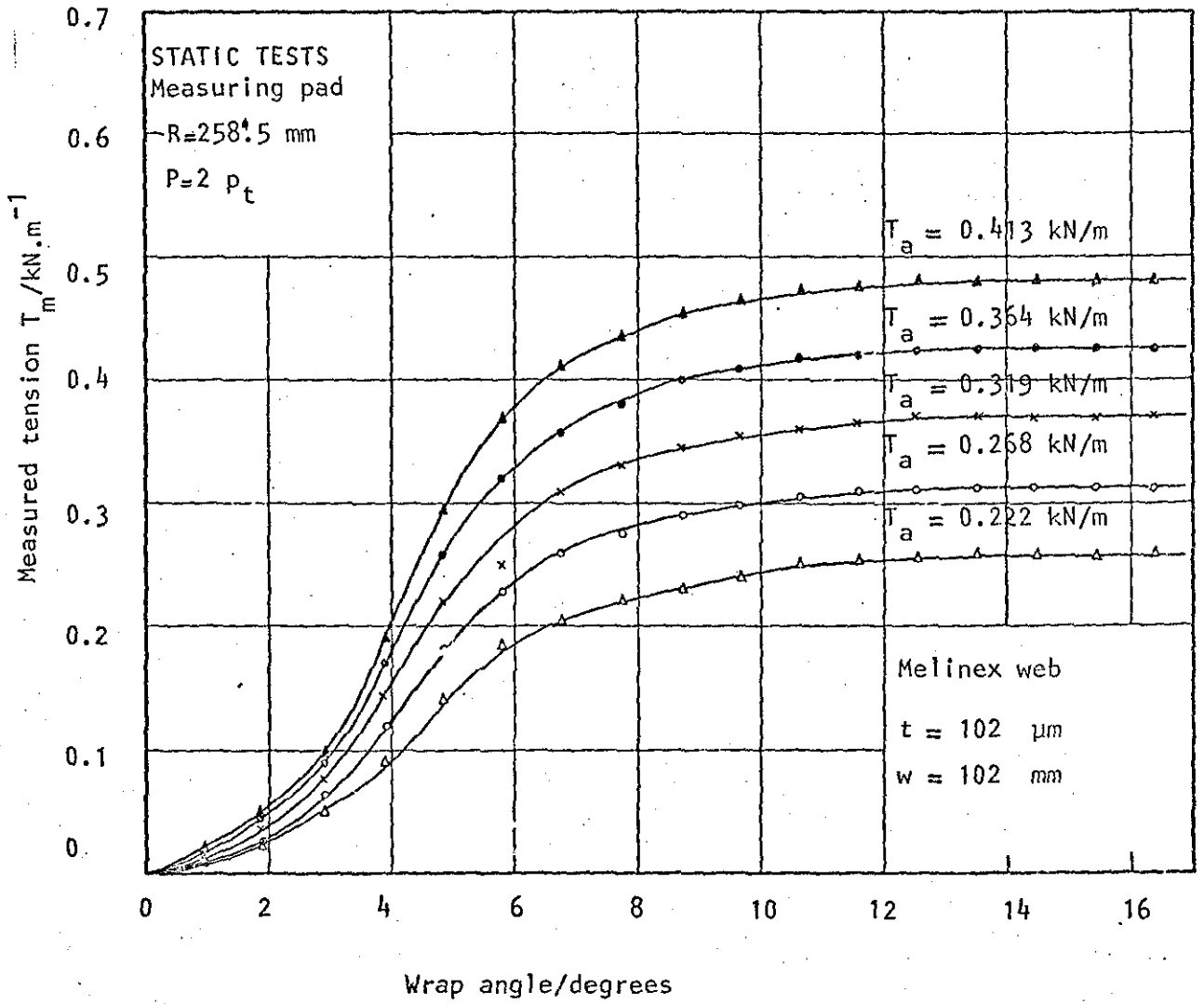


Fig. 6.41 Optimum wrap angle for a 102 mm wide Melinex web.

STATIC TESTS - Optimum Wrap Angle

- Measuring Pad ;  $R = 258.5 \text{ mm}$  ;  $P = 2 P_t$
- Web Material : Melinex ;  $t = 102 \mu\text{m}$   
 $w = 260 \text{ mm}$

Distance moved by the pad against the web			Measured tension in the web at different applied tensions ( $T_m = P_m \cdot R$ ) kN/m				
mm	in	Wrap angle degrees	$T_{a1}$	$T_{a2}$	$T_{a3}$	$T_{a4}$	$T_{a5}$
0.00	0.0	0.0	0.000	0.000	0.000	0.000	0.000
2.54	0.1	0.98	0.015	0.019	0.023	0.036	0.052
5.08	0.2	1.88	0.037	0.047	0.060	0.082	0.117
7.62	0.3	2.92	0.075	0.072	0.118	0.162	0.221
10.16	0.4	3.88	0.096	0.151	0.184	0.251	0.344
12.70	0.5	4.84	0.156	0.191	0.237	0.322	0.434
15.24	0.6	5.82	0.178	0.213	0.264	0.363	0.494
17.78	0.7	6.78	0.188	0.228	0.278	0.383	0.531
20.32	0.8	7.76	0.193	0.233	0.288	0.394	0.553
22.86	0.9	8.72	0.197	0.237	0.293	0.399	0.566
25.40	1.0	9.68	0.199	0.241	0.295	0.402	0.576
27.94	1.1	10.64	0.202	0.243	0.299	0.404	0.586
30.48	1.2	11.60	0.204	0.245	0.303	0.407	0.595
33.02	1.3	12.56	0.204	0.249	0.306	0.407	0.600
35.56	1.4	13.52	0.205	0.250	0.306	0.408	0.602
38.10	1.5	14.48	0.205	0.250	0.306	0.408	0.602
40.64	1.6	15.44	0.205	0.250	0.306	0.408	0.602
43.18	1.7	16.38	0.205	0.250	0.306	0.408	0.602

$T_{a1} = 0.103, T_{a2} = 0.122, T_{a3} = 0.159, T_{a4} = 0.236, T_{a5} = 0.312 \text{ kN/m}$

Table 6.19 Optimum Wrap Angle for a 260 mm wide web.

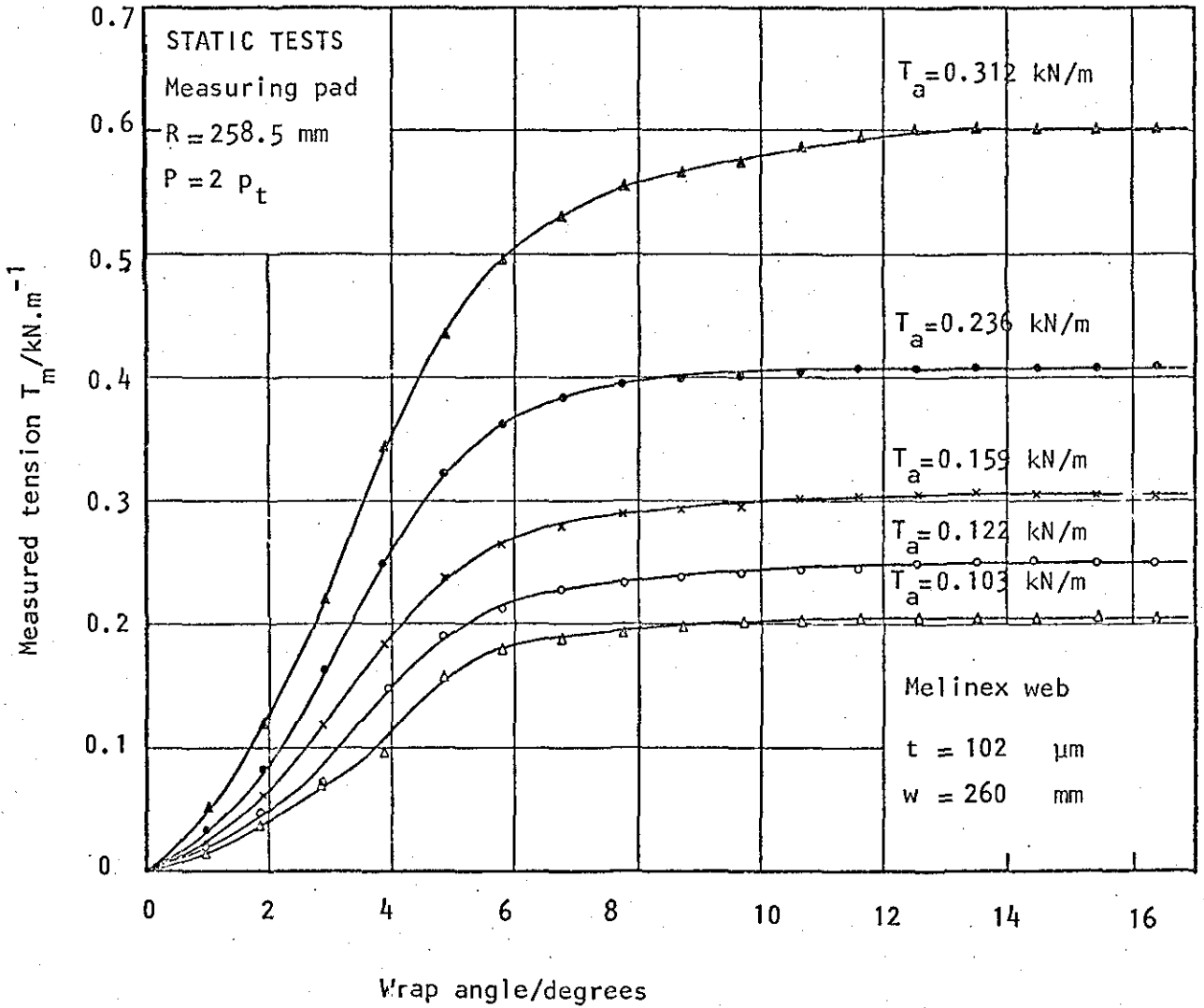


Fig. 6.42 Optimum wrap angle for a 260 mm wide Melinex web

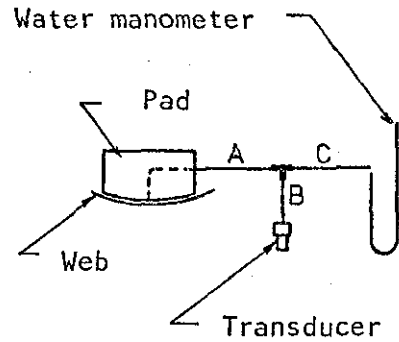
STATIC TESTS -

Optimum position for the miniature pressure transducer

- Measuring Pad :  $R = 258.5 \text{ mm}$  ;  $T = 2 P_{\text{max}}$
- Web Material : Melinex ;  $t = 102 \mu\text{m}$  ;  $w = 102 \text{ mm}$
- Stage I

Transducer in the Calibration adapter outside the pad

Experiment No.	A	B mm	C
1	1000	2300	2300
2	10	50	2300



Applied tension kN/m	Measured tension kN/m			
	(1)		(2)	
	By manometer	By transducer	By manometer	By transducer
0.000	0.000	0.000	0.000	0.000
0.018	0.018	0.023	0.015	0.010
0.094	0.108	0.111	0.107	0.101
0.211	0.235	0.239	0.237	0.239
0.259	0.287	0.294	0.290	0.277
0.308	0.341	0.345	0.342	0.340
0.354	0.391	0.395	0.390	0.396
0.402	0.442	0.446	0.443	0.451
0.452	0.494	0.502	0.494	0.506
0.500	0.545	0.552	0.546	0.562
0.547	0.594	0.598	0.595	0.608
0.595	0.645	0.645	0.645	0.654

Table 6.20 Calibration of the Miniature pressure transducer against water manometer.

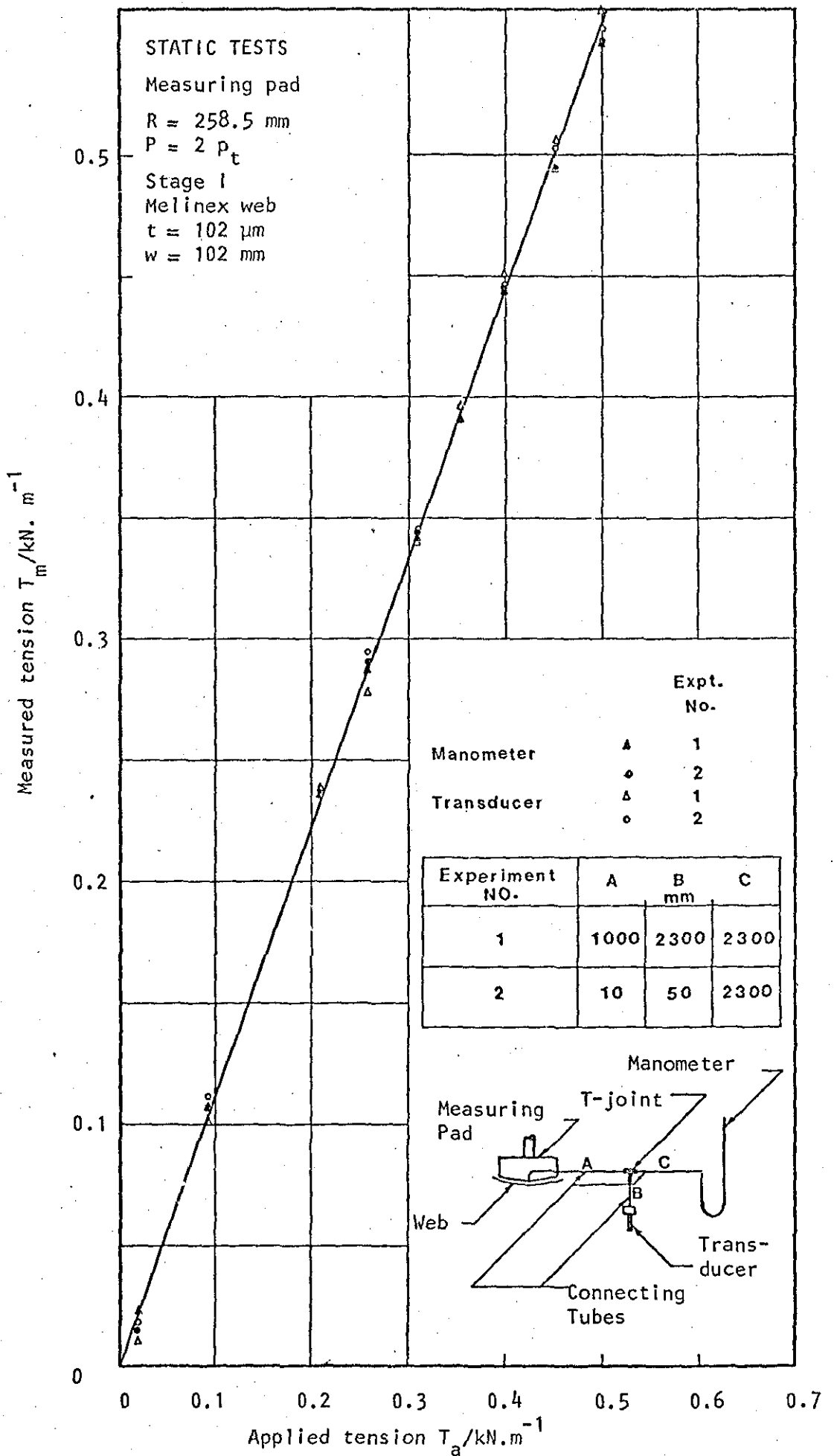


Fig. 6.43 Calibration of the Miniature pressure transducer against water manometer.



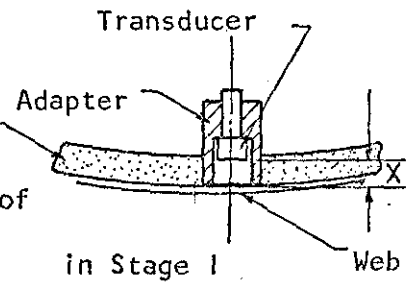
STATIC TESTS -

Optimum position of the miniature pressure transducer

- Measuring Pad ;  $R = 258.5 \text{ mm}$  ;  $P = 2 p_{\text{max}}$
- Web Material : Melinex ;  $t = 102 \mu\text{m}$  ;  $w = 102 \text{ mm}$
- Stage II

Transducer fitted into the pad within different adapters

Sintered segment of the pad



Applied tension kN/m	Measured tension at different positions of the pressure transducer kN/m						in Stage I
	$x_1$	$x_2$	$x_3$	$x_4$	$x_5$	$x_6$	
0.000	0.000	0.000	0.000	0.000	0.000	0.000	0.000
0.018	-0.019	0.009	0.005	0.009	0.014	0.023	0.017
0.094	0.019	0.024	0.014	0.046	0.097	0.101	0.106
0.211	0.115	0.111	0.106	0.176	0.225	0.231	0.239
0.259	0.176	0.171	0.157	0.231	0.271	0.277	0.286
0.308	0.212	0.231	0.207	0.277	0.323	0.332	0.343
0.354	0.272	0.267	0.253	0.328	0.374	0.383	0.396
0.402	0.336	0.323	0.309	0.374	0.429	0.442	0.449
0.452	0.396	0.369	0.359	0.438	0.480	0.489	0.504
0.500	0.451	0.438	0.424	0.493	0.535	0.548	0.557
0.547	0.511	0.502	0.451	0.548	0.590	0.599	0.603
0.595	0.567	0.557	0.521	0.608	0.645	0.654	0.654

- $x_1 = 2.31 \text{ mm}$  (0.091 in) ;  $x_4 = 5.08 \text{ mm}$  (0.200 in)
- $x_2 = 3.25 \text{ mm}$  (0.128 in) ;  $x_5 = 5.72 \text{ mm}$  (0.225 in)
- $x_3 = 3.81 \text{ mm}$  (0.150 in) ;  $x_6 = 6.17 \text{ mm}$  (0.243 in)

Table 6.21 Optimum position of the pressure transducer - Stage II

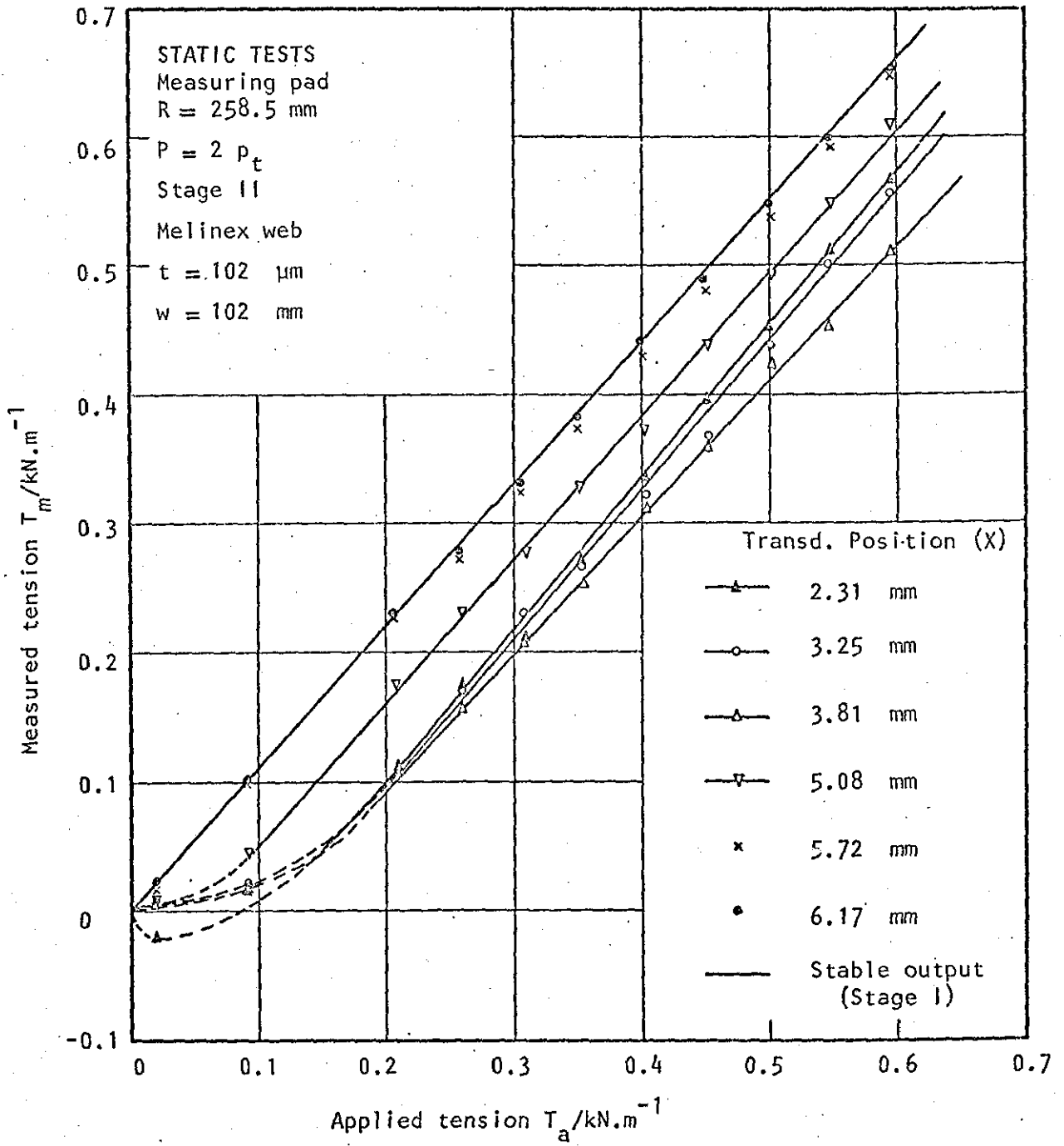


Fig. 6.44 Optimum stable position of the Miniature pressure transducer.

DYNAMIC TESTS - Measuring cylinder with Kistler transducer

- Measuring Cylinder ; "Kistler" pressure transducer
- Web Material : 1- Melinex } ; t = 51 μm  
                                   2- Steel } ; w = 102 mm
- Initial static tension . . . . . 0.52 kN/m
- Direct current applied to vibrator moving coil 1 A
- Alternating current applied to vibrator moving coil 1 A

Amplitude of sinusoidal force measured at different frequencies  
Amplitude of equivalent force measured at zero frequency

$$= A_m / A_{\omega=0}$$

Frequency of applied force (ω) Hz	$A_m / A_{\omega=0}$			
	Melinex Web		Steel Web	
	Load-cell	Transducer	Load-cell	Transducer
1.5	0.96	1.00	0.99	1.01
3	0.96	0.98	0.99	1.01
5	1.03	1.09	0.99	1.01
7	1.25	1.29	0.99	1.01
9	1.62	1.69	-	-
10	-	-	1.13	1.13
11	3.62	3.38	-	-
12	-	-	1.33	1.33
13	5.60	5.38	-	-
15	2.36	2.45	1.55	1.52
17	0.85	0.88	3.15	3.05
20	0.52	0.52	-	-
25	0.29	0.32	1.85	1.77
30	0.22	0.24	0.87	0.88
40	-	-	0.39	0.39
50	-	-	0.28	0.25

Table 6.22 Frequency response of the Kistler transducer 1.

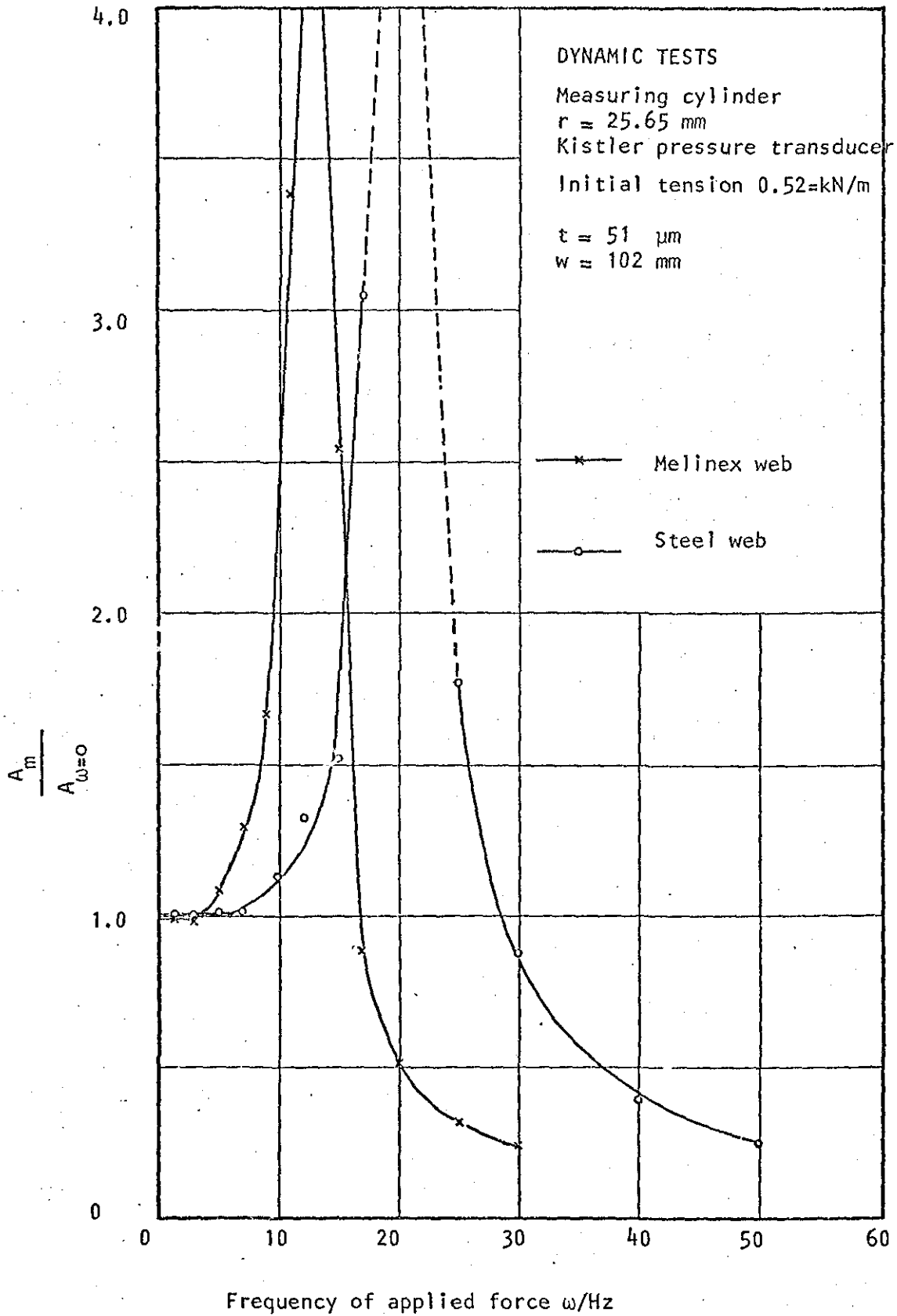


Fig. 6.45 Preliminary test on the Kistler pressure transducer.

DYNAMIC TESTS - Measuring Cylinder with Kistler transducer

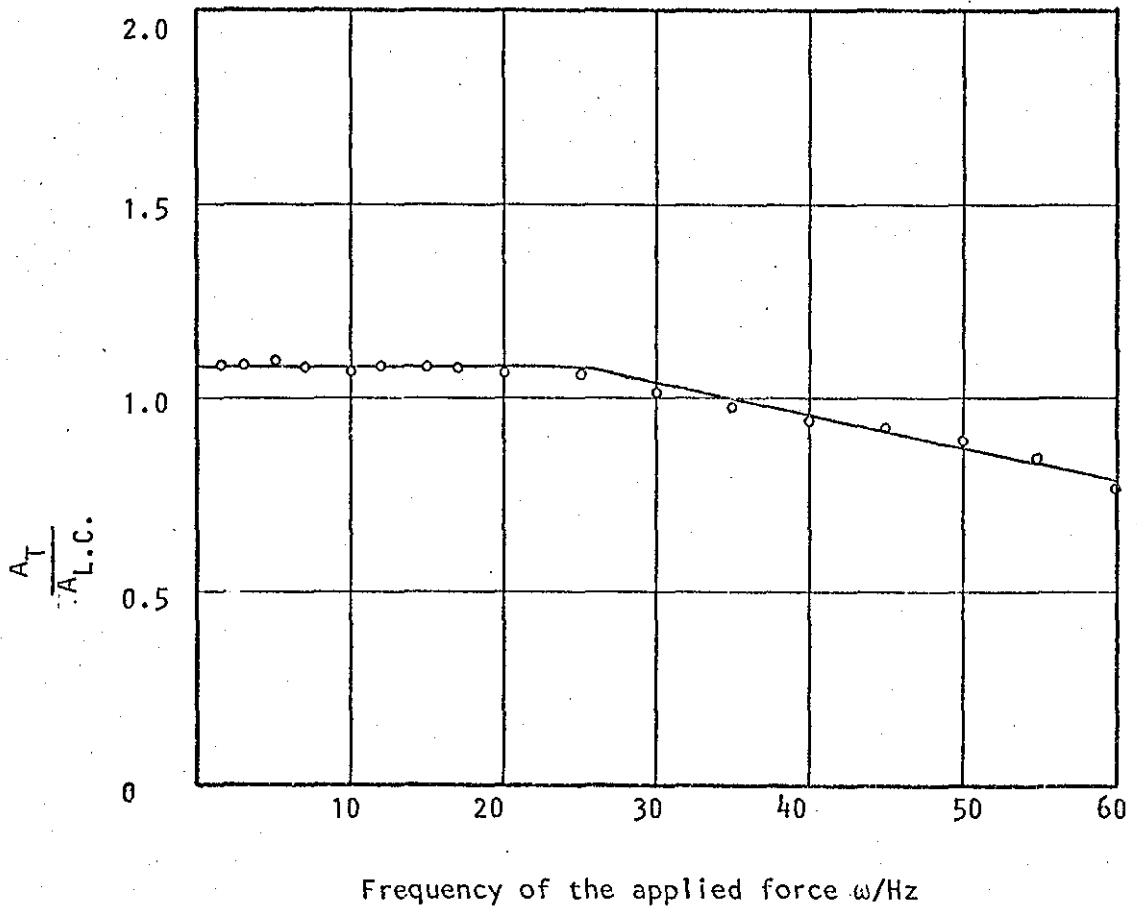
- Measuring Cylinder ; "Kistler" pressure transducer
- Web Material : Steel ; t = 51 μm  
w = 102 mm
- Initial static tension 0.52 kN/m
- Constant sinusoidal force, monitored by the load-cell, applied to the web at different frequencies.

$$\frac{\text{Amplitude of the measured force by the transducer}}{\text{Amplitude of the constant applied force measured by the load-cell}}$$

$$= A_T/A_{L.C.}$$

Frequency of applied force (ω) Hz	Amplitude of measured force mm		A <sub>T</sub> /A <sub>L.C.</sub>
	By load-cell	By transducer	
1.5	17.50	19.00	1.09
3	17.5	19.0	1.09
5	17.75	19.50	1.10
7	19.00	20.50	1.08
10	21.25	22.75	1.07
12	21.00	22.75	1.08
15	19.50	21.00	1.08
17	20.00	21.50	1.08
20	19.00	20.25	1.07
25	21.50	22.25	1.06
30	22.75	23.00	1.01
35	23.50	23.00	0.98
40	24.00	22.50	0.94
45	25.50	23.50	0.92
50	24.50	21.75	0.89
55	23.50	20.00	0.85
60	23.50	18.00	0.77

Table 6.23 Frequency response of the Kistler transducer II.



- DYNAMIC TESTS

- Measuring Cylinder ,  $r = 26.65$  mm
- Kistler pressure transducer
- Initial tension 0.52 kN/m
- Steel web ;  $t = 51$   $\mu$ m and  $w = 102$  mm

Fig. 6.46 Frequency response of the measuring cylinder associated with the Kistler pressure transducer

DYNAMIC TESTS

Tests on the measuring pad with the miniature pressure transducer

- Measuring Pad ; Miniature pressure transducer
- Web Material : Melinex ;  $t = 102 \mu\text{m}$   
 $w = 102 \text{ mm}$

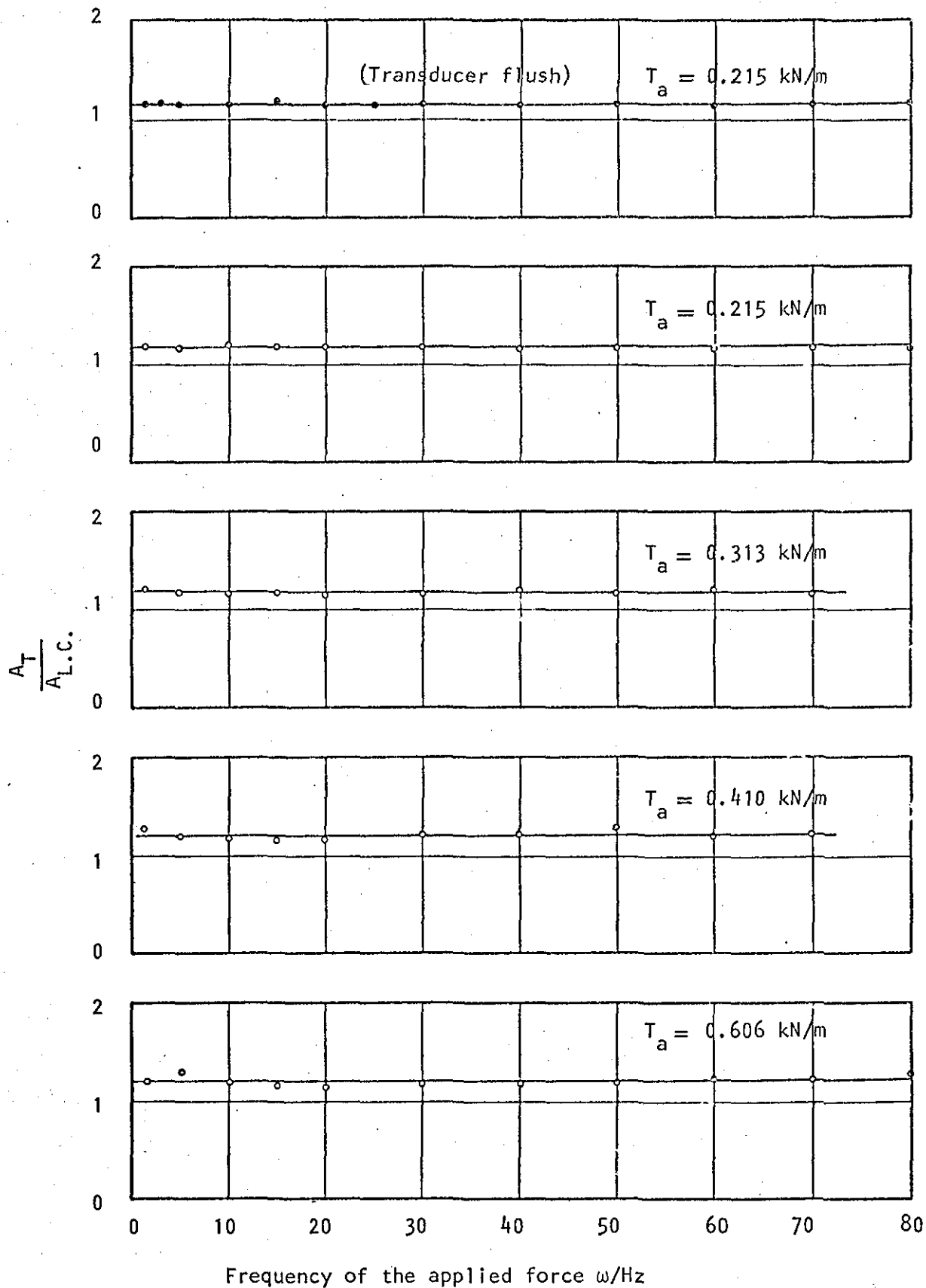
$$\frac{\text{Amplitude of the measured force by the transducer}}{\text{Amplitude of the constant applied force measured by the load-cell}} = A_T/A_{L.C.}$$

Frequency ( $\omega$ ) Hz	$A_T/A_{L.C.}$ at different initial tension				
	(Trans. flush)	(Transducer at optimum stable position)			
	$T_{a1}$	$T_{a1}$	$T_{a2}$	$T_{a3}$	$T_{a4}$
1.5	1.14	1.18	1.20	1.28	1.20
3	1.15	-	-	-	-
5	1.15	1.17	1.17	1.20	1.30
10	1.13	1.19	1.16	1.18	1.20
15	1.17	1.17	1.17	1.16	1.20
20	1.13	1.18	1.16	1.16	1.14
25	1.13	-	-	-	-
30	1.15	1.17	1.15	1.21	1.19
40	1.13	1.16	1.19	1.21	1.19
50	1.15	1.16	1.17	1.25	1.19
60	1.13	1.15	1.2	1.17	1.23
70	1.13	1.15	1.15	1.21	1.22
80	1.15	1.13	-	-	1.29

$$T_{a1} = 0.211 \text{ kN/m} \quad , \quad T_{a3} = 0.402 \text{ kN/m}$$

$$T_{a2} = 0.307 \text{ kN/m} \quad , \quad T_{a4} = 0.594 \text{ kN/m}$$

Table 6.24 Dynamic response of measuring pad on a Melinex web.



- DYNAMIC TESTS:

- Measuring pad
- Melinex web ;  $t = 102 \mu\text{m}$  and  $w = 102 \text{ mm}$
- Miniature pressure transducer

Fig. 6.47 Frequency response of the measuring pad associated with the Miniature pressure transducer (fitted at optimum stable position) at different initial tensions



DYNAMIC TESTS

Tests on the measuring pad with the miniature pressure transducer

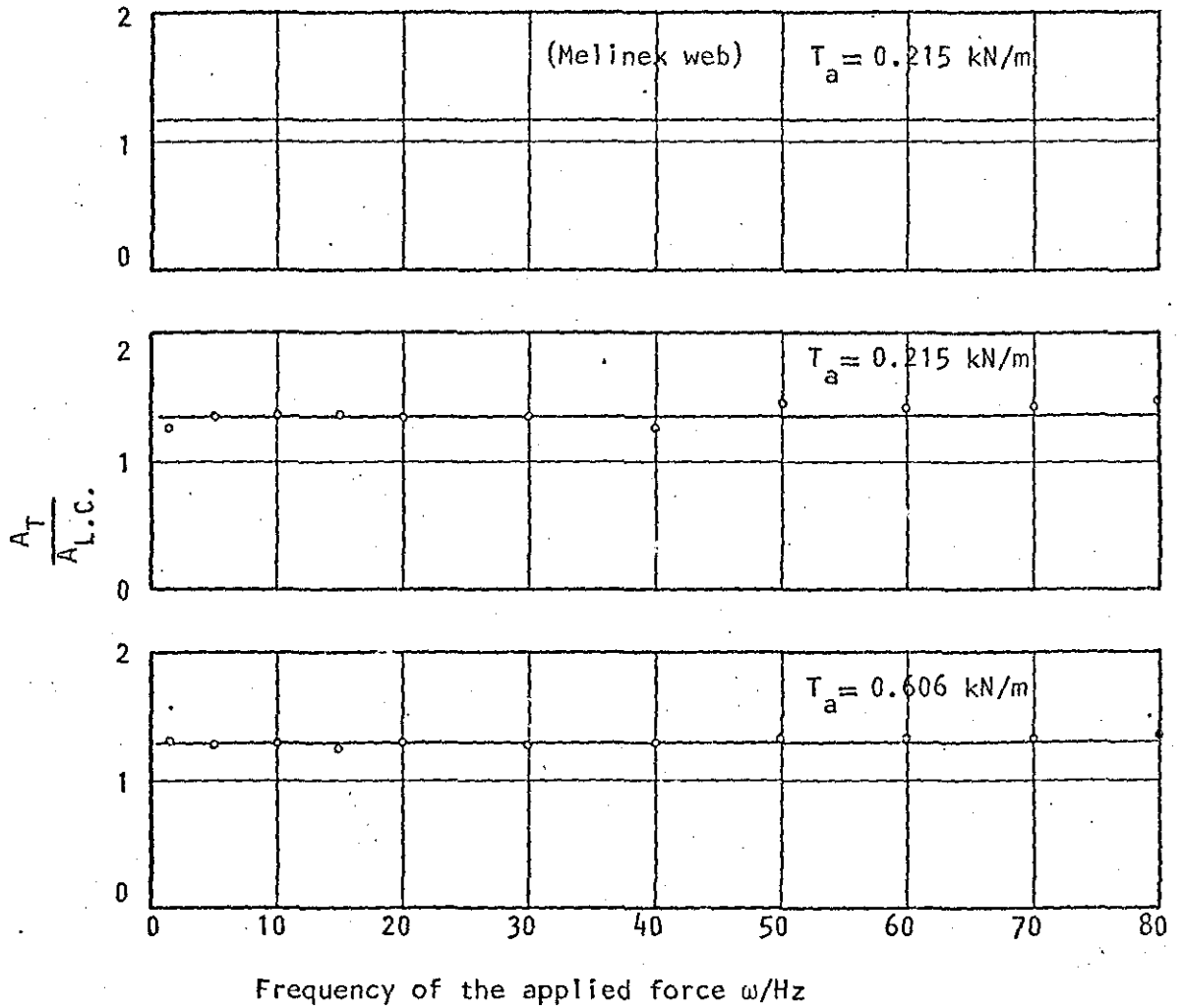
- Measuring pad ; Miniature pressure transducer
- Web material : Steel ; t = .51 μm  
w = 102 mm

$$\frac{\text{Amplitude of the measured force by the transducer}}{\text{Amplitude of the constant applied force measured by the load-cell}} = A_T/A_{L.C.}$$

Frequency (ω) Hz	A <sub>T</sub> /A <sub>L.C.</sub> at different initial tension (Transducer at optimum stable position)	
	T <sub>a1</sub>	T <sub>a2</sub>
1.5	1.24	1.31
5	1.36	1.28
10	1.36	1.28
15	1.42	1.24
20	1.39	1.28
30	1.35	1.26
40	1.22	1.28
50	1.47	1.32
60	1.43	1.32
70	1.43	1.32
80	1.47	1.34

$$T_{a1} = 0.211 \text{ kN/m} \quad , \quad T_{a2} = 0.594 \text{ kN/m}$$

Table 6.25 Dynamic response of measuring pad on Steel web.



- DYNAMIC TESTS

- Measuring pad
- Miniature pressure transducer
- Steel web ;  $t = 51 \mu\text{m}$  and  $w = 102 \text{ mm}$

Fig. 6.48 Frequency response of the measuring pad associated with the Miniature pressure transducer at two different initial tensions

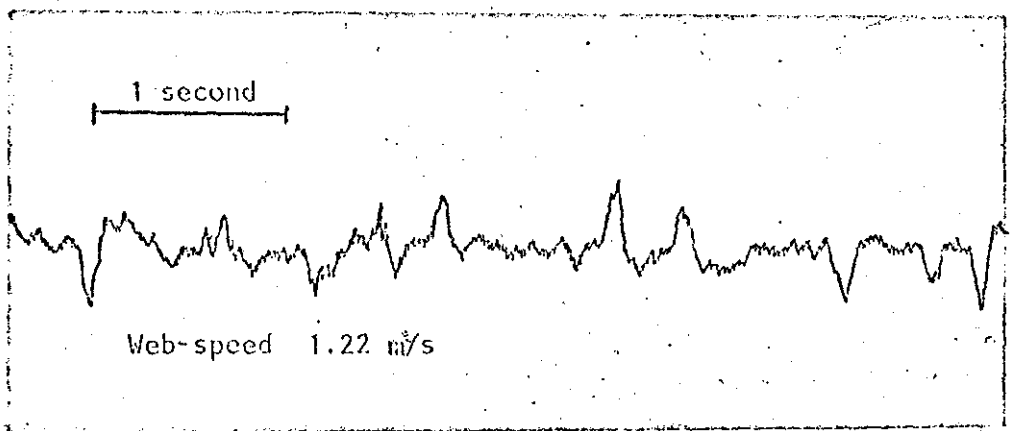
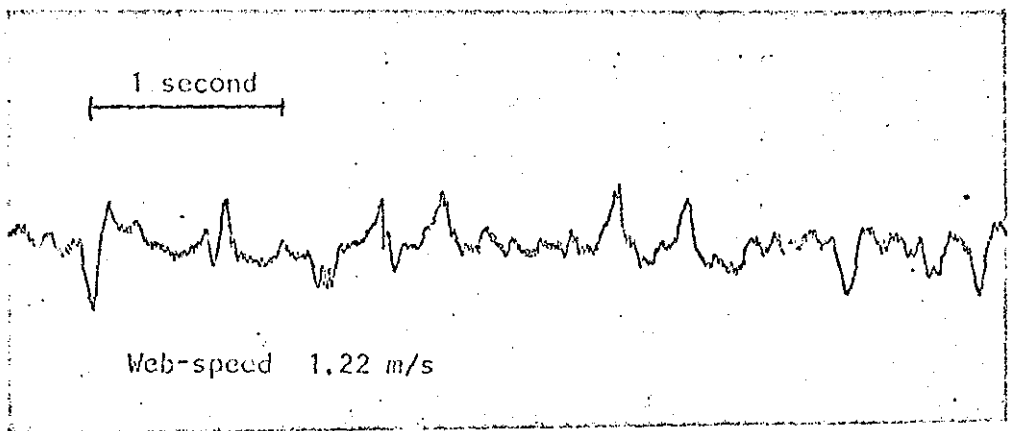
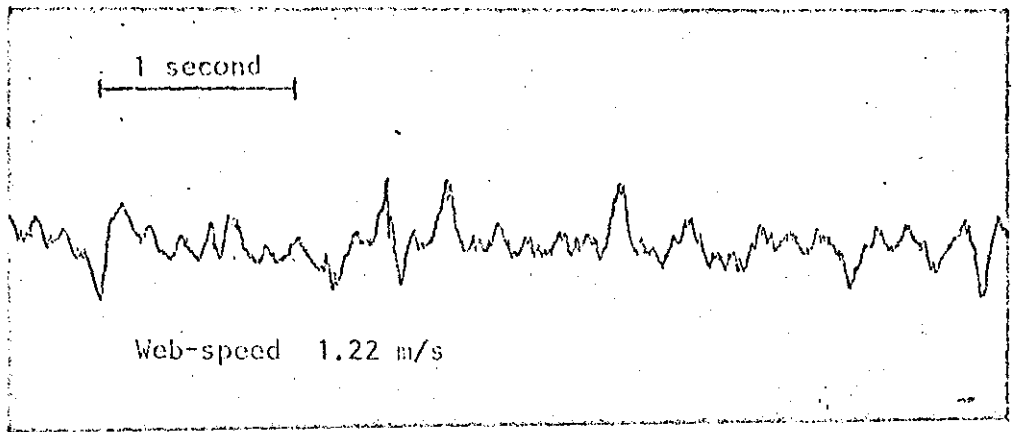


Fig. 6.49 Tension perturbations detected by the measuring pad at web speed of 1.22m/s for 3 cycles of the running loop of a 50mm wide Melinex web.

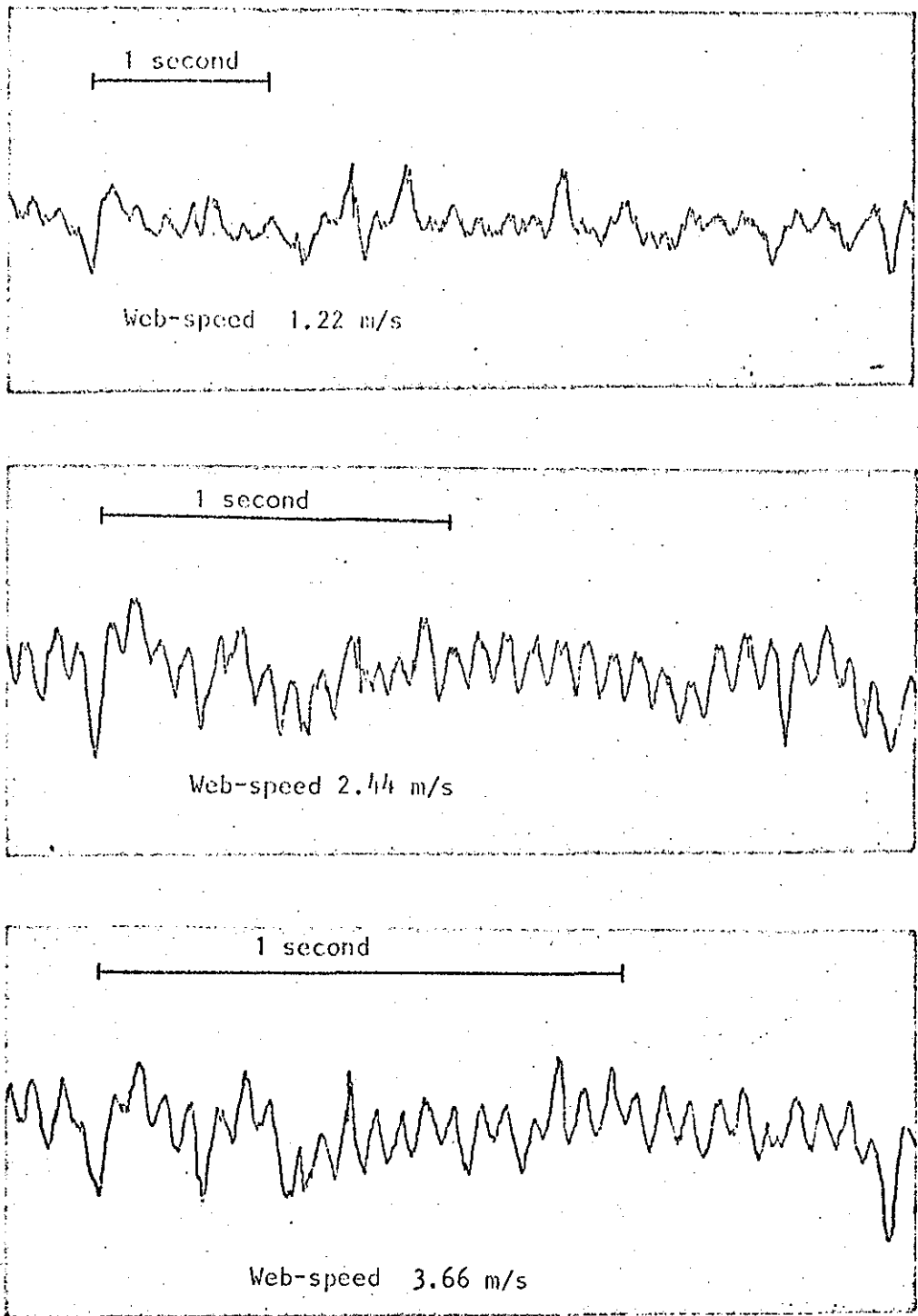


Fig. 6.50 Tension perturbations detected by the measuring pad at different web speeds over one cycle of the running loop of a 50mm wide Melinex web.

CHAPTER SEVEN

CONCLUSION AND RECOMMENDATION FOR FUTURE WORK

## 7.1 CONCLUSION

The following main conclusions are drawn from the results achieved and their analysis throughout the present investigation. Reference is made to the section of the thesis wherein the details corresponding to each conclusion were laid down.

1. The Huyck tensometer, a portable hand-held instrument for measuring web-tension, proved to have a non-linear output even within its specified measuring range under static conditions. (Ref. 6.3.1).
2. Utilising the concept of externally pressurised air foil-bearings to measure web-tension, the theoretical linear relation governing the tension in the web, the radius of the bearing and the pressure in the air film supporting the web was verified experimentally. (Ref. 6.3.2 and 6.3.4).
3. The apparent linear deviation of the measured tension values from the mean applied tensions was proved, experimentally, to be due to the tension profile across the web. This profile is a result of a combination of the distribution of the applied tensile force and the pressure distribution in the air film provided by external pressurisation. (Ref. 6.3.3 and 6.3.5).
4. The prototype of the portable hand-held device (called the web-tension measuring pad), when tested for static accuracy, proved to be capable of measuring the local tension in the web at the centre-line of the pad with a reliable accuracy. (Ref. 6.3.5).

5. Static stability of the measuring pad output, associated with a miniature pressure transducer, was achieved by setting the transducer at a distance of 6 mm from the active surface of the device. This experimental fact did not affect the dynamic response of the device to tension perturbations applied to the web with frequencies up to 80 Hz, the maximum available on the test rig. (Ref. 6.3.7 and 6.4.2).
6. The frequency response of a web-tension measuring technique, based on the electro-pneumatic principle, would be unsatisfactory if the volume of air in the pneumatic circuit is relatively large. (Ref. 6.4.1).
7. The developed measuring pad, associated with the miniature pressure transducer used, showed a very good frequency response to tension perturbations of frequencies up to 80 Hz. This improved result of the measuring pad, although it is based on an electro-pneumatic principle, is attributed to cutting down the volume of air in the pneumatic circuit to its minimum possible. The experimental investigation showed clearly that the pad is also capable of measuring tension perturbations with a reliable accuracy and with no measurable time lag between the measured and the applied tension perturbations. (Ref. 6.4.2).
8. Testing the performance of the developed prototype of the measuring pad on running webs, with different speeds up to 8.5 m/s, proved the device to be capable of detecting the tension perturbations in a practical environment. The tension perturbations in the corresponding experiments were caused by out of balance in the guide rollers on the test rig. (Ref. 6.5).

## 7.2 RECOMMENDATIONS FOR FUTURE WORK

In view of the fact that the open literature does not provide enough material relevant to the subject of the present investigation, it is believed that this field of research is a fruitful area for further investigations. The following points which have been brought about from the present study, are recommended for future work. Again, reference is made to the section of the present thesis wherein the corresponding point had been discussed.

1. The tension profile across the web, determined experimentally in the present study, is believed to be due to a combination of the distribution of the applied tensile force and the pressure distribution in the air film provided by external pressurisation. Further investigations, both analytical and experimental, to assess the contribution of each of the two factors would throw more light on this interesting phenomenon. It is also suggested to extend the present experimental work concerning the effect of the thickness, width and material stiffness of the web on the tension profile. (Ref. 2.4, 6.3.2 and 6.3.3).
2. The study of the effect of the radius of curvature of the measuring pad and the wrap angle of the web around its active surface on the peak value of the tension profile, is recommended for the case in which the web is narrower than the pad. An analytical study aiming at the prediction of the state of tension at the centreline of a web, which is wider than the measuring pad developed in the present study, would be of practical importance. (Ref. 2.4 and 6.3.4).



3. A theoretical derivation of the flow pattern of the pressurised air, in the vicinity of the area where the miniature pressure transducer was fitted into the pad, would elucidate the negative output of the measuring pad at relatively low values of applied tension. (Ref. 6.3.7).
4. The existing experimental rig can be adapted to evaluate quantitatively the performance of the developed prototype under running web conditions. This could be achieved by introducing, in the rig, a source to induce tension perturbations of known amplitudes and frequencies to the running web at different speeds.
5. Analytical determination of the frequency response of a web-tension measuring technique, based on the electro-pneumatic principle, would be beneficial. Particular reference to applied pressure and pneumatic circuit parameters, e.g. volume and resistance, would be of practical importance.

## REFERENCES

## REFERENCES

1. N.J.E. Haglov, "Web tension, rollstands, and reel changing", *Proceedings of the PATRA newspaper and rotary letterpress conference*. October (1957), pp 65-114.
2. E.R. Gibbon, "Stress/strain curves of paper", *Proc. Papermakers, Ass. G.B.I.* Vol. 25 (1944), pp 199.
3. O. Anderson, B. Ivarsson, A.H. Nissan, and B. Steenberg, "Graphical analysis of stress/strain curves of paper", *Proc. Papermakers, Ass. G.B.I.*, Vol. 30 (1949), pp 43.
4. Anon "Low cost web tension indicator", *Paperboard Packaging*, Feb. (1965), pp 134.
5. Anon "Web tension controller", *Boxboard Containers*, October (1967), pp 86.
6. Anon "Measurement and control of web-tension" *Packaging*, April (1968), pp 71-73.
7. Anon "Mechanical web tension control", *British Printer*, November (1970), pp 99.
8. D.C. Endersby and E. Zucker, "Direct tension control by strain gauges and disc brakes for rewinders", *Pulp and Paper Magazine of Canada*, September (1966), pp 393-398.
9. H. George and J. Kimball "Web tension research on rotogravure presses", *Eleventh Annual TAGA meeting*, June 15-17, (1959).
10. H. George, J. Kimball and R. Oppenheimer. "Web tensiometer frequency response". *TAGA Proceedings* (1963), pp 85-101.

11. R. Oppenheimer and H. George. "Transfer equations of the gravure press system". TAGA Proceedings (1966), pp 348-360.
12. R. Oppenheimer and H. George. "Computer simulation and control of the rotogravure press system", TAGA Proceedings (1971), pp 303-313.
13. D.L. King. "The mathematical model of a newspaper press", Interim Report, Newspaper techniques, December (1969), pp 3-7.
14. D.L. King "Tension measurements for newspaper presses", Instrumentation and control equipment for newspapers, INCA-FIEJ Research Association, September (1971) (11), pp 7-17.
15. D.L. King "Web tension study at Perscombinatie NV" Newspaper techniques, November (1972) pp 8-18.
16. D.L. King. "Tension behaviour of web-fed newspaper presses", Printing technology, Vol. 17, No. 2, (1973), pp 15-24.
17. R. Grünewald "Web tension measurements on web-offset presses", Papier Druck, Vol. 21, No. 11 November (1972), pp DV 161-164.
18. T. Curran "The application of solid-state regenerative drives and synchro phaser precision power transmissions in web tension/extension control", Pira/IARIGAI, International Conference on applied lithographic technology, October (1970), pp 23.1-23.4
19. Anon "Tension control in web-offset", British Printer February (1970), pp 98-104.
20. J.R. Martin "Tension Control for web-offset", The Penrose Annual, Vol. 66, (1973) pp 209-214.

21. Anon "The battle against web breaks" Newspaper techniques, March (1972) pp 1 and 4-21.
22. M. Graneek "Technical developments for the newspaper industry", The Penrose Annual. Vol. 65 (1972), pp 151-158.
23. W.A. Gross Gas film lubrication, Wiley & Sons, Inc., (1962).
24. N.S. Grassam and J.W. Powell (Ed.) Gas lubricated bearings, Butterworth's (1964).
25. Dudley Fuller (Ed) First International Symposium on gas-lubricated bearings, Office of Naval Research, Dept. of the Navy, ACR-49, October (1959).
26. W.E. Langlois "The lightly loaded foil bearing at zero angle of wrap", IBM Journal of Research and Development. Vol. 7, No. 2 April (1963), pp 112-116.
27. A. Eshel and H.G. Elrod, Jr. "The theory of the infinitely wide, perfectly flexible, self-acting foil bearing". Journal of Basic Engineering, Vol. 87, Series D, No. 4, December (1965) pp 831-836.
28. L.Licht "An experimental study of air-lubricated foils with reference to tape transport in magnetic recording", Report No. 7. Lubrication Research Lab., Dept. of Mech. Eng., Columbia Univ, New York. August (1966), pp 1-150.
29. A. Eshel and M. Wildmann, "Dynamic behaviour of a foil in the presence of a lubricating film", Trans. of ASME, Journal of Applied Mechanics, June (1968), pp 242-247.
30. T.B. Barnum and H.G. Elrod, Jr. "A theoretical study of the dynamic behaviour of foil bearings" Journal of Lubrication Technology, January (1971) pp 133-142.

31. E. Barlow, "Externally pressurised, axisymmetrical, foil bearing", Ampex Corp. Report, RR.63-4, April (1963), pp 1-26.
32. M. Wildmann and A. Wright. "The effect of external pressurisation on self-acting foil bearings", Journal of Basic Engineering, Vol. 87, Series D, No. 3, September (1965), pp 631-640
33. E. Barlow, "Externally pressurised foil gas bearings", Trans. of ASME, Journal of Basic Engineering, December (1965) pp 986-990
34. E. Barlow and M. Wildmann, "The axisymmetric, perfectly flexible foil bearing with porous inlet restrictor", Journal of Lubrication Technology, January (1968), pp 145-152.
35. G.W. Baumann, "Analysis of a porous gas foil bearing", Journal of Lubrication Technology, October (1971), pp 457-464.
36. W.S. Deason, "Air-blown sintered metal turner bars as an aid to web transport", Powder Metallurgy, Vol. 12, No. 24, (1969), pp 410-416.
37. A.J. Munday, "Development of gas bearing technology", CME, February (1974), pp 80-83.
38. R. Molle, "Recent Tendencies in Pneumatic Metrology" Microtecnic Vol. 10 (1956), pp 167
39. D.B. Kirk "Introduction to Principles of Pneumatic Gauging", ASME, Paper No. 52-A-113 (1952).
40. J.C. Evans "The Pneumatic Technique in its Application to Dimensional Measurement", J. Instn. Prod. Engrs., Vol. 36, (1957) pp 110.

41. J.C. Evans "Pneumatic gauging techniques", Research, Vol. 11, (1958), pp. 90.
42. I.G. Morgan and J.B. Johnson. "Dynamic behaviour of Pneumatic Gauging Systems", The Engineer, Vol. 212, November (1961), pp 879.
43. S.P. Timoshenko and D.H. Young Theory of Structure, 2nd ed. McGraw-Hill, (1965).
44. R.K. Livesley, Matrix Method in Structural Analysis, Pergamon Press (1964).
45. C.A. Brebbia and J.J. Conner. Fundamentals of Finite Element Techniques, Butterworth & Co. Ltd., (1973).
46. O.C. Zienkiewicz The Finite Element Method in Engineering Science, 2nd ed. McGraw-Hill, (1971).
47. R.D. Henshell, (Ed) PAFEC 70+ Manual, Nottingham University, Department of Mechanical Engineering.
48. K.J. Hume and G.H. Sharp Practical Metrology, Vol. 2, Macdonald and Co. Ltd., pp 25-28.
49. H. Bonrath, "Web Tension and Elongation Control in Web-Fed Presses", INCA-FIEJ Research Institute, Seminar on New Features of Newspaper Press Design.
50. Anon "On-line Shape Control for Cold-rolled Strip", Metals and Materials, June (1976), pp 26-32.
51. I.S. Gradshteyn and I.M. Ryzhik, "Tables of Integrals, Series and Products", 4th ed. by YU. V. Geronimus and M.YU. Tseytlin, Academic Press (1965) pp.249, 904 and 905.
52. Anon "An Introduction to Melinex Films", Bulletin MX 100. Third ed. Film Group, ICI Plastic Division, Welwyn Garden City, pp 12.

REFERENCES NOT CITED:

53. H.L. Wunsch, "Design Data for Flat Air Bearings" Metalworking production, September, 26 (1958), pp 1697-1704.
54. K. Arthur, Transducer Measurements, 1st ed. Tektronix, Inc. (1970).
55. E. Ower and R.C Pankhurst. The Measurement of Air Flow, 4th ed. Pergamon Press, (1966).
56. C.E. Crede, Shock and Vibration Concepts in Engineering Design, Prentice-Hall Inc. (1965).
57. L.A. Pipes, Applied Mathematics for Engineers and Physicists, 2nd ed. McGraw-Hill, (1958)
58. M.C. Shaw and E.F. Macks. Analysis and Lubrication of Bearings, McGraw-Hill, (1949).



APPENDICES

APPENDIX I

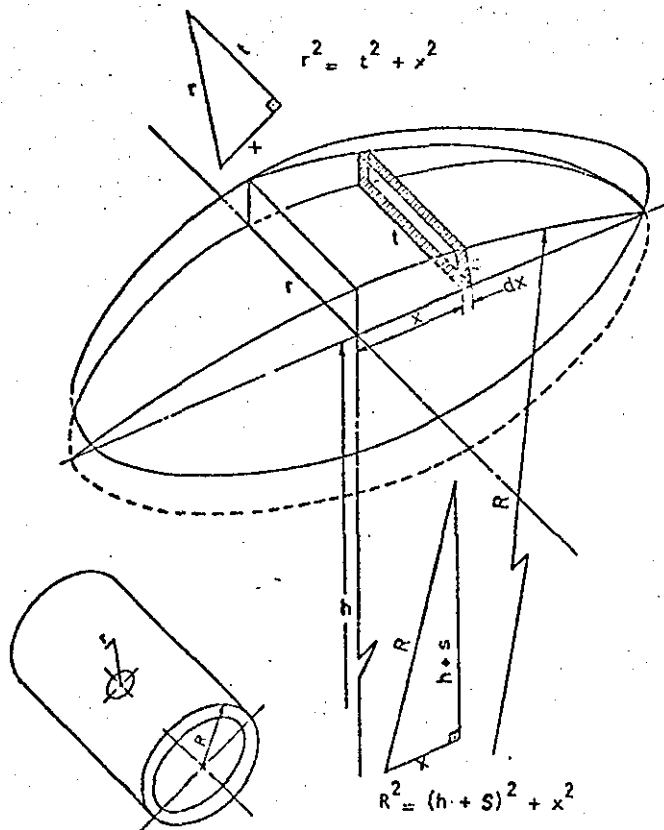
MINIMUM VOLUME OF PNEUMATIC CIRCUIT

Fig. (1.1) shows the geometry of the volume of air pocket resulting from the intersection of two cylinders perpendicular to each other (see 2.1).

Terminology:

- R Outer radius of the cylindrical sintered segment
- r radius of the pressure transducer = radius of intersection circle (between sintered segment and transducer).
- h distance between the centre line of the cylindrical segment and the plane containing the intersection circle.
- t length of the element of volume.
- s height of the element of volume.
- dx width of the element of volume.
- v 1/4 the resulting volume
- V total resulting volume = 4 v.

FIG. 1.1



Referring to Fig. (1.1) it can be seen that one can work on one quarter of the resulting volume. Due to symmetry the total resulting volume is four-fold of the calculated one.

$$v = \int t.s. dx \dots\dots\dots (1)$$

$$\text{But we have } t = \sqrt{r^2 - x^2} \dots\dots\dots (2)$$

$$\text{and } h + s = \sqrt{R^2 - x^2}$$

$$\text{since } h = \sqrt{R^2 - r^2}$$

$$\text{hence } s = \sqrt{R^2 - x^2} - \sqrt{R^2 - r^2} \dots\dots\dots (3)$$

Substituting in (1) for t and s we get

$$v = \int_0^r \sqrt{r^2 - x^2} \cdot \sqrt{R^2 - x^2} dx - \sqrt{R^2 - r^2} \int_0^r \sqrt{r^2 - x^2} dx$$

$$= I - \sqrt{R^2 - r^2} \cdot \left[ \frac{x}{2} \sqrt{r^2 - x^2} + \frac{r^2}{2} \sin^{-1} \left( \frac{x}{r} \right) \right]_0^r$$

$$v = I - \frac{\pi r^2}{4} \sqrt{R^2 - r^2} \dots\dots\dots (4)$$

$$\text{where } I = \int_0^r \sqrt{r^2 - x^2} \cdot \sqrt{R^2 - x^2} dx \dots\dots\dots (5)$$

Referring to "Tables of Integral Series and Products" by Gradshteyn and Ryzhik<sup>51</sup> we get

$$\int_u^b \sqrt{(a^2 - x^2)(b^2 - x^2)} dx = \frac{a}{3} \left\{ (a^2 + b^2) E(\xi, t) - (a^2 - b^2) F(\xi, t) \right\} + \frac{u}{3} (u^2 - 2a^2 - b^2) \sqrt{\frac{b^2 - u^2}{a^2 - u^2}}, [a > b > u > 0] \dots (6)$$

A quick look at equations (5) and (6) reveals the resemblance between the right hand side of the first and the left hand side of the second except for one thing; the lower limit of integration  $u$  in equation (6) equals zero in (5). Hence equation (6) becomes

$$\int_0^b \sqrt{(a^2 - x^2)(b^2 - x^2)} \, dx = \frac{a}{3} \left\{ (a^2 + b^2)E(k) - (a^2 - b^2)K(k) \right\} \dots \quad (7)$$

where  $k = \frac{b}{a}$  and  $E$  and  $K$  are the complete elliptic integrals of the 2nd and 1st kind respectively<sup>51</sup>.

In our case  $b = r$ ,  $a = R$  and  $k = \frac{r}{R}$

The complete elliptic integrals are defined by<sup>51</sup>:

$$K(k) = \int_0^{\frac{\pi}{2}} \frac{d\theta}{\sqrt{1 - k^2 \sin^2 \theta}} \dots \dots \dots \quad (8)$$

$$E(k) = \int_0^{\frac{\pi}{2}} \sqrt{1 - k^2 \sin^2 \theta} \, d\theta \dots \dots \dots \quad (9)$$

They could also be given in series representation as follows:

$$K(k) = \frac{\pi}{2} \left\{ 1 + \left(\frac{1}{2}\right)^2 k^2 + \left(\frac{1 \times 3}{2 \times 4}\right)^2 k^4 + \dots + \left[ \frac{(2n-1)!!}{2^n n!} \right]^2 k^{2n} + \dots \right\} \quad (10)$$

$$E(k) = \frac{\pi}{2} \left\{ 1 - \frac{1}{2^2} k^2 - \frac{1^2 \times 3}{2^2 \times 4^2} k^4 + \dots - \left[ \frac{(2n-1)!!}{2^n n!} \right]^2 \frac{k^{2n}}{2n-1} \dots \right\} \quad (11)$$

where  $(2n-1) !! = (2n-1) \cdot (2n-3) \cdot (2n-5) \dots \quad (1)$

Turning now to equation (5), if we put

$$x = r \sin \theta \quad \text{then} \quad dx = r \cos \theta \, d\theta$$

equation (5) becomes

$$\begin{aligned}
 I &= \int_0^{\frac{\pi}{2}} \sqrt{r^2 - r^2 \sin^2 \theta} \cdot \sqrt{R^2 - r^2 \sin^2 \theta} \cdot r \cos \theta \, d\theta \\
 &= r^2 R \int_0^{\frac{\pi}{2}} \cos^2 \theta \sqrt{1 - \frac{r^2}{R^2} \sin^2 \theta} \, d\theta \dots\dots\dots (12)
 \end{aligned}$$

Substituting for  $\frac{r^2}{R^2}$  by  $k^2$  &  $\cos^2 \theta$  by  $\frac{1}{2} (\cos 2\theta + 1)$  we get

$$I = \frac{r^2 R}{2} \int_0^{\frac{\pi}{2}} \cos 2\theta \sqrt{1 - k^2 \sin^2 \theta} \, d\theta + \frac{r^2 R}{2} \int_0^{\frac{\pi}{2}} \sqrt{1 - k^2 \sin^2 \theta} \, d\theta$$

The second integration in the last equation equals  $E(k)$ , equation (9), and integrating the first one by parts we get

$$\begin{aligned}
 \int_0^{\frac{\pi}{2}} \sqrt{1 - k^2 \sin^2 \theta} \cdot \cos 2\theta \, d\theta &= \left[ \sqrt{1 - k^2 \sin^2 \theta} \cdot \frac{1}{2} \sin 2\theta \right] - \int_0^{\frac{\pi}{2}} \frac{\sin 2\theta}{2} \\
 &\quad \frac{-k^2 \sin \theta \cos \theta}{\sqrt{1 - k^2 \sin^2 \theta}} \, d\theta = 0 + \int_0^{\frac{\pi}{2}} k^2 \frac{\sin^2 \theta \cos^2 \theta}{\sqrt{1 - k^2 \sin^2 \theta}} \, d\theta
 \end{aligned}$$

$$\therefore I = \frac{r^2 R}{2} \int_0^{\frac{\pi}{2}} k^2 \frac{\sin^2 \theta \cos^2 \theta}{\sqrt{1 - k^2 \sin^2 \theta}} \, d\theta + \frac{r^2 R}{2} E(k)$$

$$= \frac{r^2 R}{2} \int_0^{\frac{\pi}{2}} \frac{\cos^2 \theta - \cos^2 \theta (1 - k^2 \sin^2 \theta)}{\sqrt{1 - k^2 \sin^2 \theta}} \, d\theta + \frac{r^2 R}{2} E(k)$$

$$= \frac{r^2 R}{2} \int_0^{\frac{\pi}{2}} \frac{\cos^2 \theta}{\sqrt{1 - k^2 \sin^2 \theta}} \, d\theta - \frac{r^2 R}{2} \int_0^{\frac{\pi}{2}} \cos^2 \theta \sqrt{1 - k^2 \sin^2 \theta} \, d\theta + \frac{r^2 R}{2} E(k)$$

Substituting by  $\frac{1}{2}$  from equation (12) for the second term of the last equation and for  $\cos^2\theta$  by  $1-\sin^2\theta$  in the first term we get:

$$I = \frac{r^2 R}{2} \int_0^{\frac{\pi}{2}} \frac{d\theta}{\sqrt{1-k^2 \sin^2 \theta}} - \frac{r^2 R}{2} \int_0^{\frac{\pi}{2}} \frac{\sin^2 \theta}{\sqrt{1-k^2 \sin^2 \theta}} d\theta - \frac{1}{2} + \frac{r^2 R}{2} E(k)$$

Substituting by  $K(k)$  from equation (8) for the first integral and multiplying and dividing the second term by  $k^2$  we get

$$3I = r^2 R \cdot K(k) - \frac{r^2 R}{k^2} \int_0^{\frac{\pi}{2}} \frac{k^2 \sin^2 \theta}{\sqrt{1-k^2 \sin^2 \theta}} d\theta + r^2 R \cdot E(k) \dots \tag{13}$$

Subtracting (9) from (8) yields

$$K(k) - E(k) = \int_0^{\frac{\pi}{2}} \frac{1-1+k^2 \sin^2 \theta}{\sqrt{1-k^2 \sin^2 \theta}} d\theta$$

$$= \int_0^{\frac{\pi}{2}} \frac{k^2 \sin^2 \theta}{\sqrt{1-k^2 \sin^2 \theta}} d\theta$$

Substituting in (13) for the integration in the middle term

$$3I = r^2 R \cdot K(k) - \frac{r^2 R}{k^2} \left[ K(k) - E(k) \right] + r^2 R \cdot E(k)$$

$$\therefore I = \frac{r^2 R}{3k^2} \left[ (1+k^2)E(k) - (1-k^2)K(k) \right] \dots \tag{14}$$

Substituting for  $E(k)$  and  $K(k)$  from (10) and (11) in (14) reveals

$$\begin{aligned}
 I &= \frac{r^2 R}{3k^2} \cdot \frac{\pi}{2} \left[ \left\{ (1+k^2) \left( 1 - \frac{k^2}{4} - \frac{3}{64} k^4 - \frac{5}{256} k^6 - \frac{175}{256 \times 64} k^8 \dots \right) \right\} \right. \\
 &\quad \left. - \left\{ (1+k^2) \left( 1 + \frac{k^2}{4} + \frac{9}{64} k^4 + \frac{25}{256} k^6 + \frac{175 \times 7}{256 \times 64} k^8 + \dots \right) \right\} \right] \\
 &= \frac{r^2 R}{3k^2} \cdot \frac{\pi}{2} \left( \frac{3}{2} k^2 - \frac{12}{64} k^4 - \frac{6}{265} k^6 - \frac{120}{256 \times 64} k^8 \dots \right)
 \end{aligned}$$

$$\therefore I = \frac{\pi}{4} \cdot r^2 R \left( 1 - \frac{1}{8} k^2 - \frac{1}{64} k^4 - \frac{5}{1024} k^6 \dots \right) \dots \dots \quad (15)$$

Substituting for I from (15) in (4) yields

$$v = \frac{\pi}{4} \cdot r^2 R \left( 1 - \frac{1}{8} k^2 - \frac{1}{64} k^4 - \frac{5}{1024} k^6 - \dots \right) - \frac{\pi}{4} \cdot r^2 R \sqrt{1 - \left(\frac{r}{R}\right)^2}$$

Since total volume  $V = 4v$

$$\begin{aligned}
 \therefore V &= \pi r^2 R \left\{ \left( 1 - \frac{1}{8} k^2 - \frac{1}{64} k^4 - \frac{5}{1024} k^6 - \dots \right) - (1-k^2)^{\frac{1}{2}} \right\} \\
 &= \pi r^2 R \left( \frac{3}{8} k^2 + \frac{7}{64} k^4 + \frac{59}{1024} k^6 + \dots \right) \\
 V &= \frac{3\pi}{8} \cdot \frac{r^4}{R} \left( 1 + \frac{7}{24} \left(\frac{r}{R}\right)^2 + \frac{59}{384} \left(\frac{r}{R}\right)^4 + \dots \right) \quad (16)
 \end{aligned}$$

## APPENDIX II

### ADJUSTABLE SPEED DRIVE SYSTEM AND SWINGING ROLL GUIDE UNIT

#### 1. The Drive System

The system used was the Morse SCR adjustable speed drive system for controlling the speed and torque of a direct current motor. It consisted of the following:

- Main Control Unit
- Remote Control Station
- Primary Circuit Protector
- D.C. Motor

#### D.C. MOTOR DATA

Type	G/N60K
Rating	0.75 kW(1 hp)
Maximum speed	1500 rev/min
Power requirements	220-240V, 50 Hz

Suppliers: Morse Chain, division of Borg-Warner Ltd.,  
Letchworth, Herts. England.

#### 2. The Guide Unit

The unit, used to control the lateral alignment of the moving webs throughout this investigation, consisted of:

- Power Unit
- Sensing Head
- Swinging roll displacement guide



GUIDE UNIT DATA

Power Unit Model

AH71 Air jet/hydraulic sensing and control system

Sensing Head

Type J1 guiding head

Swinging roll

Unit will correct a maximum of 1 inch on either side of the centreline

Manufacturers: Mount Hope Machinery Ltd., Dartford, Kent. England

### APPENDIX III

#### PROPERTIES OF THE MELINEX WEB USED

"Melinex" is the trade mark for a range of biaxially drawn films manufactured by ICI Plastics Division from polyethylene terephthalate polymer. The use of Melinex films in many industries, such as printing, manufacturing of magnetic tapes and photographic films and packaging industries, made it a favourable choice for a material of the web used in the present investigation.

The following are values for a 23  $\mu\text{m}$  thick Melinex Type S film<sup>52</sup>. They are included to give an idea about the properties of such films.

#### PROPERTIES (along the machine direction)

Density	1.395 - 1.405 g/ml
Yield strength	$10.3 \times 10^4 \pm 1.4 \times 10^4 \text{ kN/m}^2$
Tensile strength	$19.6 \times 10^4 \pm 2.0 \times 10^4 \text{ kN/m}^2$
Elongation at yield	5%
Elongation at break	110 - 140%
Thermal coefficient of expansion	$2.7 \times 10^{-5} \text{ } / ^\circ\text{C}$

## APPENDIX IV

### SPECIFICATIONS OF INSTRUMENTS USED

#### 1. The Electro-magnetic Vibrator and the associated Power Amplifier

##### VIBRATOR DATA

Model	405
Maximum thrust (sine vector with force cooling	196 N
D.C. Force factor (force/A)	7.7 N
Maximum working current:-	
Naturally cooled	9 A
Force cooled	18 A
Maximum acceleration	981 m/s <sup>2</sup>
Useful frequency range	1.5 Hz to 9 k Hz with TPO 300 Amplifier
Maximum stroke	± 8.8 mm
Suspension stiffness	14.1 N/mm
Fundamental armature resonance	9 k Hz

##### AMPLIFIER AND OSCILLATOR DATA

Model	TPO 300
Output power	300 V.A. at any load power factor of between 0.1 to 1.0
Output voltage	19 V R.M.S. at 300 watts
Power requirements	240 - 210 V, 50 Hz, 850 Watts
Oscillator frequency range	1.5 Hz - 25 k Hz in four ranges
Scale accuracy	3% between 25 Hz - 25 k Hz
Manufacturers:	Ling Dynamic Systems, Herts. England.

2. The reference Load-cell and the associated charge amplifier

LOAD CELL DATA

Model	Force transducer type 9203
Maximum measuring range	$\pm 50 \text{ kp}^*$ (490.4 N)
Resolution	0.1 p* ( $1 \times 10^{-3}$ N)
Maximum force	$\pm 60 \text{ kp}^*$ (588.4 N)
Resonant frequency	27kHz
Rise-time	15 $\mu\text{s}$
Linearity	$\pm 1\%$
Tightening torque for M3	5 cm.kp* (0.49 N.m)
Working temperature range	- 150 to + 240°C

\* 1 kp = 1 kg force , 1 p = 1 g force

CHARGE AMPLIFIER DATA

Model	566
Ranges (for + 10 V or $\pm 5$ V output)	0.05, 0.1, 0.2, 0.5, 1.0, 2.0, 5.0, 10, 20, 50 and 100 mV/pC
Output voltage (to high impedance load)	+ 10V, - 5V
Output current (to low-impedance load)	$\pm 10$ mA
Frequency response (nominal)	d.c. to 150 k Hz
Linearity error	0.1 %
Input and output connectors	BNC co-axial
Manufacturers:	Kistler Instrument Corporation, Switzerland.

3. The miniature pressure transducer and the associated circuit

MINIATURE PRESSURE TRANSDUCER DATA

Model	EPA-125-15
Range	15 psi (103.4 kN/m <sup>2</sup> )
Over range	50 psi (344.8 kN/m <sup>2</sup> )
Sensitivity (Nominal)	30 mV full scale
Resonant frequency (Nominal)	60 k Hz
Excitation	6.0 V d.c. or a.c.
Combined non-linearity and hysteresis	± 1% full scale
Repeatability	0.25%
Operating temperature range	-40°C to 121°C
Dimensions	3.18mm diameter (See Fig. 3.8)
Manufacturers:	Entran Devices, Inc., N.J., U.S.A.

BRIDGE SUPPLY AND BALANCE UNIT DATA

Model	FE-492 BBS
Output - Voltage Mode	
voltage	3-12 V Constant voltage
current	35 mA maximum
Current Mode	
current	3.35 mA Constant current
voltage	8 V maximum
Stability: with temperature	0.02 % /°C
against mains changes	500 : 1
Main supply requirements	200 - 240 V, 50 Hz

PRE AMPLIFIER DATA

Model	FE-251-GA
Gain: (Voltage)	Switched 20, 50, 100, 200, 500, 1000
accuracy	$\pm 1\%$ maximum
linearity	<0.1% deviation from best straight line
Stability	better than 0.02% / $^{\circ}$ C " " 0.1% long term
Output: voltage	$\pm 8V$ maximum
current	$\pm 1.5$ mA maximum
impedance	<2 $\Omega$
Shift	$\pm 8$ V referred to output
Bandwidth	d.c. to 20 k Hz
Power supply	200-240 V, 50 Hz
Manufacturers: Fylde Electronic Laboratories Ltd., Preston, England.	

APPENDIX V

INTERNATIONAL SYSTEM OF UNITS (SI) CONVERSION FACTORS

Symbol given		Multiply by	To obtain	Symbol
in	inch	25.4*	millimeters	mm
ft.	feet	0.3048*	meters	m
ft <sup>3</sup>	cubic feet	0.02832	cubic meters	m <sup>3</sup>
ft/min	feet per minute	0.00508*	meters per second	m/s
lb	pound mass	0.4536	kilograms	kg
kgf	kilogram-force	9.807	newtons	N
kgf/cm	kilogram-force per centimeter	0.981	kilonewtons per meter	kN/m
kgf/cm <sup>2</sup>	kilogram-force per square centimeter	98.1	kilonewtons per square meter	kN/m <sup>2</sup>
lbf/in <sup>2</sup>	pound force per square inch	6.895	kilonewtons per square meter	kN/m <sup>2</sup>

\* Indicates exact value.

